



HAL
open science

Identification of the Genetic Basis of Childhood Melanoma

Alexandra Vargas Chavez

► **To cite this version:**

Alexandra Vargas Chavez. Identification of the Genetic Basis of Childhood Melanoma. Cancer. Université Paris-Saclay, 2022. English. NNT : 2022UPASL036 . tel-04510274

HAL Id: tel-04510274

<https://theses.hal.science/tel-04510274v1>

Submitted on 18 Mar 2024

HAL is a multi-disciplinary open access archive for the deposit and dissemination of scientific research documents, whether they are published or not. The documents may come from teaching and research institutions in France or abroad, or from public or private research centers.

L'archive ouverte pluridisciplinaire **HAL**, est destinée au dépôt et à la diffusion de documents scientifiques de niveau recherche, publiés ou non, émanant des établissements d'enseignement et de recherche français ou étrangers, des laboratoires publics ou privés.

Identification of the genetic basis of childhood melanoma

Identification des bases génétiques du mélanome de l'enfant

Thèse de doctorat de l'université Paris-Saclay

École doctorale n°582, Cancérologie : biologie - médecine - santé
(CBMS)

Spécialité de doctorat : Aspects moléculaires et cellulaires de la biologie

Graduate School : Sciences de la vie et santé

Référent : Faculté de médecine

Thèse préparée dans l'unité de recherche **Institut des neurosciences Paris-Saclay**,
(université Paris-Saclay, CNRS), et **Dynamique des Cellules Tumorales** (université

Paris-Saclay, Inserm, Institut Gustave Roussy), sous la direction de **Brigitte**

BRESSAC-DE PAILLERETS, PH université Paris Saclay, la co-direction de **Sophie**
CREUZET, DR, université Paris-Saclay

Thèse soutenue à Paris-Saclay, le 10 juin 2022, par

Alexandra VARGAS CHAVEZ

Composition du Jury

Jean-Loup DUBAND

DR CNRS, INSERM

Université Paris-Est Créteil

Président

Julie CAMEL

CR, INSERM

Université Claude Bernard Lyon

Rapporteuse & Examinatrice

Berta LÓPEZ SANCHEZ

CR, Consejo Superior de
Investigaciones Científicas

Rapporteuse & Examinatrice

Anne-Hélène MONSORO-BURQ

PU, université Paris Saclay

Examinatrice

Titre : Identification des bases génétiques du mélanome de l'enfant

Mots clés : Mélanome cutané, Cancers pédiatriques, Crête Neurale

Résumé : En France, le cancer est la première cause de décès par maladie chez l'enfant. Chaque année, 2500 enfants et adolescents se voient diagnostiquer un cancer, dont la moitié chez les enfants de moins de cinq ans et 700 chez les jeunes de 15 à 18 ans. Le pronostic des cancers pédiatriques est souvent mauvais, avec des conséquences dévastatrices. Cependant, les tumeurs malignes détectées chez les enfants et les adolescents ne sont pas de la même nature que celles des adultes et ne peuvent donc pas être comprises et traitées de la même manière. Comparé au mélanome de l'adulte, le mélanome pédiatrique est une maladie rare qui représente moins de 1 % de tous les diagnostics de mélanome. De plus, la plupart des cas pédiatriques sont sporadiques et surviennent parfois au sein de naevus congénitaux géants, ce qui favorise l'hypothèse de mutations de novo. Notre hypothèse est que les "accidents" génétiques de novo se produisent soit dans un gamète parental, soit post zygotiquement pendant le développement de l'embryon. Pour tester cette hypothèse, nous avons séquencé des exomes constitutionnels sur de l'ADN extrait du sang d'enfants atteints de mélanome et de leurs parents sains (trios) et de 6 tumeurs de mélanome congelées. Nous avons identifié des mutations germinales ou post-zygotiques de novo dans 14 gènes impliqués dans le développement de la crête neurale, du mélanome ou du cancer.

Mon projet de thèse vise à étudier le rôle biologique inconnu de gènes candidats de novo au cours du développement des lignées NC et mélanocytaires. Nous avons effectué une analyse fonctionnelle des gènes candidats de novo *FBXO32*, *SOX10*, *DSCAM* et *ALDH1L1*. Pour répondre à ce défi, les modèles transgéniques conventionnels ne sont pas entièrement adaptés, nous avons donc conçu des modèles originaux *in vivo*, *ex vivo* et *in vitro* pour éclairer la signification biologique de ces variantes.

Dans le NC céphalique, nos résultats montrent que les quatre gènes candidats, lorsqu'ils sont désactivés, altèrent la prolifération et la différenciation des mélanocytes de manière différente, suggérant que ces gènes exercent des rôles dans la biologie normale des mélanocytes. Ensuite, nous nous sommes concentrés sur le gène *FBXO32* dans lequel une mutation germinale de novo, p.G139S, a été identifiée chez un enfant de sept ans présentant un mélanome de niveau III. Nos résultats montrent que l'inactivation de *FBXO32* altère la prolifération, la différenciation et la vascularisation des mélanocytes dans le tronc NC. Pour étudier l'expression de la spécificité endogène de *FBXO32*, nous avons réalisé des expériences de sauvetage par coélectroporation de *dsFBXO32* avec la forme humaine sauvage ou mutée de *FBXO32*. Alors que le sauvetage de *FBXO32* est capable de compenser l'extinction du gène endogène et de restaurer la différenciation normale des mélanocytes, l'ADNc mutant, *FBXO32*^{G139S}, a un effet néfaste sur la lignée mélanocyttaire. Afin de décrypter le rôle de *FBXO32* dans la lignée mélanoblastique dans la NC céphalique, nous avons mis en place un modèle d'explant de peau 3D *in vitro*, qui nous a permis de suivre la différenciation des appendices cutanés et de caractériser la différenciation normale des mélanocytes dans l'épiderme, et/ou leur migration aberrante vers le derme. Plus précisément, *FBXO32* induit la prolifération des mélanocytes, associée à la migration des mélanocytes vers le derme. Au niveau cellulaire, *FBXO32* déclenche la transformation des mélanocytes et le remodelage du cytosquelette. Nous montrons ainsi que *FBXO32* entrave l'adhésion focale et l'organisation des filaments d'actine, suggérant l'implication de ce mécanisme dans les processus d'invasion. Grâce au profilage transcriptionnel, nous avons constaté que *FBXO32* orchestre un enrichissement différent des gènes au niveau de la CN du tronc et de la CN crânienne. Nos résultats montrent que *FBXO32* pourrait être un **gène crucial dans le développement** des mélanocytes et potentiellement impliqué dans la mélanomagenèse.

Title : Identification of the genetic basis of childhood melanoma

Keywords : Cutaneous melanoma, Pediatric cancers, Neural Crest

Abstract: In France, cancer is the leading cause of death by disease in children. Every year, 2500 children and adolescents are diagnosed with cancer, half of them in children under five years old and 700 in young people between 15 and 18 years old. The prognosis of pediatric cancers is often poor, with devastating consequences. However, oncology research mainly focuses on understanding the cancer mechanisms in adults. However, malignant tumors detected in children and adolescents are not of the same nature as those of adults and, therefore cannot be understood and treated in the same way. Compared to adult melanoma, pediatric melanoma is a rare disease accounting for less than 1% of all melanoma diagnoses. Furthermore, most pediatric cases are sporadic and sometimes arise within giant congenital nevi, favoring the hypothesis of *de novo* mutations. Our hypothesis is that *de novo* genetic "accidents" occur either in a parental gamete or post zygotically during embryo development. To test this hypothesis, we sequenced constitutional exomes on DNA extracted from the blood children with melanoma and their healthy parents (trios) and 6 frozen melanoma tumors. We identified *de novo* germline or post-zygotic mutations in 14 genes involved in the development of the neural crest, melanoma, or cancer.

My thesis project aims to study the unknown biological role of *de novo* candidate genes during the development of NC and melanocyte lineages. We performed functional analysis of *FBXO32*, *SOX10*, *DSCAM*, and *ALDH1L1* *de novo* candidate genes. To address this challenge, the conventional transgenic models are not fully suitable, so we designed original *in vivo*, *ex vivo*, and *in vitro* models to enlighten the biological significance of these variants.

In the cephalic NC, our results show that the four candidate genes, when knocked down, impair melanocyte proliferation and differentiation in a different way, suggesting these genes exert roles in the normal biology of the melanocytes. Then, we focused on the *FBXO32* gene in which *de novo* germline mutation, p.G139S, was identified in a seven-year-old child with melanoma level III. Our results show that the silencing of *FBXO32* impairs melanocyte proliferation, differentiation, and vascularization in the trunk NC. Then, we performed rescue experiments by co-transfecting the human wild-type or mutated form of *FBXO32*. While the rescue of *FBXO32* is able to compensate for the silencing of the endogenous gene and restore normal melanocyte differentiation, the mutant cDNA, *FBXO32*^{G139S}, has a detrimental effect on the melanocyte lineage. To decipher the role of *FBXO32* in the melanoblast lineage in the cephalic NC, we set up an *in vitro* 3D skin explant model, which allowed us to follow the differentiation of skin appendages and to characterize the normal differentiation of melanocytes in the epidermis, and/or their aberrant migration to the dermis. Specifically, *FBXO32* induces melanocyte proliferation, associated with melanocyte migration towards the dermis. At the cellular level, *FBXO32* triggers melanocyte transformation and cytoskeleton remodeling. At a subcellular level, we show that *FBXO32* hinders focal adhesion and actin filaments organization suggesting the involvement of this mechanism in invasion processes. Through transcriptional profiling, we found that *FBXO32* orchestrates different gene enrichment at the trunk NC and cranial NC. . Our data show that *FBXO32* could be a **crucial gene in melanocyte development** and potentially involve melanomagenesis.

*This work was supported by La Ligue Contre le Cancer
Financement de thèse 1^{er} - 4^{ème} année*

Para ti Daniel

*Aunque me miras desde el cielo hace 16 años,
te siento todos los días a mi lado hermano mío*

Synthèse en Français

En France, le cancer est la première cause de décès par maladie chez les enfants. Chaque année, 2500 enfants et adolescents sont diagnostiqués d'un cancer, dont la moitié chez l'enfant de moins de 5 ans et 700 chez les jeunes de 15 à 18 ans (l'Institut National du Cancer-SFCE, 2014). Le pronostic des cancers pédiatriques est souvent sombre avec des conséquences dévastatrices. Cependant, la recherche en Oncologie est essentiellement axée sur la compréhension des mécanismes cancérologiques des adultes ; or, les tumeurs malignes détectées chez les enfants ne sont pas de même nature que celles des adultes et ne peuvent donc pas être appréhendées et soignées de la même manière. Dans le cas du mélanome, les cancers pédiatriques sont sporadiques, ce qui suggère que « l'accident génétique » se produit soit dans les gamètes parentaux, soit de manière post-zygotique au cours du développement embryonnaire. Le mélanome cutané de l'enfant ou de l'adolescent est rare mais son incidence augmente. L'étude du gène *CDKN2A* (principal gène de prédisposition au mélanome de l'adulte) chez des jeunes ayant développé un mélanome avant 18 ans, a montré que ce gène était rarement impliqué. Notre projet vise à étudier les mécanismes génétiques et moléculaires, responsables de la survenue de mélanomes pédiatriques. Notre hypothèse de travail est que des « accidents » génétiques *de novo* se produisent soit dans un gamète parental, soit de manière post-zygotique pendant le développement de la crête neurale. L'analyse de ces événements génétiques chez le patient jeune, ayant accumulé peu de mutations dues à l'environnement (principalement l'exposition aux UVs), permet une identification rapide d'évènements oncogéniques pouvant être également impliqués dans le mélanome de l'adulte. Nous avons obtenu des données de séquençage d'exomes (WES) constitutionnels de 55 trios, et tumorales de 6 cas. Les analyses bioinformatiques ont montré l'existence de mutations *de novo* de 14 gènes impliqués dans le développement

Afin de mieux comprendre les « accidents génétiques » qui contribuent au mélanome infantile, nous avons identifié 14 gènes porteurs de mutations *de novo*, soit germinales, soit post-zygotiques, potentiellement impliquées dans le mélanome infantile. L'objectif de ma Thèse était donc d'explorer le lien entre les mutations identifiées *de novo* et l'apparition de mélanome. Pour ce faire, mon projet de thèse a nécessité de mettre en œuvre des modèles et des stratégies expérimentales innovantes. En effet, le mélanome dépend d'une transformation cancéreuse de mélanocytes, les dérivés pigmentaires de la crête neurale. Or, la crête neurale est une structure transitoire et multipotente de l'embryon, méconnue du grand public, et qui est difficile à

manipuler génétiquement par les outils et lignées transgéniques conventionnels. Pour cela nous avons choisi de travailler avec l'embryon de poulet. Dans mon laboratoire d'accueil « Développement & Évolution de la Crête Neurale » à l'Institut de Neurosciences de Paris-Saclay, cet organisme-modèle est utilisé comme alternative à l'utilisation de souris transgéniques. Du fait de son accessibilité à tous les stades du développement embryonnaire, permet de combiner avec une grande fiabilité spatio-temporelle, tout un ensemble de techniques et notamment, des manipulations d'expression de gènes, grâce auxquelles les cribles fonctionnels sont menés par des stratégies de gain- et de perte-de-fonction contrôlées. En outre, le pourcentage d'homologie en acide aminé entre les séquences du poulet et de l'homme varie de 95 à 99%.

Sur la base des cartographies des lignages cellulaires, les analyses fonctionnelles sont réalisées dans ce système en utilisant la technique d'électroporation *in vivo*, qui consiste à effectuer un transfert de séquences nucléiques exogènes dans le tissu ciblé. Dans notre système, la mise en silence du gène cible est obtenue par interférence ARN (ARNi), à partir d'une molécule d'ARN double brin (ARNdb) synthétisé sur une séquence spécifique de l'ADN complémentaire. Cela permet d'inactiver le gène endogène et de comprendre son implication physiologique dans la biologie des mélanocytes. Mon projet de doctorat se concentre sur deux compartiments différents de la crête neurale, afin de reproduire les sites principaux d'émergence de ces mélanomes pédiatriques : le tronc et crête neurale céphalique, pour étudier le rôle biologique inconnu des gènes candidats *de novo* pendant le développement. Nous nous sommes concentrés sur le gène *FBXO32* dans lequel une mutation germinale *de novo*, p.G139S, a été identifiée chez un enfant de sept ans présentant un mélanome de niveau III dans le genou. L'Analyse fonctionnelle de la diminution d'expression du gène a démontré le gène *FBXO32* entrave la prolifération, la différenciation des mélanocytes et la vascularisation au niveau dermique dans la crête neurale du tronc. Pour étudier l'expression de la spécificité endogène de *FBXO32*, nous avons réalisé des expériences de sauvetage par coélectroporation de *dsFBXO32* en combinaison avec des ADNc humaines de type sauvage pour lequel nous avons restauré une différenciation normale des mélanocytes. En parallèle, pour démasquer le phénotype spécifique résultant de l'expression de la forme mutée, nous avons réalisé des expériences de sauvetage par coélectroporation de *dsFBXO32* en combinaison avec la séquence ADNc muté du gène : *hFBXO32*^{G139S} montrant un effet néfaste dans la lignée mélanocytaire.

Pour analyser les cellules précurseurs des mélanocytes, les mélanoblastes, j'ai également mis au point en place une technique d'explants de peau embryonnaire de poulet, *ex vivo*. Le peau embryonnaire, explantée avant la différenciation de téguments, et avant la différenciation des mélanocytes, est placée sur une boîte de culture non - embryotoxique. Placée en incubateur, la

peau se différencie *in vitro* et on voit se différencier les bourgeons plumaires et l'apparition du pigment, et récapitule le programme spatio-temporel similaire aux mécanismes *in vivo*. Avec cette expérience, j'ai observé que les mélanocytes différenciés sont capables de migrer à nouveau vers le derme. Par la suite, je me suis interrogée sur la capacité des cellules à migrer vers le derme, comment y parviennent-elles ? Pour répondre à cette question, j'ai isolé des cellules de l'épiderme et les ai récoltées par culture *in vitro* et j'ai analysé la morphologie de ces cellules. Les résultats ont été surprenants : les cellules témoins présentaient une morphologie bipolaire et de longs filopodes, en revanche les cellules transformées changent leur morphologie en multipolaire, elles ont des filopodes plus courts, elles forment des lamellipodes courts et des agrégats entre eux. Les cellules transfectées sont difficiles à maintenir *in vitro* car elles se détachent des plaques de fibronectine (un ligand de la membrane cellulaire). Ainsi, la capacité des cellules à former des agrégats pourrait leur permettre de migrer en groupe et la perte de la capacité d'adhésion à la fibronectine pourrait leur permettre de migrer vers d'autres tissus. Pour entrer dans les détails, j'ai analysé un composant de la structure cellulaire, la paxilline, une protéine intracellulaire qui est impliquée dans la migration cellulaire (Dubois et al., 2017). De manière surprenante, dans les cellules témoins, la paxilline est localisée dans les structures des cellules appelées adhésions focales, qui sont des sites de contact cellulaire étroit dans la matrice cellulaire sous-jacente (Dubois et al., 2017; Turner, 2000; Webb et al., 2002). En revanche, dans les cellules transfectées, la paxilline est fortement localisée dans les filopodes et les lamellipodes qui permettent l'attachement cellule-cellule. L'analyse de la mutation de gène *hFBXO32^{G139S}*, pourrait donc intervenir dans la transformation des mélanocytes et le développement du mélanome infantile. L'application de la connaissance de ce gène au cours des mécanismes de développement peut améliorer la compréhension du possible rôle de l'initiation du mélanome et du traitement des cancers dérivés de la crête neurale.

Acknowledgements

First of all, I would like express my sincere gratitude to my supervisors Dr. Sophie Creuzet and Dr. Brigitte Bressac-de Paillerets for their invaluable continuous support advice during my PhD. I am deeply grateful for all your guidance and all the time of research discussions that helped me to develop and writing this thesis. Your insightful feedback pushed me to sharpen my thinking and brought my work to a higher level.

I would also like to thank the members of my jury thesis including: Dr. Julie Caramel, Dr. Berta López Sanchez, Pr. Anne-Hélène Monsoro-Burq and Dr. Jean-Loup Duband. My sincere thanks to Dr. Julie Caramel, Dr. Berta López Sanchez for dedicating some of your time to review my project and for your valuable feedback. Thanks to Dr. Jean-Loup Duband who is the president of the jury and was part of my thesis committee. Thank for your enlightening recommendations to extend my work in the trunk neural crest.

I wish to extend my special thanks to the donors form La Ligue Contre le Cancer, whose contributions made possible the development of this thesis.

I would like to thank all the members in the Development and the Evolution of the Neural Crest Team: Emmanuel, Diego, Tatiana, and all the past members. I am grateful to have the pleasure of working with them and to have a such incredible laboratory team. I want to thank Diego for being there these four years with your technical advice and the cheerful moments that we shared. I would like to thank Tatiana for conduct the experiments on Western Blots. Special thanks to Emmanuel for the unconditional support in each step during my PhD journey. Thanks for making the past four years much more enjoyable and all the discussions that we have along the road. This PhD would never have been the same without you.

I want to thank the NeuroPsi PhD's students and Post Docs who has made me fell welcoming even if my research work is far away from their field. Specially to my Italian colleagues Mariagiovanna and Giovanny, with whom I share such a great moment.

Prior to start my PhD, I had the opportunity to learn from different scientist to which I owe inspiration in science. I have the pleasure of working with one of the most influential women scientists in Ecuador and South America, Dr. Eugenia del Pino. She was a motivation for me to continue my graduate studies in Developmental Biology. I also would like to like to Dr. Anne

Poliard from the bottom of my heart for their constant support, guidance, and encouragement during my Master internship.

I am deeply grateful with my Parisian friends: Natalia, Leonor, Hudson, Maria Alejandra, Mathilde, Guillermo. Coming to France alone was not easy but I found in you a family far for home. These words be short to express all my love for you. Nati y Leonor, sin ustedes estos años no hubieran sido lo mismo. Estaré profundamente agradecida por nuestra comprensión y nuestro apoyo mutuo. Las quiero.

I wish to thank my loving and supportive boyfriend and parents. Merci Chéri, tu es arrivé dans ma vie et tu l'as rendu plus heureuse, merci pour ton soutien et ta compréhension tout au long de ces années de ma thèse. Merci également à ta famille qui m'a accueillie comme un membre de leur famille. Finalmente, un fuerte agradecimiento a mis padres, sin su incondicional apoyo esto no hubiera sido posible. Gracias mil gracias por su amor, su guía, su comprensión. Gracias por apoyarme a seguir mis sueños. A ti mami gracias por nuestras interminables conversaciones en donde tus palabras me tranquilizaban y me alentaban a continuar con más fuerza. A los dos por su ejemplo de perseverancia y de resiliencia. Y a ti Daniel por tu presencia ausencia a lo largo de estos años, que significa el renacer en cada día.

Contents

RÉSUMÉ	III
ABSTRACT	IV
SYNTHÈSE EN FRANÇAIS	VII
ACKNOWLEDGEMENTS.....	X
CONTENTS.....	XIII
FIGURES	XVI
TABLES	XVII
MOVIES.....	XVIII
ABBREVIATIONS.....	XIX
1 GENERAL INTRODUCTION	1
1.1 SKIN ANATOMY OVERVIEW	1
1.1.1 Epidermis	1
1.1.2 Dermis	1
1.1.3 Hypodermis	2
1.2 THE MELANOCYTE LINEAGE	2
1.2.1 The NC embryonic origin	2
1.3 NCCS MIGRATION PATHWAYS.....	9
1.3.1 Cephalic NCCs migration	9
1.3.2 Trunk NCCs migration.....	9
1.4 MELANOBLAST SPECIFICATION FROM NCCS PRECURSORS	10
1.5 MELANOGENESIS PATHWAY	14
1.6 MELANOCYTES TRANSFORMATION TOWARDS MELANOMA	16
1.6.1 Melanocytic naevus	16
1.6.2 Dysplastic nevus (Intermediated neoplasm)	16
1.6.3 Melanoma <i>in situ</i>	17
1.6.4 Invasive melanoma	17
1.6.5 Metastatic melanoma.....	18
1.7 MELANOCYTIC TUMOR CLASSIFICATION	20
1.8 GERMLINE AND SOMATIC VARIANTS IN ADULT CUTANEOUS MELANOMA	24
1.8.1 Germline events in adult melanoma	24
1.8.2 Somatic events in adult melanoma	25
2 CHILDHOOD MELANOMA	30
2.1 THE INCIDENCE OF CHILDHOOD MELANOMA	30
2.2 CHILDHOOD MELANOMA RISK FACTORS	31
2.2.1 Xeroderma pigmentosum.....	31
2.2.2 Immunosuppression	31
2.3 ABDC CRITERIA IN CHILDHOOD MELANOMA DIFFER FROM ADULT MELANOMA	32
2.4 HISTOPATHOLOGY CRITERIA.....	32
2.4.1 Superficial spreading melanoma (SSM)	32
2.4.2 Melanoma arising from a congenital melanocytic naevus (CMN).....	33

2.4.3 Atypical Spitz tumor and Spitzoid melanoma.....	33
2.4.4 Conventional or adult-type melanoma.....	34
2.5 WHAT IS KNOWN ABOUT CHILDHOOD MELANOMA GENETICS?.....	34
2.5.1 Germline mutations (inherited) in childhood melanoma.....	35
2.5.2 Somatic mutations (tumoral) in childhood melanoma.....	38
3 DE NOVO MUTATION CONCEPT AND THE ROLE IN CHILDHOOD MELANOMA.....	42
3.1 NEXT-GENERATION SEQUENCING, A BIG STEP IN THE HUMAN GENETIC RESEARCH.....	42
3.1.1 NGS germline sequencing of parent-child trios.....	42
3.2 <i>DE NOVO</i> MUTATIONS.....	46
3.2.1 Mosaicism in <i>de novo</i> mutations.....	46
3.2.2 Timing of <i>de novo</i> mutations.....	46
3.3 PRELIMINARY DATA ON CHILDHOOD MELANOMA CASES.....	47
3.3.1 Previous work done by Fanélie Jouenne in 2017.....	47
4 <i>FBXO32</i> GENE IN CANCER RESEARCH.....	55
4.1 <i>FBXO32</i> GENE IN CANCER RESEARCH.....	55
5 OBJECTIVES.....	59
6 MATERIAL AND METHODS.....	61
6.1 EXPERIMENTAL MODEL.....	61
6.1.1 The chick embryo as an experimental model.....	61
6.2 GENE SILENCING IN THE CHICK EMBRYO.....	61
6.3 <i>IN OVO</i> ELECTROPORATION AT THE TNC AND CNC.....	62
6.4 <i>EX VIVO</i> SKIN EXPLANT ELECTROPORATION.....	63
6.5 MELANOCYTE CELL CULTURE.....	63
6.6 PLASMIDS AND CONSTRUCTS.....	67
6.6.1 Construct to visualize CNC and TNC cell migration.....	67
6.6.2 Chicken gene cloning and construct preparation.....	67
6.7 BACTERIA TRANSFORMATION FOR PLASMID REPLICATION.....	68
6.8 NUCLEIC ACID PREPARATION.....	68
6.9 <i>IN SITU</i> HYBRIDIZATION.....	76
6.9.1 <i>in situ</i> DIG-labelled riboprobe synthesis.....	76
6.9.2 <i>in situ</i> hybridizations on whole-mount embryos.....	76
6.9.3 <i>in situ</i> hybridization on paraffin sections.....	79
6.10 PARAFFIN EMBEDDING FOR IMMUNOCYTOCHEMISTRY.....	79
6.11 IMMUNOCHEMISTRY.....	79
6.11.1 Whole embryos.....	79
6.11.2 Truncal paraffin section.....	80
6.11.3 Culture cells.....	80
6.12 FLUORESCENCE IMAGES AND DATA ANALYSIS.....	81
6.12.1 Statistical analysis.....	81
6.13 BULK RNA SEQUENCING.....	81
6.13.1 Computational analysis.....	82
6.14 FLUORESCENCE IMAGES AND DATA ANALYSIS.....	85
7 FUNCTIONAL ANALYSIS OF <i>FBXO32</i>, <i>SOX10</i>, <i>DSCAM</i>, AND <i>ALDH1L1</i> CANDIDATE GENES.....	86
7.1 CHILDHOOD MELANOMA CANDIDATE GENES <i>FBXO32</i> , <i>SOX10</i> , <i>DSCAM</i> , AND <i>ALDH1L1</i> ARE EXPRESSED AT THE NC.....	86
7.2 <i>FBXO32</i> , <i>SOX10</i> , <i>DSCAM</i> , <i>ALDH1L1</i> LOSS OF FUNCTION YIELDS ABNORMAL MELANOCYTE DIFFERENTIATION AT THE CNC.....	90

7.3	SETTING AN <i>IN VITRO</i> 3D SKIN EXPLANT TO UNRAVEL <i>FBXO32</i> , <i>SOX10</i> , <i>DSCAM</i> , <i>ALDH1L1</i> CONSEQUENCE AT THE MELANOBLAST/MELANOCYTE LINEAGE	93
8	RESULTS (MANUSCRIPT IN PREPARATION).....	96
9	DISCUSSION.....	146
9.1	MAIN FINDINGS AND SIGNIFICANCE	146
9.2	SILENCING OF <i>FBXO32</i> , <i>SOX10</i> , <i>DSCAM</i> , AND <i>ALDH1L1</i> IMPAIRS MELANOCYTE DIFFERENTIATION AT THE CNC	148
9.3	<i>FBXO32</i> INDUCES MELANOCYTE TRANSFORMATION	148
9.4	<i>FBXO32</i> TRIGGERS EUMELANIN SYNTHESIS	149
9.5	<i>FBXO32</i> 'S EFFECT ON MELANOCYTE CELL EXTENSION FORMATION	150
9.6	<i>FBXO32</i> INDUCES CYTOSKELETON REMODELING	153
9.7	<i>FBXO32</i> ^{G139S} UNFOLDS NOVEL TARGETS IN MELANOCYTE TRANSFORMATION	153
9.8	IS <i>FBXO32</i> A TSG IN CHILDHOOD MELANOMA?	156
10	CONCLUSION	158
11	SUPPLEMENTARY INFORMATION	159
12	BIBLIOGRAPHY	171

Figures

FIGURE 1.1 SKIN ANATOMY	4
FIGURE 1.2 THE NC FATE MAP	8
FIGURE 1.3 NC MIGRATION AND FATE.....	12
FIGURE 1.4 MELANOCYTE DEVELOPMENT.....	13
FIGURE 1.5 BIOSYNTHESIS PATHWAYS INVOLVED IN PHEOMELANIN AND EUMELANIN.....	15
FIGURE 1.6 THE MORPHOLOGY PROGRESSION OF MELANOCYTES TO MELANOMA	19
FIGURE 1.7 THE MITF RHEOSTAT MODEL.....	28
FIGURE 2.1 PREVALENCE IN COPY NUMBER VARIATIONS BETWEEN ADULT AND PEDIATRIC CONVENTIONAL MELANOMA...	36
FIGURE 3.1 MECHANISM OF <i>DE NOVO</i> MUTATIONS.....	45
FIGURE 3.2 INHERITED MUTATIONS AND <i>DE NOVO</i> MUTATIONS.....	49
FIGURE 3.3 WORKFLOW FOR THE DETECTION OF DE NOVO MUTATIONS IN CHILDHOOD MELANOMA.	52
FIGURE 4.1 THE SCF COMPLEX.....	57
FIGURE 6.1 3D <i>IN VITRO</i> SKIN EXPLANT SYSTEM.....	65
FIGURE 6.2 MELANOCYTE CHARACTERIZATION BY <i>IN VITRO</i> CELL CULTURE, CREATED WITH BIORENDER.COM	66
FIGURE 6.3 pCAGGS- MCHERRY PLASMID TO VISUALIZED NCC MIGRATION	71
FIGURE 6.4 PLASMIDS USED FOR GENE SILENCING	72
FIGURE 6.5 PCR™ II TOPO® TA_ SOX10, FBX032, ALDH1L2 SEQUENCING RESULTS	74
FIGURE 6.6 PLASMID USED FOR RESCUE EXPERIMENTS	75
FIGURE 7.1 FBX032, SOX10, DSCAM AND ALDH1L1 TRANSCRIPTS ARE EXPRESSED IN THE CNC AND TNC AT DIFFERENT DEVELOPMENTAL STAGES	89
FIGURE 7.2 SILENCING OF dsFBX032, dsSOX10, dsDSCAM, dsALDH1L1 YIELDS ABNORMAL MELANOCYTE DIFFERENTIATION AT THE CNC.....	92
FIGURE 7.3 SILENCING <i>dsSOX10</i> , <i>dsDSCAM</i> AND <i>dsALDH1L1</i> AT THE MELANOBLAST LINEAGE YIELDS ABNORMAL MELANOCYTE DIFFERENTIATION AND FEATHER BUD MORPHOGENESIS.....	95
FIGURE 9.1 SCHEMATIC VIEW OF <i>FBX032</i> NETWORK PROPOSAL IN MELANOCYTE TRANSFORMATION	155

Tables

TABLE 1. THE WHO 2018 CLASSIFICATION OF MELANOMA ACCORDING TO ETIOLOGY ASSOCIATION WITH UV RADIATION EXPOSURE AND PATHWAYS.	23
TABLE 2 4 OUT OF 14 CHILDHOOD MELANOMA CANDIDATE GENES CARRYING A <i>DE NOVO</i> MUTATIONS IDENTIFIED BY WES.	53
TABLE 3. VECTORS USED IN THIS STUDY.....	70
TABLE 4. HYBRIDIZATION BUFFER SOLUTION COCKTAIL.....	78
TABLE 5. TOTAL NUMBER OF SKIN EXPLANT ANALYSIS.....	83
TABLE 6. SAMPLES COMPARISONS FOR DIFFERENTIAL EXPRESSION ANALYSIS.....	84
TABLE 7 <i>FBXO32</i> INDUCES MORPHOGENESIS DISRUPTION IN MELANOCYTE DIFFERENTIATION	147

Movies

MOVIE 1. CELL DYNAMICS FROM DURING 24H ISOLATED FROM CONTROL SKIN EXPLANT 152

Abbreviations

AF:	Allelic frequency
ALDH1L1:	Aldehyde Dehydrogenase 1 Family Member L1
ALL:	Acute lymphoblastic leukemia
ALM:	Acral lentiginous melanoma
ASIP:	Agouti signaling protein
AST:	Atypical Spitz
SM:	Spitzoid melanoma
α-MSH:	alpha melanocyte stimulating hormone
BAP1:	Breast cancer 1 (BRCA1) associated protein 1
CADD:	Combined annotation dependent depletion
CAMs:	Cell adhesion molecules
CDK6:	Cell division protein kinase 6
CDK4:	Cyclin dependent kinase 4
CDKN2A:	Cyclin dependent kinase inhibitor 2A
cDNA:	Complementary DNA
CM:	Conventional melanoma
CMN:	Congenital melanocytic naevi
CMV:	Cytomegalovirus
CNC:	Cephalic neural crest
CNRGH:	Centre National de Recherche en Génomique Human
CNS:	Central nervous system
CSD:	Cumulative solar damage
CTC:	Circulating tumor cells
ctDNA:	Circulating cell-free tumor DNA
DEPC:	Diethyl pyrocarbonate
Dfb:	Distal feather buds
DMEM-F12:	Dulbecco's Modified Eagle Medium: Nutrient mixture F12
DOPA:	Dihydroxyphenylalanine
DSCAM:	DS cell adhesion molecule
DZNep:	3-Deazaneplanocin A
E:	Embryonic day
ECM:	Extra cellular matrix
EMT:	Epithelial mesenchymal transition
ENS:	Enteric nervous system
FBS:	Fetal bovine serum
FBXO32:	F-box protein 32
FNC:	Facial neural crest

FPKM:	Reads per kilobase of exon per million reads mapped
GNAQ:	Guanine nucleotide binding protein α q polypeptide
GO:	Gene Ontology
HH:	Hamburger-Hamilton
Ifb:	Intermediate feather buds
IPA:	Ingenuity Pathway Analysis
ISH:	<i>in situ</i> hybridization
KEEG:	Kyoto Encyclopedia of Genes and Genomes
KLF4:	Krüppel-like factor 4
LB:	Luria-Bertani medium
LFS:	Li-Fraumeni syndrome
LMM:	Lentiginous melanoma
MC1R:	Melanocortin 1 receptor
MITF:	Microphthalmia associated transcription factor
NC:	Neural crest
NCCs:	Neural crest cells
NER:	Nucleotide excision repair
NF:	Next-generation sequencing
NM:	Nodular melanoma
NT:	Neural tube
PCA:	Principal component analysis
PBS:	Phosphate Buffer Saline
PBST:	PBS Tween-20
PFA:	4% formaldehyde
Pfb:	Proximal feather buds
PNS:	Peripheral nervous system
PTEN:	Phosphatase and Tensin homolog gene
RGP:	Radial growth phase
RNAi:	RNA of interference
RT:	Room temperature
SEER:	Surveillance, Epidemiology, and End result program
SF3B1:	Splicing factor 3b subunit 1
SKP1:	S-phase kinase associated protein 1
SN:	Spitzoid naevus
SNV:	Single nucleotide variant
SOX10:	SRY-box transcription factor 10
SS:	Somite stage
SSM:	Superficial spreading melanoma
TERT:	Telomerase reverse transcriptase
TNC:	Trunk neural crest
TP53:	Tumour protein 53

TSG:	Tumor suppressor gene
TYR:	Tyrosine
TYRP1:	Tyrosinase related protein 1
Ub:	Ubiquitin
UV:	Ultraviolet
VGP:	Vertical growth phase
WES:	Whole exome sequencing
WGS:	Whole genome sequencing
WHO:	World Health Organization
XP:	<i>Xeroderma pigmentosum</i>

1 General Introduction

1.1 Skin anatomy overview

Skin is the largest organ in the human body. The central role of the skin is to form a physical barrier to the external environment by protecting internal tissues from ultraviolet (UV) radiation, pathogens, and chemicals. Additional functions include sensory perception, immunologic surveillance, thermoregulation, and synthesis of vitamin D. The skin is composed of three layers: the epidermis (the outer layer), the dermis (the inner layer), and the hypodermis (the deeper subcutaneous tissue) (**Figure 1.1**). The hypodermis consists of fatty tissue connecting the dermis to the underlying skeletal component.

1.1.1 Epidermis

The epidermis is the outermost layer of the skin composed of keratinized squamous epithelium. Most cells in this layer are keratinocytes, 95% of all skin cells. The primary function of keratin is to protect the skin and underlying tissue from ultraviolet radiation. The remaining cells include melanocytes, Langerhans cells, and Merkel cells. Melanocytes correspond to 2 to 4% of cells in the epidermis and are responsible for melanin production. Langerhans cells correspond to 3 to 5% of cells in the epidermis and are antigen-presenting immune cells involved in T-cell responses to pathogens. Langerhans cells are mobile, dendritic, and antigen-presenting cells in stratified epithelia (Kanitakis, 2002). Meckel's cells, 2 to 5% of the epidermis cells, play a role in the skin's sensitivity. They are in contact with the nerve endings and play the role of mechanoreceptors.

1.1.2 Dermis

The dermis is the second layer underneath the epidermis. It consists of different cell types that build sweat glands and blood vessels. It is divided into two layers: the superficial, the papillary region, and the deeper and thicker, known as the reticular region. Through these vessels, melanoma can spread during the vertical growth phase. The dermis harbors many mechanoreceptors that provide the sense of touch. A basement membrane layer separates the epidermis and dermis. The central role of the basal membrane consists in controlling the traffic of molecules between the dermis and epidermis and reservoir for inflammatory and growth factors during physiological

repair processes. In a pathological context, the basement membrane forms the limit between *in situ* versus invasive melanoma.

1.1.3 Hypodermis

The hypodermis is a connective tissue composed of fat cells and adipocytes. This layer plays the role of energy reserve, thermal insulator, and protector of the deep organs against shocks and injuries.

1.2 The melanocyte lineage

Melanocytes are derived from the neural crest (NC) lineage in higher vertebrates (Dupin & Le Douarin, 2003a). Their primary function is to transfer melanin pigment to the adjacent keratinocytes to prevent UV-induced DNA damage (Slominski et al., 2015). The anatomical relationship between keratinocytes and melanocytes is known as the "Epidermal melanin unit". It has been estimated that each melanocyte is connected with around 30-40 keratinocytes in the basal or suprabasal layer (Costin & Hearing, 2007).

1.2.1 The NC embryonic origin

The NC is a migratory embryonic cell population unique to the vertebrate embryo. In 1868, the Swiss embryologist Wilhelm His described a band of cells lying between the dorsal ectoderm and the underlying neural tube (NT), which he called a "Zwischenstrang" = "intermediate cord", in the chick embryo. Wilhelm His named the tissue "ganglionic crest" the cells away from their source and accumulated laterally to form the spinal ganglia (His & His, 1868). This tissue was later renamed NC by Arthur Milnes Marshall (1879) with a more precise description of its anatomical position. Since then, the NC has been broadly analyzed because of its stem cell properties, multipotency, and migratory abilities.

The formation of the NC starts during neurulation at the borders of the neural plate where neural crest cells (NCCs) become specified, hence being interposed between the future central nervous system (CNS), and the non-neural ectoderm fated to form the epidermis. While the neural plate invaginates to the neural folds and fused to form the NT, NCCs engage their emigration from the neural primordium. During this transient phase, NCCs exhibit profound changes which convert their original neuroepithelial traits into a mesenchymal morphology. The NCCs undergo delamination and they acquire migratory properties and detach from the basal lamina to spread

as mesenchymal cells and colonize varied sites where they differentiate into a broad range of derivatives and lineages. Conceptually speaking, the formation of NC and emigration represents a developmental model of Epithelium to Mesenchyme Transition (EMT). NCCs are multipotent *in vivo* in pre-migratory and migratory cells in the mouse embryo (Baggiolini et al., 2015). The NCCs have the capacity to migrate throughout the embryo and colonized different organs and tissues where they settle and differentiated: their contribution is notable and essential to the morphogenesis and the development of the peripheral nervous system (PNS), the craniofacial structures, and the brain (Creuzet et al., 2004, 2005; Creuzet, 2009; Creuzet et al., 2006; Creuzet, 2009; Dupin et al., 2006; Le Douarin et al., 2004; Le Douarin et al., 2007, 2012) through an epithelial-mesenchymal transition (EMT). Then, the NC cells (NCCs) acquire the capacity to migrate throughout the embryo and colonize different organs and tissues, where they settle and differentiate in tissues of the peripheral nervous system (PNS) to the craniofacial skeleton structures (Baggiolini et al., 2015).

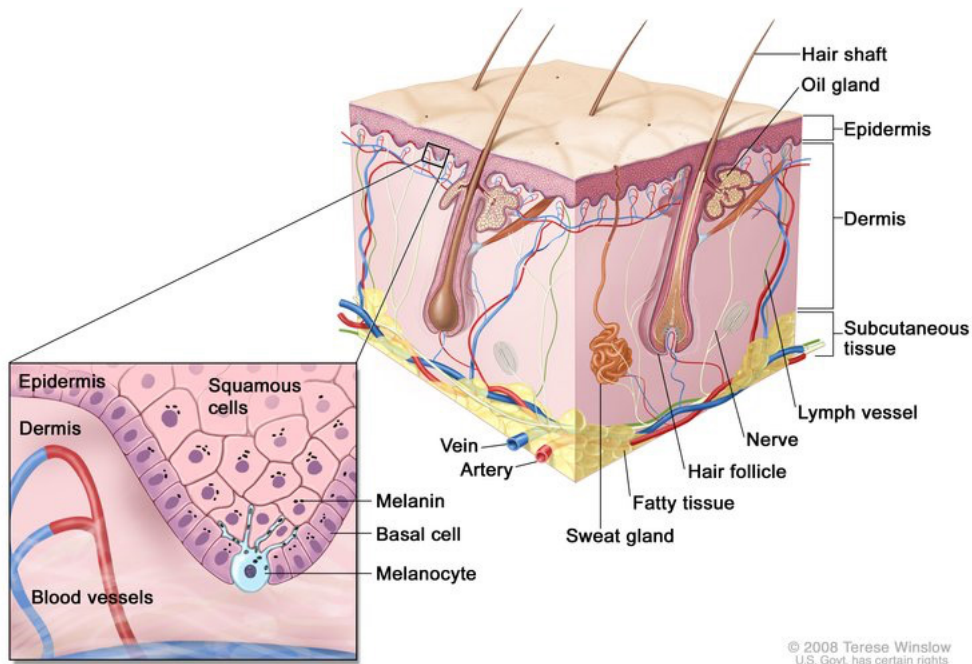


Figure 1.1 Skin anatomy

Schematic representation of normal skin anatomy, including the epidermis, dermis, hair follicles, sweat glands, hair shaft, veins, arteries, fatty tissue, nerves, lymph vessels, oils glands, and subcutaneous tissue. Magnification shows the epidermis's squamous cell and basal layer above the dermis with blood vessels. Melanin is shown in the cells. A melanocyte is shown in the basal layer at the deepest part of the epidermis. From National Cancer Institute. Teresa Winslow 2008.

A broad set of techniques has been developed to map the fate of NCCs migration and differentiation through cell transplantation by embryonic chimeras, tissue ablation, and cell labeling with vital dyes between others.

However, each strategy of exogenous labeling suffered from a lack of precision and a short coverage. In 1969, Nicole Le Douarin developed an inspirational technique of quail-chick chimeras ("chimeras" from Greek: meaning fabulous monster) which allowed to follow the NCCs' fate and migration along the anterior-posterior axis, whatever the state of cell differentiation (Le Douarin et al., 2004). This technique consisted of the replacement of the neural tube bearing NCCs, before the onset of their migration, in the chicken embryo by its stage-matched counterpart taken from a quail embryo. Quail and chicken share similar developmental morphological traits during the first half of ontogenesis. However, the quail cells harbor a specific pattern of heterochromatin accumulation at the nucleolus, making a unique and dense spot of nucleolar chromatin, while chick cells are euchromatic evenly distributed throughout the nucleus. The singularity of the quail nucleus was exploited as a decisive advantage to trace the fate of transplanted cells into an heterospecific environment (Le Lievre & Le Douarin, 1975). Later on, this technique was enriched with and a monoclonal antibody, QCPN (for *Quail non-Chick Peri-Nucleolar antigen*) which eased the migration and fate of the NCCs to be followed during the development of embryos and post-hatching chimeric animals. These studies revealed the contribution of the NC to the cranial, sacral, trunk, and vagal NC (**Figure 1.2**). The NCCs that contribute to the peripheral nervous system (PNS) and enteric nervous system (ENS) derivate from restrictive areas along the neural axis. To further characterized the differentiation potential of NCCs, researchers have done heterotopic transplantations from cranial NCCs to the trunk level or trunk NCCs to the vagal compartment. These experiments demonstrate that the fate NCCs, that form PNS and ENS, is not entirely determined before these cells migrate. Still, instead, NCCs have the plasticity to develop in the predeterminate cell type and the environmental signaling controls their fate choice during migration (Le Douarin & Teillet, 1974; Le Lièvre & Le Douarin, 1975).

Quail-chick chimeric demonstrates that NC compromises cell populations that differ in fate, migration pathways, and derivatives. The anterior-posterior position in which NC delaminates defines their future and, based on the localization, can be sub-divided into cranial, vagal, trunk, and sacral NC. The cephalic NC (CNC) compromises NCCs formed between the forebrain and the 6th rhombomere of the hindbrain and gives rise to bone and cartilage structures of the head, face, and nerve ganglia, smooth muscle, connective tissue, and pigment cells (melanocytes). The NC forms the forebrain's meninges at the cephalic level, while the other parts of the CNS are of mesodermal origin (Etchevers et al., 2001). At the trunk level, NC the NCCs from somite 8th to 27th and gives rise to neurons and glia, contributing to the PNS and pigmented cells of the skin.

Moreover, the NC is considered at the “four germ layer” due to their astonishing developmental plasticity and the ability of neural ectoderm-derived NCCs to differentiate into both neural and mesenchymal-like derivatives.

More recently, other methods for tracking NCCs migration were developed, including staining with different dyes, *in ovo* electroporation or viral-mediated introduction of GFP encoding constructs at the NT (Aguiar et al., 2014; Garcez et al., 2014). These studies involved the tracking of NCCs migration and gene regulation analysis. The development of *in ovo* electroporation in the chick embryo offers a straightforward methodology to transfect cells of interest spatially and temporally controlled (Wilson & Stoeckli, 2011) and conduct gain and loss-function experiments (Muramatsu et al., 1997; Pekarik et al., 2003). Katahira and Nakamura, 2003, introduced the double-stranded RNA, known as RNA interference (RNAi), in the chick embryo (Andermatt et al., 2014; Katahira & Nakamura, 2003). RNAi has been the technique used in the chick embryo for gene silencing since cytomegalovirus (CMV) enhancer is used in a vector and gives a transient expression for at least 72h and can be maintained long-term misexpression. Misexpression is restricted to descendants of the transfected cells, allowing for tracing the lineage during development (Nakamura et al., 2004). Moreover, our laboratory has further refined the electroporation system involving the designing an own set of electrodes (Creuzet et al., 2002; Garcez et al., 2014), a triple electrode has the advantage of conducting selective and bilateral transfection in the CN population (Aguiar et al., 2014). Nonetheless, other techniques have been used for functional analysis as (1) morpholinos antisense oligonucleotides, but they can interfere with translation, so it is necessary the use an antibody against the molecule to have a relevant result (Kos et al., 2003), (2) Knockdown experiment by gene targeting to make mutants in the chick embryo, but it provokes early embryonic lethality that prevents their analysis in later developmental stages.

The NC migratory and plasticity capacities studies enrich understanding of congenital malformations, pediatric cancers, and evolutionary biology. Valérie Castellani and her team developed a neuroblastoma avian model study to understand the *in vivo* formation of neuroblastoma (Delloye-Bourgeois & Castellani, 2019). Neuroblastoma is a highly heterogeneous pediatric cancer that develops from immature nerve cells. By performing micro-grafts of patient samples in the avian host organism, it is possible to replicate scale-down samples from these patients within days. They demonstrated that these cells retained the memory of their original cells' NC properties. Another example is the chick chorioallantois membrane used *in vivo* assays to study both angiogenesis in response to tissues, cells, or soluble factors (Kalirai et al., 2015; Pawlikowska et al., 2020; Ribatti & Tamma, 2019). Furthermore, Busch and colleagues used the

chick embryo as a biological model for melanoma cell invasion. They demonstrated the invasive behavior induced by embryonic oncogenes and target manipulation of melanoma cells (Busch et al., 2013). These experimental examples show the powerful chick model as an excellent tool in research cancer studies.

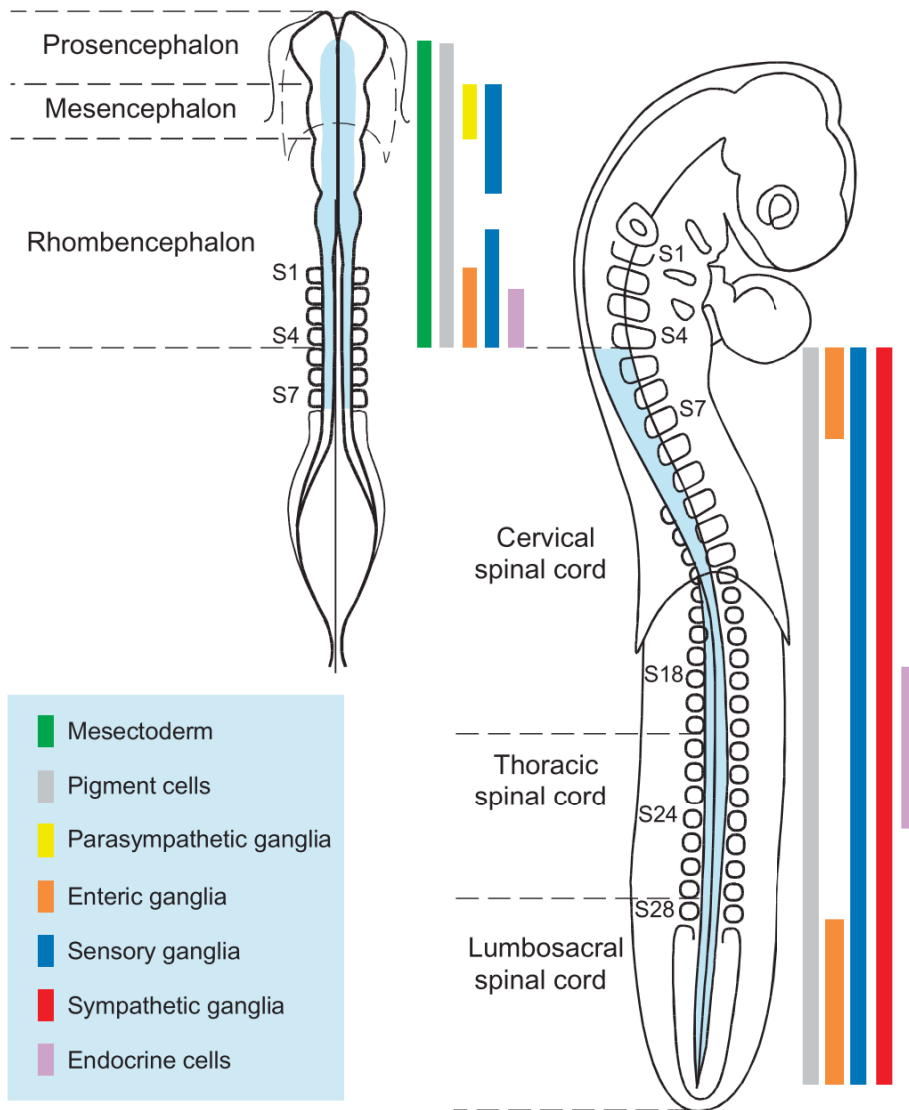


Figure 1.2 The NC fate map

Left up, tissue that arise from the cranial NC. Right, tissue that arise from the trunk NC in cervical thoracic and lumbosacral regions of the spinal cord. The Mesectoderm (green line) extends from the level of mid-diencephalon down to somite 4. The melanocytes (grey line) are produced along the entire length of the neural axis. The parasympathetic ganglia (yellow line) originate from the mesencephalon area. The enteric ganglia (orange line) arise from both vagal and lumbosacral. The trunk NC yields PNS sympathetic ganglia (red line). Sensory ganglia originate from both CNC and trunk NC from posterior rhombencephalon to lumbosacral levels. Endocrine cells (purple

1.3 NCCs migration pathways

After NC induction, NCCs delaminated by the EMT program and migrated extensively throughout the developing embryo (Bronner, 2012). NCCs migration follows two different pathways, a ventral pathway, and a dorsal pathway. Melanocytes residing in the skin of the head originate from the CNC, while the remaining parts of the body are mainly from the trunk NC (TNC).

1.3.1 Cephalic NCCs migration

At the cephalic level, NCCs migrate predominantly in the dorsolateral pathway (i.e., between the ectoderm and the underlying mesoderm). They differentiate into the various components of the head and neck (Kuo & Erickson, 2010). Cephalic NCCs migration occurs in three phases, (1) dorsolateral migration of NCCs, cephalic NCCs from the hindbrain rich contact with the surface ectoderm and cephalic mesenchyme adjacent to the hindbrain, (2) NCCs homing the branchial arches, (3) NCCs entry into and invasion of the branchial arches (reviewed in (Kulesa et al., 2010). In mouse and *Xenopus* embryos, delamination occurs while the neural plate is still open, while in chick embryos occurs with the fusion of the neural folds (Le Douarin & Kalcheim, 1999). Neurons and glial cells developing from the cranial NC stop dorsally, whereas NCCs differentiated into bone and cartilage continue the migration toward the branchial arches.

1.3.2 Trunk NCCs migration

After delamination, the NCCs at the trunk level of the embryo start to migrate along two different routes. In the ventral pathway, NCCs migrate either along blood vessels in the intersomitic space, between the NT and the anterior half of developing somites, or through invasion of the anterior region of the sclerotome. According to the ventral to dorsal order of colonization, the cells migrating ventrally will form the sympathetic ganglia, Schwann cells along the nerve fibers, and the dorsal root ganglia, according to the ventral to dorsal order of colonization (Bronner-Fraser, 1986; Serbedzija et al., 1994). NCCs follow migration superficially between the ectoderm and the dermomyotome in the dorsal pathway. In chicken and mice, this route is used mainly by the NCC to enter the epidermis and later differentiate into melanocytes (Thomas & Erickson, 2008) (**Figure 1.3**). In mouse and chick embryos, the trunk NCCs migrate ventrally between the somites and NT. NCCs which follow the ventral path differentiated as neurons and glial cells of the PNS, while later emigrating NCCs that follow the dorsal path differentiate as melanocytes cells of the skin (Le Douarin & Kalcheim, 1999). Evidence suggests that NCCs are determinate before their migration

(Reedy et al., 1998). NCCs are specified as a previous melanoblast to the onset of dorsolateral migration, and only these cells will follow the dorsolateral pathway. Erickson and Goins (1995), in an elegant study using avian graft, demonstrated that the melanoblast cells could migrate immediately on the dorsal path (Erickson & Goins, 1995). On the contrary, early migrating NCCs grafted in older embryos follow the ventral pathway through the anterior sclerotome and become neurons and glia cells. In contrast, the oldest NCCs follow the dorsal path between the ectoderm and the somites through the developing dermis and become melanocytes (Erickson & Goins, 1995). This study demonstrates that the migratory pathway does not determine the fate of the cells; instead, the cells are specified before leaving the NC.

In the chick embryos, the late migration of NCCs at the trunk region is exclusively melanoblast progenitors. Only melanoblast localized in the epidermis germ layer differentiated (Le Douarin & Kalcheim, 1999). NCCs that have seeded at the epidermis germ layer in the feather bud or have remained in the dermis do not undergo melanogenesis. It is likely that they will function later as stem cells and contribute to feather pigmentation. In the dorsal region where feathers are developed, melanoblast starts to massively invade the epidermis from eleven days of development, embryonic day (E) 11, to differentiate towards melanocytes and undergoes melanogenesis processes toward the periphery of the feather filament.

1.4 Melanoblast specification from NCCs precursors

Melanocytes differentiate from NC progenitors, melanoblast, that have migrated towards the skin during embryonic life. Melanoblast are unpigmented cells that originate from embryonic NCCs. A dual NC origin of melanocytes has been proposed by a common bipotent NC progenitor and the other from a Schwann cell (Dupin & Le Douarin, 2003a). Studies in mice using lineage-tracing experiments suggest a significant contribution of melanocytes from Schwann cell progenitors in the postnatal skin. In this scenario, NCC, which fails to acquire neural fate, is associated with nerves and gains a Schwann cell precursor fate. The spinal nerve's dorsal and ventral arches guide these precursors to cutaneous locations. When reaching the end of the nerves, some Schwann precursors acquire a melanocyte fate and migrate to the skin, where they proliferate and populate the skin (reviewed in Ernfors, 2010).

After the closure of the NT, melanoblast migrates extensively by EMT to various regions of the embryo to develop into melanocytes. This process involves the transcription factors SRY-box transcription factor 10 (*SOX10*), microphthalmia-associated transcription factor (*MITF*), paired domain- and homeodomain- containing transcription factor (*PAX3*). *SOX10* and *MITF* are involved

in specifying NC stem cells into melanoblast via *SOX10*- positive bipotent melanoblast/glia progenitor and differentiation in melanocytes (**Figure 1.4**) (Mort et al., 2015).

The Microphthalmia associated transcription factor (MITF) is the earliest expressed marker of melanoblast and essential for melanogenesis. MITF is expressed shortly after melanoblast emigration from the neural tube. MITF is crucial for melanocyte specification; loss of MITF causes the cell to switch to the glia phenotype (Thomas & Erickson, 2009). In avian embryos, MITF expression is observed as early as stage 15 in the trunk. At the same time, the SRY-box transcription factor 10 (*SOX10*) is expressed explicitly in the migratory NCCS at the dorsolateral melanoblast migratory pathway (Southard-smith et al., 1998). Loss-of-function mutations in the *SOX10* locus cause dominant, cell-autonomous defects in Schwann cells and melanocyte differentiation, while homozygous mutants exhibit embryonic lethality with failure of migration and/or differentiation of glia and neurons. *SOX10* transiently regulated *Dct* expression during early melanogenesis development in a *MITF* independent regulation (Potterf et al., 2001). *MITF* also regulates the expression of tyrosinase, tyrosinase-related protein 1 (TYRP1), and dopachrome tautomerase (*Dct*) genes required for melanogenesis.

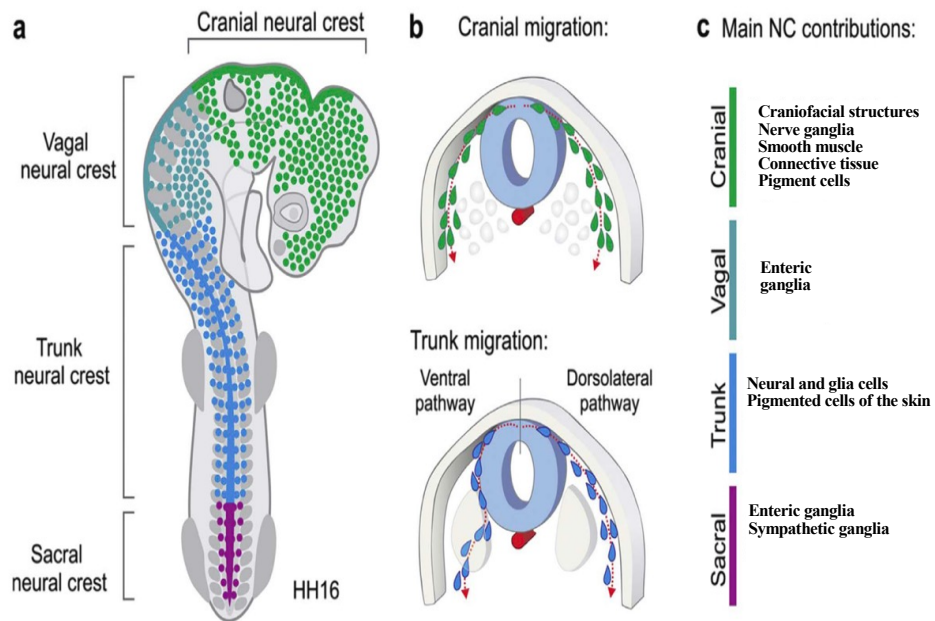


Figure 1.3 NC migration and fate

(A) NC sub-populations: CNC, vagal NC, TNC and sacral NC in a HH16 chick embryo. (B) Migratory pathways of NCCs at the cephalic and trunk level. Cephalic NCCs migrates dorsolateral, while trunk NCCs migrates either by the ventral pathway or the dorsolateral pathway. (C) Main NCCs derivatives. *Adapted from Rothstein et al., 2018*

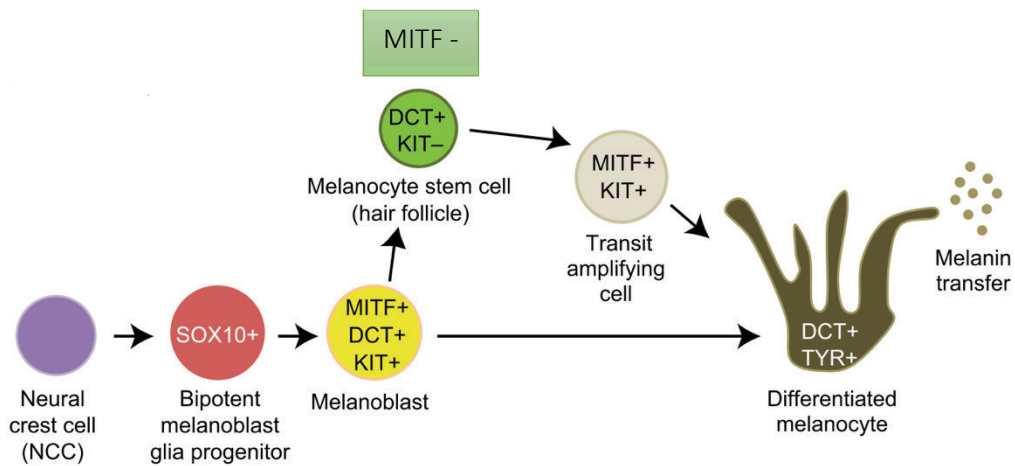


Figure 1.4 Melanocyte development

Melanocytes differentiated from stem cells of the NC. In mammals, melanoblast are specified for NCCs via SOX10 positive melanoblast/glia progenitor, and then acquired MITF, DCT, KIT expression. The melanoblast differentiated in melanocyte after reaching the embryonic hair follicle and produce melanin via DCT and TYR positive expression. A subset of melanocytes determined to form melanocyte stem cell in the hair follicle bulge by losing MITF expression. Adapted from Mort et al., 2005.

1.5 Melanogenesis pathway

The biosynthesis of melanin pigments occurs in differentiated melanocytes and the retinal pigmented epithelium derived from the optic cup of the brain. At the subcellular level, the production and store of melanin occur in the melanosomes, which are subcellular lysosome-like organelles (D'Mello et al., 2016). In humans, two types of melanin are found in human skin red/yellow pheomelanin and black/brown eumelanin.

In the melanogenesis pathway, tyrosinase (TYR) is a crucial enzyme for melanin biosynthesis, catalyzing the two initial steps. The first step is the oxidative hydroxylation of L-tyrosine to L-dihydroxyphenylalanine (DOPA), and the second step is the oxidation of L-DOPA to DOPA quinone (reviewed in (Lin & Fisher, 2007)). Two other enzymes, the tyrosinase-related protein 1 (TYRP1) and tyrosinase-related protein 2 (TYRP2), also called DOPA chrome tautomerase, are explicitly involved in eumelanin synthesis. In the presence of cysteine, DOPA quinone reacts with it, which is then oxidized and polymerized, giving rise to yellow-brown-red soluble melanin-pheomelanin. In the absence of cysteine, the two enzymes TYRP1 and TYRP2 react to the product black pigment melanin, eumelanin (**Figure 1.5**).

Eumelanin production is regulated primarily by the melanocortin one receptor (MC1R) signaling. Two different MC1R ligands have opposite activities: α -MSH (alpha-melanocyte-stimulating hormone) is an agonist, whereas agouti signaling protein (ASIP) is an antagonist (**Figure 1.5**). The binding of α -MSH to MC1R activates adenylate cyclase. It ultimately leads to the generation of secondary messenger cAMP, which triggers the signaling cascade for the transcription of enzymes required for eumelanin production. On the contrary, ASIP inhibits eumelanin synthesis by directing competing for receptor binding of MITF for promoter activation of all three enzymes TYR, TYRP1, and TYRP2, whose absence favors pheomelanin synthesis (Nasti & Timares, 2015). In addition, several studies have highlighted the association of MC1R variants with melanoma risk (Matichard et al., 2004; Valverde et al., 1996). Together with MCR1, the ASIP, tyrosinase the TYRP1 variants are considered a low risk for inherited melanomas (Ghanem & Fabrice, 2011), while in another study, authors have demonstrated that variants at *ASIP*, *TYR*, and *TYRP1* showed significant association with melanoma and multiple polymorphisms of pigmentation genes included *TYRP1* was found associated with risk for melanoma (Gudbjartsson et al., 2008).

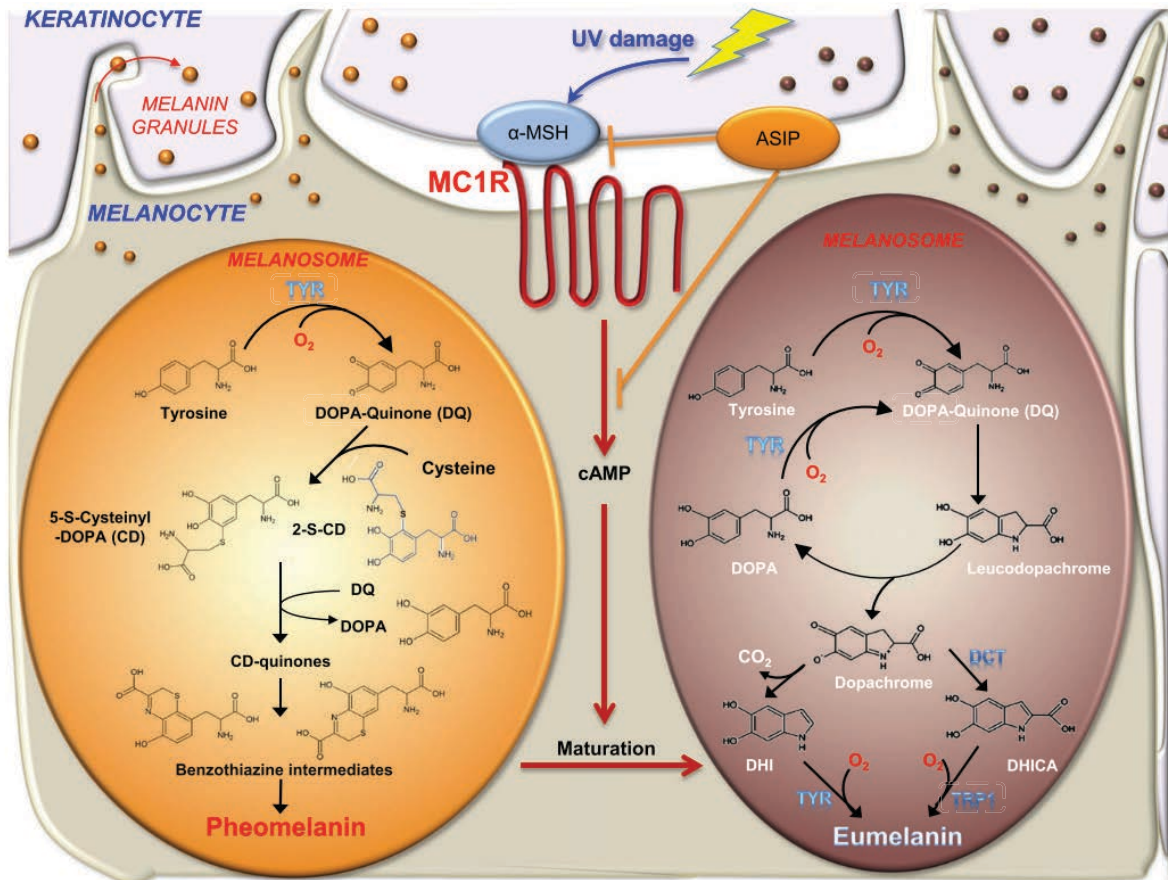


Figure 1.5 Biosynthesis pathways involved in pheomelanin and eumelanin

Tyr is engaged in both pheomelanin and eumelanin synthesis, whereas Tyrp1, TYRP2 (DCT) are only involved in eumelanin synthesis. Synthesis of eumelanin requires higher O₂ consumption than pheomelanin. MC1R, melanocortin 1 receptor, ASIP, agouti signaling protein, α-MSH, alpha melanocyte stimulating hormone. Adapted from Timares & Nasti, 2015

1.6 Melanocytes transformation towards melanoma

Melanoma results from the malignant transformation of melanocytes. Melanocytes can give rise to a diverse set of neoplasm from melanocytic naevi or benign lesions to malignant ones, termed melanoma. These lesions vary in anatomical distribution, clinical features, histopathological appearance, and biological behavior. Primary melanomas are often associated with different types of precursors lesions, ranging from benign naevi and dysplastic naevi to melanoma *in situ*.

1.6.1 Melanocytic naevus

Melanocytic naevus is a benign clonal lesion of melanocytes proliferation at the basal layer of the epidermis. Benign transformed melanocytes (nevus cells) become somewhat free from regulation by surrounding keratinocytes and initially proliferate as solitary units at the dermo-epidermal junction. Then, some nest of melanocytes enters the dermis by uncontrolled proliferation and accumulation of melanocytes at the junction; thereby, the nevus is established (**Figure 1.6**).

Caucasians, on average, have 25 naevi on their skin that measure at least 2 mm in diameter. Several lines of evidence indicate that the common naevi that progress is associated with non-cumulative solar damage (CSD) melanomas. Approximately 30% of non-CSD melanoma show areas representing a pre-existing common naevus, but some studies have found that 90% of superficial spreading melanoma (a common histological presentation of non-CSD) is associated with naevus. An evolutionary relationship between common naevi and non-CSD is also reflected in the high proportion of $BRAF^{V600E}$ mutations found in both types of neoplasm. An individual's constitute genotype strongly influences naevus number and size. The frequency and size of initiating mutations such as $BRAF^{V600E}$ and their penetrance would be modulated by germline mutations. The role of $BRAF^{V600E}$ in melanoma development is further described in section 1.8.2.1.

1.6.2 Dysplastic nevus (Intermediated neoplasm)

Dysplastic nevus are a subset of melanocytic nevi that are clinical atypical and characterized histologically by no well-defined border, size >5 mm, with a variable pigmentation, asymmetry and/or irregular borders (Elder et al., 2020). Dysplastic naevus are relative common with a frequency of 10% in population of North European descent. In terms of their clinical and microscopy morphology, dysplastic nevi are intermediate between common acquired nevi and the radial growth phase melanoma.

A dysplastic nevus is a symptom of systematic melanoma susceptibility and the inheritance of genes functionally involved in the proliferation of melanocytes that have acquired oncogenic mutations in genes such as *BRAF*, *NRAS* mutations, and TERT promoter mutation (cf. section 1.8.1). However, the risk of melanoma progression of these nevi appears to be low. The MITF E318K variant, known as the medium penetrance melanoma gene, is associated with an increase in nevus number and a higher incidence of multiple primary melanomas

1.6.3 Melanoma *in situ*

The first phase of melanoma progression results in the proliferation of melanoma cells in the epidermis. Clark's classification defines this type of melanoma as *in situ* melanoma or radial growth. At this stage, melanoma cells are limited to the epidermis without invasion to deeper layers of the skin.

Melanoma *in situ* can be a precursor lesion to both non-CSD and CSD invasive melanomas. Two main patterns of melanoma *in situ* can be distinguished, and they are associated with a pagetoid growth pattern a lentiginous growth pattern (**Figure 1.6**). The pagetoid growth pattern is associated with *BRAF*^{V600E} mutations, thus this neoplasm correspond to non-CSD or superficial spreading melanoma. By contrast, the lentiginous pattern is inversely correlated with *BRAF*^{V600E} mutations, and therefore is associated with CSD trajectory. Melanoma *in situ* lesions also has a high frequency of telomerase reverse transcriptase (TERT) promoter mutations and heterozygous *CDKN2A* alterations (Shain et al., 2015). But also other genes involved in genome stability (TP53), signaling induction proliferation and survival (PI3K, AKT, PTEN), and cell differentiation and adhesion of melanocytes (MITF, WNT, β -catenin).

1.6.4 Invasive melanoma

Once melanoma cells have migrated through the epithelium of the epidermis and entered to the dermis, the melanoma has become invasive (**Figure 1.6**). For melanoma, the risk of metastatic disease and death correlates with the depth on invasion. Indeed, most invasive melanomas arise from melanomas *in situ*. Following progression, invasive malignant melanoma cells grow into the dermis where they interact with many others cell types and gain physical access to both lymphatics and blood vessels, as vertical growth. To melanoma invasion occurs in necessary to acquired driver mutations activating the MAPK pathway as well as *TERT* mutations that

accumulated during earlier stages of progression. Moreover, Bi-allelic inactivation of CDKN2A emerged exclusively of invasive melanomas (Shain et al., 2015).

1.6.5 Metastatic melanoma

This phase occurs when melanoma cells have disseminated through the body and colonized distant organs (Hudson, 2001). Cutaneous melanoma metastasizes more frequently to lymph nodes (Karaman & Detmar, 2014) first and later to distant organs, such as the brain, liver, bones, and lungs (Olmeda et al., 2017).

To invade the underlying epidermis, melanoma cells downregulate some molecules involved in cell-cell adherent junctions, such as E-cadherin, leading to their detachment from the basal lamina and adjacent keratinocytes. Melanomas do not show a classical EMT, and they adopt more mesenchymal features (MET) (out of focus in this project). E-cadherin expression may be repressed by Slug, Snail, or Twist at the transcriptional level.

In the context of this thesis, this chapter emphasized the migration and differentiation of NCCs towards the transformation of malignant melanocyte. One of my goals is to focus in understanding the biology of melanocytes, proliferation, migration, differentiation in the developing chick embryos that might highlight new research approaches of melanoma disease in a developmental context.

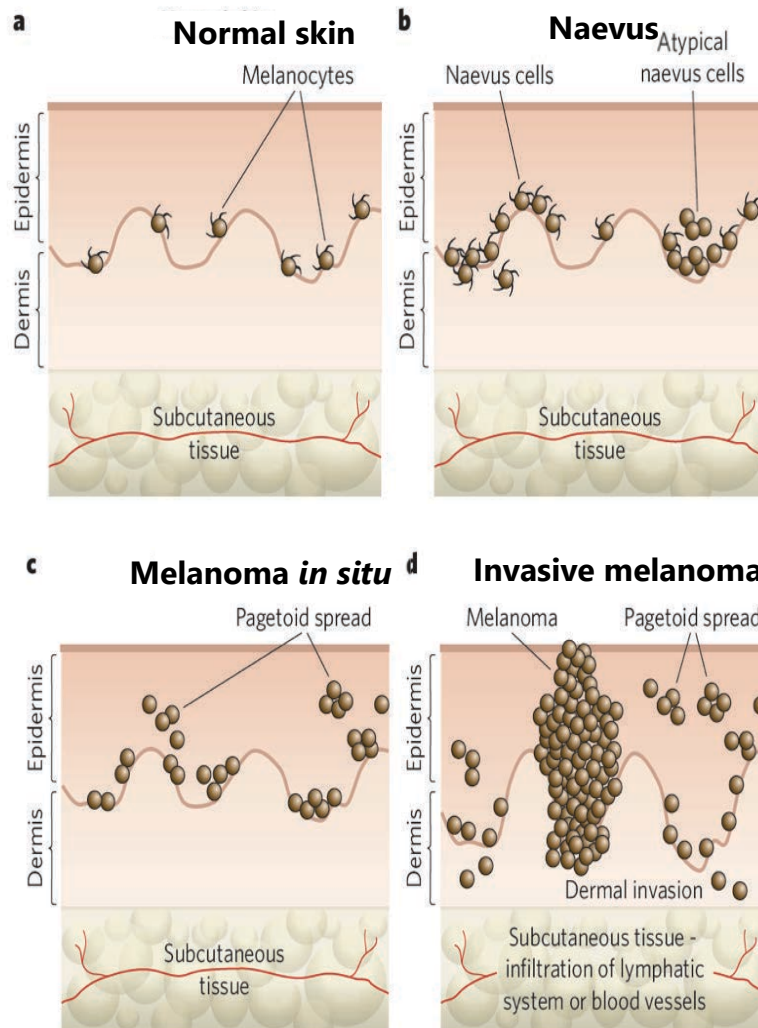


Figure 1.6 The morphology progression of melanocytes to melanoma

(A) Normal skin showing a dendritic polarization within the basal layer of the epidermis (B) Naevus is benign melanocytic naevi occur with an increased number of dendritic melanocytes. According to their location, naevus is termed either junctional, dermal, or compound. Some naevus are dysplastic with morphologically atypical melanocytes (C) Melanoma *in situ* or radial growth phase, considered as primary malignant state. Pagetoid spread describes the horizontally migration of solitary or small groups of melanocytes in the superficial layer of the epidermis (D) Invasive melanoma or vertical growth phase. This is the first state that is considered to have malignant potential and lead directly to metastatic malignant melanoma state by infiltration to vascular and lymphatic system. Adapted from Gray-Schopfer et al., 2007.

1.7 Melanocytic tumor classification

The World Health Organization (WHO) 2018 of melanocytic tumors classification is based on etiologically related to sun exposure and those that are not, mutational signature, anatomical site (localization), and epidemiology (Elder et al., 2020). Indeed, the currently used clinic-pathologic classification of melanoma is based on the melanoma progression proposed by Clark and colleagues in 1969 (Clark et al., 1969; Hudson, 2001). Authors suggested that melanocytic transformation is a stepwise transition from normal melanocytes proliferating, leading to a benign nevus along with the epidermis and basal layer to early (radial) growth. Such lesions are in the radial growth phase (RGP) because transformed melanocytes proliferate and expand along the surface at the level of the basal epidermis. RGP melanomas have an excellent prognosis until deeper/ticker invasion of the dermis occurs with the formation of a tumor mass, termed the vertical growth phase (VGP). In the next step of progression, tumor cells can spread into other areas of the skin, subcutaneous tissue, and organs proliferate increase and metastasize. For the presence or absence of RGP, three major categories of melanoma have been described. The initially recognized RGP variants were superficial spreading melanoma (SSM), also called pagetoid melanoma, characterized by neoplastic cells throughout the epidermis. Another variant is the nodular melanoma (NM), defined as VGP melanoma without identifiable RGP but forms a tumor from its earliest recognition. Therefore, it has the potential to metastasize from the first diagnosis. The third variant of melanoma, termed lentiginous melanoma (LMM), is associated with histological evidence of severe solar damage and has a lentiginous rather than pagetoid growth pattern.

These three categories' distinction was later supplemented by epidemiological and genomic observation, leading to the concept of alternative pathways in the development of melanoma. Two major pathways are described based on the etiology of skin susceptibility to solar damage. CSD and non-CSD melanomas differ in their anatomical site of origin, degree of cumulative exposure to UV radiation, hostage, mutation burden, and types of oncogenic alteration (**Table 1**):

- Low degree-CSD typically affects the more intermittently sun-exposed areas such as the trunk and proximal extremities of younger individuals (<55 years of age) that do not show marked solar elastosis (Shain & Bastian, 2016). Low-CSD melanomas include superficial spreading melanoma (SSM) and a subset of nodular melanomas. This type of melanoma is strongly associated with *BRAF* mutations.

- High-CSD melanomas typically affect the more intermittently sun-exposed areas such as the trunk and proximal extremities of younger individuals (<55 years of age) that do not show marked solar elastosis. This type of melanomas includes lentigo maligna and a subset of nodular melanomas. These melanomas occur later than non-CSDs.

Melanoma arising in the skin with some degree of CSD harbors a higher number of point mutations, mostly cytosine to thymidine (C>T) transitions. The most recurrent somatic mutations, in high CSD and non-CSD melanoma, affecting genes that govern proliferation are *BRAF* V600K and not V600E, *NRAS* and *NFI*; in growth-metabolism are *PTEN* and *KIT*; in resistance to apoptosis is *TP53*; in the G1/S cell cycle checkpoint control is *CDKN2A*, which encodes p16^{INK4A} and p14^{ARF} (Goldstein et al., 2007; Kamb et al., 1994). Moreover, the most common mutation event in cells' replicative lifespan is the *TERT* promotor, commonly mutated at an early stage in melanoma development.

Other melanoma arises via pathways in which solar damage does not appear to play any role are:

- Acral melanoma originates in the glabrous skin, nails, and mucosal melanomas from melanocytes originate in the anogenital and sinonasal mucosa. These melanomas develop in areas with limited sun exposure. *BRAF* mutations are found in acral (but not mucosal) melanomas, *KIT*, and *NRAS* mutations. These melanomas have a low mutation burden but highly rearranged genomes with numerous copy number changes, including multiple focused amplifications.
- Uveal melanomas originate from melanocytes within the choroid or iris. This type of melanoma also has a low mutation burden. It is characterized by frequent activating mutations in guanine nucleotide-binding protein α q polypeptide (*GNAQ*) or *GNA11*, accompanied by inactivating mutations of the tumor suppressor gene BRCA1 associated protein 1 (*BAP1*) or mutations in splicing factor 3b subunit 1 (*SF3B1*).
- Spitz melanomas are most frequent in childhood and adolescent melanoma. The relationship of malignant Spitz tumors with benign Spitz naevi is uncertain, and diagnostic distinction from these mutations is often difficult. Histologically, the lesions are composed of large spindle and /or epithelioid melanocytes. CSD is usually absent or minimal. Genetic alterations are also distinctive, including *HRAS* and kinase fusions *ROS1*, *NTRK1*, *NTKR3*, *ALK*, *BRAF*, *MET* and *RET*, and *TERT* promoter mutations in rare highly aggressive or rare lethal variants are less stable than others.

- Melanomas in congenital nevi develop *in utero* or are acquired just after birth. There is no apparent etiological relationship with sun exposure, CSD is typically absent. The *NRAS* mutation is the predominant somatic event in giant congenital naevi and in the melanoma that arises therein, at least in childhood (Bauer et al., 2007).

During development, congenital melanocytic nevi of substantial size may be caused by the accelerated proliferation of melanoblast during migration from the neural crest to the epidermis. The *NRAS* mutation may underlie the abnormal proliferation. If the abnormal proliferation take place at early developmental stages, the distribution of mutated melanoblast (nevus cells) will cover large areas, producing a wide and deep lesion. Thus, the time of proliferation determinates the size of the nevus; the later the proliferation begins, the smaller the size is. Furthermore, dermal and subcutaneous components of large congenital nevi are formed by the excess melanocyte proliferation from the neural crest.

Table 1. The WHO 2018 classification of melanoma according to etiology association with UV radiation exposure and pathways.

Pathway(s)	Type of melanoma			
	Melanomas arising in sun exposed skin		Melanoma arising to sun shielded sites or without known etiological associations with UV radiation exposure	
	Low-CSD (melanoma superficial spreading melanoma)	High-CSD melanoma (including lentigo maligna melanoma and high CSD nodular melanoma)	Acral/Mucosal melanoma	Maligna Spitz tumours (Spitz melanoma)
MAPK pathway activation	<i>BRAF</i> (p.V600E), <i>NRAS</i>	<i>NF1</i> (loss), <i>NRAS</i> , <i>BRAF</i> (p.V600T), <i>KIT</i>	<i>NRAS</i> , <i>KIT</i> , <i>NF1</i> (loss), <i>SPRED1</i> (loss), <i>BRAF</i> (p.V600E), <i>CCND1</i> (amplification), kinase fusions of <i>ALK</i> , <i>ROS1</i> , <i>RET</i> , <i>NTRK1</i>	<i>HRAS</i> , fusions of <i>ROS1</i> , <i>NTRK1</i> , <i>NTRK3</i> , <i>ALK</i> , <i>RET</i> , <i>BRAF</i>
G1/S checkpoint	<i>CDKN2A</i> (loss)	<i>CDKN2A</i> (loss)	<i>CDKN2A</i> (loss), <i>CDK4</i> (amplifications)	<i>CDKN2A</i> (loss)
P53 pathway	<i>CDKN2A</i> (loss), <i>TP53</i>	<i>CDKN2A</i> (loss), <i>TP53</i>	<i>CDKN2A</i> (loss), <i>TP53</i>	<i>CDKN2A</i> (loss)
Other alterations	<i>TERT</i> (promotor mutations)	<i>TERT</i> (promotor mutations)	<i>TERT</i> (amplification)	<i>TERT</i> (promotor mutations)

1.8 Germline and somatic variants in adult cutaneous melanoma

Cutaneous melanoma is an extremely complex disease involving genetic and environmental factors, such as germline and/or somatic mutations, skin color, number and type nevi, and sun exposure. This section will focus on the current knowledge of germline and somatic mutations in adult melanoma.

1.8.1 Germline events in adult melanoma

Cyclin-dependent kinase inhibitor 2A (CDKN2A)

The *CDKN2A* gene was the first predisposition gene identified in melanoma-prone families (Kamb et al., 1994). Germline mutations and/or deletions of *CDKN2A* were identified in 20-40% of families with three or more members with melanoma (Goldstein et al., 2007).

The *CDKN2A* gene is a tumor suppressor gene (TSG) localized at chromosome 9p21 that encodes two alternative reading frames: p16^{INK4A} and p14^{ARF}, both of which can function as TSG. The p16 protein is a member of the INK4 family of Cdk4/6 kinase inhibitors. The protein 16 blocks the transition of the cell cycle G1-S by inhibition of the cyclin-dependent kinase 4 (CDK4) or cell division protein kinase 6 (CDK6) complex leading to Rb protein inhibition. This inhibition results in non-phosphorylation of Rb that leads to the arrest of cell growth at the G₁ state of the cell cycle (Gruis et al., 1995). The p14^{ARF} (protein 14 alternate reading frame) acts as a TSG by inhibiting ribosome biogenesis or initiating p53-dependent cell cycle arrest and apoptosis. In mice, the model has shown that the INK4A allele (*INK4a*^{-/-}) and depletion eliminates p16^{INK4A} and p19^{ARF} (in humans, p14^{ARF}) proteins, resulting in the development of spontaneous tumors (Serrano et al., 1996). The p14^{ARF} protein function as a TSG by arresting the cell cycle or promoting apoptosis through the p53 pathway.

Telomerase reverse transcriptase (TERT) gene

In normal development, somatic cells have the capacity to avoid senescence by the telomerase enzyme, which maintain the length of the telomers, the repetitive DNA at the end of the chromosomes. On the contrary, in cancer cell development, telomere length maintenance is essential for uncontrolled proliferation. Specifically mutations that increase the telomerase activity

results in cell immortalization by extension the replicative lifespan of cells, allowing them to avoid senescence by telomere shortening.

The gene *TERT* confers an oncogenic advantage in adult melanoma by enabling melanocytes to sustain their telomere length and become immortalized. (Hodis et al., 2012; Huang et al., 2013). Promoter mutations create a new transcription factor binding site that activates *TERT* transcriptional constitutively (Vallarelli et al., 2016). Horn and colleagues (2013) identify a germ line mutation affecting the *TERT* promotor in adult melanoma, which encodes telomerase's catalytic reverse transcriptase subunit. The nucleotide change (T>G) located in the promotor of the *TERT* gene creates a new binding motif for transcription factor sites which activates *TERT* transcriptional constitutively. *TERT* promotor mutations when combined with *BRAF/NRAS* mutations correlates with adverse outcome in adult melanoma (Horn et al., 2013)

Tumour protein 53 (TP53)

Germline *TP53* variant is a genetic cause of Li-Fraumeni syndrome (LFS) (de Andrade et al., 2021). Li and Fraumeni defined LFS in 1969 as a genetic cancer predisposition manifested by the early onset of various malignant tumors within an individual and multiple affected family members (F. P. Li & Fraumeni, 1969). LFS is an autosomal dominant cancer predisposition disorder in which clinical diagnosis is based on personal and family history of cancer. This syndrome is manifested in soft tissue and bone sarcomas, in early-onset female breast cancer, brain tumors (choroid plexus tumors), leukemia, and adrenal cortical carcinomas.

1.8.2 Somatic events in adult melanoma

Neuroblastoma ras viral oncogene homolog (NRAS) and v-raf murine sarcoma viral oncogene homolog B1 (BRAF)

Adult melanomas show activation of the MAPK/ERK pathway by *NRAS* and *BRAF* oncogenic mutations. *BRAF*^{V600E} mutations are found in 80% of human naevus, a benign lesion that can remain for long periods. The *p.V600E* mutation found in *BRAF* is a substitution of glutamic acid for valine at position 600, considered to induce senescence in melanocytes and the formation of a nevus. Mutational activation of *BRAF* is the earliest event in melanoma. However, the oncogenic *BRAF*^{V600E} mutation is insufficient for a fully activated the melanogenesis program. In low-CSD

melanomas, *BRAF p.V600E* mutation account for most MAPK pathway-activation mutations. In contrast, high-CSD melanomas rarely harbor *BRAF p.V600E* mutations (Bauer et al., 2007), whereas *NF1*, *RNAS*, and *KIT* mutations (all mutually exclusive) predominate in melanoma in the skin with a high degree of CSD.

The microphthalmia-associated transcription factor (MITF), the master regulator

The microphthalmia-associated transcription factor (*MITF*) is a transcription factor considered the master gene regulator of melanocyte survival, growth, and differentiation. *MITF* is a basic helix-loop-helix leucine zipper (b-HLH-ZIP) DNA domain that binds to DNA sequences (E-box, M-box), consisting of a 5'-CATGTG-3' or 5'-CACGTG-3' motif (Bell & Levy, 2011). Mutation in *MITF* results in the Waardenburg syndrome type 2, hypopigmentation of the skin, hair, and iris associated with deafness resulting from NC-derived melanocytes deficiency (Cheli et al., 2010; Tassabehji et al., 1994).

The *MITF* level activity can lead to the expression of cell cycle genes, a switching of differentiated to invasive melanoma cells described as the *rheostat model* by Carreira and colleagues in 2005 (**Figure 1.7**). This model explains that *MITF* alters the expression of different target genes depending on their expression and activity level (Goding, 2011). A low level of *MITF* induces an actin cytoskeleton reorganization, cells undergo cycle arrest in P27 dependent manner and promote invasion. By contrast, high *MITF* levels activate cell differentiation, and medium *MITF* level promotes cell proliferation (Carreira et al., 2005).

Furthermore, *MITF* controls the transcription of different genes involved in: the **pigmentation cascade** as *Tyr* (Paterson et al., 2015), *TRP1*, *DCT*, and *PDE4D3* (Khaled et al., 2010) in cAMP, **cell cycle** exit in G1 by *INK4A* regulation (coding P16 TSG) (Loercher et al., 2005) and *CDK4* (Du et al., 2004), which codes for a serine/threonine kinase that is essential for G1/S transition. Indeed, *MITF* induces and maintains the cell cycle exit in melanocytes, which can be a reversal in *INK4A* melanoma inactivation. *MITF* is also implicated in melanocyte survival and melanoma progression by direct *BCL2* regulation, an antiapoptotic factor (McGill et al., 2002), melanocyte invasion and proliferation regulation via *DIAPH1* gene regulation with the control of actin polymerization, microtubules remodeling, and cell cycle progression through regulation of P27 (Cyclin-dependent kinase CDK inhibitor) (Carreira et al., 2006) and induce G0/G1 arrest thus the entry to senescence (Giuliano et al., 2010).

In adult melanoma, *MITF* has been proposed to act as an oncogene and confer a genetic predisposition to occurring melanoma. *MITF* plays a role at the post-transcriptional level, including SUMOylation. SUMOylation is a post-translational modification involved in the covalent conjugation of SUMO1, a small ubiquitin-like modifier, to a protein in a ψ KXE sequence context (ψ represents a large hydrophobic amino acid) which results in fate modifications and function (Rodriguez et al., 2000). The most common germline variant of *MITF* is *p.E318K*, which alters its binding affinity for the ubiquitin-like protein SUMO, thus enhancing the binding of *MITF* protein to the *HIF1A* promoter and increasing its transcriptional activity (Rodriguez et al., 2000; Bertolotto et al., 2011). Bertolotto and colleagues have shown *in vitro* that *MITF* harboring Mi-E318K enhances migration, invasion, and the ability of immortalized melanocytes to colonies formation in melanoma cells, consisting of a gain-of-function role in tumorigenesis (Ballotti & Bertolotto, 2017). In a parallel study in 2011, authors identified an individual carrying the germline variant (coding DNA sequence c.G1075A protein sequence p.E318K) in the melanoma-lineage-specific oncogene *MITF*, demonstrated that *MITF* is a melanoma predisposition gene (Yokoyama et al., 2011).

In pediatric melanoma, *MITF* knowledge is limited. To date, only one article directly reports a pediatric case with a tandem duplication of *MITF* present in CNM (Lu et al., 2015).

Breast cancer 1 (BRCA1) associated protein 1 BAP1

The BAP1 (located at chromosome 3p21) is a deubiquitinate protein categorized as TSG. BAP1 has roles in numerous cells process, including DNA damage response, cell cycle regulation, cell growth, metabolism, and the regulation of inflammatory responses (Conway et al., 2021; Ji et al., 2014; Yu et al., n.d.; Zarrizi et al., 2014). A new form of the cutaneous melanocytic tumor was also associated with this syndrome (Wiesner et al., 2011) or BAP1-inactivated melanocytic nevus/melanocytoma by the WHO Classification of Skin Tumours (Elder et al., 2020). Wisner and colleagues (2011) identified families that developed cutaneous melanoma in affected individuals with multiple cutaneous spitzoid melanocytic neoplasms and predisposed to increased risk of developing cutaneous and uveal melanoma (Wiesner et al., 2011). The majority of tumors lost the remaining wild-type BAP1 allele by various somatic alterations and lacked immunohistochemical expression of BAP1 (Wiesner et al., 2011). Furthermore, almost all familial BAP1-negative neoplasms showed *BRAF*^{V600E} mutations typically absent in Spitz nevi (Wiesner et al., 2012).

POST-TRANSLATIONAL: SUMO, UBQ

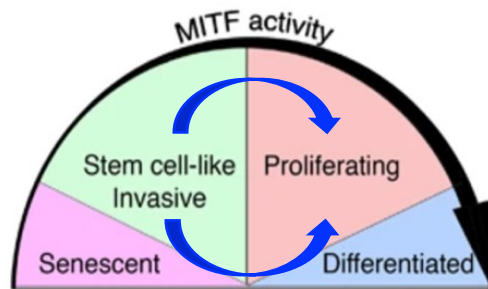


Figure 1.7 The MITF rheostat model

In adult melanoma, low levels of MITF cause G1 arrested, invasive, stem-like cells with high p27. Cells expressing MITF either proliferate or differentiate depending on the level of MITF expression, moderate level, and high level respectively or its post-translational modification. Long-term small interfering RNA-mediated depletion of MITF leads to DNA-damage and mitotic catastrophe-induced senescence, though this may be prevented in vivo by up-regulation of anti-proliferative signaling pathways. Adapted from Goding (2011)

Key points of Chapter 1 – General Introduction

- Melanocytes arise from the entire CNC and TNC.
- NC techniques allow for tracking NCCs migration and performing functional analysis.
- Melanocytes migrate either at the CNC or at the TNC regions. At the CNC, melanocytes migrate in a cohort in a wave-like pattern. At the trunk level, melanocytes adopted either ventral or dorsolateral migration.
- Melanogenesis involves the enzymes TYR, DOPA, TYRP1, and TYRP2 to synthesize pheomelanin or eumelanin.
- Activation of MC1R by α -MSH is positively coupled to the cAMP signaling pathway. It leads to a stimulation of melanogenesis and a switch from the synthesis of pheomelanin to the production of eumelanin.
- *ASIP* prevents α -MSH from binding to MC1R on melanocytes to inhibit the α -MSH mediated elevation of cAMP, leading to eumelanin production, which shifts the production of eumelanin to pheomelanin.
- Melanoma is a stepwise transition: from uncontrolled melanocyte proliferation towards radial to vertical growth to metastatic melanoma.
- WHO 2018 melanoma classification in adults is based on the sun exposure etiology in low-CSD and High-CSD with different genetic signatures.
- Germline events in adult melanoma involve *CDKN2A*, *TERT*, and *TP53*.
- The somatic event in adult melanoma involves *NRAS*, *BRAF*, *MITF*, and *BAP1*.

2 Childhood melanoma

Childhood melanomas represent a heterogeneous group of malignant melanocytic tumors with variable clinical, histopathology, and genetic features that differentiate them from adult melanomas. Patient age is used to classify pediatric melanoma into two subtypes, prepubertal (congenital and childhood) melanoma occur in patient under the age of <10-12 years, and post-pubertal (adolescent) melanoma occur in patient aged between 10-12 years and 19 years. The upper age cut-off for pediatric melanoma is <20 years consider by the Surveillance, Epidemiology, and End Results (SEER) database (<https://seer.cancer.gov/>) and the National Cancer Institute (<https://www.cancer.gov/>). The prepubertal incidence rate is <1 per 100 000 person/year, whereas post-pubertal incidence has increased over the past 20 years, in relation to unprotected sun exposure (Eggen et al., 2017). This chapter will describe what is known about the incidence, histopathology, risk factor, and genetics in childhood melanoma.

2.1 The incidence of childhood melanoma

Melanoma in the pediatric melanoma population has not been studied as extensively as adult melanoma. Melanoma accounts for about 4% of all cancer in children aged 15 to 19 years (National Cancer Institute, 2018),. The incidence is around 5-6 per million in children under the age of 20 years (Strouse et al., 2005). Pediatric melanoma remains a health concern because incidences rates (IR) have been a reported to increase (Hamre et al., 2002; Strouse et al., 2005). Melanoma IR differed by age; prepubertal have lower IRs of melanoma than post-pubertal groups. Melanoma accounts for 7.1% of cancer in 15 to 19 years olds with an increase of 10.4 per million. Post-pubertal accounts for most cases of pediatric melanoma (73.2%), followed by 10- to 14-years old (17.3%), 5- to 9- years old (5.7%), and 1- to 4- years old (3.8%) (Campbell et al., 2015).

Pediatric melanoma behaves heterogeneously across race, age (Campbell et al., 2015; Wong et al., 2013), sex (Strouse et al., 2005; Wong et al., 2013), anatomical location of the lesion, and geographical residence across the age groups. Increased age confers greater risk in the white gender than black individuals (Strouse et al., 2005). In the first year of life, the incidence of melanoma is similar by race, but it diverges by age 5 to 9 years and is 40-fold higher in white individuals around age 20. This pattern may reflect increased susceptibility to UV radiation exposure in white individuals, other environmental factors, and/or differences in genetic

predisposition (Strouse et al., 2005) which favors genetic accident origin. Regarding sex, females are mostly affected by this disease in childhood/adolescence, with a ratio of 1.6 compared to males (Eggen et al., 2017; Hamre et al., 2002). The incidence of melanoma by anatomical localization is not uniform across age and sex. In younger children (age, ten years old), melanoma IRs are fairly equal across all anatomical locations, except for truncal melanomas being especially rare in 0- to 14- years old. On the other hand, the incidence in children aged 10 to 19 years is highest in the trunk (Campbell et al., 2015; Strouse et al., 2005).

In terms of clinical evolution, children with melanoma had a 5-year survival of 93.6% (95% CI, 91.9 to 94.9). When melanoma is early detected and wide local incision of early disease, the prognosis is good but decreases with advanced melanoma, like in adult melanoma.

2.2 Childhood melanoma risk factors

The risk of melanoma is increased in children with a high number of melanocytic naevi, giant congenital naevi, and dysplastic nevus syndrome. Other risk factors include predisposing syndromes such as *Xeroderma Pigmentosum*, immunodeficiency conditions, and family history (reviewed in Stefanaki et al., 2017; Strouse et al., 2005).

2.2.1 Xeroderma pigmentosum

Xeroderma pigmentosum (XP) is a rare hereditary autosomal recessive disorder characterized by sensitivity to sunlight, photophobia, and early-onset freckling followed by neoplastic changes in sun-exposed sites (Kraemer et al., 1994). There is a hypersensitivity due to defects in the nucleotide excision repair (NER). Patients are unable to repair UV-induced DNA damage, resulting in a 1000-fold increased risk of skin cancer at an early age (Bahrami & Barnhill, 2018; Ceballos et al., 1995). Melanoma arises in approximately 5% of post-pubertal patients diagnosed at 19 years (Pappo, 2003).

2.2.2 Immunosuppression

Children with genetic immunodeficiency tend to develop light sensitivity and/or freckles with a 3 to 6-fold risk of developing melanoma. Moreover, children who acquired immunodeficiency syndromes such as post-organ transplantation, chemotherapy for malignancy, and human

immunodeficiency syndrome (HIV) have a 3 or 4-fold increase in melanoma risk (Jen et al., 2009; Pappo, 2003)

2.3 ABDC criteria in childhood melanoma differ from adult melanoma

Pediatric melanoma molecular transcriptomic signature is different from the adult counterpart. Cordoro and colleagues (2013) reported that childhood and adolescent melanoma differs in the adult ABCDE conventional criteria: Asymmetry, Border irregularity, Color, Diameter >6mm, and Evolution. They observed that 60% of children between 0 to 10 years old and diagnosed with melanoma did not meet the common adult criteria. Childhood melanoma is present as Amelanotic; Bleeding, Bump (papulonodules: bumps), Color uniformity; variable Diameter, and *de novo* development (Cordoro et al., 2013). This study shows that establishing a diagnosis of pediatric melanoma can be difficult due to the atypical appearance of some melanocytic lesions. Due to pediatric melanoma's scarcity and complexity of pediatric melanoma, the diagnosis challenges clinicians who need expertise in pediatric melanocytic neoplasm to analyze the evolving naevus to be biopsied and examined histologically (reviewed in Ferrari et al., 2021). For the diagnosis is necessary to consider a physical examination, dermoscopy analysis, patient history biopsy, molecular testing, and imaging (reviewed in Ferrari et al., 2021). The skin examination should also consider the presence and number of typical and atypical naevus and congenital naevus.

2.4 Histopathology criteria

In this section, I will describe the types of cutaneous melanoma that can arise during childhood considering the clinical and pathological outcomes as (1) superficial spreading melanoma, (2) melanoma arising from CMN, and (3) Spitzoid melanoma, (4) conventional adult-type melanoma. The genetics undergoing childhood melanoma will be further discussed in section 2.5

2.4.1 Superficial spreading melanoma (SSM)

These lesions are similar in post-pubertal, adolescent to SSM found in adults. Histologically, SSM develops in a radial or horizontal growth phase, initially intraepidermal (*in situ*) or micro-invasive melanoma. The distribution is asymmetrical with intraepidermal nest and isolated melanocytes with a wide hyperpigmented cytoplasm. The lateral pagetoid scatter of such melanocytes is the

histological hallmark of these tumors (reviewed in de la Fouchardière et al., 2021). In advanced SSM, the dermis is invaded, often by nest or large melanocytes with similar morphology. A dense lymphocytic infiltrate is commonly present on the invasive front of the tumor. These tumor-infiltrating lymphocytes are in close connection with melanocyte (reviewed in de la Fouchardière et al., 2021). Breslow thickness, dermal mitotic activity, and epidermal ulceration will be assessed. A *BRAF p.V600E* mutation is frequently present at >80% in the melanoma and the nevus from which it arose.

2.4.2 Melanoma arising from a congenital melanocytic naevus (CMN)

CMN are benign melanocytic tumors that can appear at birth or become apparent in early childhood. CMN is the result of a mutation *in utero*, after the embryo has already begun to develop, leading to mosaicism (reviewed in Kinsler et al., 2017). Genetic events occurring in melanoblast can explain the development of such lesions (reviewed in de la Fouchardière et al., 2021). During development, a single multipotent NCCs bearing a somatic mutation can be differentiate into a melanoblast competent progenitor that, after proliferation and dissemination along the peripheral nerves, will cause the formation of CMN at the periphery. Due to the early nature of this development abnormality, the resulting nevus can be involved in the thickness of the skin but also can involve the CNS (de la Fouchardière et al., 2021). Moreover, the nevi growth is proportional to the state of occurrence of the oncogenic mutation during development. When the mutation occurs early in development can give rise to the development of a Large CMN.

Conventional criteria categorize CMN in relation to size from small (<1.5 cm in diameter), medium (1.5 to 20 cm), and, or large to giant (>20 cm) by projected adult size (PAS) of the largest nevus and by a total number of naevus (Kinsler et al., 2017). Small and medium CMN are homogeneous with lesions with either reticular or globular patterns.

At the molecular level, CMN is caused by a mosaicism post-zygotic mutation in *NRAS* at the codon 61 (Q61K) found in 60% to 80% of the largest lesions (reviewed in Kinsler et al., 2013), and upregulation of *TERT*. These somatic mutations will be further described in section 2.5

2.4.3 Atypical Spitz tumor and Spitzoid melanoma

Atypical Spitz tumors and Spitzoid melanoma (AST/SM) are usually seen in younger patients. It often appears as melanocytic neoplasia of epithelial or fusiform cells. Sophie Spitz described, in

1948, a “juvenile melanoma” as a melanocytic tumor, present in childhood, with clinical and pathological characteristics similar to melanoma but with benign behavior (Spitz, 1948). Benign Spitz nevi are frequent during childhood, especially after puberty, and are very difficult to diagnose and to classify due to the histopathological similarities between naevus and melanoma. These lesions are mostly located in the lower limbs, especially on the knees or on the face. Spitz tumors enclose many morphological subtypes (pigmented, hyperpigmented spindle (Reed), plexiform, pagetoid, desmoplastic angiomatoid, among others) and have specific, mutual exclusive genetic anomalies (reviewed in de la Fouchardière et al., 2021).

AST/SM is characterized by copy number aberrations that can be detected by fluorescence *in situ* hybridization or comparative genomic hybridizations, including biallelic loss of *CDKN2A*. These tumors typically lack *TERT* promoter mutations and have fusion kinase involving *MAP3K8*, *NTRK*, *ALK*, *ROS1*, *RET*, *BRAF*, or *MET*. (reviewed in Bahrami & Barnhill, 2018; Lee et al., 2015). These tumors rarely disseminate, but when they do, they acquire *TERT* activity by promoter mutation, including structural arrangement (Lee et al., 2015)

2.4.4 Conventional or adult-type melanoma

Convention melanoma (CM) classification shares the histological and clinical features of melanoma arising in intermittently sun-exposed skin in adults. CM is rare and occurs almost exclusively in adolescents (Barnhill et al., 1995; Lu et al., 2015). FISH analysis has shown that CM constitutes a more uniform and well-defined disease entity in comparison with spitzoid melanoma (Lu et al., 2015). Pediatric melanoma patient with CM harbors the MC1R receptor, which is associated with sun-sensitivity skin and an increase in melanoma susceptibility. As in adults, these tumors have evidence of a UV signature with a preponderance of C>T transitions, *CDKN2A* homozygous deletions, *BRAF*^{V600E}, *TERT* promoter, and *PTEN* mutations. This predisposition of genes will further be described in detail in the following section.

2.5 What is known about childhood melanoma genetics?

Early-onset cancer is a classical hallmark of a genetic predisposition; nevertheless, most pediatric melanomas are clinically sporadic. This section, I will focus on the known genetic variants in pediatric melanoma as **germline**: *CDKN2A*, *MC1R*, *TP53*, and **somatic mutations**: *NRAS* and *BRAF*, *PTEN*, *TERp*.

2.5.1 Germline mutations (inherited) in childhood melanoma

CDKN2A and CDK4

The main predisposing gene *CDKN2A* in adult melanoma is rare in childhood melanoma (Berg et al., 2004; Goldstein et al., 2018; Lu et al., 2015; Markovic et al., 1997). Lu and colleagues have worked on understanding the pediatric genomic landscape, demonstrating copy variants similarities with adult melanoma and 15 CM from 23 total pediatric patients (**Figure 2.1**). None of their patients carried *CDKN2A* or *CDK4* mutations, but 67% of CM patients carried germline *MC1R* variant reported to be associated with increased melanoma risk in adults.

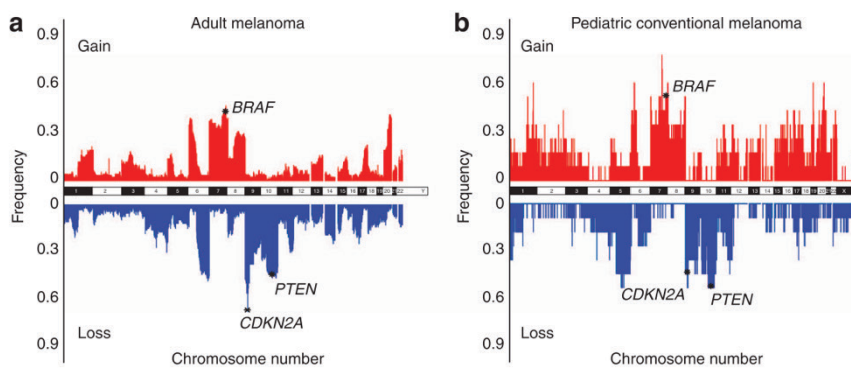


Figure 2.1 Prevalence in copy number variations between adult and pediatric conventional melanoma

(A) frequency of CNVs in adult melanoma by single-nucleotide polymorphism array from the study (Hodis et al., 2012) (B) frequency of conventional melanoma in 11 pediatric patients from Lu and colleagues study (Lu et al., 2015). The 7q34 locus harboring *BRAF* was a common region of gain, whereas 9p21 and 10q23.3, covering *CDKN2A* and *PTEN*, were common regions of loss in both adult and pediatric melanomas Adapted

Melanocortin 1 receptor (MC1R)

The *MC1R* gene on human chromosome 16q24.3 encodes a G-protein-coupled receptor expressed on melanocytes, melanoma cells, and CMN. Their role is to activate the signaling pathways involved in melanocytic proliferation and melanin (Nasti & Timares, 2015). *MC1R* is highly polymorphic, and specific variants were identified as *R* variants (p.D84E, p.R142H, p.R151C, p.I155T, p.R160W, and p.D294H) according to their strong association with red hair color phenotype. In contrast, those with a weak association are designed as *r* variants allele (p.V60L, p.V92M and p.R163Q) (Sturm et al., 2003). *R* alleles have been found to have a significant effect on pigmentation and UV sensitivity. By contrast, *r* alleles confer a normal impaired *MC1R* activity, with a low-strength association with the fair skin phenotype.

MC1R variants are associated with CMN in pediatric melanoma with red hair pigmentary phenotype and family history (Kinsler et al., 2017; Kinsler et al., 2012). The clinical correlation between children with red hair and freckles phenotype with CMN diagnosis was determinant in investigating the role of the *MC1R* gene in childhood melanoma. Kinsler and colleagues reported the association between CMN and red hair/*MC1R* variants. *MC1R* promotes the growth of CMN during embryogenesis (Kinsler et al., 2012). In a case study of monozygotic twins (with red hair, green eyes, fair-skinned) without a family history of melanoma and the absence of both *CDKN2A* and *CDK4* mutation gene, authors identified two *MC1R* heterozygous variants in both twins: the c.451C>T (p.Arg151Cys) and the c.456C>A (p.Tyr152) (Pellegrini et al., 2012). They concluded that the *MC1R* variant possible is associated with melanoma risk. Then, Pellegrini and colleagues (2019) analyzed *MC1R* prevalence in childhood or adolescent patients (from 20 years or younger) with CMN in a worldwide cohort study (U.S.A, Canada, Australia, France, Italy, Greece, Sweden, Turkey). Children and adolescents younger than 18 years were found to have higher odds (OR 1.80, 95% CI 1.06 -3.07) of carrying *MC1R* *r* variants than adults patients. This study reveals that *MC1R* variant *r* is more associated with young patients than the adult counterpart (Pellegrini et al., 2019). In another study, one or two germline *MC1R* variants (V60L, V92M, R151C, and R160W) were detectable at 67% in CM and SN, but controversially not in CMN (Lu et al., 2015). In brief, *MC1R* variants, mainly *r* variants, are a genetic risk factor in childhood and adolescent melanoma, possibly through a pigmentation-independent pathway.

Moreover, in a clinical study from a 15-year patient diagnosed with melanoma, brain metastasis, and family uveal melanoma history, the predisposition melanoma genes *CDKN2A*, *CDK4*, and *BAP1* were not found. The genomic analysis did not show any rearrangement, copy number neutral changes, point mutations, or other alternations that could not explain her death

(Rabbie et al., 2017). Interestingly, the authors found only *MC1R* variants in this patient, R142H and V60L alleles. This study emphasized the elevated prevalence of *MC1R* variants related in young patients. Still, the few numbers of available genomic studies and the small number of cases per study make it difficult and challenging to propose conclusions in this population.

BRAC1-associated protein 1 (BAP1)

The *BAP1* gene is located at chromosome 3p21 and encodes a nuclear-localized deubiquitin carboxyl-terminal hydrolase enzyme. Loss of function of *BAP1* in adults has been associated with an enhanced risk of uveal and cutaneous melanoma, renal cell carcinoma (de la Fouchardière et al., 2015), and atypical cutaneous melanocytic proliferations. The majority of the tumors lost the remaining wild-type *BAP1* allele by various somatic alterations and lacked immunohistochemical expression of BAP1 (Wiesner et al., 2012). Childhood carriers frequently develop benign BAP1-inactivated melanocytic nevi, and immunohistochemical studies in childhood samples showed loss of nuclear BAP1 expression as in adult melanoma samples. The presence of a dense, possibly pigmented, clonal sheet-like area within BAP1 inactivated nevus hints at this diagnosis (reviewed in de la Fouchardière et al., 2021).

TP53

As described before, *TP53* is a pathogenic germline variant involved in LFS. LFS patients are at risk of multiple primary tumors. However, melanoma is considered a controversial component of LFS. Report cases show the relation between LFS and pediatric melanoma. In the case of a child who had choroid plexus carcinoma and then developed Spitzoid melanoma in the field of radiation treatment, *TP53* variant was confirmed as a germline mutation (Kollipara et al., 2014). More recently, in 2019, the first case in a postpubertal patient was demonstrated in which cutaneous melanoma was the initial malignant tumor in a child with LFS (Baek et al., 2019).

2.5.2 Somatic mutations (tumoral) in childhood melanoma

Neuroblastoma RAS viral oncogene homolog (NRAS) and v-RAF murine sarcoma viral oncogene homolog B1 (BRAF)

NRAS is altered in 15-20% of melanoma at exons 2 or 3. The most common *NRAS* point mutation affects codon 61 with amino acid substitution at c.181C>A p.Q61K and c.182A>G, p.Q61R. *NRAS* mutations are responsible for CMN formations in 70 to 95% of cases in large and giant CMN, respectively (Charbel et al., 2014). Furthermore, this post-zygotically mutation is found in different affected cutaneous and neurological lesions from the same patients (Kinsler et al., 2013).

CMN is known to be a risk factor for malignant melanoma in childhood melanoma. Due to discrepancies in the incidence in both mutations in CMN, different authors have demonstrated that *NRAS* mutation at codon 61, *NRAS*^{Q61R}, is prone to drive 70% *in utero* CMN while *BRAF*^{V600E} mutation is less common, occurring in a 30% of small congenital naevus or *BRAF* as a chromosomal translocation (Charbel et al., 2014; Dessars et al., 2007; Lu et al., 2015). The high risk of *NRAS* mutation in naevus that develops in the non-sun-exposure area demonstrated that UV is not a requirement for *NRAS* mutations in CMN (Bauer et al., 2007).

Nonetheless, pediatric melanoma cases are characteristic of low UV exposure with few acquired or somatic mutations compared to the adult. The point mutation *BRAF* (V600E, V600K) were found to be linked to conventional melanoma in 13 of 15 patients (87%), and 12 of 13 patient had *TERT* promoter mutations (Lu et al., 2015). These mutations share histopathological characteristics with adult melanoma counterparts with high somatic SNV.

Phosphatase and tensin homolog gene (PTEN)

The *PTEN* tumor suppressor gene, the negative regulator of the phosphatidylinositol 3 kinase/AKT pathway, is commonly disrupted in CM (Lu et al., 2015). It has been proposed possible cooperation between *BRAF* activation and loss of either p16/ARF or *PTEN* contributes to melanoma development (Hodis et al., 2012; Lu et al., 2015).

Telomerase reverse transcriptase (TERT)

Melanoma initiation requires melanocyte proliferation bypassing senescence. After a certain number of divisions, cells enter a process of senescence. To bypass this process and keep the cells growing, the telomere length and cell cycle need to be increased (Bahrami & Barnhill, 2018; Bertrand et al., 2020). In melanoma, *TERT* expression can also be deregulated through aberrant promoter methylation (Lee et al., 2015) or by structural rearrangement of the gene; the latter occurs in a manner mutually exclusive of promoter mutation. Such lesions in *TERT* occur commonly in malignant adult melanomas (Horn et al., 2013) and biologically aggressive

adolescent melanomas (Seynnaeve et al., 2017), but are not observed in low-grade pediatric melanomas (Seynnaeve et al., 2017). In childhood melanoma, the *TERT* promoter is mutated in pediatric CM (*TERT-p* C->T mutation) (Lu et al., 2015).

To conclude the section 2.5 is clear that the occurrence of the *CDKN2A* germline mutation in childhood melanoma is rare, and the few variants in childhood melanoma are correlated with adult melanoma. Although these few variants were identified in childhood based on adult melanoma knowledge, there is a clear necessity for genetic research in childhood melanoma. We hypothesize that pediatric cases are sporadic and sometimes arise with giant congenital nevi **favoring the hypothesis of *de novo* mutations as the causative role of childhood melanoma.**

Key points of Chapter 2 – Pediatric Melanoma

- Childhood melanoma is a sporadic disease.
- The conventional ABCDE criteria in adults do not fit with childhood lesions.
- The histological diagnoses of childhood melanoma are congenital melanocytic naevus, spitzoid naevus, and conventional melanoma.
- The main predisposition gene in adult melanoma, *CDKN2A*, is rare in childhood melanoma.
- Only a few variants characterized in adult melanoma are described in childhood melanoma as germline: *CDKN2A* (*very rare*), *MC1R*, *TP53*, and somatic mutations: *NRAS* and *BRAF*, *PTEN*, *TERT*.
- Most pediatric cases are sporadic, without a family history, supporting the hypothesis of *de novo* mutations

3 *de novo* mutation concept and the role in childhood melanoma

3.1 Next-generation sequencing, a big step in the human genetic research

The development of the Sanger method for DNA sequencing in 1977 allowed deciphering genetic mutations (Sanger et al., 1977). The next-generation sequencing (NGS) has revolutionized DNA sequencing by dramatically reducing cost-effectively and increasing sequencing output. In both Sanger and NGS techniques, the DNA polymerase adds fluorescent nucleotides one by one onto a DNA template strand. Each incorporated nucleotide is identified by its fluorescent tag. The main advantage of NGS is the high sensitivity level to detect low-frequency variants and the ability to analyze thousands of genes or genes regions simultaneously. NGS is a massive sequencing of millions of DNA fragments in parallel. The first step in the sequencing is accomplished by breaking the entire genome into small fragments, between 200 to 600 base pairs. Then, short fragments of DNA called "adapters" are attached to the fragments during DNA synthesis by the DNA polymerase. In NGS, millions of DNA segments are sequenced at the same time. After sequencing the region, the read (the number of sequenced segments) is used to assemble and aligned to a reference genome, recreating the complete DNA sequence. The millions of reads resulting can be used in the *de novo* assembly or compared to a reference human genome. The accuracy of NGS approaches relies on high sequencing coverage, which corresponds to the number of short reads that overlaps each other within a specific genomic region.

Two types of DNA sequencing have been developed to sequence the human genome: the whole-genome sequencing (WGS) and whole-exome sequencing (WES). WES is a cost-effective genomic technique for sequencing all the protein-coding regions of genes in a genome (exons) which represent approximately 1% of the genome. To enrich for this fraction, genomic DNA is randomly sheared into small fragments that are subsequently hybridized into a biotin-labelled probe specific to the region of interest. The enriched regions are then processed into a sequencing library that is read for the NGS platform. By contrast, interpreting the WGS of non-coding variants is very difficult today even in known genes.

3.1.1 NGS germline sequencing of parent-child trios

NGS is crucial for the identification of *de novo* mutations. *de novo* mutations are detected by trio-based sequencing through WEG or WES from trios (parents and offspring) allows the analysis of the variation in the human rate between individuals (reviewed in Veltman & Brunner, 2012). Trio-based sequencing consists of performing WES or WEG in an individual and both his or her parents. This trio-based strategy allows the identification of *de novo* candidates' variants present in the offspring but absent in the parents in order to elucidate genetic diseases (Jin et al., 2018).

NGS approaches also enable to study of the occurrence of all types of *de novo* mutation through the genome, from SNVs to small insertions-deletions (indels), to larger structural variations, including deletion, duplications, and other chromosomal arrangement (reviewed in Acuna-Hidalgo et al., 2016; Ku et al., 2013). The timing of *de novo* mutagenesis during development determines the proportion of variant cells and the tissue distribution phenotype in the offspring. The NGS technologies enable researchers to dissect the molecular basis of complex phenotypes that arise from *de novo* mutations. This has been demonstrated in common neurodevelopmental disorders such as severe intellectual disability, epileptic encephalopathies, schizophrenia, and an autism spectrum disorder. The rate of *de novo* variation of an SNV was estimated from 0.82 to 1.58 per base per generation (Gilissen, Hehir-Kwa, Thung, et al., 2014; Sanders et al., 2012; Ségurel et al., 2014; Veltman & Brunner, 2012), and for *de novo* early post-zygotic the average *de novo* SNV mutations burden with a rate of 0.04×10^{-8} - 0.34×10^{-8} in a monozygotic twin pair (Dal et al., 2014).

Importantly, the NGS strategy has been crucial for detecting disease-causing genes involved in sporadic diseases. *De novo* mutations has been primarily described in sporadic early-onset neurodevelopmental disorders including epilepsy, autism spectrum disorders (O'roak et al., 2012; Sanders et al., 2013), intellectual disability (Gilissen, Hehir-Kwa, Tjwan Thung, et al., 2014; Vissers et al., 2010) and pediatric disorders. *De novo* mutation in these diseases revealed a high genetic heterogeneity with many different genes affected by *de novo* mutations (McRae et al., 2017). Concerning the role of *de novo* mutations in cancer research, Renaux-Petel and colleagues demonstrated that LFS not only carries *TP35* mutation (discussed earlier), but also the mutation was described as a *de novo* mosaic mutation, occurring post-zygotic in embryonic developmental (Renaux-Petel et al., 2018). Additionally, a clinical case of a 2-year-old child with LFS aggressive metastatic neuroblastoma and two soft tissue mesenchymal tumors without a family history of cancer demonstrated the role of *TP53* as a *de novo* mosaic germline mutation affecting two germ layers. The occurrence of separate tumors derived from different germ layers suggests that *TP53* *de novo* mutation occurred early in embryogenesis, prior to gastrulation (Behjati et al., 2014). Evidence from twin studies of neonatal blood spots indicates that the most initiating event of

acute lymphoblastic leukemia occurs during fetal development *in utero* (Bateman et al., 2015) (Bateman et al., 2015). The most frequent *FBXW7* were identified in T cell ALL. These studies demonstrated the importance and the powerful advances in NGS technology to find *de novo* mosaicism mutations that arose in early developmental stages (mosaicism in *de novo* mutations will be further described in section 3.1.2).

To sum up, the *de novo* concept is a set of erroneous incorporation nucleotides during DNA replication involved in sporadic diseases (**Figure 3.1**) (Acuna-Hidalgo et al., 2016; Ségurel et al., 2014). The development of WES allows the detection of new genetic drivers. For this reason, gaining insight into childhood melanoma genetics knowledge is crucial to improving early diagnosis and therapies.

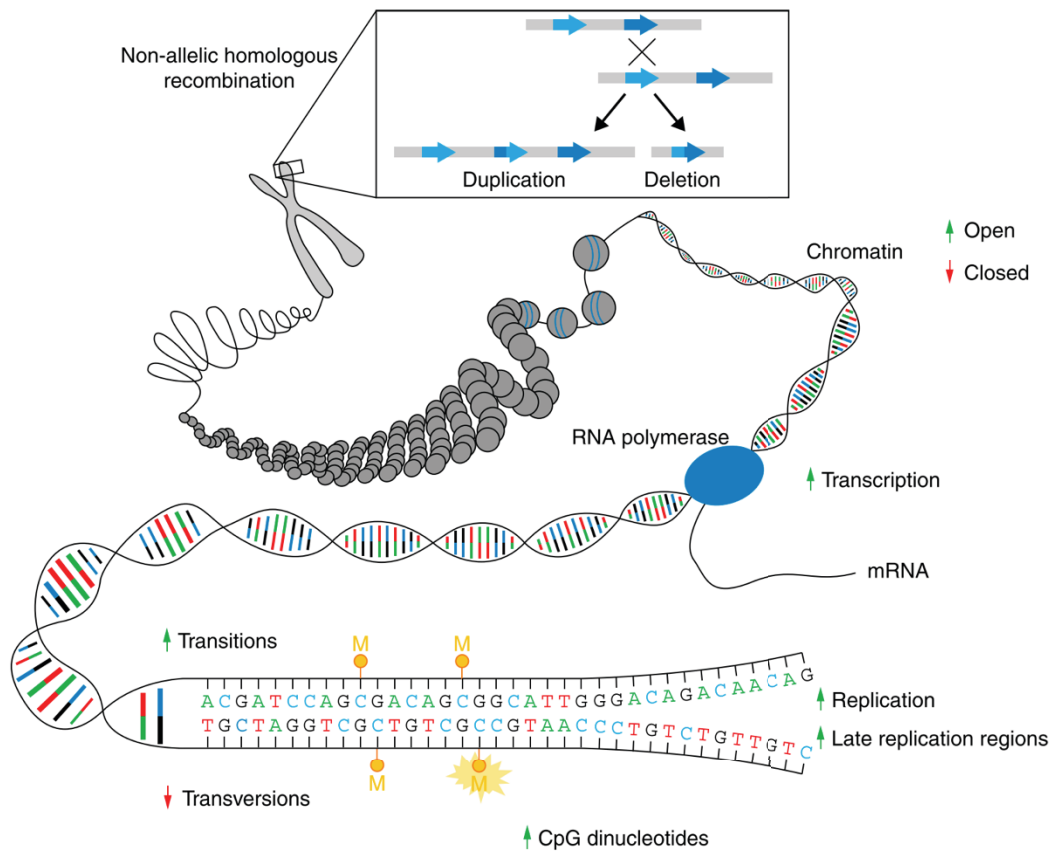


Figure 3.1 Mechanism of *de novo* mutations

De novo mutations can arise due to transitions, transversions or erroneous pairing of nucleotides during DNA replication. Moreover, de novo mutations can also occur in relation of chromatin state transcriptional state and gene expression levels. Green arrows pointing upwards indicate high mutability, while red arrows pointing downwards indicate lower mutability. Adapted from Acuna-Hidalgo (2016).

3.2 *De novo* mutations

De novo mutations are recognized both as an important source of genetic variation and as a prominent cause of sporadic disease in humans. *De novo* mutations are thought to occur predominantly in the egg or sperm cell, and this results in an embryo with a constitutive mutation. A *de novo* mutation can occur pre-zygotically in an oocyte or sperm cell, and upon fertilization, it results in an embryo with a germline mutation. The zygote carries a constitutive germline mutation present in all cells of the organism (reviewed in Acuna-Hidalgo et al., 2016). However, *de novo* mutations can also appear post-zygotically, leading to embryonic mosaicism, a state in which two or more genetically distinct cell populations in an individual develop from a single fertilized cell.

3.2.1 Mosaicism in *de novo* mutations

Due to technological improvements allowing the detection of low-level mosaic mutations at a genome-wide scale, mosaicism has been recognized to have an important role in human biology and disease. A somatic *de novo* mutation can occur post-zygotically in early embryonic cells leading to embryonic mosaicism. The post zygotically *de novo* mutation results in two or more cell lines with different genotypes implicated in several human diseases, ranging from developmental disorders to cancer (Biesecker & Spinner, 2013; Dal et al., 2014). Mosaicism arises from genetic alterations, including SNVs, CNVs, and simple or complex chromosomal rearrangements.

3.2.2 Timing of *de novo* mutations

The timing of a *de novo* mutation influences the risk of recurrence of disease and the tissue distribution of the cells in the offspring (Acuna-Hidalgo et al., 2015). Germline *de novo* mutations originate from errors in DNA replication during gametogenesis. To discriminate between germline *de novo* mutations from early and late post-zygotically mutations by DNA sequencing, it is crucial to estimate the biological allele frequency (AF) generated by WES. The AF represents the percentage of sequence reads carrying a mutant allele on an individual disease patient. In other words, the allelic ratio is the proportion of variant reads from the total number of sequencing reads covering a given base pair and is expressed as a percentage (Acuna-Hidalgo et al., 2015). A Sanger sequencing method is necessary when AF is lower than 15% to verify errors in repeated

sequences in the genome produced by either hybridization or bio information NGS sequencing. Sanger sequencing is less sensitive but does not present these artifacts.

An inherited germline mutation originates from errors during gametogenesis in one zygote of the parents. The variants are assumed to be germline origin when the allele frequency is approximately 50%, but a range between 30% and 70% is commonly accepted as representative of a heterozygous pathogenic variant. Once the mutation is transmitted to the embryo, they are present in all tissues of the offspring (reviewed in Acuna-Hidalgo et al., 2016; Poduri et al., 2013) **(Figure 3.2)**. Another possible event is *de novo mutation* presented in the affected offspring but not detected in the parents. These *de novo* mutations are present in the sperm or egg of one parent and not detectable in their blood; once transmitted to the embryo, they are present in all tissues of the offspring (Poduri et al., 2013). If the AF is lower than 50%, it can be considered an early post-zygotic mutation **(Figure 3.2)**.

A late post-zygotically *de novo* mutation is detectable in the affected lineage tissue through biopsies/tumor, from early development to when the samples were analyzed (reviewed (Acuna-Hidalgo et al., 2016; Jonsson et al., 2021). For metastasis disease in which the primary tumor cannot be biopsied, those mutations can also be detectable in a blood sample as circulating tumor cells (CTC) and circulating cell-free tumor DNA (ctDNA) (Haber & Velculescu, 2014). CTC in cancerous melanocyte cells undergoing EMT from the primary tumor site disseminates through the bloodstream and forms secondary tumors. The ctDNA are small nucleic acid fragments that freely circulate through the bloodstream without association with specific cells or fragments (De Souza et al., 2017). The AF in the blood can give an idea of the timing of the mutation in embryo development. In tumors, the percentage of tumoral cells helps to interpret the AF. If the percentage of tumor cells is high, the AF is purely related to tumoral cells. In the case of low AF, the AF is artificially decreased by normal cells contamination. Notably, *de novo* mutations, either as early or late post-zygotically, activating oncogenes or tumor suppressor genes could explain the occurrence of childhood melanoma (Bressac-de Paillerets, 2020).

3.3 Preliminary data on childhood melanoma cases

3.3.1 Previous work done by Fanélie Jouenne in 2017

Previous PhD project from Fanélie Jouenne "*Apport du séquençage d'exomes constitutionnels dans l'identification de nouveaux gènes de prédisposition aux cancers, sarcomes et mélanomes pédiatriques*" in 2017 (HAL Id: tel-01587772) at the Institute Gustave Roussy yield a list of

candidate genes of childhood melanoma from a collection of blood and a 6 frozen tumor samples from 55 trios, children with melanoma and their healthy parents. The WES were generated at the French National Centre for Genotyping (CNG, Evry, France), CEA, Dr JF Deleuze.

The hypothesis in Fanélie Jouenne's thesis project was that sporadic pediatric melanomas occur due to a *de novo* genetic "accident" occurring either in a parental gamete or post zygotically during NC development (**Figure 3.2**). As a result, a ***de novo* germline mutation** corresponds to a mutation absent in the parents and present in all child's cells body, and a ***de novo* somatic mutation** corresponds to a mutation absent in their parents and present in one fraction of a child's cells, with a postzygotic origin.

The collection analyzed constitutes the blood and six frozen tumor samples of children before 19 years old without a family history of melanoma. Trios have been studied in two series considering the developmental melanoma timing and cell lineage affected. The first series consists of 30 trios considered a priority on the criteria of precocity of the melanoma of occurrence the melanoma, children between 3 to 18 years old. The second series consisted of 11 trios and 14 solos. Of the 11 trios, six children developed prepubertal melanoma (1 to 10 years old), and five children developed melanoma post-pubertal. Two children develop melanoma pre-puberty and 12 post-puberty in the solo samples. From these two series, six frozen tumors samples were available. A parameter considered was the presence of congenital naevus as a risk factor for developing melanoma. The risk of developing melanoma is higher in children with a giant CMN (as discussed above). Among the samples, the type of histology presented in the samples was mostly SSM, followed by NM, SMM, *in situ* melanoma (1 sample), and polypoïde.

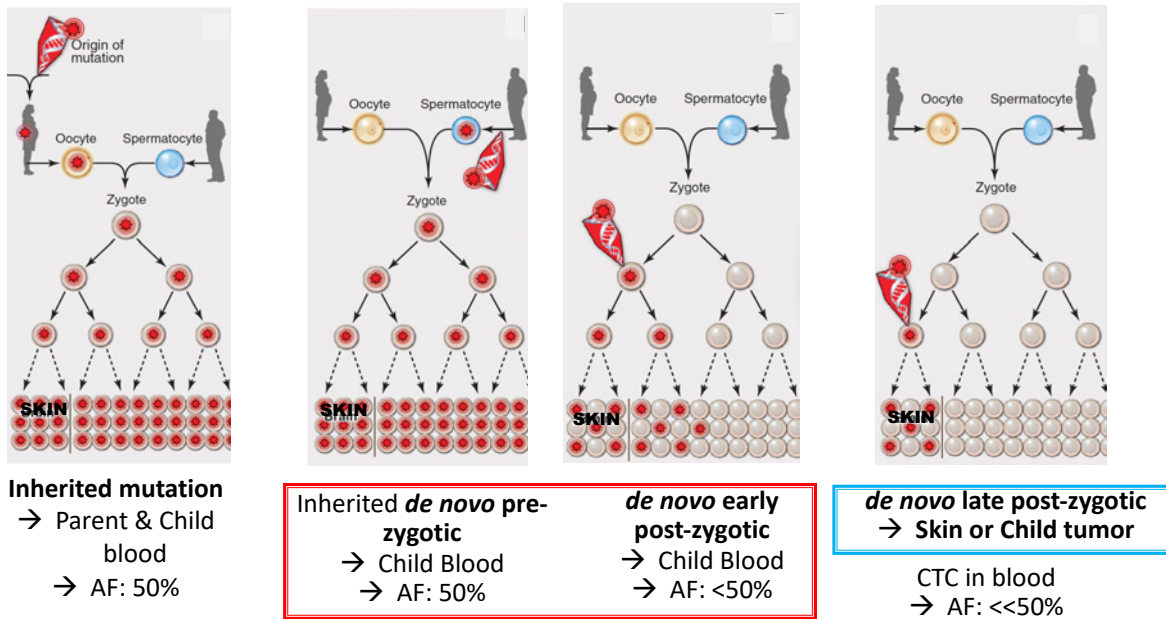


Figure 3.2 Inherited mutations and *de novo* mutations

The origin of an inherited mutation is related with the parental germ cell either from the father or the mother. It can be detected in blood samples from both parents and child. The AF is about 50%. A *de novo* mutation may arise sporadically during gametogenesis in one of the parents. It is present in the zygote and thus all cells of the affected child. The AF is about 50%. A *de novo* early post-zygotic mutation results in a mutation present in most or all tissues of the organism but in a mosaic fashion, with only a portion of all cells in each tissue harboring the mutation. The AF is about lower than 50%. A *de novo* late post-zygotic mutation can be detected in tumours or in blood of metastatic CTC. These mutations lead to individuals who are mosaic, only a subset of their cells harboring the mutation. The AF is less than 50%. AF= allelic frequency. Adapted from Poduri et al. (2013).

From this collection, the DNA extracted from 41 trios and 14 solos was analyzed by WES using 200X depth sequencing. WES analysis was performed at 200X for six frozen tumors to identify somatic events, an *extremely rare material*. The increased sequencing depth of 200X was used to improve mutation calling performance. Then, data mining was carried out by bioinformatic resources of the potential *de novo* variants using Ingenuity Variant Analysis (IVA) (Qiagen) software. The parameters used in the analysis were: 1) filter terms in the development of the NC or melanoma or cancer in the biology context filter and 2) using Combined Annotation Dependent Depletion (CADD). CADD is an integrative annotation that can score human SNV and short insertion and deletions in the reference assembly. CADD integrates the information from many various functional annotations and condenses the information into a single score (Rentzsch et al., 2019). They used a scaled CADD score above 20, meaning that a variant is predicted to be amongst the top 1% of deleterious variants in the human genome. Another parameter considered was the AF from blood and tumor samples, which hinted at the mutation timing in embryo development. In this study, the range accepted was between 26 to 60%, and higher than 60% for tumoral cells. If the AF is lower, it was possible to conclude that the mutation occurred early post-zygotically. As described above, *de novo* early or late post-zygotically mutations are possible to detect in samples tumors and CTCs.

After the genomic analysis, 14 genes were identified as *de novo* germline or post-zygotic in 14 trios out of 55 (**Figure 3.3**). All 14 genes are *in silico* connecting through literature information within a functional network of 13 known melanoma drivers and 16 cancer drivers using Ingenuity Pathway Analysis (Qiagen). Of the 14 candidate genes, we selected in this PhD project research, four candidate genes carrying *de novo* mutation as *de novo germline* and *de novo late post-zygotically* to perform functional analysis (**Table 2**).

In **trio 2**, a 12-year child developed an NM level IV and Breslow of 3.1 mm at the back, without non-congenital detection. The mutation corresponds to DS cell adhesion molecule, **DSCAM**, identified as c.4378G>A, p.G1460R, detected in the tumor and not in the blood sample, suggesting a *de novo* somatic late post zygotically mutation. The allelic frequency was 31%, and the percentage of tumoral cells was 50-80%.

In **trio 25**, then 7 years old child presented a melanoma at the knee level III and thickness of 1 mm, without ulceration. The mutation identified was the F-box protein 32, **FBXO32**, detected in blood samples as c.415G>A, p.G139S. The mutation corresponds a *de novo* germline mutation, AF 51%.

In **trio 28**, then 14 years old child presented melanoma at the back level IV, and Breslow 2.4 mm. The mutation identifies the gene Aldehyde dehydrogenase 1 family member L, **ALDH1L1**, as c.179G>A, p.R60H. The AF was 47%, considered a *de novo* germline mutation.

In **trio 30**, the child developed melanoma at the right eyebrow with congenital naevus of SMM type at level IV and thickness of 4,3 mm. The lesion was ulcerated. Unfortunately, the child died of brain metastasis. He presented a mutation at the gene **SOX10** identified at c.1298G>A, p.R433Q. The AF was 26% and considered as *de novo* germline mutations unaffected. Furthermore, his healthy twin brother carried the same mutation at AF12%.

At **trio 50**, the child developed melanoma at the back of the big toe level V, Breslow 1.1mm. Unfortunately, the child died at 13 years old. A somatic *DSCAM* mutation was identified at c.5473 G>C, p.E1825Q. AF 60%, 80% of tumoral cells.

At **Trio 52**, two mutations were detected, **NRAS** and **DSCAM**. *NRAS* somatic mutation was detected at c.181C>A, p.Q61K, and considered *de novo* late post-zygotically. With an AF of 90% and tumoral cells in 80%, they conclude that *NRAS* mutation is the earliest driver, as the mutation is identified in about 100% of tumoral cells. *DSCAM* mutation was detected in c.2905A>G, p.S969G identified as *de novo germline*. *DSCAM* mutations are considered constitutional since they were detected in the child's blood and tumoral cells, AF:49%, tumor samples, and 80% of tumor cells.

The identification of *de novo* variants in childhood melanoma by Dr. Fanélie Jouenne (2017) has been crucial for the elaboration of my thesis project. Four candidates' genes out of fourteen have been selected to perform functional analysis due to their **private** state as *de novo* mutation and the malignant melanocytic tumors in the patient's children sample. **My project will be one of the first research projects to understand childhood melanoma in a developmental biology environment to understand the role of *de novo* mutations. Furthermore, my PhD project attempt to understand the putative role of the selected candidate genes responsible for the occurrence of sporadic pediatric melanomas. To further elucidate the melanocyte's transformation under the transfection of *DSCAM*, *FBXO32*, *ALDH1L1*, *SOX10* candidates' genes in an NC developmental context and to give some hints from the unknown role of these genes in pediatric melanoma.**

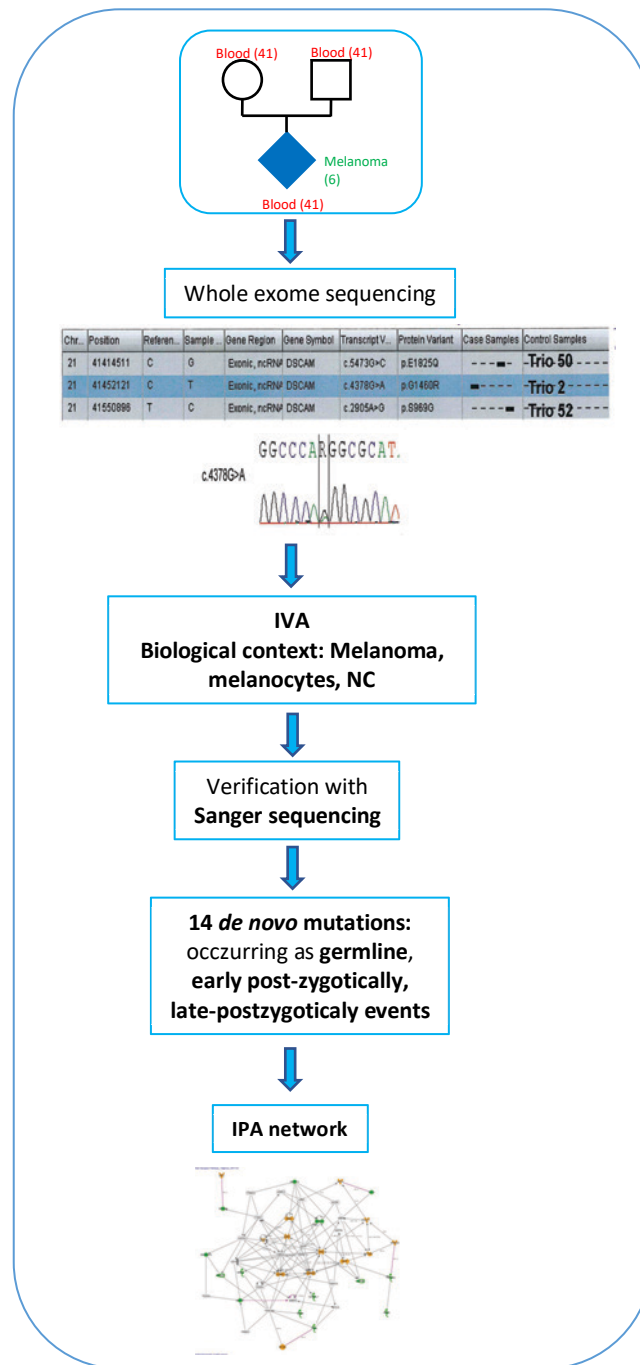


Figure 3.3 Workflow for the detection of de novo mutations in childhood melanoma.

PhD thesis done by Fanélie Jouenne (2017). HAL Id: tel-01587772, version 1 <https://tel.archives-ouvertes.fr/tel-01587772>

Table 2 4 out of 14 childhood melanoma candidate genes carrying a *de novo* mutations identified by WES.

Trio N°	Melanoma localization	Age at diag.	Congenital naevus	AF mutant (%)	Tumoral cells (%)	Identified gene	Locus	Mutation stage	Transcript Variant	Protein variant
2*	Back	12	NO	31	[50-80%]	<i>DSCAM</i>	21q22.2	somatic	c.4378G>A	p.G1460R
25	Knee	7	NO	51		<i>FBXO32</i>	8q24.13	<i>de novo</i> germline	c.415G>A	p.G139S
28	Dorsal	14	NO	47		<i>ALDH1L1</i>	3q21.3	<i>de novo</i> germline	c.179G>A	p.R60H
30	Eyebrow	11	NO	26		<i>SOX10</i>	22q13.1	<i>de novo</i> germline	c.1298G>A	p.R433Q
50*	Back of the left big toe	13	NO	56	[80-80%]	<i>DSCAM</i>	21q22.2	somatic	c.5473G>C	p.E1825Q

*Samples from freeze tumors, AF=Allelic frequency.

Key points of Chapter 3 – *de novo* mutation concept and the role in childhood melanoma

- of WES or WGS has revolutionized human genetic research for the identification of new cancer drivers, as well as new predisposition genes.
- *De novo* mutations have been shown to cause early-onset genetic disorders, including cancers.
- The timing during development and the AF is crucial for *de novo* mutation classification.
- *De novo* mutation could develop as *de novo* pre-zygotically, early or late post-zygotically.
- 14 variants in childhood melanoma were identified as *de novo* germline and somatic post zygotically detected by WES on TRIO samples collection (blood or six tumors) and datamining by AF, CADD, *in silico* connecting through literature by IPA and verification by Sanger sequencing.
- The starting line of my PhD thesis is the identification of genetic variants in children under 19-years with melanoma, previous work done by Fanélie Jouenne.

4 *FBXO32* gene in cancer research

4.1 *FBXO32* gene in cancer research

Among the four genes identified as childhood melanoma variants, we focused on the gene ***FBXO32*** to unravel its potential role during melanocyte development. F-box protein 32 (*FBXO32*), also known as atrogin-1/ MAFBX, is a recognition subunit of the SKP1–Cullin1–F-box protein E3 ligase involved in protein ubiquitination and degradation through the proteasome pathway (Bodine et al., 2001).

The F-box proteins were described as components of the SCF ubiquitin-ligase (E3) complex, which functions in phosphorylation-dependent ubiquitination and regulate a network of proteins with central roles in cell division, and cell growth, and differentiation (reviewed in (Wang et al., 2014). Structurally, the SCF complex consists of four subunits, an adaptor protein \underline{S} -phase kinase-associated protein 1 (SKP1), essential for the recognition and binding of F-box proteins for ubiquitination, a scaffold protein \underline{C} ullin, the RING proteins RBX, which recruits the E2 ubiquitin-conjugation enzyme binding and \underline{E} -box proteins that recognize specific substrates (Kipreos & Pagano, 2000) (**Figure 4.1**). The SCF complex facilitates interaction between substrates and ubiquitin-conjugated enzymes, which covalently transfer ubiquitin into substrates. Then, the poly-ubiquitinated substrates are degraded by the 26S proteasome.

F-box proteins are divided into three subclasses in relation to the specific substrate recognition and binding domains. The FBXW proteins contain WD-40 amino acid domains, FBXL proteins containing leucine-rich amino acid repeats, and FBXO, F-box only with uncharacterized domains (Randle & Laman, 2016). The F-box proteins are known for their function as a key regulator of the cell cycle and hallmark pathways in cancer (Randle & Laman, 2016) through modulation of ubiquitin-protein status.

The gene *FBXO32*, localized at 8q24.13 in humans, has been reported as TSG through different mechanisms. Chou and colleagues (2010) demonstrated that *FBXO32* is epigenetically silencing in ovarian cancer cells through DNA methylation, which disruption of TGF- β /SMAD4 signaling. Restoration of *FBXO32* reduced tumor growth *in vivo* and *in vitro* due to increased apoptosis of the cells (Chou et al., 2010). Furthermore, *FBXO32* targets the oncogenic protein c-Myc for

ubiquitination and degradation through the proteasome system. Overexpression of *FBXO32* suppresses c-Myc activity and inhibits cell growth, but knockdown of *FBXO32* enhances the c-Myc activity and promotes cell growth (Mei et al., 2015). In colorectal cancer, *FBXO32* expression levels were reported as high in normal colorectal and low in colorectal carcinoma cells with impaired TGF- β /SMAD4 signaling. Promoter hypermethylation may be one of the mechanisms for the inactivation of *FBXO32* in colorectal carcinoma cells (Yuan et al., 2018). In breast cancer, *FBXO32* is repressed in primary breast cancer tumors and contributes to 3-Deazaneplanocin A (DZNep), a chromatin modulator, in the apoptosis of MCF-7 breast cancer cells (Tan et al., 2007). Moreover, *FBXO32* degrades a zinc-finger transcription factor KLF4 (Krüppel-like factor 4) to suppress the breast cancer progression via the p38 mitogen-activated protein kinase pathway (Zhou et al., 2017).

The F-box family proteins have been described in their role in regulating EMT (Song et al., 2019). *FBXO32* dysregulation promotes the EMT process in urothelial carcinoma after-acquired platinum resistance. This was verified by the accumulation of MyoD proteins and the subsequent increase in the expression of mesenchymal marker Snail and vimentin, leading to enhanced migratory potential and reduced expression of the epithelial molecule E-cadherin (Tanaka et al., 2016). Recently, Sahu and colleagues (2017) reported the role of *FBXO32* in EMT regulation as a promoter of tumorigenicity and metastasis. They found that *FBXO32* was strongly amplified in metastatic cancers, and its depletion in an immunodeficient mouse xenograft model significantly inhibits tumor growth and metastasis, suggesting the potential as an oncogene (Sahu et al., 2017). In the same study, the author demonstrates that *FBXO32* directly targets CtBP1 for its ubiquitination and degradation, thereby controlling EMT activation and cancer metastasis in breast cancer cells with invasive properties (Sahu et al., 2017) .

Finally, Bertolotto and Balloti team in 2021 have shown that *FBXO32* is a new target of MITF (Habel et al., 2020). The authors demonstrated that *FBXO32* inhibits migration and proliferation *in vitro* and *in vivo* assays in adult melanoma cells. Moreover, they elucidate that *FBXO32* controls transcription by regulation of chromatin remodeling complex. Nonetheless, to date, we do not know the role of *FBXO32* in childhood melanoma.

Based on the extensive bibliographic research, the questions that come to mind for this research project are 1) are *de novo* mutations responsible for childhood melanoma, 2) Does *FBXO32*^{G139S} alter normal melanocyte development in a development environment using the chick embryo?

(a) The SCF E3 complex (plus Ubc and substrate)

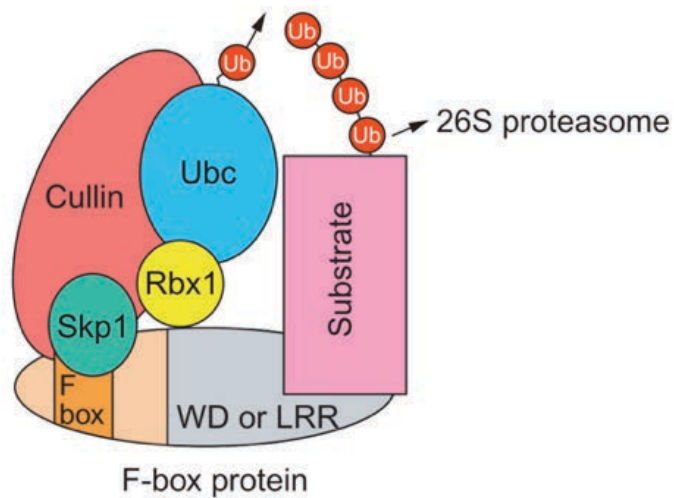


Figure 4.1 The SCF complex

This complex comprises of scaffold CULLIN, SKP1, RBX1/2 and F-box receptor. A ubiquitin-conjugating enzyme (Ubc) binds to the SCF complex and transfers ubiquitin (Ub) onto substrates bound by the F-box protein. When the substrate becomes poly-ubiquitinated, it is degraded by the 26S proteasome Adapted from Kipreoset and Pagano (2000).

Key points of Chapter 4 – *FBXO32* gene in cancer research

- *FBXO32* is a protein E3 ligase member of the F-Box protein family.
- F-box protein family is part of the SCF complex (SKP1, Cullin, and RING proteins) involved in the protein ubiquitination and degradation through the proteasome system.
- *FBXO32* is implicated in several cancers, such as ovarian, colorectal carcinoma, breast cancer, adenocarcinoma as TSG, and an oncogene in breast cancer.
- The role of *FBXO32* in childhood melanoma during development is unknown.

5 Objectives

Childhood melanoma is a heterogeneous group of malignant melanocyte tumors with variable genetic features that differentiate them from adult melanomas. This PhD project is a collaboration between Dr. Bressac-de Paillerets, whose expertise in the genetics field identified *de novo* candidates as drivers of childhood melanoma, and Dr. Creuzet, a developmental biology researcher with long expertise in NC research. The sequencing by WES from 55 pediatric melanoma cases and their healthy parents (blood and six frozen tumors) identified *de novo* germline or post-zygotic mutations in 14 genes. From this study, we have chosen four candidate genes, *FBXO32*, *SOX10*, *DSCAM*, and *ALDH1L1*, for pilot functional analysis.

The goal of this project has been first to **elucidate** the role between the candidate genes carrying *de novo* mutations and the occurrence of childhood melanoma during development. To understand the potential role of these variants in melanocyte development, I analyzed the consequences resulting from the silencing of these genes in the chick embryo. I used a powerful technique for the delivery of *dsRNA* by *in vivo* and *ex vivo* electroporation. Both techniques allowed me to investigate whether the silencing of these *de novo* variants could impair abnormal melanocyte differentiation at different developmental stages.

Because it has been described the role of the *FBXO32* gene as TSG/oncogene in various cancer, together with the unknowledge role of *FBXO32* in melanoma at the start of this project. We focused on *FBXO32* to study the **biological effect** of *FBXO32* and its variant during **neural crest cells and melanocyte development**. To this goal, I analyzed the consequences of the gene silencing in melanocyte differentiation, first at the trunk due to childhood tumors mostly arising in the extremities and trunk and second at a cephalic level in the chick embryo.

In parallel, I aimed to **elucidate the specificity** of **endogenous expression** of *FBXO32*. To do this, I investigated whether *FBXO32* impairs melanocyte development by restoring the normal melanocyte differentiation through the human cDNA wild-type form of the gene and the specific impact of the mutation by the human cDNA mutated form, *FBXO32*^{G139S}.

To **analyze** the potential role of *FBXO32* and its variant in the melanocyte progenitor cells, and the melanoblasts, I set up an *ex vivo* chicken embryonic skin explant technique. From this experiment, I observed that differentiated melanocytes are able to migrate back to the dermis.

Then, I wondered about the ability of the cells to migrate to the dermis. I studied **cell morphology** during **melanocyte transformation** by *in vitro* culture to answer this question.

Furthermore, I intend to identify the link between *FBXO32*^{G139S} and melanocyte transformation signaling pathway.

6 Material and Methods

6.1 Experimental model

6.1.1 The chick embryo as an experimental model

The chick embryo was used as an experimental model for functional studies at different developmental stages. Fertilized eggs were delivered every two weeks to the laboratory. For all experiments, eggs were incubated at $38.5\pm 0.5^{\circ}\text{C}$ until reaching the desired developmental stage. Embryos were staged according to Hamburger-Hamilton developmental table (HH: stage; E: embryonal day) (Hamburger & Hamilton, 1951). During the neurulation, the exact stage of development was further determined by counting the number of somite-pairs flanking the neural tube (ss: somite stage). *In vivo* experiments were performed at two levels along the anteroposterior axis, in order to involve different neural crest cell populations: the CNC and the TNC. Each of them was manipulated at different developmental stages to adapt the experimental design to their respective developmental program of neural crest cells or on the melanoblast/melanocyte specified lineage. *In vivo* functional studies in CNC were performed while the FNC cells are pre-migratory and still neuroepithelial, i.e. at 5ss, corresponding to 29 hours of incubation (E1.5). *In vivo* functional experiments in TNC were performed at 22ss, corresponding to 50-35 hours of incubation. For explants, functional assays were performed on CNC-derived melanocyte precursors at E10. To access and manipulate the developing chick embryo, a hole is made in the chamber air to pull down the vitellus and allow the opening of the shell without damaging the embryo. Then, a window is made by removing a small piece of the shell and after embryo manipulation, the window is sealed with a transparent tape before placing again the egg in the incubator at $38.5\pm 0.5^{\circ}\text{C}$ to allow the development until reaching the desired stage for analysis.

6.2 Gene silencing in the chick embryo

To analyze the role of the candidate genes in the normal development of the melanoblast/melanocyte lineage, we first performed loss-of-function experiments in a precise temporal and spatial manner by using the RNAi strategy to mediate gene silencing. The strategy was also used to switch off the activity of the endogenous gene and restore its function by using

the exogenous human wild-type sequence and comparing the specific effect of its mutated form. For both purposes, long-double stranded RNA molecules were synthesized from the complementary DNA molecule (cDNA) encoding the targeted gene (Aguiar et al., 2014; Pekarik et al., 2003). Gene silencing was assessed by *in vivo* and *ex vivo* electroporating the exogenous RNAs molecules in the CNC and TNC before the onset of cell migration, during chicken embryo development. According to this technique, *RNAi* molecules were produced against the transcripts of the following genes of interest: *FBXO32*, *SOX10*, *DSCAM*, and *ALDH1L1*

6.3 *In ovo* electroporation at the TNC and CNC

Two different strategies were designed to selectively electroporate TNC and CNC cells. At the trunk level, electroporation was achieved using a double electrode system, with one cathode flanking one side of the neural tube, and the anode flanking the other side. In this context, one truncal region becomes transfected while the contralateral region remains un-transfected (and can serve as an internal control). Before electroporation, nucleic acids were contrasted with a vehicle solution of 0.01% Fast Green solution (Sigma) diluted in *Phosphate Buffer Saline* (PBS) to carefully control the site of injection.

During neurulation at the cephalic level, the CNC cells mingle at the midline before spreading laterally. To avoid the mixture of transfected and un-transfected cells (which may bias the phenotypes), we optimized the transfection of CNC by performing bilateral electroporation at E1.5. In this context, the electroporation was achieved using a triple electrode system placed on the vitelline membrane with two cathodes flanking the developing head with a gap of 5 mm, and the anode facing the anterior neuropore (Creuzet et al., 2002). The triplex of electrodes allows generating a triangular electric field and yields the bilateral dispersion of nucleic acid sequences into the target cells (Creuzet et al., 2002; Garcez et al., 2014). The iterative electrical pulses lead to transient permeabilization of the cell membrane and allow the polarized displacement of exogenous nucleic acids which eventually become trapped in the cytoplasm of the permeabilized cells, as their cell membrane recovers its integrity (Garcez et al., 2014).

For both TNC and CNC, electroporation was achieved with five pulses of 27 Volts delivered by a square pulse generator (ECM 830 BTX, Harvard Bioscience). After electroporation, eggs were sealed and re-incubated at $38.5 \pm 0.5^\circ\text{C}$ until reaching E13.

6.4 *Ex vivo* skin explant electroporation

We set up a 3D *ex vivo* skin explant culture at the CNC level, to specifically target melanoblast lineage shortly before their differentiation into melanocytes. Skin explant was taken from E10 embryos. The head of the chick embryos was stabilized on a rubber holder (**Figure 6.1A**). The molecules of interest (RNAi) or cDNA encoding human sequences (*hFBXO32 WT* or *hFBXO32^{G1395}*) were micro-injected intradermally, at the level of the dorsal head, and then electroporated using a triplex of electrodes (**Figure 6.1B**). The skin corresponding to the dermis-epidermis area subjected to electroporation was then carefully dissected using micro-scissors for iridectomy (**Figure 6.1C**), and transferred into a Nunc IVF Dish (ThermoFisher), then plated to mimic the *in vivo* conditions (**Figure 6.1D**). Exogenic nucleic acids were selectively transfected into the dermis, without electroporating the epidermal layer of keratinocytes (**Figure 6.1E**). Explants were grown *ex vivo* for 4 days at 37°C, in 2 ml of Dulbecco's Modified Eagle Medium: Nutrient mixture F12 (DMEM-F12, without phenol red) enriched with 5% Goat Serum (Gibco™ by life Technology) + 1% Penicillin-Streptomycin (10000 U/mL) (Gibco™) + 1% Amphotericin B solution (Sigma). This 3D culture system favors the differentiation of feather buds (corresponding to the hairy buds in mammals) and preserves the capacity of the skin to develop according to anteroposterior and mediolateral body axes. For all genes of interest, we tracked melanocyte differentiation after 4 days.

6.5 Melanocyte cell culture

Melanocytes were isolated from the 3D *in vitro* skin explants (**Figure 6.2A, B**). After 4 days of *in vitro* culture, skin explant was washed with PBS + 1% Penicillin-Streptomycin (10000 U/mL) (Gibco™) + 1% Amphotericin B solution (Sigma). To separate epidermis from dermis, feather buds were dissected using micro-scissors and incubated in TrypLE™ recombinant enzyme (ThermoFisher) for 1h at 37°C (**Figure 6.2C**). Dissociation was stopped by adding the cell culture medium (the same cell culture medium as we used for 3D skin explants). After centrifugation for 5 min at 12,000g (**Figure 6.2D**), the pellet containing the epidermal tissue and the differentiated melanocytes was recovered in DMEM/F12. Feather buds and/or dissociated cells were cultivated Lab-Tek chamber slides previously coated with bovine fibronectin (20µm/ml, F1141, Sigma-Aldrich) containing 300µl of cell culture medium (Dulbecco's Modified Eagle Medium/Nutrient Mixture F-12 (DMEM/F12, Gibco) + 10 % fetal bovine serum (FBS, Sigma) + 1% PS + 1% fungizone. Cells were incubated in cell culture incubator Midi 40 (3404, ThermoFisher), at 37°C with 5% CO₂ conditions (Figure 14E) until confluence and fixed in 4% formaldehyde (PFA). Cell culture was

analyzed by immunocytochemistry and image acquisition performed on an Epifluorescence Leica microscope (**Figure 6.1F**). To evidence cell viability, we used LysoTracker™ deep red (Invitrogen, ThermoFisher Scientific) staining to track acidic organelles in live cells (Schaefer et al., 2004). Cell culture was incubated with LysoTracker (75nM) solution for 1h at 37°C, 5% CO₂, prior to cell fixation in PFA.

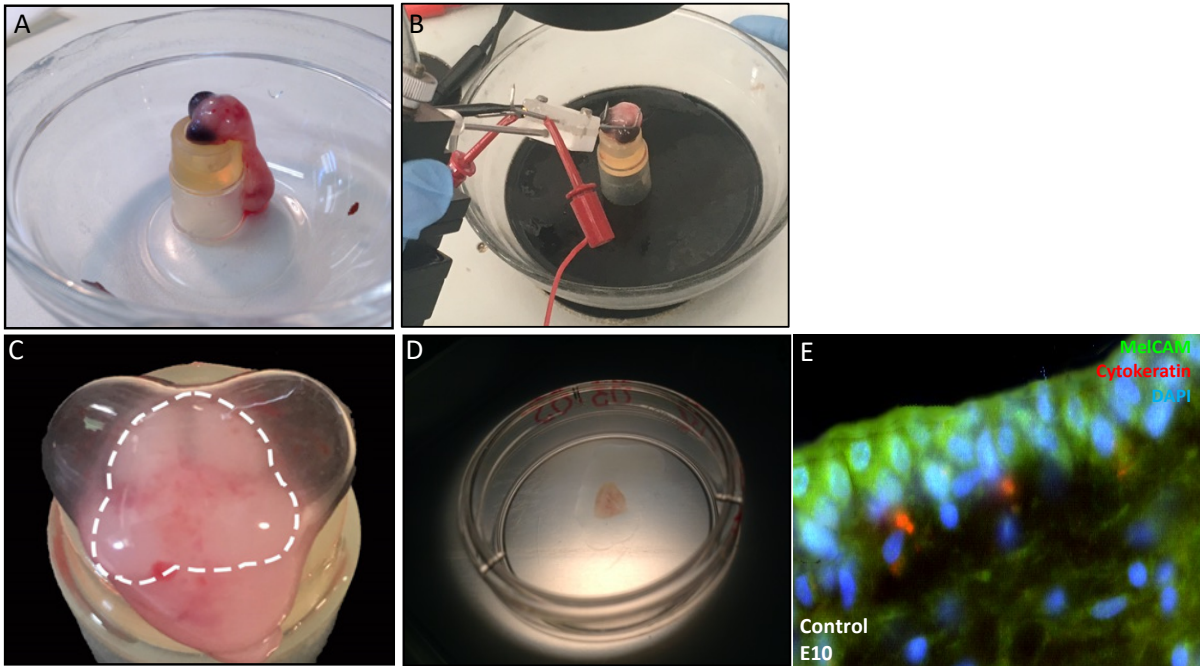


Figure 6.1 3D *in vitro* skin explant system.

A) Chick embryo E10 **B)** Melanoblast electroporation into the dermis, leaving keratinocytes un-transfected. **C)** Skin explantation. **D)** 3D *in vitro* skin explant. **E)** Immunofluorescence on skin explant against MelCAM, Cytokeratin

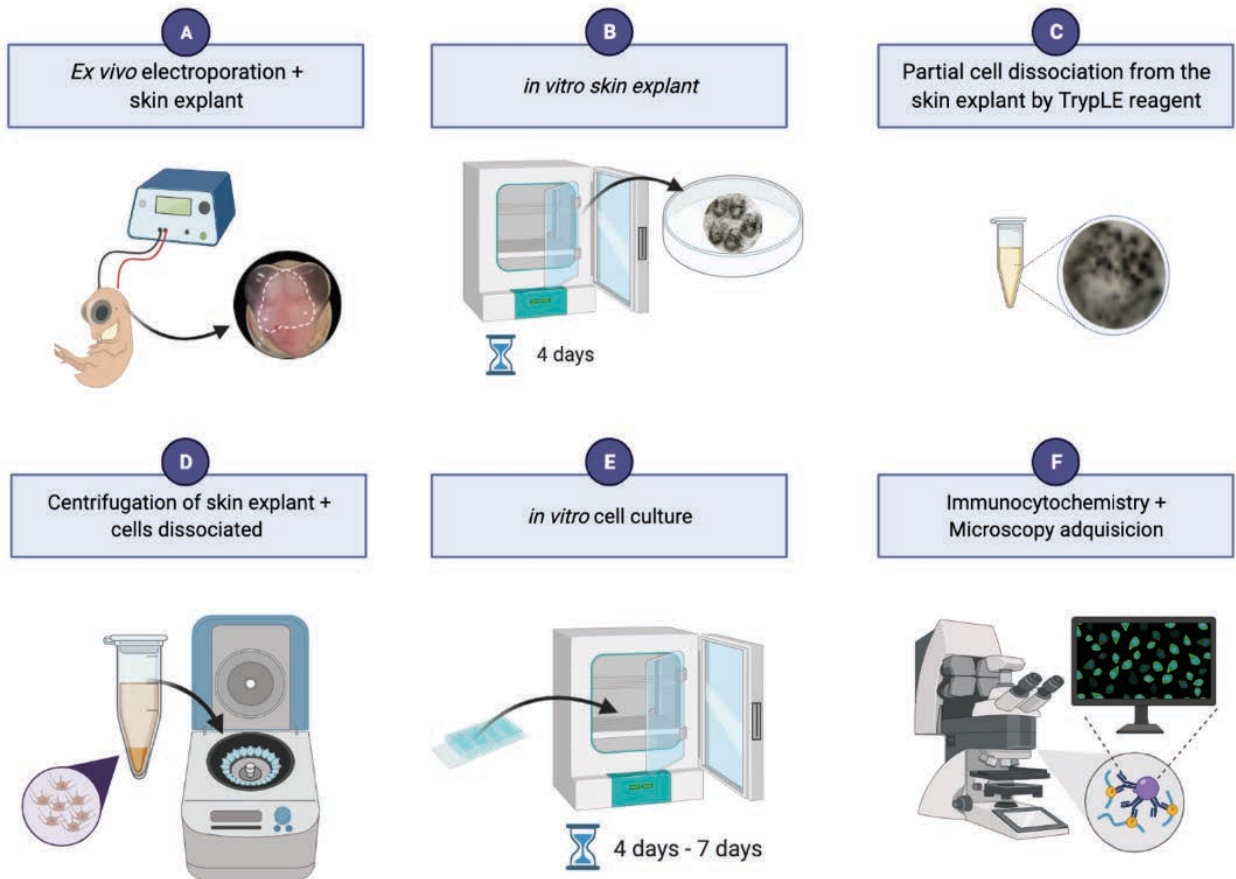


Figure 6.2 Melanocyte characterization by *in vitro* cell culture, created with Biorender.com

6.6 Plasmids and constructs

6.6.1 Construct to visualize CNC and TNC cell migration

To follow the migration of CNC and TNC embryos, pCAGGS-mCherry plasmid (Addgene n°41583; **Figure 6.3**) was injected in the lumen of the neural tube and electroporated in CNC cells at 7ss and in TNC at 14ss, respectively. Embryos were collected either 20h or 72h post-electroporation and fixed in PFA.

6.6.2 Chicken gene cloning and construct preparation

Chicken sequences encoding for *FBXO32*, *SOX10*, and *ALDH1L1* were cloned at the molecular biology platform I2GB (CNRS, Gif-sur-Yvette). Total RNAs from *Gallus gallus* tissues were extracted using the Qiacube automation robot (Qiagen) using the RNeasy Plus Mini kit (Qiagen). The corresponding cDNAs were synthesized by reverse transcription using the Maxima H Minus First-strand DNA synthesis kit (Thermo Scientific). For each of the three genes, two specific primers have been designed. The amplification of the sequence of interest was performed with the high-fidelity polymerase PFX (Invitrogen). This amplification product was then subcloned into the vector pCRII_TOPO_TA using the TOPO® TA Cloning® Kit (Invitrogen) (**Figure 6.4**). The subcloned sequence was validated by sequencing (**Figure 6.5**). The *DSCAM* plasmid was kindly donated by Dr. Yagamata (Department of Molecular and Cellular Biology and Center for Brain Science, Harvard University, Cambridge, Massachusetts 02138, USA; **Figure 6.4**): *DSCAM* fragment of 2kb was amplified from a chicken retina and cloned it into pGEMTeasy vector (Promega; (Yamagata & Sanes, 2008).

To investigate the specific role of the variant *FBXO32*, we performed rescue experiments by co-electroporating *dsFBXO32*, which generates the silencing of the endogenous gene, in combination with either human wild type: h*FBXO32* WT or mutated: h*FBXO32*^{G139S}. The simultaneous silencing of the endogenous gene and the expression of the mutant version of this gene allowed to unmask the specific role of the mutation. For rescue experiments, we used the pcDNA3.1 + C-eGFP plasmid carrying the human genes under the control of a cytomegalovirus (CMV) promoter (**Figure 6.6**). This rescue strategy does not rely on homologous recombination with the chick genome, but the CMV promoter yields a powerful expression of the exogenous sequence over 72h. Even though the plasmid is transiently active, its activity is sufficient to durably impact the fate of the cells until their final differentiation (Nakamura et al., 2004).

6.7 Bacteria transformation for plasmid replication

For transformation, 50µl library efficiently DH5α bacteria competent cells (Invitrogen) were thawed on ice and mixed with 3 µl plasmid of interest. Tubes were gently homogenized and incubated in ice for 30 min. After incubation, cells were heat-shocked in a 42°C water bath for 45 sec and immediately transferred on ice for 2 min. Then, 2 mL of Luria-Bertani (LB) medium (Invitrogen) was added to the cells and incubated for 1h at 37°C, to allow bacteria growth. Bacteria containing the plasmid were selected on LB agar (Invitrogen) containing the appropriated antibiotic-resistant gene, encoded by the plasmid, and incubated at 37°C overnight. The following day, we performed colonies screening for selection of recombinants and further incubated the colonies in 4-6 mL of LB medium at 37°C, overnight. Bacteria transformed were centrifugated at 4,000g for 30 min at 4°C. For long-term storage, glycerol stocks of transformed bacteria were prepared with 800 µL bacteria transformed and 200 µL glycerol and stored at -80°C. To recover bacteria from the glycerol stocks, we scraped some of the frozen bacteria off with a pipette tip, in sterilized conditions and incubated overnight with a 200 mL LB medium at 37°C.

6.8 Nucleic acid preparation

For loss-of-function experiments, RNA sense and antisense strands were synthesized from the cDNA encoding the target genes: *FBXO32*, *SOX10*, *ALDH1L1* and *DSCAM*. First, plasmid DNA purification was done using QIAfilter Plasmid Midi kits (QiAGEN). We followed the manufacture protocol which consists in (1) bacteria transformed pellet resuspended in lysis buffer, (2) adsorption of DNA into the QiAGEN membrane, (3) washing and elution of the plasmid DNA. Then, 10 to 20 µg of plasmid containing the cDNA of the interest gene was linearized by restriction enzymes for 2h30 at 37°C (Table 3). Linearized cDNA was used to enable *in vitro* transcription of antisense and sense strands. Synthesis of RNA sense and antisense strands was done by (1) *in vitro* using the matching RNA polymerases (**Table 3**) for 2 hours at 37°C, (2) DNA template degradation by the DNaseI free (Promega), and (3) RNA strands were precipitated by LiCl (0.5M), EDTA and EtOH 100% and cooling at -20°C, overnight. The RNA was isolated and stored at -80°C in 25µL DEPC-H₂O.

For silencing experiments, the stoichiometry of the sense and antisense strands were adjusted, and the single strands (ssRNA) were annealed for 5 min at 95°C, then purified (Pekarik et al., 2003). Non-annealed single-strand RNAs were eliminated by RNasin® ribonuclease inhibitor (Promega). To conduct efficient loss-of-function, the concentration of *dsFBXO32*, *dsDSCAM*, *dsSOX10*, and

dsALDH1L1 was set at 300ng/ μ l (Creuzet et al, 2004; Creuzet 2009; Garcez et al., 2014). For rescue experiments, *dsFBXO32* RNAs were co-transfected with the human wild-type and human mutated, *hFBXO32*^{G139S} cDNA at the concentration of 1.25 μ g/ μ l. For control experiments, ssRNA without annealing was electroporated according to the same paradigm.

Table 3. Vectors used in this study

Gene	Vector	Restriction enzymes		RNA polymerase		Size in pb	Authors
		Antisense	Sense	Antisense	Sense		
FBXO32	PCR TM II						
	TOPO [®] TA_	BamHI	XhoI	T7	SP6	3900	--
SOX10	PCR TM II						
	TOPO [®] TA_	BamHI	XhoI	T7	SP6	3900	--
ALDH1L2	PCR TM II						
	TOPO [®] TA_	BamHI	XhoI	T7	SP6	3900	--
DSCAM	pGEM- T Easy	SacI	NcoI	T7	SP6	3015	Yagamata, Sanes 2008

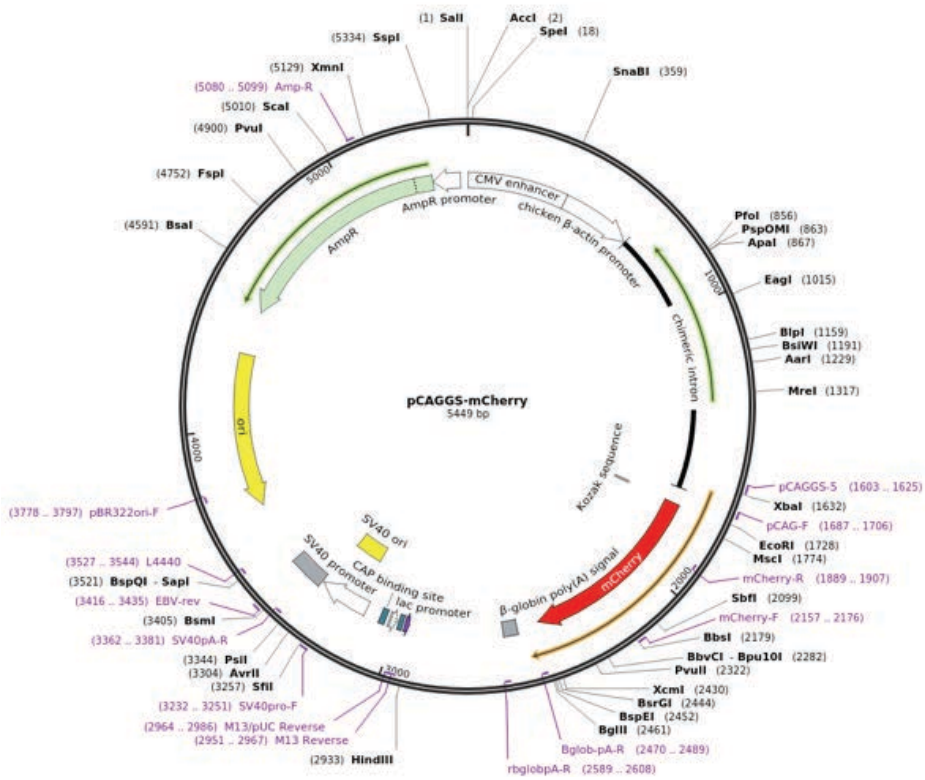


Figure 6.3 pCAGGS- mCherry plasmid to visualized NCC migration

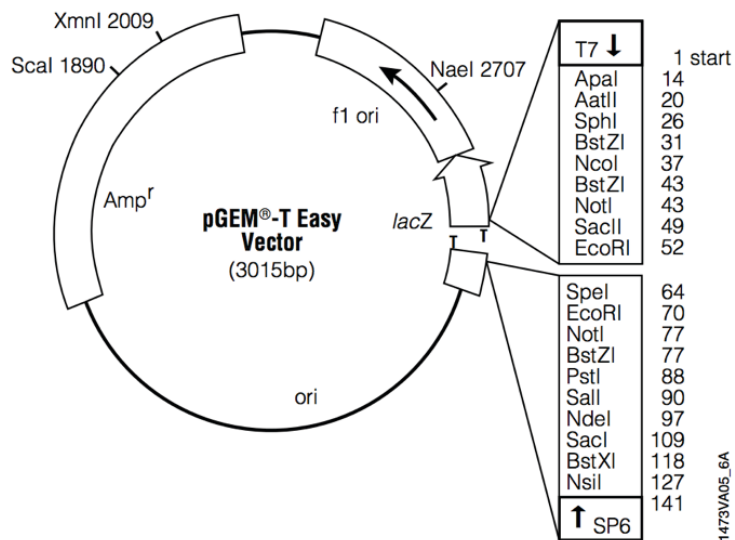
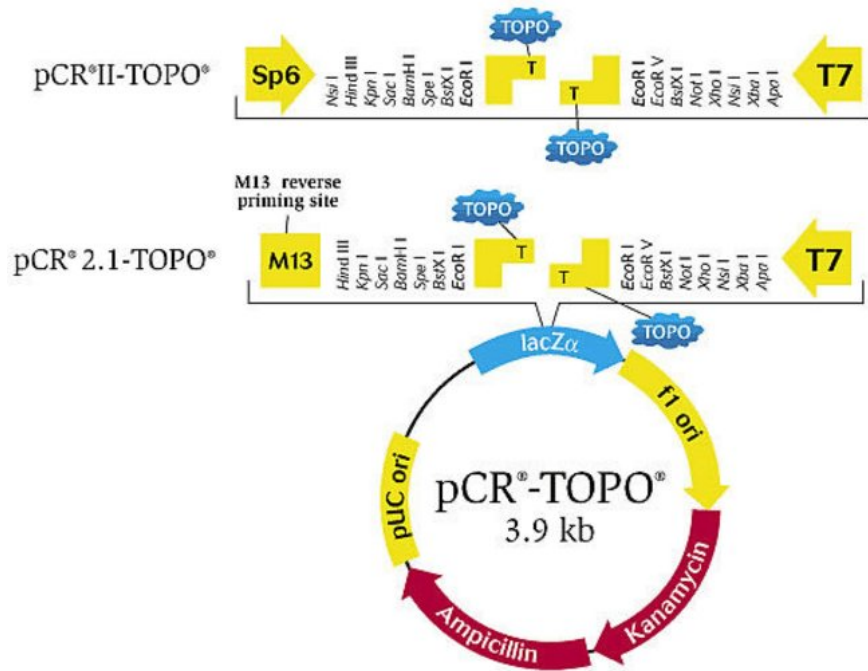


Figure 6.4 Plasmids used for gene silencing

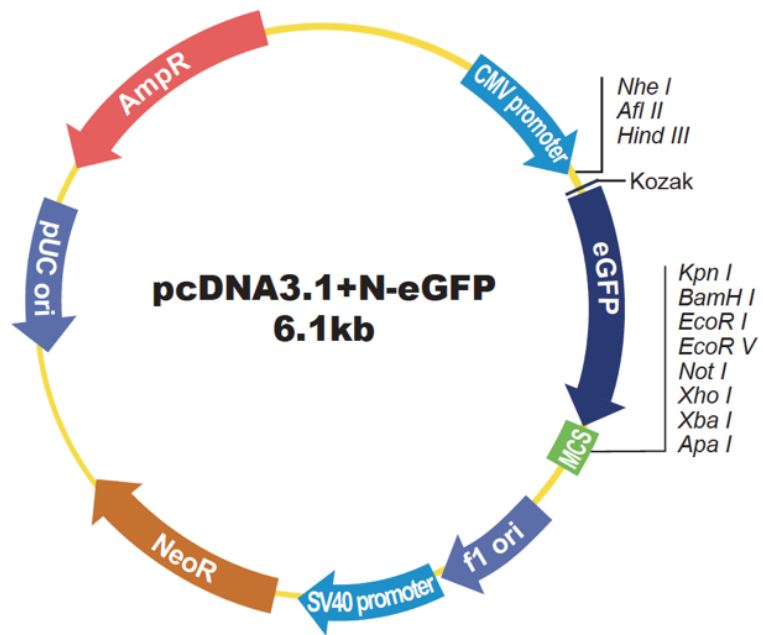


Figure 6.6 Plasmid used for rescue experiments

6.9 *in situ* hybridization

6.9.1 *in situ* DIG-labelled riboprobe synthesis

FBXO32, *SOX10*, *DSCAM*, and *ALDH1L1* antisense riboprobes were generated by *in vitro* transcription from the T7 RNA polymerase recognition sequence at one end. We used the RNA polymerase in the presence of a mixture of ribonucleotides, including DIG-UTP for 3h at 37°C. During this reaction, the DNA is transcribed to generate a large amount of full-length DIG-labelled RNA copies (10-20 µg RNA from 1 µg DNA in a standard reaction). After *in vivo* transcription DNaseI (10U/µL) was done to eliminate DNA strains. RNA probes precipitation was done by LiCl (0.5M), EDTA, and EtOH 100% and cooling at -20°C, overnight. The RNA probes were stored at -80°C in 25 µl sterile-filtered water treated with diethyl pyrocarbonate (DEPC) (SIGMA) before use.

6.9.2 *in situ* hybridizations on whole-mount embryos

Whole-mount *in situ* hybridizations (ISH) for *FBXO32*, *SOX10*, *ALDH1L1*, and *DSCAM* were performed on chicken embryos at 8ss, 14ss and 22ss fixed in 4% PFA. To verify gene inactivation in NCC, *in situ* hybridization was performed after dsRNA silencing in embryos 7-10ss. Fixed embryos in 4% PFA were washed in PBS 1X containing 0.1% Tween-20 (PBST). Embryos were dehydrated in a graded series of 25% and 50% methanol in PBST and incubated in 100% methanol for a cold shock at -20°C for 30 min. Then, embryos were progressively rehydrated in methanol + PBST for 10 min and rinsed twice in PBST for 10 min. Embryos were digested with 20µg/ml proteinase K (8, 14, 22 min for 8ss, 14ss, and 22ss, respectively) and post-fixed in 4% PFA + 0.1% glutaraldehyde for 20 min each. Prehybridization was performed by incubation with hybridization buffer (**Table 4**) for 1h at 70°C. Then, embryos were incubated with the corresponding DIG-labelled riboprobes diluted in 1 µg/mL hybridization buffer at 70°C, overnight.

On the second day, riboprobes were harvested and stored at -20°C, which can be re-used up to 4 times. The embryos were rinsed with pre-warmed hybridization buffer for 45 minutes, twice, then in MABT (2M maleic acid, 5M NaCl, 0.1% Tween-20, pH 7.5). Non-specific antibody binding was prevented by incubation in MABT with 2% blocking reagent and 20% goat serum for 60 minutes. Then embryos were incubated in AP-conjugated anti-DIG antibody (Roche, 1:1000 diluted in the blocking buffer) overnight at RT.

On the third day, the embryos were rinsed in MABT for 3h before a half-hour treatment with NTM (100 mM Tris, 100 mM NaCl, 50 mM MgCl₂, pH 9.5). Cephalic vesicles for embryo 22ss were opened to avoid the non-specific accumulation of the staining solution. The hybridization staining was developed in 20 µL /1mL of NBT/BCIP (Roche) at 37°C and protected from light.

Table 4. Hybridization buffer solution cocktail

Hybridization buffer solution
50% Formamide
1.3X SSC 20X pH5
5mM EDTA 500mM pH8
50µg/mL Yeast RNA (20mg/mL)
0.2% Tween 20X
0.5% CHAPS
100µg/mL Heparine (50mg/mL)
H ₂ O qsp

6.9.3 *in situ* hybridization on paraffin sections

Paraffin sections of 7 μ m-thick were used for *in situ* hybridization with a DIG-UTP-labelled probe in a 1 μ g/mL hybridization buffer. First, the sections were deparaffined by 3 times toluene baths, progressively rehydrated in graduate ethanol dilution (100%, 90%, 70%, and 30%), then digested with 20mg/mL proteinase K for 14 min, post-fixed in 4% PFA and rinsed with PBS + saline- sodium citrate (SSC) buffer (3M NaCl, 0.3 M Sodium citrate), pH 7.5.

After overnight hybridization at 70°C with the corresponding riboprobe, the slides were washed twice in 50% formamide + 1X SSC at 65°C, then in MABT, pH 7.5 at room temperature (RT). Nonspecific antibody binding was blocked by incubation in MABT with 20% goat serum and 2% blocking reagent for 90 minutes. Blocking solution was replaced with anti-DIG antibody (1:2000) diluted in MABT and 20% blocking reagent on each slide and covered with a glass slide for overnight incubation at RT. The following day, slides were rinsed in MABT for 3h before a half-hour treatment with NTM. NBT/BCIP diluted in NTM was finally applied and kept in a humid chamber at 37°C until the revelation. Slides were mounted in Aquatex (Merck).

6.10 Paraffin embedding for immunocytochemistry

Chick embryos at E13 were processed for paraffin embedding and sectioning. First, embryos were first fixed in 4% PFA, to take photos avec their gross-anatomy and feather phenotypes, and then further fixed in 60% ethanol, 30% formaldehyde (37%, stock solution), and 10% acetic acid (100%, stock solution), for 48 at RT for paraffin embedding. Then, E13 embryos were dehydrated in ethanol 100% (Probal) and permeabilized for paraffin embedding in Toluene (Fisher) for at least 24h. Once impregnated with toluene, the embryos were placed on the surface of hardened paraffin (Paraplast, Sigma) and incubated at 60°C overnight. Embryos were included in a block of paraffin block, and their orientation was precisely controlled according to the desired sectioning plan. Once embedded, embryos were cut into 7 μ m sections in a LEICA RM2235 microtome, collected on super frost-plus slides (Thermo Scientific), and dried at 37°C for 24h.

6.11 Immunocytochemistry

6.11.1 Whole embryos

Immunocytochemistry was performed on whole-mount embryos to visualize the NCC and check the efficacy of their transfection after electroporation. To do so, we used two monoclonal antibodies (Abs), HNK1 (Santa-Cruz) to evidence NCC, and anti-FBXO32 (Abcam) to evidence the protein produced by the gene of interest. After incubation with the corresponding secondary Abs, embryos were imaged under Leica MZFLIII fluorescence stereo zoom microscope and AxioImager M2 (Apotome, ZEISS).

6.11.2 Truncal paraffin section

Paraffin sections at cephalic and trunk levels were deparaffinized by successive baths in toluene, then ethanol 100%, and finally PBS 1X (10 min each). Slides were blocked for 2h using PBS 1X + goat serum and 0.1% Triton-X 100 at RT. The sections were incubated with primary monoclonal Abs against DOPA decarboxylase (Invitrogen), FBXO32 (Abcam), and polyclonal Abs against TYR (ThermoFisher), TYRP1 (ThermoFisher), MITF (ThermoFisher) and MelCAM (Santa Cruz Biotechnology). The following day, slides were rinsed three times in PBS 1X and incubated with secondary Abs conjugated to Alexa fluor® 488, Alexa fluor® 59 as fluorophores, then mounted in Fluoromount-G™ with DAPI (Invitrogen). Imaging acquisition was carried out on a Leica Epifluorescence DM100 or a Confocal Leica SP8 microscope.

6.11.3 Culture cells

Cell cultures were fixed in 4% PFA for 20 min at RT and rinsed three times with PBS 1X. Cells were permeabilized in 0.1% Triton-X 100 in PBS 1X for 15 min at RT, then, rinsed three times in PBS 1X and incubated with primary monoclonal Abs against MelCAM (Santa Cruz Biotechnology SC-18837); polyclonal Abs against Phospho-Paxillin (ThermoFisher 44-720G); Cytokeratin (ThermoFisher MA5-13205); FBXO32 (Invitrogen PA5-66751); MITF (ThermoFisher). Before incubation with the secondary Abs, cells were treated with Alexa Fluor™ 633-conjugated phalloidin, a high-affinity F-actin probe (1:40 diluted in methanol) for 40 min at RT to evidence actin filament cytoskeleton and rinsed 3 times with PBS 1X. Incubation with the fluorophore-conjugated secondary Abs was performed all day long. Slides were mounted with Fluoromount-G™ with DAPI (Invitrogen). Imaging acquisition was done in a Leica Epifluorescence DM100, digital camera HAMAMATSU ORCA-R² C10600, or Confocal Leica SP8 microscope.

6.12 Fluorescence images and data analysis

Embryos were imaged under a stereomicroscope Leica Wild M10 equipped with a digital camera micropublisher 3.3 RTV and digitalization using Q-capture 6.0 software. Whole embryos *in situ* hybridization were imaged using a Leica MZFLIII fluorescence stereo zoom microscope, digitalization was done in InfinityAnalyze 6.3.0 software. *In situ* hybridization sections were imaged using transmitted light under the EVOS M5000 microscope (Invitrogen). Whole-mount staining was imaged under Leica MZFLIII fluorescence stereo zoom microscope and Axiolmager M2 (Apotome) (ZEISS). Immunohistochemistry sections were imaged under a fluorescent microscope (Leica) equipped with a digital camera C10600 Hamamatsu Orca-R², Germany. Digitized images were adjusted in contrast and brightness by the Adobe Photoshop software. For 3D rendering, we used Imaris Software. Methodology images were created in BioRender.com

6.12.1 Statistical analysis

ImageJ2 software was used for all image analysis. All data plots and statistical analysis was determined by Prism 9.3.1(Graphpad) software. Quantification results were compared using Bartlett's with Dunnett's multiple comparisons test. A P value of <0.05 was considered as significantly difference.

6.13 Bulk RNA sequencing

For RNA sequencing analysis, 3 biological samples were harvested for each sample. Each condition was analyzed in triplicates on samples involving either CNC or TNC experiments. The only exception is the rescue *hFBXO32 WT* in CNC for which only 2 replicates could be collected (**Table 5**). RNA extraction was performed by (1) precipitation with TRI reagent® (SIGMA-AIDRICH) and 2-propanol, (2) RNA pellets were washed with 75% ethanol, follow by (3) RNA pellet air-drying and (4) RNA was recovered in DEPC-H₂O (SIGMA). RNA concentration was 200ng/μl for each sample. Then, the first cDNA strand synthesis was synthesized randomly by hexamer primer M-MuLV reverse transcriptase and the second cDNA strand was synthesized using DNA polymerase I and RNase. Libraries fragments were purified and sequenced on Illumina Novaseq platform, and 150 bp paired ends reads were generated. Gene model annotation files were downloaded from genome website directly and we used as reference genome *Gallus gallus* (genome ID: ensembl_gallus_gallus_grcg6a_gca_000002315_5).

6.13.1 Computational analysis

For quantification of gene expression level, FeatureCounts v10.5-p3 was used to count the read numbers mapped for each gene. Then, the reads per kilobase of exon per million reads mapped (FPKM) of each gene was calculated on the length of the gene and the reads count mapped for this gene. The expected number of FPKM considers the effect of the sequencing depth and gene length for the reads count at the same time. This method is currently the most used method for estimating gene expression levels. Differential expression between two conditions/groups (**Table 6**) was performed using DESeq2 R package (1.20.0), based on the negative binomial distribution by Novogene company. The resulting P-values were adjusted using Benjamini and Hochberg's method for controlling the false discovery rate. Adjusting the rate helps to control the fact that sometimes small P-values (less than 5%) happen by chance and will result in false positives. Genes with an adjusted P-value <0.05 found by DESeq2 were assigned as differentially expressed.

Prior to differential expression analysis, for each sequenced library, the reads counts were adjusted by the edgeR program package. Differential expression analysis of two conditions was performed by using the edgeR package. The P values were adjusted with Benjamini and Hochberg's method. Correct P-values of 0.05 and absolute FoldChange of 2 were set as thresholds for significant differential expression. Hierarchical clustering was performed using Pearson correlations. Clustering was achieved using base principal component functions in edge R. Gene Ontology (GO) enrichment analysis of differentially expressed genes was implemented by the cluster Profiler package, in which gene length bias was correct. GO terms with a correct P-value less than 0.05 were considered significantly enriched by differential expressed genes. KEEG database resource for understating high-level functions of the biological system, such as the cell, form molecular-level information, and high-throughput experimental technologies (<https://www.genome.jp/kegg/>). Novogene company used the cluster ProfilerR package to test the statical enrichment of differential expressed genes in KEEG data.

Table 5. Total number of skin explant analysis

Neural crest anatomical level	Biological samples	Number of embryos	Replicates
Trunk	Control	9	3
	<i>dsFBXO32</i>	9	3
	hFBXO32 MUT	9	3
	hFBXO32 WT	9	3
Cephalic	Control	9	3
	<i>dsFBXO32</i>	9	3
	hFBXO32 MUT	9	3
	hFBXO32 WT	9	2

Table 6. Samples comparisons for differential expression analysis

Neural crest anatomical level	Comparisons of differential expression ("Treatment" vs "Ctl")
Trunk	<i>dsFBXO32 vs Ctl</i>
	<i>hFBXO32 WT vs dsFBXO32</i>
	<i>T-hFBXO32 MUT vs dsFBXO32</i>
	<i>hFBXO32 WT vs Ctl</i>
	<i>hFBXO32 MUT vs Ctl</i>
	<i>hFBXO32 MUT vs hFBXO32 WT</i>
Cephalic	<i>dsFBXO32 vs Ctl</i>
	<i>hFBXO32 WT vs dsFBXO32</i>
	<i>hFBXO32 MUT vs dsFBXO32</i>
	<i>hFBXO32 WT vs Ctl</i>
	<i>hFBXO32 MUT vs Ctl</i>
	<i>hFBXO32 MUT vs hFBXO32 WT</i>
Truncal vs Cephalic	<i>C-Ctl vs T-Ctl</i>
	<i>C-dsFBXO32 vs T-dsFBXO32</i>
	<i>C-hFBXO32 WT vs T-hFBXO32 WT</i>
	<i>C-hFBXO32 MUT vs T-hFBXO32 MUT</i>

6.14 Fluorescence images and data analysis

The cephalic and trunk level of the embryos were imaged under a stereomicroscope Leica Wild M10 equipped with a digital camera micropublisher 3.3 RTV and digitalization using Q-capture 6.0 software. Whole embryos *in situ* hybridization were imaged using a Leica MZFLIII fluorescence stereo zoom microscope, digitalization was done in infinity analyze 6.3.0 software. *In situ* hybridization sections were imaged using transmitted light under EVOS M5000 microscope (Invitrogen). Whole mount staining were imaged under Leica MZFLIII fluorescence stereo zoom microscope and Axiomager M2 (Apotome) (ZEISS). Immunohistochemistry sections were imaged under a fluorescent microscope (Leica) equipped with a digital camera C10600 Hamamatsu Orca-R², Germany. Digitized images were adjusted in contrast and brightness by the Adobe Photoshop software. For 3D rendering we used Imaris Software. Methodology images were created in BioRender.com

7 Functional analysis of *FBXO32*, *SOX10*, *DSCAM*, and *ALDH1L1* candidate genes

7.1 Childhood melanoma candidate genes *FBXO32*, *SOX10*, *DSCAM*, and *ALDH1L1* are expressed at the NC

To reveal the temporal and spatial regulation expression of *FBXO32*, *SOX10*, *DSCAM*, and *ALDH1L1* during NCCs development, we performed a series of *in situ* hybridizations at different developmental stages from emigrating NCCs to melanocyte differentiation at the epidermis level (**Figure 7.1**). The *FBXO32*, *SOX10*, *DSCAM*, and *ALDH1L1* transcripts were all detected in the early neural stage (7 somite stage: ss) at the margin of the neural plate in the anterior midbrain and posterior midbrain (**Figure 7.1A, D, G, J**), the *ALDH1L1* expression was also observed down to the anterior rhombencephalon NF and further down to r6 (**Figure 7.1J**).

After the onset of NCCs migration, CNC migrated in *FBXO32*, *SOX10*, *DSCAM*, *ALDH1L1*, and expression was observed in the facial neural crest (FNC) derived mesenchymal cells at stage 24-26ss. The *FBXO32* expression was observed in migrating NCC from the nasofrontal to the retro-ocular region and in the neuroepithelium of the future pigmentary retina at 24ss (**Figure 7.1B**). Similarly, this gene is expressed in the olfactory placode of the nasofrontal region. The cephalic vesicles were negative for *FBXO32* transcripts except for the outer edges. The *SOX10* and *ALDH1L1* expression was limited to the retro-ocular region of embryos 26ss and 24ss, respectively (**Figure 7.1E and K**). The *DSCAM* transcripts were delimited at the nasofrontal neuroepithelium, and the cephalic vesicles were negative except for the junction between the hindbrain and midbrain (**Figure 7.1H**). These areas are significant because they constitute the organizing centers of the midbrain and forebrain, the isthmus, and the anterior neural ridge. All genes are expressed in the 3rd branchial- arch, the territory of the epibranchial placode at the origin of the petrous ganglion of the glossopharyngeal nerve (IX) (**Figure 7.1B, E, H, K**).

After melanocyte differentiation, at thirteen days of development (E13), transcripts of *FBXO32*, *SOX10*, *DSCAM*, and *ALDH1L1* were detected at the epidermis level with polarization toward the dermis and not in the bud soma/pulp of the feather bud (corresponding to the dermis) (**Figure**

7.1C, F, I, L). Moreover, At the trunk level, *FBXO32* transcripts were confirmed at the TNC by *in situ* hybridizations in embryos 28ss (**Figure 7.1M and N**).

We can decipher that the candidate genes are defined in the melanocyte lineage. Thus, the genes whose mutations have been identified in children with melanoma are well expressed in the chicken model at different developmental stages. Therefore, we assessed the potential role of the genes by functional analysis in the NC differentiation and melanoblast/melanocyte lineage.

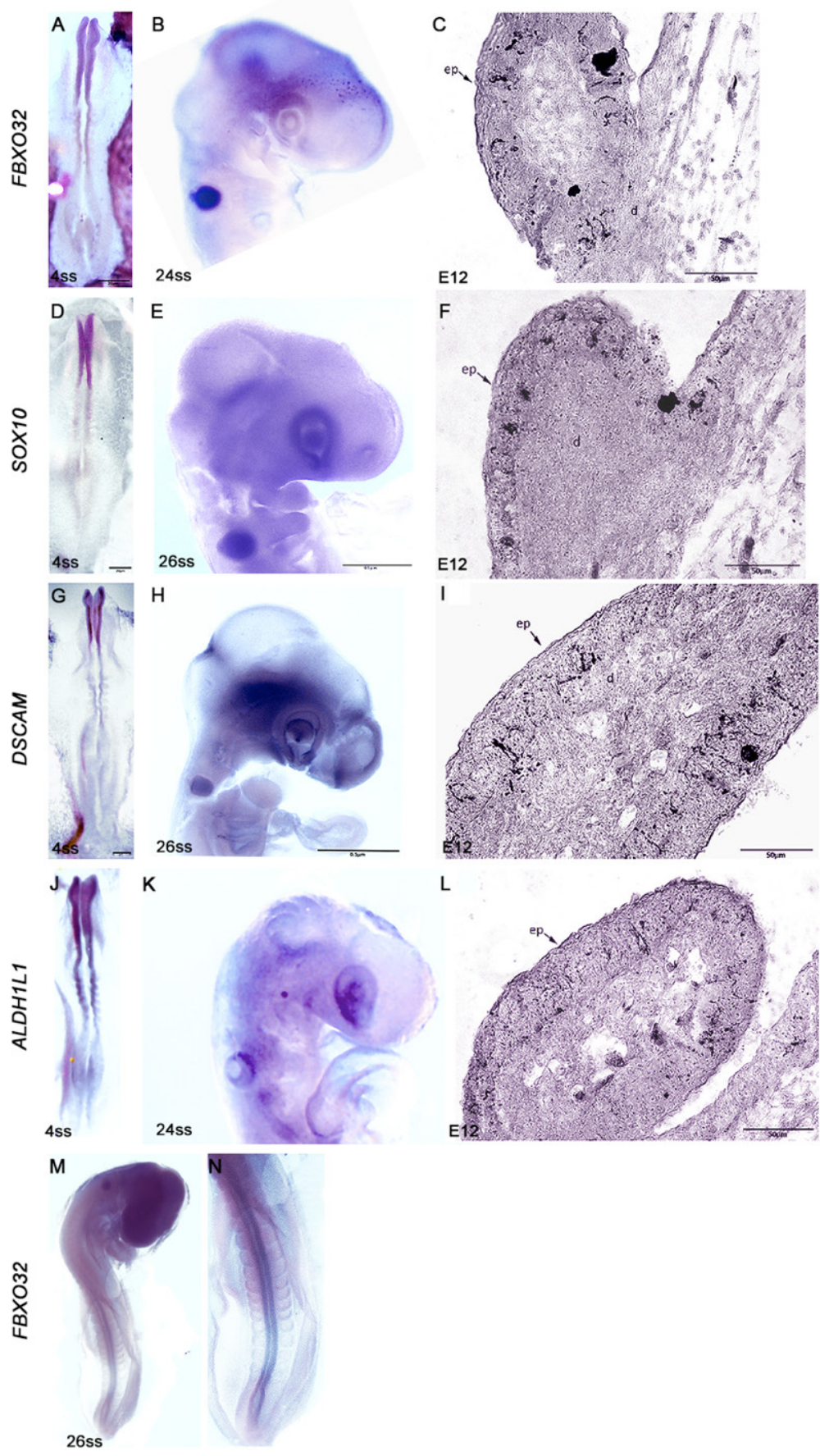


Figure 7.1 FBXO32, SOX10, DSCAM and ALDH1L1 transcripts are expressed in the CNC and TNC at different developmental stages

A) *FBXO32*, **D)** *SOX10*, **G)** *DSCAM*, **J)** *ALDH1L1* transcripts are expressed in migratory FNC at 4ss embryos. Lateral views of hybridizations for **B)** *FBXO32*, **E)** *SOX10*, **H)** *DSCAM*, **K)** *ALDH1L1* at 24-26ss embryos. Transcripts are accumulated in migrating NCC at naso-frontal, retro-ocular, olfactory placode, and branchial-arches regions. Feather bud transversal sections of control embryos showing transcripts accumulation of **C)** *FBXO32*, **F)** *SOX10*, **I)** *DSCAM* **L)** *ALDH1L1* at the melanoblast-melanocyte lineage. **M-N)** Hybridization for *FBXO32* in the neural tube at 26-24ss.

7.2 *FBXO32*, *SOX10*, *DSCAM*, *ALDH1L1* loss of function yields abnormal melanocyte differentiation at the CNC

To understand whether *de novo* variants could impair melanocyte development, we delivered double-strand RNA molecules designed against chick *FBXO32* (*dsFBXO32*), *SOX10* (*dsSOX10*), *DSCAM* (*dsDSCAM*), *ALDH1L1* (*dsALDH1L1*), and bilaterally electroporated in the CNCs at 4ss (**Figure 7.2A**). At the neural 4ss stage, CNCs are pre-migratory and still neuroepithelial, hence being efficiently targeted by electroporation. In chick embryos, *in ovo* electroporation, gene silencing by vector-based RNAi has shown to be effective for studying gene expression cascades (Kimura et al., 2004; Nakamura et al., 2004). We confirmed gene silencing efficiency by *in situ* hybridization after gene inactivation at 4ss. Three hours after gene silencing, the genes expression of all genes was abolished (data not shown). We electroporated with m-cherry the neural tube of 4ss chick embryos to validate cell transfection efficiency (**Figure 7.2B, B'**). At three days of development, delaminating CNCs transfected with m-cherry are localized at retro-ocular and dorsal head regions (**Figure 7.2C and C'**). To analyze the effect of *FBXO32*, *SOX10*, *DSCAM*, and *ALDH1L1* loss of function, we focused on embryos at thirteen embryonic days (E13), where feather buds are developing, and melanocyte differentiation appears at the epidermis (**Figure 7.2D**). Normal feather buds' development is established in anterior-posterior polarity with foxy (pheomelanin) pigmentation (**Figure 7.2E**). We observed that each inactivated gene yields distinct abnormal phenotypes at the level of feather morphology (hypoplasia or hyperplasia), pheomelanin, or eumelanin pigmentation, polarity, and spatial arrangement compared with controls embryos (**Figure 7.2 E- I**). Surprisingly, embryos against *dsFBXO32* exhibit melanocytes with eumelanin synthesis (black spots pigment) synthesis, vascularization ongoing (**Figure 7.2F**), and abnormal feather hypoplasia (**Figure 7.2J**) compared to controls.

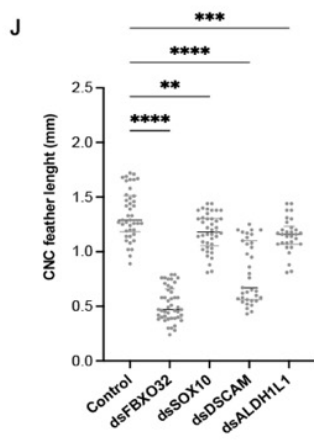
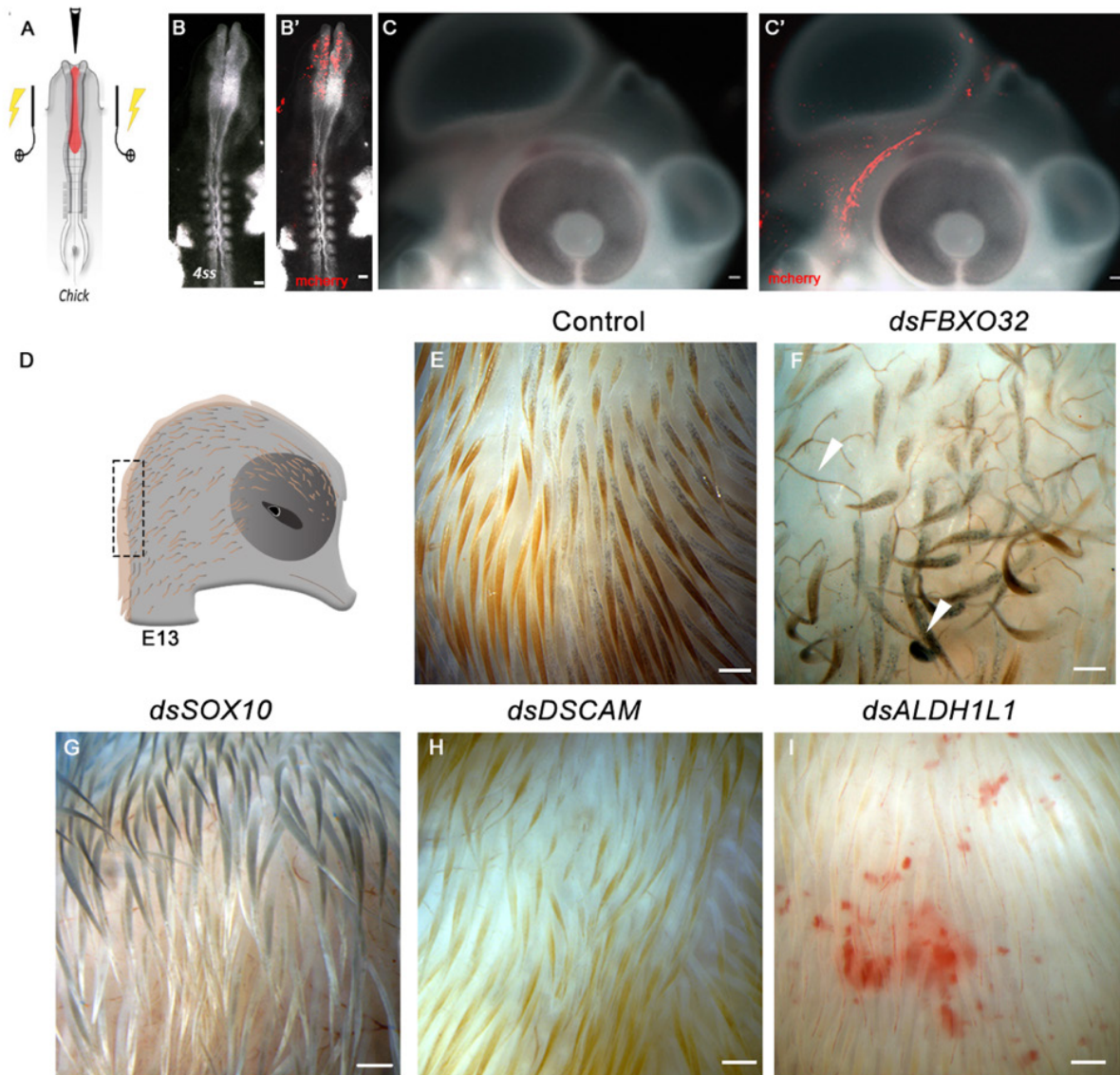


Figure 7.2 Silencing of *dsFBXO32*, *dsSOX10*, *dsDSCAM*, *dsALDH1L1* yields abnormal melanocyte differentiation at the CNC

A) Experimental design for FNC transfection by bilateral electroporation **B)** Whole-mount embryo **B')** and m-cherry NCCs labelling at 4ss after 3h of bilateral electroporation. **C)** 4ss of and embryo head **C')** and dorsal migration of NCCs visualized by m-cherry after two three of bilateral electroporation. **D)** Schematic representation of phenotyping analysis in an embryo E13. **E)** Eleven days after electroporation, control feather buds exhibit foxy pigmentation and anterior-posterior polarity. **F)** *FBXO32*, **G)** *SOX10*, **H)** *DSCAM* and **I)** *ALDH1L1* silencing impairs feather polarity and melanogenesis. Arrowheads indicate the vascularization in F. **J)** Box and whiskers plots showing the CNC feathers length in controls, *dsFBXO32*, *dsSOX10*, *dsDSCAM* and *dsALDH1L1* embryos. Statistical significance was assessed with a Dunnett's multiple comparison test against with control embryos. 4 electroporated control embryos and 3 silencing embryos of *dsSOX10*, *dsFBXO32*, *dsDSCAM* and *dsALDH1L1* were analyzed for quantifications in all conditions. * $P \leq 0.001$, **** $P < 0.0001$

7.3 Setting an *in vitro* 3D skin explant to unravel *FBXO32*, *SOX10*, *DSCAM*, *ALDH1L1* consequence at the melanoblast/melanocyte lineage

Melanoblast, the melanocyte precursor, is exclusively derived from the NC. Differentiated melanocytes synthesize and transfer melanin pigment to neighbouring keratinocytes (Bertolotto, 2013; Dupin & Le Douarin, 2003b). To further characterize the effect of the candidate genes in melanoblast progenitors, we set up an original *in vitro* skin explant culture. We performed intradermal injection of RNAi followed by bilateral electroporation shortly before melanocyte differentiation in embryonic day 10 (E10) at the CNC. The skin corresponding to the epidermis-dermis area subjected to electroporation is then micro-dissected using micro-scissors for iridectomy, transferred into a Petri dish, and then maintained *in vitro* for a week. At this stage, melanoblasts are mesenchymal and localized in the dermis. **(Figure 7.3A-B)**. This 3D culture system allows the association of dermis and epidermis to be maintained, favors the differentiation of feather buds (corresponding to the hairy buds in mammals), and preserves the capacity of the skin to develop according to anteroposterior and mediolateral body axes **(Figure 7.3C-D)**. Furthermore, the development of melanocytes and pigmentation patterns mimic the *in vivo* melanogenesis. Four days after *in vitro* culture, the skin explant exhibited the melanocytes organization in rows observed in our *in vivo* models **(Figure 7.3E)**. Silencing *dsSOX10*, *dsDSCAM*, and *dsALDH1L1* resulted in disrupted feather morphogenesis with a square-shaped organization and impairment in melanocyte differentiation (Figure S7). Melanocytes differentiate at the dermis level in *dsSOX10* **(Figure 7.3F)**, surrounding the feather buds in *dsDSCAM* **(Figure 7.3G)**, although differentiation was inhibited in *dsALDH1L1* **(Figure 7.3H)**.

The *in vivo* and *in vitro* system results of my PhD research contributed to the obtention of the INSERM Grant in *Developmental and integration of new experimental models relevant in research oncology: Optimisation of the 3R principle* in 2018. This funding call was dedicated to *New Experiments Models* in which we positioned the innovative *in vitro* 3D skin explant fulfilling the 3R aims in:

- Replace: Experiments are designed to reduce the use of animal models, replacing them with *in vitro* systems when eligible and refining their environmental conditions as per best practices.
- Refine, reduce: The skin explant system addressed our question at the later developmental stages, between melanoblasts migration from the dermis to epidermis and differentiation into melanocytes. The *in vitro* system provides the analysis of interactions between

epidermis and dermis. This model needs fewer eggs, as embryos are not maintained until hatching.

- Reduce: The skin explants corresponding to electroporation for gene silencing and rescue experiments were used for *in vitro* cell culture to characterized cell transformation.

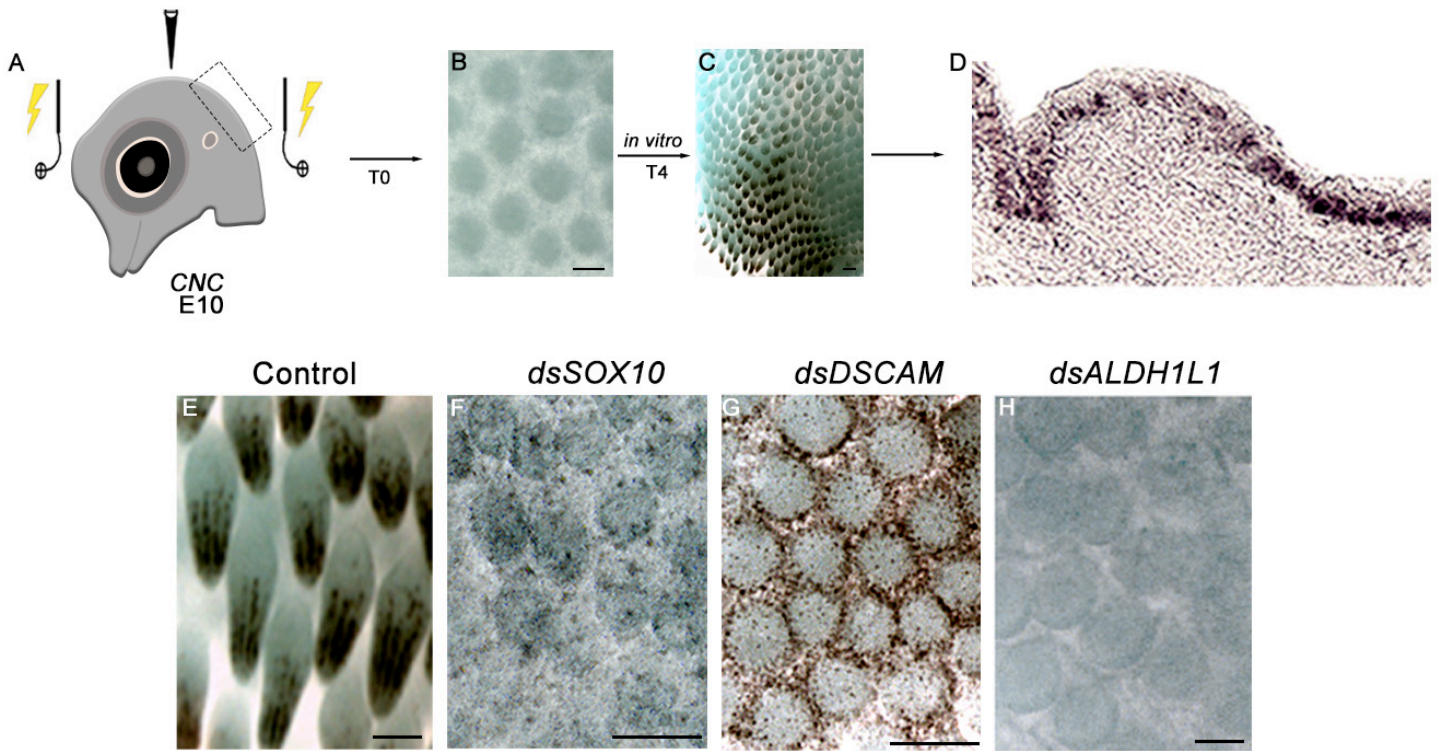


Figure 7.3 Silencing *dsSOX10*, *dsDSCAM* and *dsALDH1L1* at the melanoblast lineage yields abnormal melanocyte differentiation and feather bud morphogenesis

A) Bilateral electroporation technique at the CNC level in E10 embryos. **B)** After CNC electroporation, the *in vitro* 3D skin explant is maintained for four days at *in vitro* condition. **C)** Melanogenesis and feather morphogenesis take place at the central longitudinal axis. **D)** Melanocytes are normally distributed at the skin epidermis. **E)** Control skin explant 4 days after electroporation. Aberrant patterns of melanogenesis are observed after the inhibition of **F)** *dsSOX10*, **G)** *dsDSCAM*, **H)** *dsALDH1L1*. Scale bar: 500 μ m.

8 Results (Manuscript in preparation)

This section will be presented in the form of a manuscript in preparation, including abstract, introduction, material and methods, results, discussion and figures. The experiments presented compromises my main PhD work in the *de novo* candidate gene *FBXO32*.

Research article

(In preparation for submission)

Unraveling the significance of *FBXO32* variant, a childhood melanoma candidate gene, during neural crest and melanocyte development

Authors:

Alexandra Vargas Chavez^{1,2}, Tatiana Gorjankina², Brigitte Bressac-de Paillerets¹ and Sophie Creuzet²

1. NeuroPsi, Development and Evolution of the Neural crest Team. CNRS. Saclay, France

2. Institute Gustave Roussy, Villejuif, France.

*Corresponding author

Sophie Creuzet, PhD
Department of Development, Evolution and Cellular Signalling
Development and Evolution of the Neural Crest Group
Institute des Neurosciences Paris-Saclay, CNRS UMR9197
Campus CEA, 151 Rte de la Rotonde, 91400 Saclay
E-mail: sophie.creuzet@cnrs.fr

Keywords: Childhood melanoma, *FBXO32*, melanocytes, melanocyte transformation, neural crest, neural crest cells

Abstract

Melanoma is rare cancer in children and adolescents. It is a malignant tumor that develops from the transformation of melanocytes, the pigment cells that derive in the embryo from the neural crest (NC). We aim to elucidate the biological role of previously unknown mutations in candidate genes in pediatric melanoma during development. We studied the *FBXO32* gene for which a *de novo* germline mutation has been identified in a seven-year-old child. Using innovative experimental models, functional analysis in trunk NC cells demonstrated that inhibition of *FBXO32* induces melanocyte proliferation and differentiation. In parallel, to unmask the specific impact of the mutation, we performed rescue experiments with either the normal human gene sequence or the mutated human gene sequence. While the intact gene is able to restore normal melanocyte differentiation, the mutant gene, *FBXO32*^{G139S}, shows a devastating effect on the melanocyte lineage. Notably, *FBXO32*^{G139S} triggers the melanocyte transformation, changes in pigment pattern, and provokes cell aggregates. Cytoskeletal remodeling leads to focal adhesion disassembly, defective cell movement, cell misorientation in the epidermis, and aberrant back migration and dissemination toward dermal tissues. Similarly, we show that at the cephalic level, *FBXO32*^{G139S} induces melanocyte proliferation, as well as melanocyte migration to the dermis, but also the dissemination to the vasculature, suggesting the involvement of this mechanism in metastatic processes. Transcriptomic analyses point to the unexpected interactions of *FBXO32*^{G139S} with *ASIP* in eumelanogenesis and *BAP1* in the post-transcriptional ubiquitination proteasome system. We propose that *FBXO32* acts as a tumor suppressor gene capable of preventing the onset of pediatric melanoma, while the variant *FBXO32*^{G139S} may enhance the dysfunction of the ubiquitin proteasomal pathway and aberrant expression of E3 ligases associated with tumorigenesis.

Introduction

Childhood and adolescent melanoma are a heterogeneous group of malignant melanocytic tumors with clinical, histopathology, and genetic features different from the adult melanoma counterpart. Melanoma accounts for about 4% of all cancer in children aged 15 to 19 years (National Cancer Institute, 2018). The incidence is stable in pre-pubertal <1 per 100 000 person/year, whereas in adolescents, melanoma's incidence has increased over the past 20 years concerning unprotected sun exposure (Eggen et al., 2017). Although the risk of developing melanoma increases in children with a high number of melanocytic nevi, giant congenital nevi, and predisposition syndrome *Xeroderma pigmentosum*, most pediatric cases are sporadic (Pappo, 2003). Children who develop *in utero* congenital melanocytic nevi (CMN) are extremely rare. A unique driver has been described in congenital nevi carrying *NRAS*^{Q61R} post-zygotically mutation (Charbel et al., 2014) or *BRAF* oncogene through chromosomal translocations (Dessars et al., 2007). Furthermore, inactivating germline mutations of the main predisposition *CDKN2A* gene are rare in childhood melanoma before 18 years (Berg et al., 2004; Goldstein et al., 2018; Lu et al., 2015), while in adult melanoma-prone families, it has been identified in approximately 20 – 40% (Goldstein et al., 2018), supporting the hypothesis of *de novo* mutations in pediatric cases. The early detection of melanoma contributes to a favorable prognosis, but the difficulty of treating metastatic melanoma emphasizes the importance of defining how this cancer develops and the need for new therapies.

Few germline variants have been reported in pediatric and adolescent melanomas through whole-exome sequencing (WES) (Chang et al., 2016; Lu et al., 2015). A collection of 15 cases in conventional or adult-type melanoma had a high burden of somatic single-nucleotide variations as telomerase reverse transcriptase (*TERT*) promoter mutations and activation *BRAF V600* mutations. In addition, the germline melanocortin 1 receptor (*MC1R*) variants are associated with congenital melanocytic nevi with increased susceptibility to melanoma as red hair pigmentary phenotype and family history (Pellegrini et al., 2019). Exceptional cases of adolescent melanoma have been described in the onset of Li-Fraumeni syndrome associated with the germline mutation of the *TP53* tumor suppressor gene (Baek et al., 2019). Other events include mutations in the somatic *PTEN* tumor suppressor gene (Lu et al., 2015) and the germline BRCA1-associated protein-1 (*BAP1*) loss of nuclear expression in melanocytic neoplasms (de la Fouchardière et al., 2015). Nevertheless, the genetic mechanism in the occurrence of melanoma in pre-pubertal and post-pubertal melanomas < age of 18 is poorly understood.

Despite the significant advances in understanding the genetic landscape of pediatric cancers (Gröbner et al., 2018), rare variations are still unknown. Considering that most pediatric cases are sporadic, we hypothesize that *de novo* genetic "accident" occurs either in parental gametes or post-zygotically during development. To gain new insights into the *de novo* genetic "accident" that contribute to childhood melanoma, we performed a trio-base sequencing of affected children and their healthy parents by WES. We sequenced constitute exomes from blood extracted DNA of 55 pediatric cases (200X) before 19 years. To identify somatic events, we sequenced six frozen tumors (extremely rare material) by WES at 200X. We based our selective gene identification on the allelic frequency to determine the timing of *de novo* mutation. Our data mining of *de novo* variants using Ingenuity Variant Analysis (Qiagen) software identified disease-causing variants by applying classical and biological filters related to neural crest, melanoma, or cancer. To avoid bioinformatic artifacts, we verified all variants by Sanger sequencing or NGS (if the allelic frequency was <15%). This study identified 14 genes as *de novo* germline or post-zygotic potentially involved in childhood melanoma. All 14 genes are interconnected with a functional network using Ingenuity Pathway Analysis. Among these 14 genes, a *de novo* germline mutation in *FBXO32*, *p.G139S*, was identified in a seven-year-old child with melanoma level III in the knee. Previous studies established that *FBXO32*, which belongs to the SKP1-cullin F-box (SCF) type E3 ligase complex to directly binds to a substrate for degradation by ubiquitination, functions as a tumor suppressor gene in breast cancer (Tan et al., 2007; Zhou et al., 2017), ovarian cancer cells (Chou et al., 2010; Mei et al., 2015), colorectal cancer (Yuan et al., 2018), urothelial carcinoma (Song et al., 2019). Other authors reported *FBXO32* as a highly potent regulator of EMT in both development and disease by promoting emigration and tumorigenicity along with metastasis, respectively (Sahu et al., 2017). However, the potential role of the *FBXO32* gene to cause childhood melanoma remained to be uncharacterized.

Here, we analyzed the biological role of *de novo* childhood melanoma candidate genes and the occurrence of melanomas in two distinct anatomical levels, the trunk NC (TNC) and the cephalic NC (CNC) in the developing chick embryo. The chick embryo is an accessible and tractable system for experimentation where the developmental processes related to the NC's differentiation and its derivatives are well characterized (Creuzet et al., 2005; Le Douarin, 2004). Furthermore, the chick embryo is a functional model successfully used to unravel the mechanism of neural crest oncogenesis (Delloye-Bourgeois & Castellani, 2019; Kain et al., 2014). We carried out functional analyses of *de novo* germline and post-zygotic mutations on *FBXO32* by RNAi-mediated gene silencing to uncover the role of *FBXO32* in the normal development of NC cells and in the differentiation of the melanoblast/ melanocyte lineage. We show that *FBXO32* silencing at TNC and CNC is consistent with aberrant melanocyte proliferation and differentiation, supporting a

leading developmental role in this lineage. Next, we challenged the phenotype resulting from the gene silencing by rescue experiments. This approach shows that the human *FBXO32* WT sequence can inter-specifically alleviate the detrimental effect of the endogenous gene and restore normal melanocyte development. On the contrary, the human *FBXO32*^{G139S} reveals a specific impact on melanocyte differentiation and eumelanin synthesis. In addition, *FBXO32*^{G139S} induces the back migration of melanocytes from the epidermis, where they differentiate. We developed a model of skin explant to further characterize these processes *ex vivo*. Both 3D skin explant model and 2D cell cultures demonstrate the specific role of the mutation on melanocyte transformation, their cytoskeleton remodeling, and focal adhesion rearrangement leading to hyperpigmentation and cell aggregates formation. To analyze gene expression levels resulting from *FBXO32* silencing and the rescue experiments using human WT or mutated *FBXO32*, RNA-seq analysis was performed. Bioinformatic analyses unravel a specific effect of *FBXO32*^{G139S} on the *MC1R* signaling pathways. It turns out that *ASIP*, the *MC1R* antagonist, is downregulated in both TNC and CNC, suggesting that *FBXO32* is upstream of *ASIP*, controlling the binding of *MC1R* and α -*MSH* stimulating eumelanin synthesis. Our data indicate that *FBXO32*^{G139S} is involved in a malignant transformation of melanocytes during development at the cellular and molecular level and may enhance understanding of its putative role in melanoma initiation.

Materials and Methods

The chick embryo as an experimental model

The chick embryos were used as an experimental model to unravel the unknown biological significance of melanoma candidate genes. Embryos were staged according to the number of somite-pair (somite-stage, ss). Experiments were performed either at 7ss or 22ss for *in vivo* electroporation of pre-migratory cephalic or truncal NC, respectively. For experiments performed on explants, electroporation of undifferentiated melanoblasts were performed *ex vivo* at embryonic day 10 (E10).

Nucleic acid injection and *in vivo* electroporation

Before electroporation, nucleic acid solutions were contrasted with 0.01% Fast Green solution in PBS (Sigma) to carefully control the site of injection. Electroporation was achieved at the cephalic level using a triple electrode system placed on the vitelline membrane with two cathodes flanking the development head with a gap of 5 mm, and the anode facing the anterior neuropore (Creuzet et al., 2002). This electrode placement generates a triangular electric field yielding the bilateral dispersion of nucleic acid sequences in the target region (Creuzet et al., 2002; Garcez et al., 2014). At the trunk level, electroporation was carried out using a double electrode system, with the anode flanking the transfected side, and the cathode flanking the contralateral untransfected side, the latter being used as an internal control. For both TNC and CNC, electroporation was achieved by delivering five pulses of 27 volts using the electroporator system (ECM 830 BTX, Harvard Bioscience). After electroporation, eggs were sealed and re-incubated at $38.5 \pm 0.5^\circ\text{C}$ until reaching embryonic day 13 (E13).

Ex vivo electroporation on explant

Undifferentiated melanoblasts were transfected in 3D skin explant embryonic day 10. Briefly, the molecules of interest (RNAi) or cDNA human rescue sequences (*hFBXO32 WT* or *hFBXO32^{G139S}*) were injected into the dermis of the dorsal skin, followed by electroporation using a triplex of electrodes. In this context, exogenic nucleic acids were transferred exclusively to the melanocyte precursors in the dermis, while the epidermis corresponding to keratinocytes and where melanocytes differentiate is left untransfected. The skin subjected to electroporation was then

dissected using micro-scissors for iridectomy and transferred into a Nunc IVF Dish (ThermoFisher) to mimic the *in vivo* conditions. This 3D culture system supports the differentiation of skin appendages and the development of feather buds *ex vivo*. Skin appendages develop in 4 days according to anteroposterior and mediolateral body axes and exhibit a pattern of pigmentation recapitulating the *in vivo* melanogenesis. Therefore, for each gene of interest, we tracked melanocyte differentiation on Day 4.

Construct preparation

For silencing experiments, the chicken sequences encoding for *FBXO32*, *SOX10* and *ALDH1L1* were sequenced and subcloned at Imagif campus platform (I2GB, CNRS, Gif-sur-Yvette). The *DSCAM* plasmid was kindly provided by Dr. Yagamata (Yamagata & Sanes, 2008). Loss-of-function experiments were carried out by using the plasmid constructs, PCR-TOPO-*FBXO32*; PCR-TOPO-*SOX10*; PCR-TOPO-*ALDH1L1* and pGEM-*DSCAM*. To investigate the specificity of the endogenous expression of *FBXO32*, we performed rescue experiments by co-electroporating *dsFBXO32* in combination with the pcDNA3.1 + C-eGFP plasmid bearing either human wild type: h*FBXO32* WT or mutated: h*FBXO32*^{G139S}, carrying a CMV/enhancer-promoter to drive exogenous sequence transcription. The cytomegalovirus (CMV) promoter yields a powerful expression for at least 72h: Even though the plasmid is transiently active, its activity is sufficient to durably impact the fate of the cells until their final differentiation (Nakamura et al., 2004).

Double-strand RNA preparation

To follow the fate of the transfected migratory NCC, pCAGGS-mCherry plasmid (Addgene n°41583) was electroporated either in CNC or TNC cells at 7ss and 14ss respectively. For loss-of-function experiments, gene silencing was mediated by RNA interference. Briefly, sense and antisense RNA strands were synthesized from the complementary DNA molecule (cDNA) encoding the target genes: *FBXO32*, *SOX10*, *ALDH1L1*, and *DSCAM*. After digestion of the cDNA template, the stoichiometry of RNA single strands was calibrated before annealing at 95°C for 5 min (Pekarik et al., 2003). The concentration of dsRNA against *FBXO32*, *SOX10*, *DSCAM*, and *ALDH1L1* was adjusted at 300ng/μl (Garcez et al., 2014) to yield rapid and efficient silencing. For the control series, we used non-annealed single strands RNA of the target genes for injection at a concentration of 300ng/μl. For the rescue experiment, *dsFBXO32* was co-transfected together with

the construct at 1.25µg/µl, driving either the human wild-type gene (*FBXO32 WT*) or the mutated gene (*FBXO32^{G139S}*) gene.

Melanocyte cell culture

Melanocytes cells were isolated from the 3D *ex vivo* skin explants. The epidermis was separated from the dermis after micro-dissection and incubation in TrypLE™ recombinant enzyme (ThermoFisher). Dissociated cells were cultivated on Lab-Tek chamber slides previously coated with fibronectin (20µm/ml; F1141, Sigma-Aldrich), 300µl Dulbecco's Modified Eagle Medium/Nutrient Mixture F-12 (DMEM/F12, Gibco) + 10 % fetal bovine serum (FBS, Sigma) + 1% PS + 1% fungizone, in cell culture incubator Midi 40 (3404, ThermoFisher), at 37°C and 5% CO₂. To control cell viability, we used LysoTracker™ deep red (75nM; Invitrogen, ThermoFisher Scientific; (Schaefer et al., 2004) for 1h at 37°C, before fixation in PFA.

***In situ* hybridization**

Whole-mount and paraffin section *in situ* hybridizations (Creuzet et al., 2006) were performed using the following probes: *FBXO32*, *SOX10*, and *ALDH1l1* (Imagif campus platform, I2BC and *DSCAM* (Yamagata & Sanes, 2008).

Whole-mount staining and Immunocytochemistry

The accumulation of *FBXO32* in NCC was evidenced by immunocytochemistry using monoclonal antibodies (Abs), HNK1 (CD57; Sigma), and anti-*FBXO32* (Abcam). Image acquisition was performed on AxioImager M2 (Apotome; ZEISS) and 3D rendering with ImarisViewer 9.7.0. software.

Melanogenesis on paraffin sections was analyzed by immunocytochemistry using monoclonal Abs against DOPA decarboxylase (Invitrogen), *FBXO32* (Abcam), and polyclonal Abs against TYR (Thermo Fisher), TYRP1 (Invitrogen), MITF (ThermoFisher), anti-MelCAM (Santa Cruz Biotechnology) and detected with fluorophore-conjugated secondary Abs: Alexa fluor® 488, Alexa fluor® 594. Slides were mounted with Fluoromount-G™ with DAPI (Invitrogen). Imaging acquisition was done in a Leica Epifluorescence DM100 and Confocal Leica SP8 microscope. *In vitro* melanocyte differentiation was analyzed by immunocytochemistry using Abs against

Cytokeratin, (ThermoFisher), FBXO32 (Abcam), and polyclonal Abs against MelCAM (Santa Cruz Biotechnology), and Phospho-Paxillin (Tyr31) (ThermoFisher), and MITF (ThermoFisher). Before incubation with the second Abs, cells were incubated with Alexa Fluor™ 633-conjugated phalloidin. Incubation with fluorophore-conjugated secondary Abs, Alexa fluor® 488, Alexa fluor® 594 was carried out over the day. Slides were mounted with Fluoromount-G™ with DAPI (Invitrogen). Cell death was detected by LysoTracker Red (LTR; Invitrogen) staining before fixation (Garcez et al., 2014). Image acquisitions were carried out using Leica Epifluorescence DM100, equipped with a digital camera HAMAMATSU ORCA-R² C10600, on EVOS M5000 microscope, or Confocal Leica SP8 microscope.

Histology

Embryos were first fixed in 4% PFA, to take photos of their gross anatomy before paraffin embedding. Then embryos were further fixed in 60% ethanol, 30% formaldehyde, and 10% acetic acid, for 48h. After dehydration in ethanol, and impregnation in toluene, embryos were embedded in paraffin, then cut into 7µm sections in a LEICA RM2235 microtome.

Bulk RNA sequencing

For RNA sequencing, we analyzed 3 biological samples per triplicate per condition, involving CNC and TNC (2 replicates on the cephalic rescue *hFBXO32 WT*). RNA extraction was performed by precipitation with TRI reagent® (SIGMA-AIDRICH) and 2-propanol, in a concentration was 200ng/µl. cDNA synthesis and library preparation were performed by Novogene company. Briefly, the first cDNA strand synthesis was synthesized randomly by hexamer primer M-MuLV reverse transcriptase and the second cDNA strand was synthesized using DNA polymerase I and RNase. Libraries fragments were purified and sequenced on Illumina Novaseq platform, and 150 bp paired ends reads were generated. Gene model annotation files were downloaded from the genome website directly and we used them as reference genome *gallus* (genome ID: ensembl_gallus_gallus_grcg6a_gca_000002315_5).

Computational analysis

Feature counts v10.5-p3 were used to count the read numbers mapped to each gene. For quantification of gene expression level, the FPKM of each gene was calculated based on the length

of the gene and the reads count mapped of this gene. Genes were considered differentially expressed if they had a Benjamini-Hochberg adjusted p-value less than 0.05 for controlling the false discovery rate. Genes with an adjusted P-value <0.05 found by DESeq2 were assigned as differentially expressed. Hierarchical clustering was performed by clustering the FPKM values of genes and homogenizing the row (Z-score). Clustering was achieved using base principal component functions in EdgeR. Gene Ontology (GO) enrichment analysis of differentially expressed genes was implemented by the cluster ProfileR package. GO terms with a correct P-value less than 0.05 were considered significantly enriched by differential expressed genes. KEEG database resource for understating high-level functions of the biological system, such as the cell, form molecular level information, and high-throughput experimental technologies (<https://www.genome.jp/kegg/>). Novogene company used the cluster ProfileR package to test the statical enrichment of differential expressed genes in KEEG data.

Results

Childhood melanoma candidate gene *FBXO32* is expressed in NC

To reveal the temporal and spatial regulation expression of *FBXO32* during NCCs development, we performed a series of *in situ* hybridizations at different developmental stages, from emigrating NCCs to late melanocyte differentiation at the epidermis level (**Figure S1**). The *FBXO32* transcripts were all detected in the early neurula stage (7 somite stage: ss) at the margin of the neural plate in the anterior midbrain and posterior midbrain (**Figure S1A**). Twenty-four hours later, at 24ss, CNC cells that have migrated in facial processes and branchial arches, *FBXO32* transcripts were detected in the facial neural crest (FNC) derived mesenchymal cells: *FBXO32* expression was observed in migrating NCC filling the nasofrontal and the retro-ocular region. Its expression was also evidenced in the neuroepithelium of the future retinal pigment epithelium at 24ss (**Figure S1B**). Similarly, this gene was expressed in the olfactory placode of the nasofrontal region. The cephalic vesicles were negative for *FBXO32* transcripts except for the outer edges. More posteriorly, *FBXO32* transcripts were present in the 3rd branchial- arch, the territory of the epibranchial placode at the origin of the petrosal ganglion (**Figure S1B**).

Later on, in the developing skin after melanocyte differentiation at thirteen days of development (E13), transcripts of *FBXO32* were detected at the epidermis level both in feather buds and inter-feather bud spaces. However, at that stage, we evidenced neither *FBXO32* transcripts nor pigmented melanocytes in the dermis (**Figure S1C**). We can decipher that the candidate gene is defined in the melanocyte lineage. Thus, the gene whose mutations have been identified in children with melanoma are well expressed in our model at the developmental stages that are relevant for the implication of this gene in the biology of NCCs and melanocyte lineage. Therefore, we decided to evaluate the potential role of the genes in the NC differentiation and melanoblast/melanocyte lineage.

FBXO32 loss of function yields abnormal melanocyte differentiation in the CNC

To understand whether *FBXO32* *de novo* variant could impair melanocyte development, we delivered double-strand RNA molecules designed against the chick cDNA encoding for *FBXO32* (*dsFBXO32*) by bilateral electroporation in the CNCs at 4ss (**Figure 1A**). To validate cell transfection efficiency, we co-electroporated RNAi molecules together with an m-Cherry construct (**Figure 1B, B'**). At the neural 4ss stage, CNCs are pre-migratory and still neuroepithelial, hence

being efficiently targeted by electroporation. In chick embryos, *in ovo* electroporation gene silencing by vector-based RNAi introduced has shown to be effective for studying gene expression cascades (Kimura et al., 2004; Nakamura et al., 2004). We confirmed gene silencing efficacy by *in situ* hybridization after gene inactivation at 7ss. Three hours after gene silencing, gene expression was abolished (data not shown). At E3, delaminating CNCs transfected with m-Cherry were localized at retro-ocular and dorsal head regions (**Figure 1C and C'**). Next, we analyze the consequences of *FBXO32* loss of function at E13 when feather buds are developing and melanocyte differentiation occurs in the epidermis (**Figure 1D**). In normal development, feather buds develop according to an anterior-posterior polarity and exhibit pheomelanin (foxy) pigmentation (**Figure 1E**). When compared to control embryos, we observed that *FBXO32* inactivation yields abnormal feather and pigment phenotypes: first, skin development showed hypoplastic buds and a striking eumelanin pigmentation (**Figure 1F and J**). The spatial organization of feather buds attested that skin morphogenesis was also severely perturbed (**Figure 1F**). Surprisingly, the embryos subjected to *dsFBXO32* exhibit a hyperproliferation of melanocytes correlated with an expansion of the intradermal vascularization.

***FBXO32* is required for normal melanocyte proliferation and differentiation at the TNC**

To investigate the biological role of *FBXO32* in melanocyte differentiation, we performed a functional analysis in the TNC by unilateral electroporation. In pediatric melanoma, primary tumors most commonly affect the extremities, followed by the trunk, the head, and the neck (Pappo, 2003; Strouse et al., 2005). First, the presence of *FBXO32* transcripts was confirmed in the TNC by *in situ* hybridizations in embryos 28ss (**Figure S1D and E**). Then, we performed *in vivo* RNAi silencing at the TNC by unilateral electroporation to investigate the mechanism underlying *FBXO32* in TNC cells (**Figure 2A-B**). Unilateral electroporation was conducted at the trunk level before the lateral migration of melanocyte progenitors at 22ss. This technique allows us to visualize at once the experimental transfected ipsilateral side and the contralateral untransfected side (**Figure 2C-C'**). Twenty hours post-electroporation, migrating NCCs displayed robust expression of m-cherry transfection together with HNK1 and *FBXO32* markers (**Figure 2D**). Transfected embryos were then allowed to develop for 11 days until reaching E13 when the melanocyte can be evidenced (**Figure 2D'**). We observed in control embryos the normal pattern of pigment cells which form longitudinal brown stripes formed by feather buds on their back and produce pheomelanin (brown/foxy) pigment (**Figure 2E and F**). In contrast, *FBXO32* silencing resulted in melanocytes with spotted black pigmentation of eumelanin (**Figure 2G and H**) and feather hypoplasia (**Figure 2G and M**) in the transfected regions. We also observed an accumulation of melanocytes with eumelanin pigmentation towards the dermis at a transversal

feather bud level (**Figure 2H and N**). These observations strongly indicate that *FBXO32* is involved in the melanocyte biology at the trunk level.

To study the endogenous specificity expression from *FBXO32* silencing, we performed rescue experiments in the TNC. We performed co-electroporation of *dsFBXO32* in combination with the cDNA corresponding to the human *FBXO32* WT sequence in order to test whether the human wild-type sequence can inter-specifically compensate for the silencing of the endogenous genes and restore a normal melanocyte. Eleven days after electroporation (E13), the human wild-type gene fully mitigates the adverse effects of the gene silencing and restores the defect in melanocyte differentiation: feather morphology and pigment phenotypes tend to normalize (**Figure 2I and J**). In parallel, we tested the cDNA human encoding for the variant identified in the affected children, *FBXO32*^{G139S}, to unfold the specific phenotype resulting in the mutation. We observed hypoplastic feather buds, and a striking accumulation of eumelanin, along with a hyper-vascularization in the underlying tissues, at the level of the dermis (**Figure 2K-N**). Unilaterally melanocyte hyperproliferation was further observed in a feather bud's transversal section showing the condensation of melanocytes forming aggregates in the epidermis. Pigment cells were tightly condensed and characterized by a dense eumelanin accumulation. Notably, the cells were also misoriented, with the cell soma aligned along the epidermal surface and their cell extensions projecting towards the dermis (**Figure 2L**).

Encouraged by the striking phenotypes yielded by *FBXO32* silencing and mutation at the trunk region, we performed gene expression profiling by RNA-seq from control and experimental trunk skin samples harvested at E13. *FBXO32* silencing led to a significant upregulation of 297 genes and downregulation of 118 genes (**Figure 2O**). Analysis of gene ontology (GO) revealed the downregulation of some genes associated with melanogenesis: *Melan-A*, a marker of melanocyte tumors, *TUBB1*, *WNT8*, and *TYR* with a role in the melanogenesis pathway (**Figure 2P**). In contrast, we evidenced upregulation of genes involved in, e.g., adherent junctions (*CTNNA3*), MAPK signaling (*FGF18*), ECM receptor (*ITG7A*), VEGF signaling (*NFATC2*), and deregulation of genes involved in the regulation of focal adhesion and of the cytoskeleton, such as Caveolin1 (*CAV1*) and *ITGB8* (**Figure 2P**). Recent evidence has indicated that *CAV1* expression is needed for melanocyte dendricity, to promote contact with the subjacent keratinocytes, and is also a critical regulator in the production of pigment through the control of cAMP pathway (Domingues et al., 2020).

To identify other mechanisms that might account for the role of *FBXO32* in melanocyte biology, we investigated transcriptomic data using KEGG ontology. It turns out that the main signaling

pathways to be involved are linked to cell adhesion molecules, ECM-receptor interactions, melanogenesis, VEGF signaling pathways, focal adhesion, regulation of actin cytoskeleton, and MAPK signaling pathway (**Figure 2Q**).

Gene enrichment analysis was further oriented to investigate the possible synergic effect of *FBXO32*^{G139S} with the known childhood melanoma drivers, *BRAF*, *CDKN2A*, *CDK4*, *CDK6*, *PTEN*, and *TERT*. The gene *BRAF* and the genes *CDK4*, and *CDK6*, which regulate cell cycle checkpoints activity, were downregulated by *FBXO32*^{G139S} in CNC and TNC. Surprisingly, the *TERT* gene, involved in the telomere length control with aggressive clinical behaviour in pediatric patients with melanocytic neoplasm (Seynnaeve et al., 2017), was upregulated by activity *FBXO32*^{G139S} in both TNC and CNC. Recent evidence reveals that genetic and epigenetic (hypermethylation) alteration of *TERT* is associated with *TERT* upregulation in adolescents and young adults (Seynnaeve et al., 2017) (**Figure 2R**). *BAP1* childhood melanoma driver, which encodes DNA repair proteins, is downregulated *FBXO32*^{G139S} in the TNC and CNC (**Figure 2S**), indicating that *FBXO32*^{G139S} might at least counteract *BAP1* activity in the protein degradation interplay.

***FBXO32* impairs melanocyte differentiation in the cephalic NC**

We further validated the specificity of the endogenous expression of *dsFBXO32* at the CNC level. In control embryos, as observed at the TNC, feather buds are organized as strips with anterior-posterior polarity and foxy pigmentation (pheomelanin) (**Figure 3A**). In normal development, melanocytes are arranged in the barb ridges with a foxy pigmentation pattern (**Figure 3B**). On the contrary, the silencing of *FBXO32* results in feather buds misoriented with spotty melanocytes and increased vascularization (**Figure 3C**). A transversal section of one feather bud show melanocytes localized in the vicinity of the dermis with pheomelanin and eumelanin pigmentation (**Figure 3D**). Co-electroporation with the cDNA human *FBXO32* WT sequence showed an increase in melanocyte cells differentiation (hyperplasia) (**Figure 3E and I**) and partial rescue of melanocyte localization in the barb ridges (**Figure 3F**). Hyperplasia could result from the stronger cytomegalovirus (CMV) promoter driving gene expression in developing chick embryos (Yang et al., 2014). Following our strategy, the human *FBXO32*^{G139S} causes feather re-organization with hyperplastic feather buds and melanocytes with eumelanin pigmentation, such as in TNC experiments (**Figure 3G-I**). Strikingly, we observed that the human rescue *FBXO32*^{G139S} impairs bilaterally melanocyte hyperproliferation whit eumelanin synthesis and melanocyte migration towards the soma (dermis) (**Figure 3H**). We can thus conclude that *FBXO32*^{G139S} might trigger melanocyte transformation at both NC origins.

In the developing CNC, we obtained a different differential gene expression profiling compared to TNC, in which the *FBXO32* inhibition led to a significant downregulation of 227 genes and upregulation of 115 genes (**Figure 3K**). The most enriched pathways involved were tight junction, cell adhesion molecules, apoptosis, focal adhesion, cellular senescence, p53 signaling pathway, and regulation actin cytoskeleton (**Figure 3L**).

To assess specific gene expression enrichment in melanogenesis, we compared TNC and CNC experimental samples. These analyses showed that human *FBXO32*^{G139S} upregulate *TYR* at the TNC, which strengthens the role of *FBXO32* in melanogenesis (**Figure 3M**). The melanocortin 1 receptor (MC1R) gene essential for eumelanin synthesis and the tyrosine-related protein 1 (*TYRP1*) gene were predicted to increase control and human *FBXO32* WT activity samples. On the contrary, ASIP gene, an MC1R antagonist, expression was downregulated under *FBXO32*^{G139S} series in both TNC and CNC (**Figure 3N**). Together these observations raised the potential of *FBXO32*^{G139S} in melanogenesis by ASIP downregulation to stimulate the binding of MC1R receptor to α -melanocyte-stimulating hormone (α -MSH) for eumelanin synthesis and upregulating the first catalytic process of melanin synthesis at the melanosome.

Identification of distinct transcriptional signatures associated with trunk and cephalic NC

The significantly expressed genes between TNC and CNC resulted in differential expression profiling by RNAseq analysis. To gain insight into the extent of diversity between the two NCCs populations, we analyzed a principal component analysis (PCA) of expression profiles of all three replicates (**Figure 4A**). The PCA reveals that all trunk samples cluster together with no overlapping with any cephalic sample expression profile and good correlation expression levels between the biological replicates. These results demonstrated differences in NC plasticity and cues they received from their environment. Furthermore, we found in total 12573 genes uniquely expressed in the TNC and 12606 genes uniquely expressed in the CNC with overlapping regions showing the number of genes that are co-expressed in two different samples (e.g., 224 genes expressed on the TNC and 100 genes on the CNC in *dsFBXO32* samples) (**Figure 4B**). Hierarchical clustering of all NC replicates revealed statistically enriched and reduced gene differences between TNC and CNC (**Figure 4 C-D**). Specifically, the TNC displayed a high expression level inversely correlated with the CNC samples (**Figures 4E and F**). While *dsFBXO32* on TNC samples tends to upregulate genes involve in acting binding (**Figure 4E**), the CNC samples tend to downregulate genes involve in filament binding (**Figure 4F**).

***FBXO32* expression influences melanogenesis in NC lineage**

In both CNC populations, we observed an increase in eumelanin synthesis of *FBXO32* transfected embryos, which suggests that *FBXO32* impairs the melanogenesis pathway. To further confirm those results, we examined the enzymes restricted to the melanogenesis pathway: TYR, DOPA, and TYRP1 combined with MelCAM antibody to track melanocyte transformation. We analyzed the distribution patterns of these proteins by comparing the transfected cells carrying *dsFBXO32* and *FBXO32^{G139S}* insults versus the untransfected cells in truncal transversal sections (**Figure S2A**). In the developing feather buds, we focused on three morphologic compartments: proximal (Pfb), intermediate (lfb), and distal (Dfb) (**Figure S2B**).

Tyrosinase is a crucial enzyme that catalyzes the first step of L-DOPA to DOPA for melanin biosynthesis, indispensable for eumelanogenesis as well as pheomelanogenesis (Lin & Fisher, 2007). In E13 control embryos, TYR accumulation is observed in the epidermis of invaginate feather buds, Pfb, and mature Dfb (**Figure S2C**). Surprisingly, silencing of *FBXO32* results in TYR accumulation at the dermis in colocalization with MelCAM and melanocytes of mature, lfb, and Dfb (**Figure S2D**). TYR accumulation was restored in co-transfected embryos with human *FBXO32* WT (**Figure S2E**). In parallel, *FBXO32^{G139S}* highly provokes TYR accumulation in tightly melanocytes with eumelanin pigment (**Figure S2F**), demonstrating that *FBXO32^{G139S}* plays a role in the onset of melanin synthesis.

Then, we analyzed DOPA essentially for melanin pigment biosynthesis. In *dsFBXO32* embryos, DOPA is co-localized with MelCAM at the dermis (**Figure S3B**) compared to controls (**Figure S3A**), illustrating the *FBXO32* effect at melanoblast/melanocyte lineage. In the developing Pfb, lfb, and Dfb, DOPA is accumulated at the epidermis level, increasing the stratum corneum of the feather buds. DOPA accumulation was restored in the rescue with the wild-type form of the gene (**Figure S3C**). Surprisingly, DOPA was highly accumulated in feather buds and dorsolateral muscle in embryos overexpressed with *FBXO32^{G139S}* (**Figure S3D**). This result could indicate a dual effect of *FBXO32^{G139S}* alterations during development, considering that *FBXO32* gene is increased when muscles undergo atrophy (Gomes et al., 2001).

To further understand how *FBXO32* is implicated in eumelanin accumulation in transfected embryos, we studied TYRP1 directly involved in the eumelanin biosynthesis pathway (Nasti & Timares, 2015; Niwa et al., 2002). In transformed melanocytes, the expression of tyrosinase and TYRP1 is highly variable (Fang, 2002). In control embryos, TYRP1 protein was observed in the developing feather buds with a gradient of expression from invaginating (Pfb) to mature feather

buds (Dfb) (**Figure S4A**). Melanocytes with pheomelanin pigmentation deposits expressed the protein MelCAM. Silencing embryos showed a slight accumulation of TYRP1 at the dermis level in the transfected region (**Figure S4B**). Moreover, TYRP1 accumulation was observed at the epidermis and feather bud's soma (dermis) of Pfb, lfd, and Dfb. MelCAM expression accumulation was increased in melanocytes with pheomelanin deposits but not in melanocytes with eumelanin pigmentation (**Figure S4B**). In wild-type embryos, TYRP1 distribution was limited in the epidermis of all feather buds (**Figure S4C**). Although we expected to observe TYRP1 accumulation in the eumelanin pigmentation, resembling the black stripes on the transfected dorsal regions, we observed these melanocytes retaining MelCAM (**Figure S4D**). This phenotype is not surprising, accumulation of MelCAM reveals melanocyte transformation. Furthermore, pigmentation can interfere with immunostaining labeling. These observations indicate that ectopic expression of *FBXO32*^{G139S} affects the synthesis of melanin pigments and melanocyte transformation during development.

Next, we sought to investigate the epistatic relationship between MITF, the master regulator of melanocyte development. MITF promotes melanogenesis by activating TH and TYRP1, required for eumelanin synthesis. MITF also regulates specific ubiquitously expressed genes that are important for melanocyte survival (e.g., BCL2) (McGill et al., 2002) and proliferation (e.g., CDK2) (Du et al., 2004). Recently it has been described *FBXO32* as a direct transcription target of MITF with non-epistatic relation (Habel et al., 2020), thus, we investigated whether, in our model, *FBXO32* regulates MITF at the protein level. Here, *FBXO32* silencing results in MITF decreased accumulation in the developing invaginated (Pfb) and mature (lfb, Dfb) feather buds (**Figure S5**), but not in the epidermis layer. The co-immunostaining with MelCAM showed this developing feather buds with high MelCAM accumulation. Furthermore, we also observed mis-polarized melanocyte filopodia towards the dermis due to *FBXO32* transfected cells. Finally, we wanted to analyze the detection of the *FBXO32* protein itself. Although in *FBXO32* silencing embryos, we observed *FBXO32* protein accumulation in the stratum corneum of Pbf, lbf, Dfb (**Figure S6B**), its accumulation is reduced in the epidermis and dermis layers than in controls (**Figure S6E**).

***FBXO32* induces melanocyte migration towards the dermis**

Melanoblast, the melanocyte precursor, are exclusively derived from the NC. They differentiated and became mature melanocytes able to synthesize and transfer melanin pigment to neighbouring keratinocytes (Bertolotto, 2013; Dupin & Le Douarin, 2003b). To further characterize

the effect of the candidate genes in melanoblast progenitors, we set up an original *ex vivo* skin explant culture. We performed intradermal injection of RNAi followed by bilateral electroporation shortly before melanocyte differentiation on an embryonic day 10 (E10) at the CNC (**Figure 5A**). The skin is then micro-dissected and maintained *in vitro* skin explant conditions. At this stage, melanoblasts are mesenchymal and localized in the dermis (**Figure 5B**). This 3D culture system allows the association of dermis and epidermis to be maintained, favors the differentiation of feather buds (corresponding to the hairy buds in mammals), and preserves the capacity of the skin to develop according to anteroposterior and mediolateral body axes (**Figure 5C-D**).

Surprisingly, we observed melanocyte migration to the dermis in our *in vitro* system after *FBXO32* inhibition. Clearly, our observations indicate that *FBXO32* silencing induces melanocyte transformation, provoking migration to the dermis, observed by the pigmented cells (**Figure 5G-H**) in comparison with controls (**Figure 5E-H**). We also observed loss of polarity and disoriented feather buds' morphology as square morphology (**Figure 5G**). We could rescue the phenotypic alteration upon *FBXO32* depletion by overexpression with human WT *FBXO32* sequence at melanoblast lineage (**Figure 5I-J**), whereas overexpression with human *FBXO32*^{G139S} stimulates migration towards the dermis (**Figure 5K-L**). These results indicated that *FBXO32*^{G139S} enhances migration to the dermis in a developing context.

FBXO32* triggers melanocyte transformation *in vitro

To explore how *FBXO32* can affect cell morphology and induce cell migration, we characterized control and transfected cells *in vitro*. We harvest *in vitro* melanocyte dissociated from control, *dsFBXO32*, rescue with the human *FBXO32* WT and human *FBXO32*^{G139S} in cell culture chambers coated in the presence of extracellular matrix ligand fibronectin. We did only one cell passage to analyze precisely the cells carrying the uptake of the construct. We observed that control melanocytes exhibited fibroblastic-like morphology, bipolar polarity, and adhesion to fibronectin (**Figure 6A**). Surprisingly, the silencing of *FBXO32* resulted in cell remodeling to filopodia length reduction, lamellipodia formation, and the formation of cell aggregates (**Figure 6A-B**). Cell aggregates were also less adherent to the fibronectin substratum. When co-electroporated with the cDNA human WT *FBXO32* form, these constructs generated a potential restoration of cell morphology and adhesion (**Figure 6A-B**). In contrast, the human *FBXO32*^{G139S} construct showed impairment in the cell's morphology and adhesion, such as *FBXO32* silencing (**Figure 6A-B**). The formation of cells aggregates from transfected cells reinforces our previous results *in vitro*, where melanocytes tend to be more compact in the feather buds in skin explants transfected with

FBXO32^{G139S}. We can thus conclude that cell remodeling is explicitly caused by *FBXO32*^{G139S} and not by an off-target effect of the RNAi electroporation.

To understand whether *FBXO32* can induce melanocyte transformation towards melanoma phenotype, we analyzed melanoma cell adhesion molecule (MelCAM) protein by immunostaining. Normal melanocytes rarely express cell-cell adhesion receptors, whether melanoma cells show an increase in MelCAM expression. Furthermore, the expression of MelCAM is associated with an aggressive invasive phenotype, and its upregulation is strongly associated with melanoma progression. (Satyamoorthy et al., 2001). Although in normal cells, we observed accumulation of MelCAM, the loss of *FBXO32* enhances MelCAM accumulation at the cytoskeleton (**Figure 6B, second panel**). This observation strongly indicates that *FBXO32*^{G139S} induces melanocyte transformation.

***FBXO32* promotes cytoskeleton remodeling**

Migrating melanoma cells exhibit characteristic sheet-like membrane extensions called lamellipodia essential for crossing the basal membrane (Bonaventure et al., 2013; Kunitomo et al., 2014). Lamellipodia are formed at the leading edge of migrating cells with a role in driving cell migration by attaching to the substrate and generating forces to pull the cell forward (Yamaguchi & Condeelis, 2007). Our results demonstrated that *FBXO32* silencing induces lamellipodia formation and filopodia length reduction (**Figure 6B**). The average filopodia size per cell was decreased at least two-fold in *FBXO32* transfected cells compared to controls and rescue cells (**Figure 6C**) (filopodia length mean in control cells= 84.62µm, n=266 cells). A preliminary indicates that *FBXO32*^{G139S} induces the formation of bleb protrusions at the cell membrane.

To analyze focal adhesion assembly that contributes to cell migration, we analyzed phospho-paxillin Tyr31. Phospho-paxillin Tyr31 labels the adhesion near the edge of focal contacts. In melanoma cells, the levels of phospho-paxillin are much higher than in melanocytes (Velasco-Velázquez et al., 2008). We observed, in normal cells, phospho-paxillin in the focal adhesion at the edge cell (**figure 6B**). Lamellipodia in inhibited *FBXO32* cells showed prominent phospho-paxillin accumulation with tightly cell-cell contacts at the cell surface (**Figure 6B**). In addition, the cells subjected to the overexpression of human *FBXO32* WT exhibit a recovery of the bipolar morphology and normal phospho-paxillin accumulation (**Figure 6B**), whether phospho-paxillin labeling was significantly important at the cytoskeleton in *FBXO32*^{G139S} cells. (**Figure 6B**). Thus, paxillin is tyrosine phosphorylated in the dynamic adhesions, and this phosphorylation promotes

paxillin disassembly. We also observed phospho-paxillin translocation to the nucleus in *FBXO32^{G139S}* transfected cells (**Figure 6B**) compared to control cells (**Figure 6B, first row**). Although paxillin is mainly localized at the focal adhesion, it is also present at cytoplasmatic and nuclear locations. It may affect gene transcription to directly link the plasma membrane and the cytoskeleton to the nucleus (Dong et al., 2009).

To decipher whether inhibition of *FBXO32* expression disrupts cell actin filament at a cellular level, we examined F-actin organization by phalloidin staining. We observed in *dsFBXO32* cells different actin filament architectures resulting in loss of stress fibers and polymerized actin (**Figure 6D**). The actin filament structure was recovered when isolated cells were subjected to the cDNA human WT form of *FBXO32* (**Figure 6D**). These results reveal that *dsFBXO32* inactivation leads to changes in actin cytoskeleton dynamics. In contrast, a partial recovery in F-actin organization with no enrichment areas in peripheral regions results from the cDNA human *FBXO32^{G139S}* (**Figure 6D**). According to our findings, *FBXO32^{G139S}* causes cytoskeleton remodeling to induce melanocyte migration potentially.

Discussion

This study investigated the potential biological role of childhood melanoma candidate genes carrying a *de novo* mutation by a powerful RNAi-mediated silencing technique in the developing chick embryo. We focused on two anatomical levels, the TNC and CNC, to analyze melanocyte migration and transformation from both NC origins. Specifically, we explored the role of the *FBXO32* gene in the melanocytic lineage at both NC levels. We exploited gene expression profiles by RNAseq datamining in skin samples to identify novel transcriptional signatures associated with *FBXO32*. The data presented suggested *FBXO32* can act as a tumor suppressor gene in melanocytes, a role which seems to be challenged by the mutation *FBXO32*^{G139S}, hence promoting childhood melanoma.

Our functional screening established that the biological role of *FBXO32* is critical for melanocyte differentiation during development. The dsRNA driving silencing by electroporation efficiently inhibited *FBXO32* activity in pre-migratory CNC and was transient until E13. These results show that the *FBXO32* gene can impair melanocyte differentiation at the level of proliferation and differentiation. Whereas *FBXO32* results in aberrant melanocyte proliferation, pigmentation loss of feather polarity, and increased vascularization in the dermis.

We investigated the molecular mechanism by which *FBXO32* expression affects melanocyte development in the TNC. Indeed, *de novo* germline variant, p.G139S, was detected in the knee of the child with melanoma level III. We transfected NCCs at 22ss, below the level where trunk NCCs have started delaminating and migrating (Giovannone et al., 2015), and melanocyte precursors begin to enter the dorsolateral pathway by 24-28ss. We followed trunk NCCs migration by NCCs transfection with m-Cherry, along with HNK1 immunostaining and *FBXO32* colocalization. The *FBXO32* silencing by RNAi at the TNC coincides with CNC features with melanocyte proliferation, aberrant feather polarity, and vascularization. These results indicate that *FBXO32* inactivation activity triggers melanocyte transformation in both TNC and CNC.

To unravel the specific involvement of *FBXO32* in the melanocyte lineage, we performed rescue experiments in both TNC and CNC. Our rescue experiments clearly show that overexpression with the human wild-type *FBXO32* form results in normal melanocytic development in both NC regions. Surprisingly, both TNC and CNC rescue experiments carrying the human variant, p.G139S, evidenced an aberrant melanocyte differentiation at the pigment and cell polarity. Additionally, the synthesis of melanogenesis proteins in experimental embryos was accompanied by

dysregulation of MelCAM, MITF, and FBXO32 demonstrated by the accumulation in the dermis and mature feather buds immunolabelling assays.

Through RNA-seq analysis applied to control and *FBXO32* experimental series at two NC levels, we provided some evidence of the role of *FBXO32*^{G139S} as a melanoma initiator. Hierarchical clustering identified two distinct clusters signatures between the TNC and CNC. The PCA analysis also highlighted the correlation between samples, with one population entirely of TNC and other CNC. Differential gene expression upregulation was characteristic in TNC samples, whereas gene downregulation in CNC.

Two regulatory events were identified associated with *FBXO32*^{G139S} in the eumelanin synthesis. First, we analyzed *Tyr*, a critical enzyme for melanin biosynthesis, catalyzing the two initial steps of melanogenesis. RNAseq data mining showed that *FBXO32*^{G139S} upregulated *Tyr*, while *DOPA* in *FBXO32*^{G139S} samples enrichment was not detected. Together *MC1R*, *ASIP*, and *TYRP1* are among the significant regulators of pigmentation. The *ASIP* gene, an *MC1R* antagonist, inhibits eumelanin synthesis by directly competing for the receptor binding of α -MSH, thereby stimulating cAMP, which results in pheomelanogenesis (Nasti & Timares, 2015). This would suggest that the causative variant underlying the *ASIP* haplotype is a gain-of-function mutation (Gudbjartsson et al., 2008). Based on these results, *FBXO32*^{G139S} may act upstream of *ASIP*, causing *ASIP* downregulation and *TYRP1* upregulation, which stimulates eumelanin synthesis. In adults, *MC1R*, *ASIP*, and *TYRP1* are considered low risk for inherited mutations. However, its role in childhood melanoma has not been elucidated so far.

To investigate the role of *FBXO32* in the early onset of melanoma, we analyzed the epistatic relationship between childhood melanoma candidate genes. Our observations indicate that *CDKN2A* is detectable during the development of normal melanocytes, but transcriptomic analyses provide no evidence of differential *CDKN2A* enrichment expression in the RNA-seq data between our series. It also supports the notion that *CDKN2A* is rare in childhood melanoma (Berg et al., 2004; Goldstein et al., 2018; Lu et al., 2015; Markovic et al., 1997). It is important to emphasize that although we provide cues of childhood variants, our study does not exclude the possibility that other genetic events could occur. Second, we established that *CDK4* and *CDK6* genes are downregulated in the overexpression of *FBXO32* WT and *FBXO32*^{G139S}, respectively. In 15 CM out of 23 total pediatric patients, Lu and colleagues reported that none of their patients carried *CDKN2A* or *CDK4* mutations (Lu et al., 2015). Still, 67% of CM patients carried germline *MC1R* variant reported to be associated with increased melanoma risk in adults. Third, the *TERT* gene involved in telomere maintenance is upregulated under *FBXO32* silencing and *FBXO32*^{G139S}. The

upregulation in the telomere reverse transcriptase (TERT) gene observed in *FBXO32* silencing could explain melanocyte proliferation. Finally, the *BAP1* (BRCA1-associated protein-1) loss of function germline mutation is a tumor predisposition in childhood melanoma (De La Fouchardière, 2017). Both human *FBXO32* WT and *FBXO32*^{G139S} downregulated *BAP1* in both TNC and CNC. Hence, an antagonist in the ubiquitin protein degradation system *BAP1*, important in DNA damage response and cell cycle regulation, may be a partner of the *FBXO32* gene in melanocyte transformation.

To investigate the role of *FBXO32* in promoting melanocyte transformation, we silenced its activity precisely before melanoblast differentiation in an *in vitro* skin explant culture. The *FBXO32*^{G139S} expression favors proliferation and migration of melanocyte cells to the dermis recapitulating a possible invasion process. Contrary, Habel, and colleagues found a decrease in migration in melanoma patients' cells melanoma cells and 501Mel cells due to the inhibition of *FBXO32* in Boyden chambers assays, while forced *FBXO32* expression using a lentiviral vector in the cells expressing the mutant *BRAF*^{V600E} on a wild-type *NRAS*, stimulated the migration of SKmel28 melanoma (Habel et al., 2020). In our study, we forced the expression of *FBXO32* in the melanoblast cells in a developmental environment with a plasmid carrying either the human wild-type or P.G139S variant of the gene under the control of a powerful CMV promotor, leading to the inhibition and stimulation of melanocyte migration, respectively. Although the role of *FBXO32* in invading melanocytes could be further characterized, our study clearly shows that *FBXO32*^{G139S} impairs melanocyte migration and prompts pigment cell dissemination at the expense of the dermis.

Our data argue for an essential role of this gene in melanocyte transformation. A study dealing with the role of *FBXO32* in melanoma adult cells showed the oncogenic regulation in cell migration, proliferation, and transcriptional programs of melanoma cells through epigenetic mechanisms (Habel et al., 2020). Here, we demonstrate the tumor suppressor potential of *FBXO32*, while its loss-of-function and variant promotes cell proliferation and cell migration, co-expression with the human *FBXO32* WT tends to normalize melanocyte development. Even though the interplay between *ASIP* and *BAP1* would need further analysis, our transcriptomic data posit *FBXO32* as a novel tumor suppressor gene regulating the balance between *ASIP* and *BAP1* and shed a light on the mutation *FBXO32*^{G139S}, which specifically targets the transcription of these two partners to conduct melanocyte transformation in a developmental context, hence accounting for its potential role in childhood melanoma.

References

- Baek, Y. S., Seo, J. Y., Song, J. Y., Lee, S. Y., Kim, A., & Jeon, J. (2019). Li-Fraumeni syndrome presenting as cutaneous melanoma in a child: case report and review of literature. *Journal of the European Academy of Dermatology and Venereology*, *33*(4), e174–e175.
- Berg, P., Wennberg, A. M., Tuominen, R., Sander, B., Rozell, B. L., Platz, A., & Hansson, J. (2004). Germline CDKN2A mutations are rare in child and adolescent cutaneous melanoma. *Melanoma Research*, *14*(4), 251–255.
- Bertolotto, C. (2013). Melanoma: From Melanocyte to Genetic Alterations and Clinical Options. *Scientifica*, *2013*, 1–22.
- Bonaventure, J., Domingues, M. J., & Larue, L. (2013). Cellular and molecular mechanisms controlling the migration of melanocytes and melanoma cells. *Pigment Cell & Melanoma Research*, *26*(3), 316–325.
- Chang, W., Brohl, A. S., Patidar, R., Sindiri, S., Shern, J. F., Wei, J. S., Song, Y. K., Yohe, M. E., Gryder, B., Zhang, S., Calzone, K. A., Shivaprasad, N., Wen, X., Badgett, T. C., Miettinen, M., Hartman, K. R., League-Pascual, J. C., Trahair, T. N., Widemann, B. C., ... Khan, J. (2016). Multidimensional clinomics for precision therapy of children and adolescent young adults with relapsed and refractory cancer: A report from the center for cancer research. *Clinical Cancer Research*, *22*(15), 3810–3820.
- Charbel, C., Fontaine, R. H., Malouf, G. G., Picard, A., Kadlub, N., El-Murr, N., How-Kit, A., Su, X., Coulomb-L'Hermine, A., Tost, J., Mourah, S., Aractingi, S., & Guégan, S. (2014). NRAS mutation is the sole recurrent somatic mutation in large congenital melanocytic nevi. *Journal of Investigative Dermatology*, *134*(4), 1067–1074.
- Chou, J. L., Su, H. Y., Chen, L. Y., Liao, Y. P., Hartman-Frey, C., Lai, Y. H., Yang, H. W., Deatherage, D. E., Kuo, C. T., Huang, Y. W., Yan, P. S., Hsiao, S. H., Tai, C. K., Lin, H. J. L., Davuluri, R. V., Chao, T. K., Nephew, K. P., Huang, T. H. M., Lai, H. C., & Chan, M. W. Y. (2010). Promoter hypermethylation of FBXO32, a novel TGF-B/SMAD4 target gene and tumor suppressor, is associated with poor prognosis in human ovarian cancer. *Laboratory Investigation*, *90*(3), 414–425.
- Creuzet, S., Couly, G., & Le Douarin, N. M. (2005). Patterning the neural crest derivatives during development of the vertebrate head: insights from avian studies. *J. Anat*, *207*, 447–459.
- Creuzet, S., Couly, G., Vincent, C., & Douarin, N. M. Le. (2002). *Negative effect of Hox gene expression on the development of the neural crest-derived facial skeleton*. *4313*, 4301–4313.
- Creuzet, S. E., Martinez, S., & Le Douarin, N. M. (2006). The cephalic neural crest exerts a critical effect on forebrain and midbrain development. *Proceedings of the National Academy of Sciences*, *103*(38), 14033–14038.

- De La Fouchardière, A. (2017). Mélanomes de l'enfant. *Tumeurs Pédiatriques*, VI(1), 62–67.
- de la Fouchardière, A., Cabaret, O., Savin, L., Combemale, P., Schwartz, H., Penet, C., Bonadona, V., Soufir, N., & Bressac-de Paillerets, B. (2015). Germline BAP1 mutations predispose also to multiple basal cell carcinomas. *Clinical Genetics*, 88(3), 273–277.
- Delloye-Bourgeois, C., & Castellani, V. (2019). Hijacking of Embryonic Programs by Neural Crest-Derived Neuroblastoma: From Physiological Migration to Metastatic Dissemination. *Frontiers in Molecular Neuroscience*, 12.
- Dessars, B., De Raeve, L. E., Housni, H. El, Debouck, C. J., Sidon, P. J., Morandini, R., Roseeuw, D., Ghanem, G. E., Vassart, G., & Heimann, P. (2007). Chromosomal translocations as a mechanism of BRAF activation in two cases of large congenital melanocytic nevi. *Journal of Investigative Dermatology*, 127(6), 1468–1470.
- Domingues, L., Hurbain, I., Gilles-Marsens, F., Sirés-Campos, J., André, N., Dewulf, M., Romao, M., Viaris de Lesegno, C., Macé, A.-S., Blouin, C., Guéré, C., Vié, K., Raposo, G., Lamaze, C., & Delevoeye, C. (2020). Coupling of melanocyte signaling and mechanics by caveolae is required for human skin pigmentation. *Nature Communications*, 11(1), 2988.
- Dong, J. M., Lau, L. S., Ng, Y. W., Lim, L., & Manser, E. (2009). Paxillin nuclear-cytoplasmic localization is regulated by phosphorylation of the LD4 motif: Evidence that nuclear paxillin promotes cell proliferation. *Biochemical Journal*, 418(1), 173–184.
- Du, J., Widlund, H. R., Horstmann, M. A., Ramaswamy, S., Ross, K., Huber, W. E., Nishimura, E. K., Golub, T. R., & Fisher, D. E. (2004). *Critical role of CDK2 for melanoma growth linked to its melanocyte-specific transcriptional regulation by MITF*.
- Dupin, E., & Le Douarin, N. M. (2003). Development of melanocyte precursors from the vertebrate neural crest. *Oncogene*, 22, 3016–3023.
- Eggen, C. A. M., Durgaram, V. V. L., van Doorn, R., Mooi, W. J., Pardo, L. M., Pasmans, S. G. M. A., & Hollestein, L. M. (2017). Incidence and relative survival of melanoma in children and adolescents in the Netherlands, 1989–2013. *Journal of the European Academy of Dermatology and Venereology*, 32(6), 956–961.
- Fang, D. (2002). Selective down-regulation of tyrosinase family gene TYRP1 by inhibition of the activity of melanocyte transcription factor, MITF. *Nucleic Acids Research*, 30(14), 3096–3106.
- Garcez, R. C., Le Douarin, N. M., & Creuzet, S. E. (2014). Combinatorial activity of Six1-2-4 genes in cephalic neural crest cells controls craniofacial and brain development. *Cellular and Molecular Life Sciences*, 71, 2149–2164.
- Giovannone, D., Ortega, B., Reyes, M., El-Ghali, N., Rabadí, M., Sao, S., & de Bellard, M. E. (2015). Chicken trunk neural crest migration visualized with HNK1. *Acta Histochemica*, 117(3), 255–266.
- Goldstein, A. M., Stidd, K. C., Yang, X. R., Fraser, M. C., & Tucker, M. A. (2018). Pediatric

- melanoma in melanoma-prone families. *Cancer*, 124(18), 3715–3723.
- Gomes, M. D., Lecker, S. H., Jagoe, R. T., Navon, A., & Goldberg, A. L. (2001). Atrogin-1, a muscle-specific F-box protein highly expressed during muscle atrophy. *Proceedings of the National Academy of Sciences of the United States of America*, 98(25), 14440–14445.
- Gröbner, S. N., Worst, B. C., Weischenfeldt, J., Buchhalter, I., Kleinheinz, K., Rudneva, V. A., Johann, P. D., Balasubramanian, G. P., Segura-Wang, M., Brabetz, S., Bender, S., Hutter, B., Sturm, D., Pfaff, E., Hübschmann, D., Zipprich, G., Heinold, M., Eils, J., Lawerenz, C., ... Pfister, S. M. (2018). The landscape of genomic alterations across childhood cancers. *Nature*, 555(7696), 321–327.
- Gudbjartsson, D. F., Sulem, P., Stacey, S. N., Goldstein, A. M., Rafnar, T., Sigurgeirsson, B., Benediktsdottir, K. R., Thorisdottir, K., Ragnarsson, R., Sveinsdottir, S. G., Magnusson, V., Lindblom, A., Kostulas, K., Botella-Estrada, R., Soriano, V., Juberías, P., Grasa, M., Saez, B., Andres, R., ... Stefansson, K. (2008). ASIP and TYR pigmentation variants associate with cutaneous melanoma and basal cell carcinoma. *Nature Genetics*, 40(7), 886–891.
- Habel, N., El-Hachem, N., Soysouvanh, F., Hadhiri-Bziouche, H., Giuliano, S., Nguyen, S., Horák, P., Gay, A.-S., Debayle, D., Nottet, N., Béranger, G., Paillerets, B. B., Bertolotto, C., & Ballotti, R. (2020). FBXO32 links ubiquitination to epigenetic reprogramming of melanoma cells. *Cell Death & Differentiation*.
- Kain, K. H., Miller, J. W. I., Jones-Paris, C. R., Thomason, R. T., Lewis, J. D., Bader, D. M., Barnett, J. V., & Zijlstra, A. (2014). The chick embryo as an expanding experimental model for cancer and cardiovascular research. *Dev Dyn*, 243(2), 216–228.
- Kimura, J., Katahira, T., Araki, I., & Nakamura, H. (2004). Possible role of Hes5 for the rostrocaudal polarity formation of the tectum. *Development Growth and Differentiation*, 46(3), 219–227.
- Kunimoto, R., Jimbow, K., Tanimura, A., Sato, M., Horimoto, K., Hayashi, T., Hisahara, S., Sugino, T., Hirobe, T., Yamashita, T., & Horio, Y. (2014). SIRT1 regulates lamellipodium extension and migration of melanoma cells. *Journal of Investigative Dermatology*, 134(6), 1693–1700.
- Le Douarin, N. M. (2004). The avian embryo as a model to study the development of the neural crest: a long and still ongoing story. *Mechanisms of Development*, 121, 1089–1102.
- Lin, J. Y., & Fisher, D. E. (2007). Melanocyte biology and skin pigmentation. *Nature*, 445(7130), 843–850.
- Lu, C., Zhang, J., Nagahawatte, P., Easton, J., Lee, S., Liu, Z., Ding, L., Wyczalkowski, M. A., Valentine, M., Navid, F., Mulder, H., Tatevossian, R. G., Dalton, J., Davenport, J., Yin, Z., Edmonson, M., Rusch, M., Wu, G., Li, Y., ... Bahrami, A. (2015). The genomic landscape of childhood and adolescent melanoma. *Journal of Investigative Dermatology*, 135(3), 816–823.
- Markovic, O., Markovic, N., Whiteman, D. C., Milligan, A., Welch, J., Green, A. C., & Hayward, N. K. (1997). *Germline CDKN2A Mutations in Childhood Melanoma*.

- McGill, G. G., Horstmann, M., Widlund, H. R., Du, J., Motyckova, G., Nishimura, E. K., Lin, Y., Ramaswamy, S., Avery, W., Ding, H., Jordan, S. A., Jackson, I. J., Korsmeyer, S. J., Golub, T. R., & Fisher, D. E. (2002). Bcl2 Regulation by the Melanocyte Master Regulator Mitf Modulates Lineage Survival and Melanoma Cell Viability. *Cell*, *109*(6), 707–718.
- Mei, Z., Zhang, D., Hu, B., Wang, J., Shen, X., & Xiao, W. (2015). FBXO32 targets c-Myc for proteasomal degradation and inhibits c-Myc activity. *Journal of Biological Chemistry*, *290*(26), 16202–16214.
- Nakamura, H., Katahira, T., Sato, T., Watanabe, Y., & Funahashi, J. I. (2004). Gain- and loss-of-function in chick embryos by electroporation. *Mechanisms of Development*, *121*(9), 1137–1143.
- Nasti, T. H., & Timares, L. (2015). MC1R, eumelanin and pheomelanin: Their role in determining the susceptibility to skin cancer. *Photochemistry and Photobiology*, *91*(1), 188–200.
- National Cancer Institute. (2018). *SEER cancer Stat Facts: Melanoma of the Skin*. SEER Stat Fact Sheets: Melanoma of the Skin.
- Niwa, T., Mochii, M., Nakamura, A., & Shiojiri, N. (2002). Plumage pigmentation and expression of its regulatory genes during quail development – histochemical analysis using Bh (black at hatch) mutants. *Mechanisms of Development*, *118*(1–2), 139–146.
- Pappo, A. S. (2003). Melanoma in children and adolescents. *European Journal of Cancer*, *39*(18), 2651–2661.
- Pekarik, V., Bourikas, D., Miglino, N., Joset, P., Preiswerk, S., & Stoeckli, E. T. (2003). Screening for gene function in chicken embryo using RNAi and electroporation. *Nature Biotechnology*, *21*(1), 93–96.
- Pellegrini, C., Botta, F., Massi, D., Martorelli, C., Facchetti, F., Gandini, S., Maisonneuve, P., Avril, M.-F., Demenais, F., Bressac-de Paillerets, B., Hoiom, V., Cust, A. E., Anton-Culver, H., Gruber, S. B., Gallagher, R. P., Marrett, L., Zanetti, R., Dwyer, T., Thomas, N. E., ... Wong, T. H. (2019). MC1R variants in childhood and adolescent melanoma: a retrospective pooled analysis of a multicentre cohort. *The Lancet Child & Adolescent Health*, *3*(5), 332–342.
- Sahu, S. K., Tiwari, N., Pataskar, A., Zhuang, Y., Borisova, M., Diken, M., Strand, S., Beli, P., & Tiwari, V. K. (2017). FBXO32 promotes microenvironment underlying epithelial-mesenchymal transition via CtBP1 during tumour metastasis and brain development. *Nature Communications*, *8*(1), 1–18.
- Satyamoorthy, K., Muyrers, J., Meier, F., Patel, D., & Herlyn, M. (2001). Mel-CAM-specific genetic suppressor elements inhibit melanoma growth and invasion through loss of gap junctional communication. *Oncogene*, *20*(34), 4676–4684.
- Schaefer, K. S., Doughman, Y. Q., Fisher, S. A., & Watanabe, M. (2004). Dynamic Patterns of Apoptosis in the Developing Chicken Heart. *Developmental Dynamics*, *229*(3), 489–499.

- Seynnaeve, B., Lee, S., Borah, S., Park, Y., Pappo, A., Kirkwood, J. M., & Bahrami, A. (2017). Genetic and Epigenetic Alterations of TERT Are Associated with Inferior Outcome in Adolescent and Young Adult Patients with Melanoma. *Scientific Reports*, 7(1), 45704.
- Song, Y., Lin, M., Liu, Y., Wang, Z. W., & Zhu, X. (2019). Emerging role of F-box proteins in the regulation of epithelial-mesenchymal transition and stem cells in human cancers. *Stem Cell Research and Therapy*, 10(1), 1–11.
- Strouse, J. J., Fears, T. R., Tucker, M. A., & Wayne, A. S. (2005). Pediatric melanoma: Risk factor and survival analysis of the Surveillance, Epidemiology and End Results database. *Journal of Clinical Oncology*, 23(21), 4735–4741.
- Tan, J., Yang, X., Zhuang, L., Jiang, X., Chen, W., Puay, L. L., Karuturi, R. K. M., Tan, P. B. O., Liu, E. T., & Yu, Q. (2007). Pharmacologic disruption of polycomb-repressive complex 2-mediated gene repression selectively induces apoptosis in cancer cells. *Genes and Development*, 21(9), 1050–1063.
- Velasco-Velázquez, M. A., Salinas-Jazmín, N., Mendoza-Patiño, N., & Mandoki, J. J. (2008). *Reduced paxillin expression contributes to the antimetastatic effect of 4-hydroxycoumarin on B16-F10 melanoma cells.*
- Yamagata, M., & Sanes, J. R. (2008). Dscam and Sidekick proteins direct lamina-specific synaptic connections in vertebrate retina. *Nature*, 451(7177), 465–469.
- Yamaguchi, H., & Condeelis, J. (2007). Regulation of the actin cytoskeleton in cancer cell migration and invasion. *Biochimica et Biophysica Acta*, 1773(5), 642.
- Yang, C., Li, X., Li, Q., Fu, S., Li, H., Guo, Z., Lin, J., & Zhao, S. (2014). Evaluation of three different promoters driving gene expression in developing chicken embryo by using in vivo electroporation Evaluation of three different promoters in vivo. *Genetics and Molecular Research*, 13(1), 1270–1277.
- Yuan, X., Zhang, Z., Jiang, K., Wang, X., & Li, Y. (2018). Preliminary study of the role F-box protein 32 (FBXO32) in colorectal neoplasms through the transforming growth factor beta (TGF- β)/Smad4 signalling pathway. *Medical Science Monitor*, 24, 1080–1088.
- Zhou, H., Liu, Y., Zhu, R., Ding, F., Wan, Y., Li, Y., & Liu, Z. (2017). FBXO32 suppresses breast cancer tumorigenesis through targeting KLF4 to proteasomal degradation. *Nature Publishing Group*, 36, 3312–3321.

Figure 1

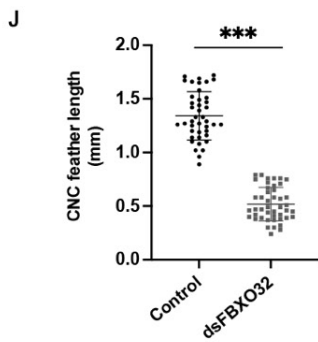
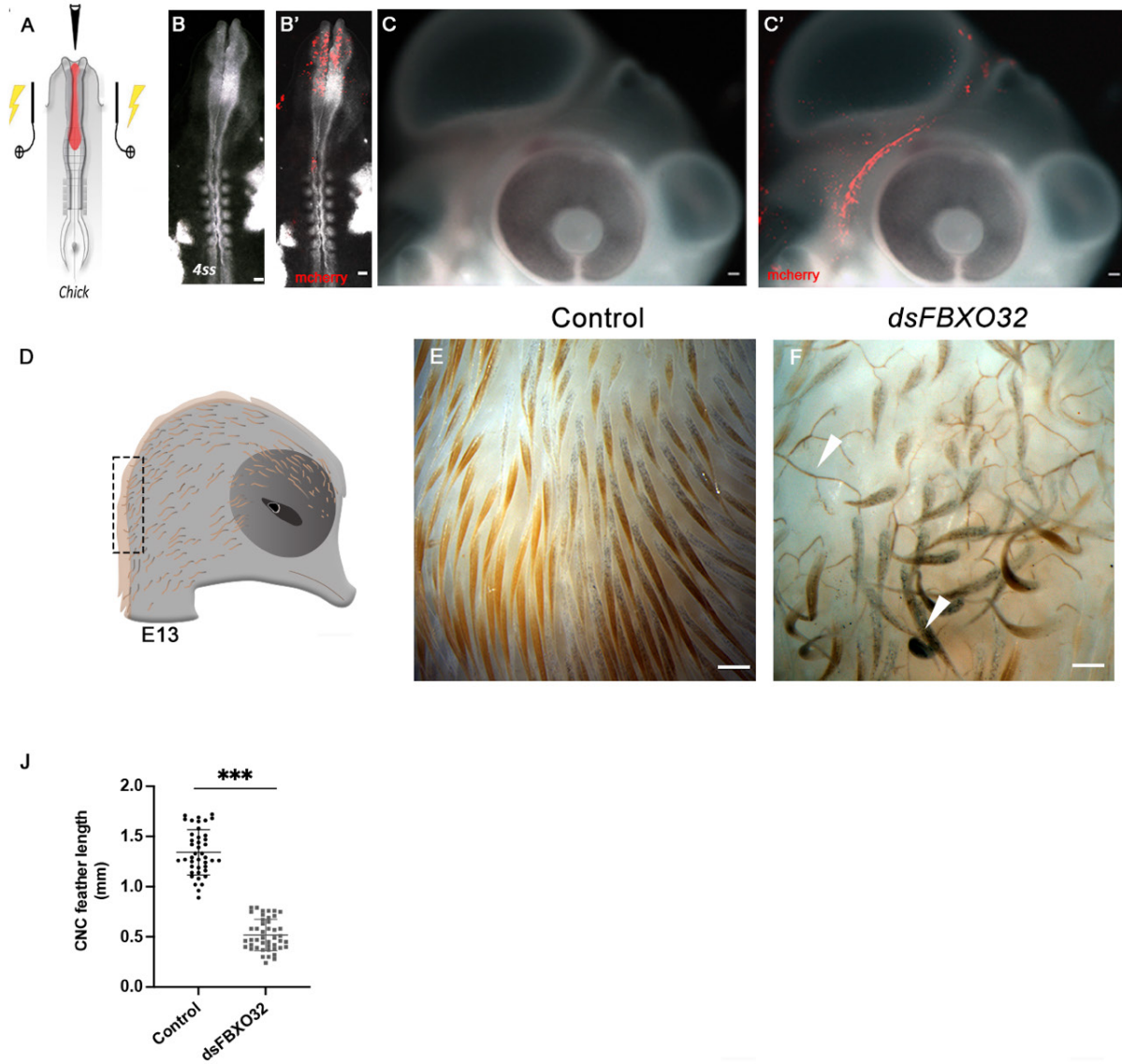
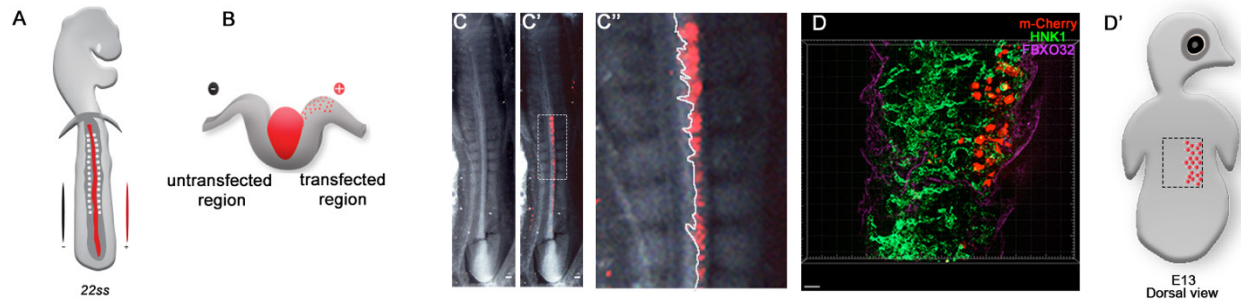


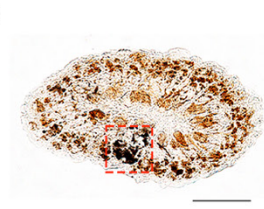
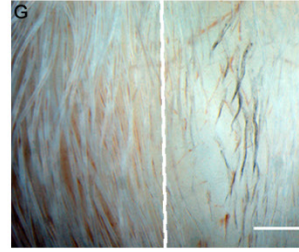
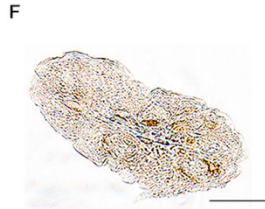
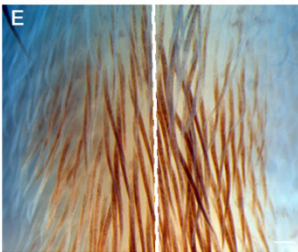
Figure 2



Control

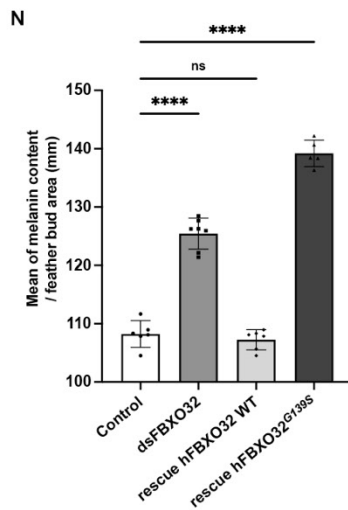
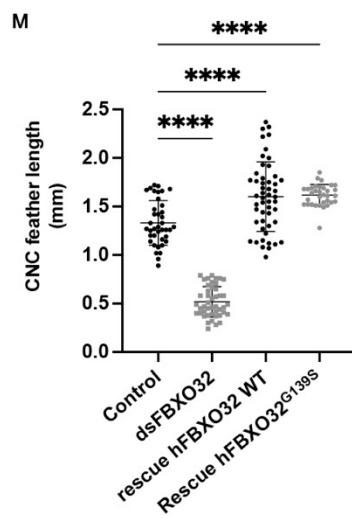
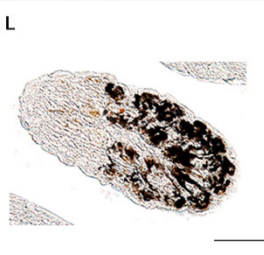
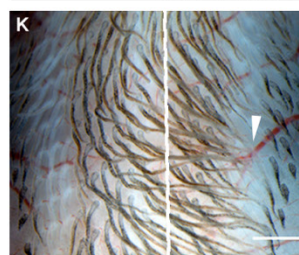
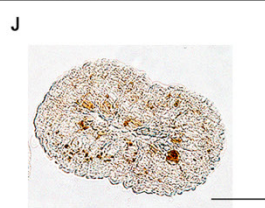
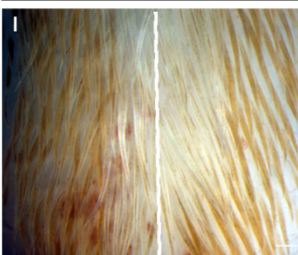
dsFBXO32

Untransfected Transfected

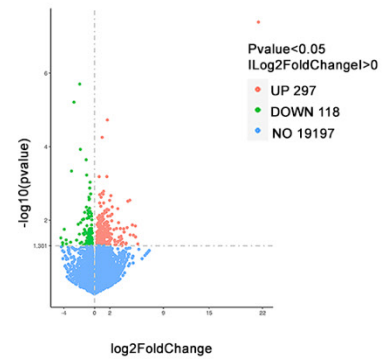


dsFBXO32 + *hFBXO32* WT

dsFBXO32 + *hFBXO32*^{G139S}



O: Volcano plot of gene enrichment/reduced in *dsFBXO32* vs Control TNC

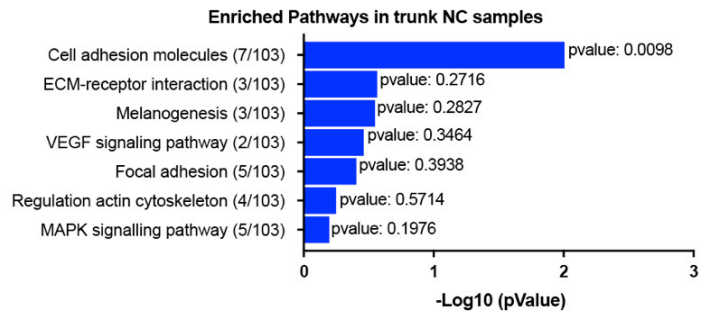


P

Signaling Pathway	Gene	Log2FoldChange
Melanogenesis	<i>melan-A</i>	-0.69975
Gap junction	<i>TUBB1</i>	-0.7029
MAPK signaling	<i>KITLG</i>	-0.805
Melanogenesis/mTor signaling	<i>WNT8</i>	-1.276
Melanogenesis	<i>TYR</i>	-1.3156

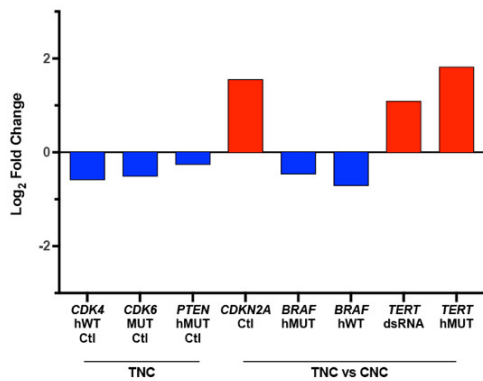
Signaling Pathway	Gene	Log2FoldChange
Adherent junctions	<i>CTNNA3</i>	1.571
MAPK signaling	<i>FGF18</i>	0.8277
ECM-receptor interaction	<i>ITG7A</i>	0.6242
VEGF signaling	<i>NFATC2</i>	0.5915
Focal adhesion	<i>CAV1</i>	0.307
Regulator of actin cytoskeleton	<i>ITGB8</i>	-0.3509

Q



R

Childhood melanoma drivers differential expression



S

BAP1 differential expression

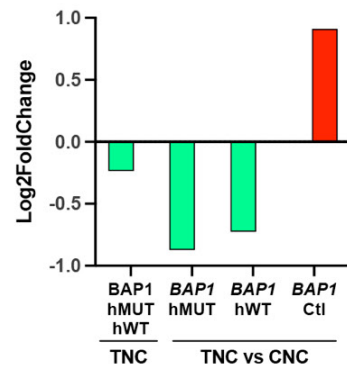
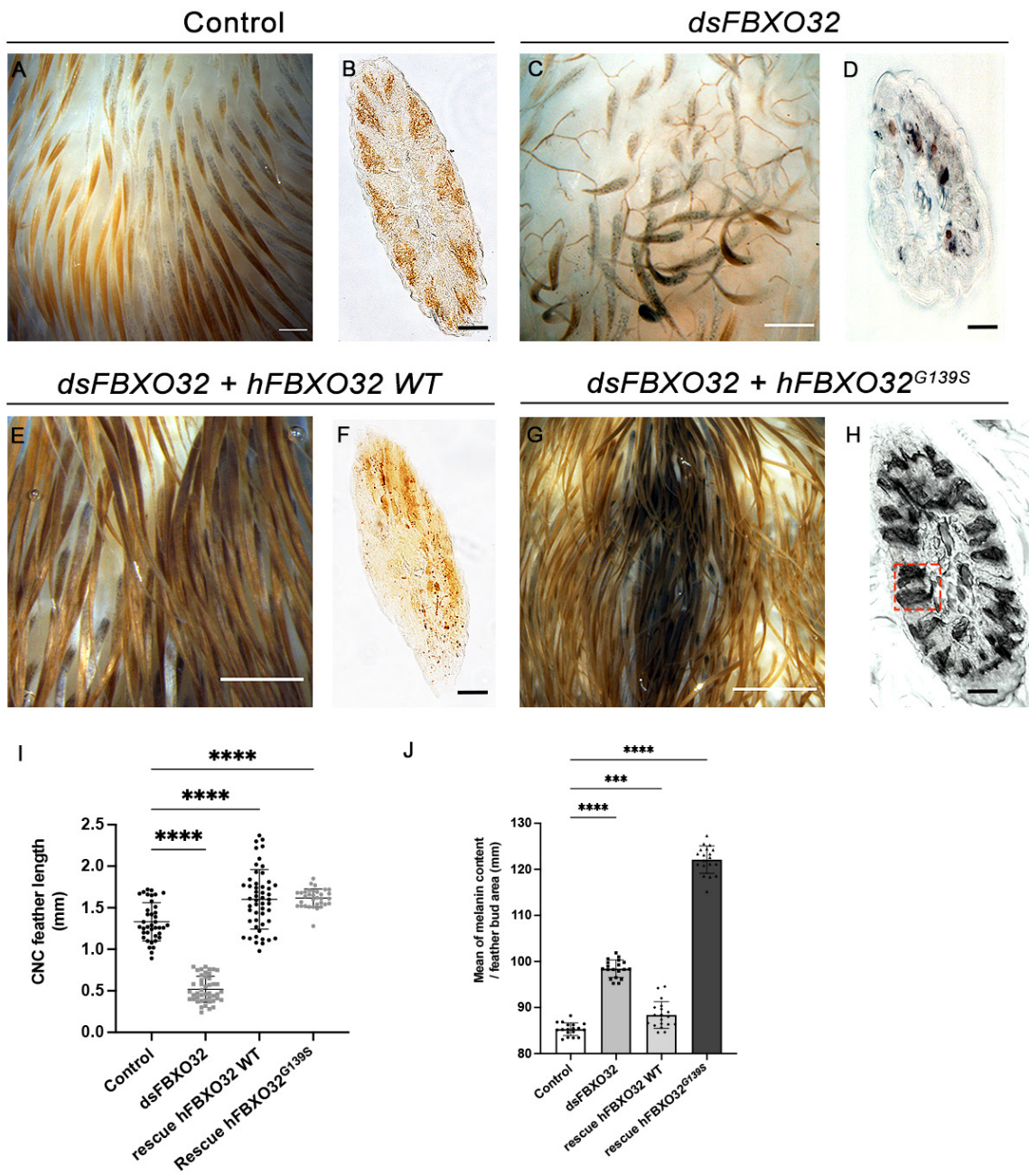
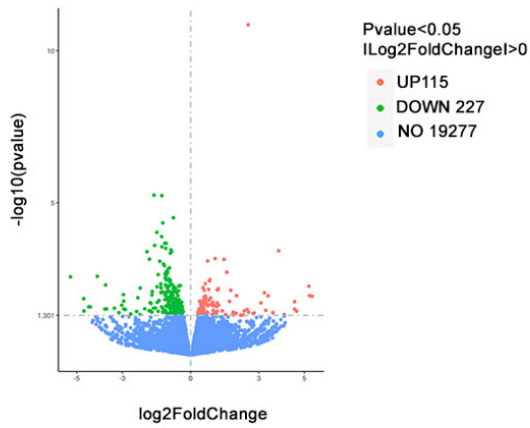


Figure 3

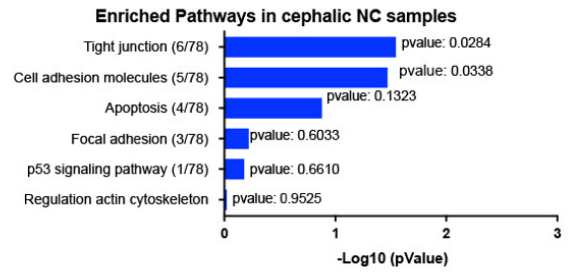


K

Volcano plot of gene enrichment/reduced in *dsFBXO32* vs Control CNC

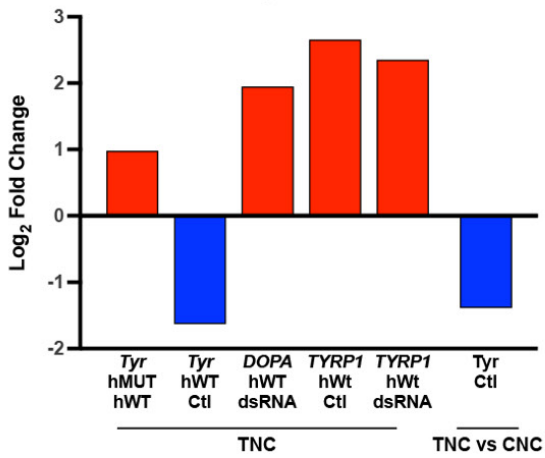


L



M

Melanogenesis genes differential expression



N

Differential expression in eumelanin synthesis regulatory genes

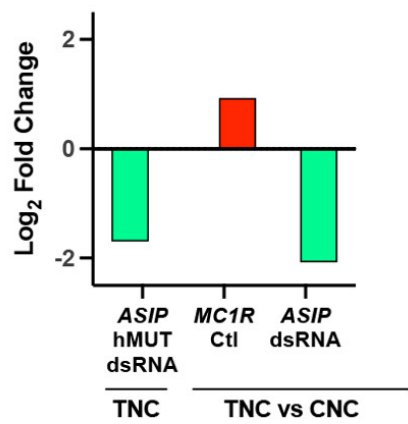
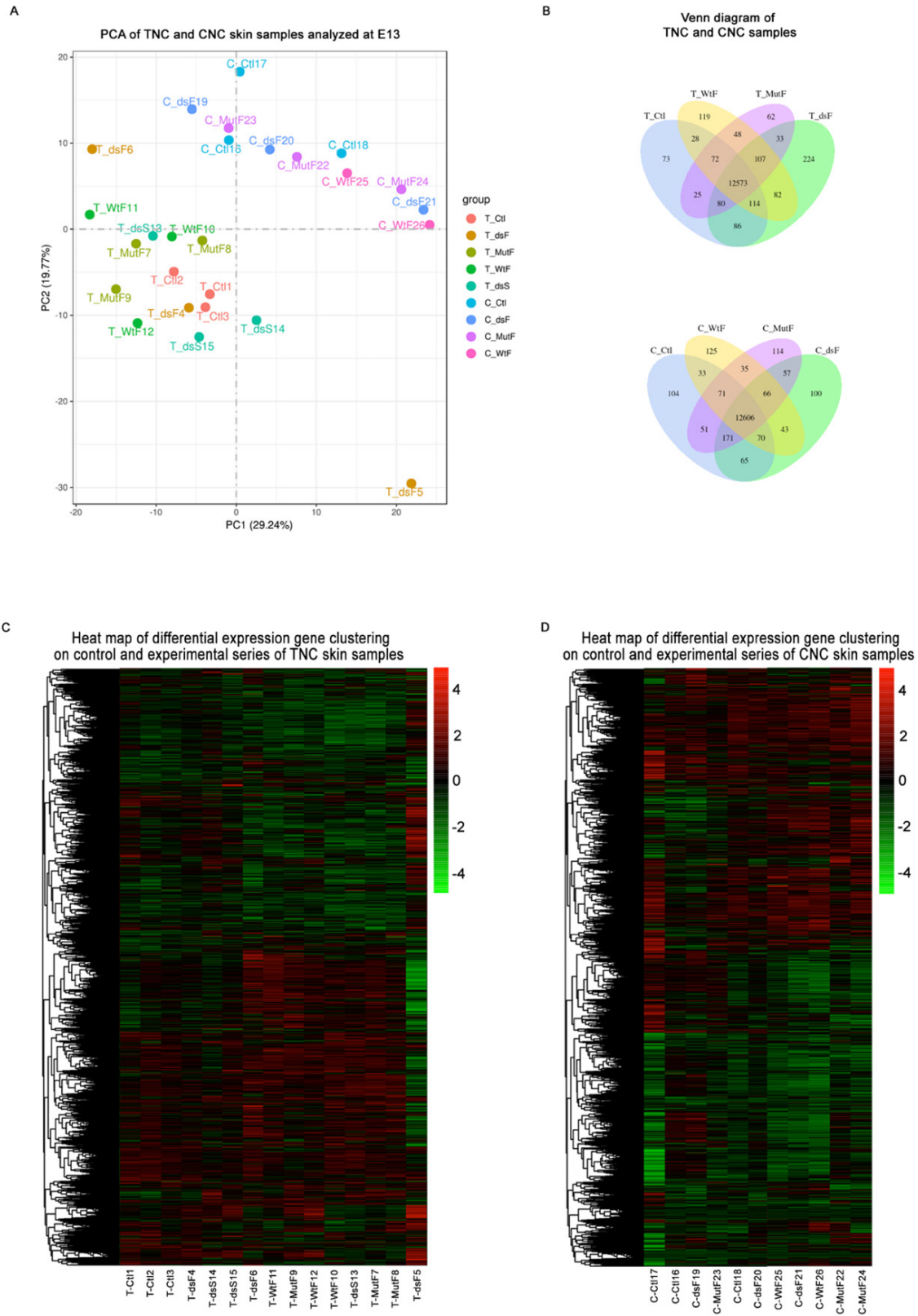
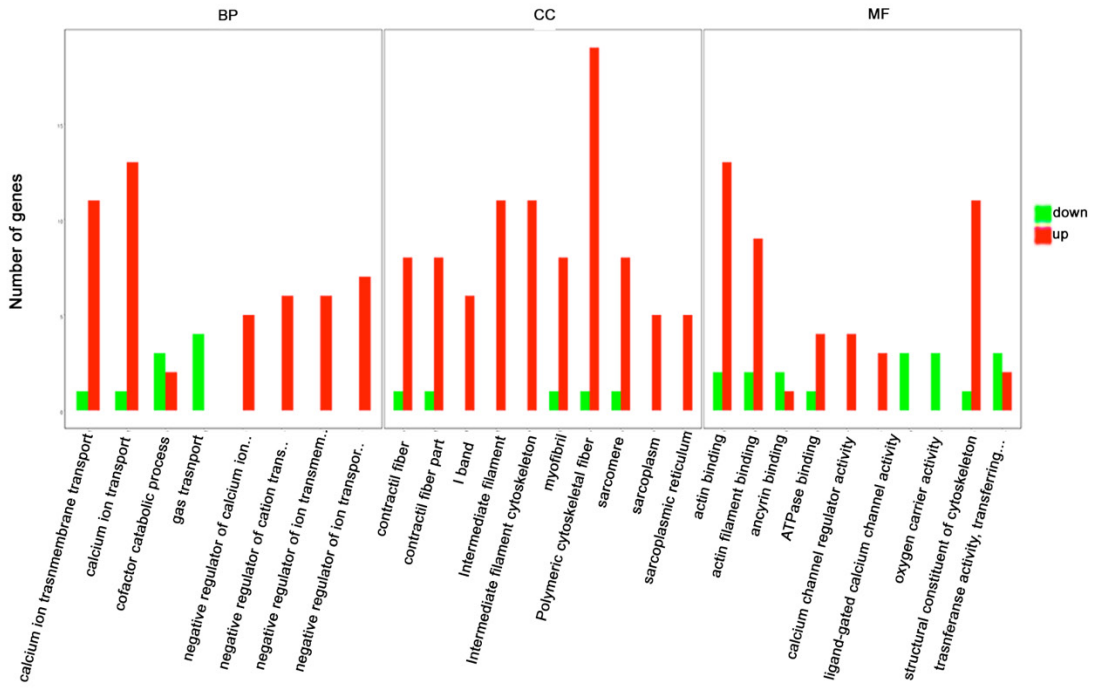


Figure 4



E

Most significant GO enrichment terms of the *dsFBXO32* and control TNC comparison



F

Most significant GO enrichment terms of the *dsFBXO32* and control CNC comparison

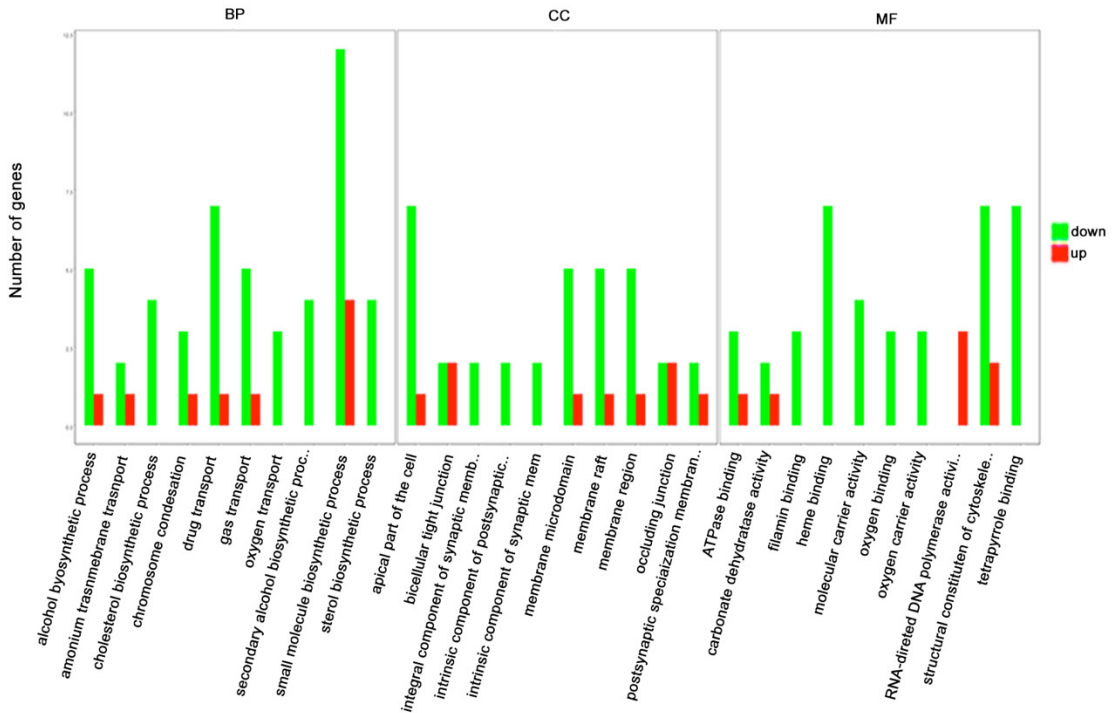


Figure 5

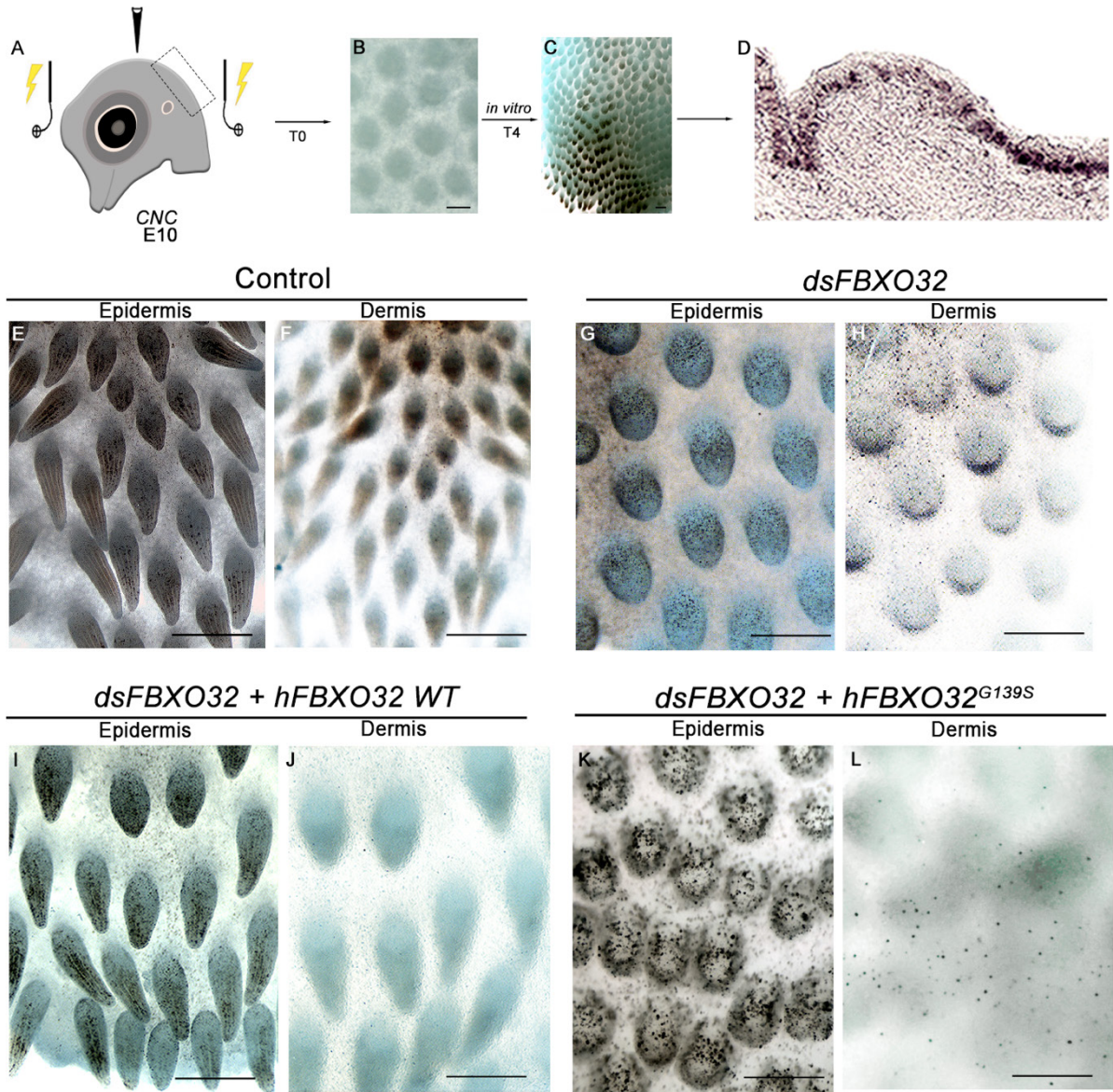


Figure 6

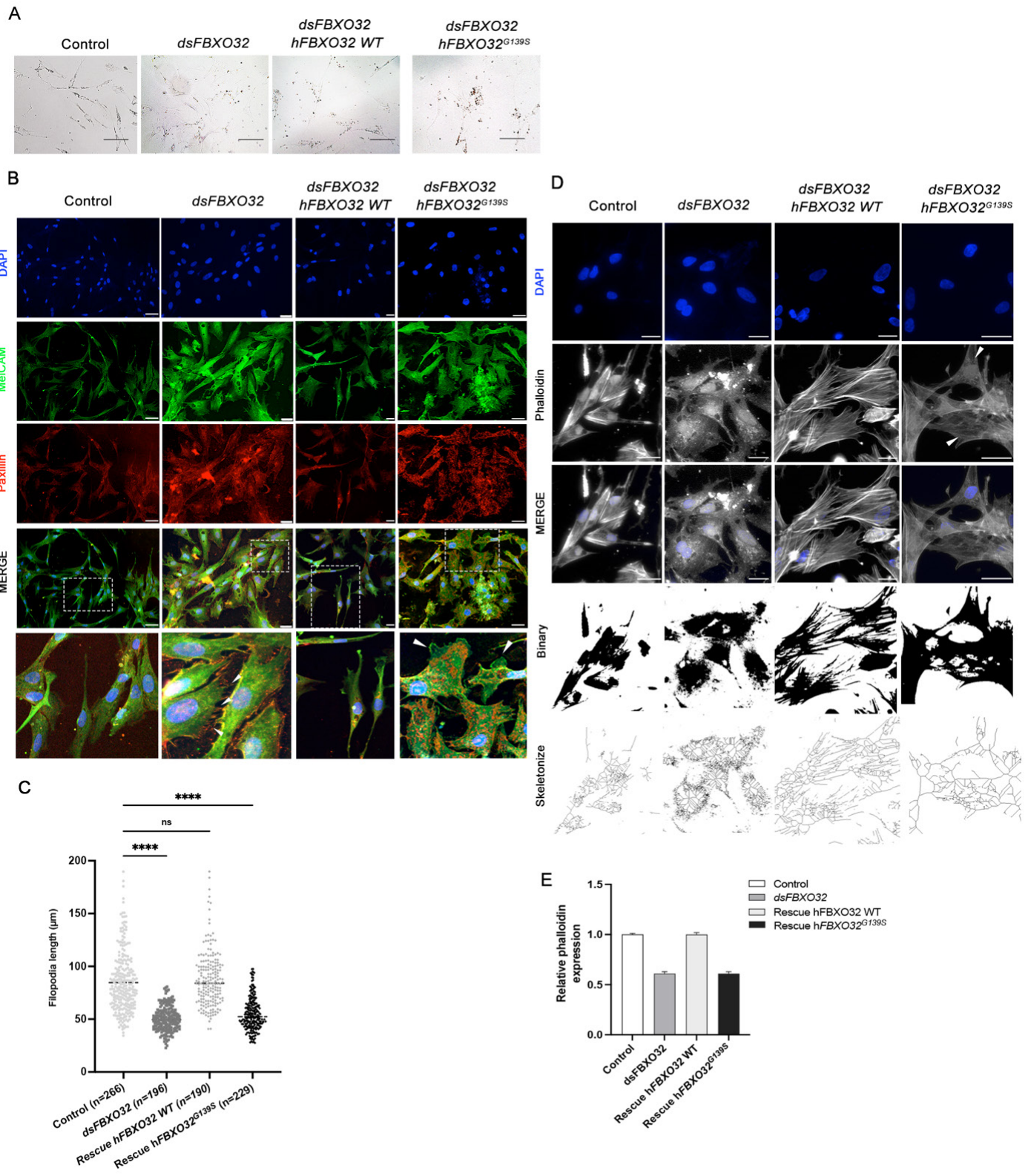


Figure legends

Figure 1. Silencing of *dsFBXO32* yields abnormal melanocyte differentiation at the CNC

A) Experimental design for FNC transfection by bilateral electroporation at 4ss chick embryo **B)** Whole-amount embryo at 4ss. **B')** and m-cherry NCCs labeling at 4ss after 3h of bilateral electroporation (telencephalon remain untransfected). **C)** 4ss of and embryo head **C')** and dorsal migration of NCCs visualized by m-cherry after two-three of bilateral electroporation. **D)** Schematic representation of phenotyping analysis in an embryo E13. **E)** Eleven days after electroporation, control feather buds exhibit foxy pigmentation and anterior-posterior polarity. **F)** *FBXO32* silencing impairs feather polarity and melanogenesis. Arrowheads indicate the vascularization in F. **J)** Box and whiskers plots showing the CNC feathers length in controls and *dsFBXO32* embryos. Statistical significance was assessed with a Dunnett's multiple comparison test against control embryos. 4 electroporated control embryos and 3 silencing embryos of *dsFBXO32* were analyzed for quantifications in all conditions. * $P \leq 0.001$, **** $P < 0.0001$.

Figure 2. *FBXO32* impairs melanocyte differentiation, feather morphology, and polarity and can be restored by overexpression of human wild-type form at the TNC

A-B) Unilateral electroporation in the neural tube at 22ss embryo. **C, C', C'')** m-cherry positive NCC delaminating after unilateral electroporation. **D)** 3D reconstruction of TNC electroporation 22ss after 20h. m-Cherry transfected cells (red), HNK1 (green), and *FBXO32* immunolabelling (magenta). **D')** Schematic representation of a dorsal embryo E13. The square represents the transfected region of interest. Dorsal view of **E)** control embryo, **G)** *dsFBXO32*, co-transfections of **I)** *dsFBXO32* + *hFBXO32* WT and **K)** *dsFBXO32* + *hFBXO32*^{G139S}. The dotted lines defined the untransfected TNC region (left) and the transfected TNC region (right). **F, H, J, L).** Transversal section of feather buds showing melanocyte localization at the barb ridges. Notice the eumelanin pigment accumulation in a feather bud in H and the tight melanocyte accumulation with eumelanin pigment in L. **M)** Box and whiskers plots showing TNC feather length in control, *dsFBXO32*, rescue *hFBXO32* WT, and rescue *hFBXO32*^{G139S}. **N)** Mean of melanin content per feather bud area (mm) in all conditions. **O)** Volcano plot of all genes statistically enriched or reduced in truncal *dsFBXO32* versus control samples, upregulated 297 and downregulated 118 genes. **P)** Genes enriched or deregulated in trunk *dsFBXO32* samples. **Q)** Significantly signaling

pathways predicted to be enriched in trunk NC samples by GO analysis. **R)** Bar chart showing differentially expressed genes related to childhood melanoma drivers. **S)** Bar chart showing downregulation of BAP1 in *FBXO32*^{G139} at TNC and CNC. Upregulated genes in red and downregulated genes in blue. *****P* <0.0001, *ns p*=0.7747. Quantifications for 5 TNC control electroporated embryos, 5 silencing embryos of *dsFBXO32*, 4 rescue embryos with the human WT form *hFBXO32*, and 4 rescue embryos with human mutant form *FBXO32*^{G139S} were analyzed in M and N. Scale bar:50µm.

Figure 3. *FBXO32* impairs melanocyte differentiation and can be restored by overexpression of the human wild type at the CNC level.

Dorsal views of **A)** control embryo **C)** *dsFBXO32* embryo, co-electroporation with **E)** *dsFBXO32* + *hFBXO32* WT and **G)** *dsFBXO32* + *hFBXO32*^{G139S}. Transversal section of feather bud in **B)** control embryos **D)** *dsFBXO32* embryo **F)** *dsFBXO32* + *hFBXO32* WT, and **H)** *dsFBXO32* + *hFBXO32*^{G139S} showing the melanocyte as black patches (eumelanin). Red squares show melanocyte filopodia towards the soma (dermis). **I)** Box and whiskers plots showing quantification of CNC feather length. **J)** Silencing of *FBXO32* results in hypoplastic feather buds. Statistical significance was assessed with a Dunnett’s multiple comparison test against the control embryos. *****P* <0.0001. Scale bar in E, G, I, K: 500µm; in F, H, J, L:25µm. **K)** Volcano plot of all genes statistically enriched or reduced in cephalic *dsFBXO32* versus control samples, upregulated genes 115 and downregulated genes 227. **L)** Significantly signaling pathways predicted to be enriched in cephalic NC samples by GO analysis. **M)** Bar chart showing examples of melanogenesis-related differential expressed genes in TNC and CNC. **N)** Bar chart showing examples of eumelanin pathway-related differential expressed genes in TNC and CNC

Figure 4. RNA-seq reveals transcript differential enrichment diversity and activated genes in *FBXO32* experimental series in CNC and TNC

A) PCA plot based on the trunk and cranial skin samples E13. Trunk and cranial NC samples populations appear clearly in two clusters indicating that NC populations have differential gene expression patterns. **B)** Venn diagram comparing all experimental series controls, *dsFBXO32* (T_dsF and C_dsF), rescue with the human wild type form of *FBXO32* (T_WtF and C_WtF), and rescue with the human mutant form of *FBXO32* (T_MutF and C_MutF) in TNC and CNC samples. **C)** Differential expression gene clustering heatmap of truncal and cephalic NC skin samples

analyzed by RNA-seq. **(C-D)** Two differential TNC and CNC clusters by NC origin. **E-F)** Bar Chart showed the 30 most terms enriched from GO enrichment analysis results. All terms are grouped according to major categories of biological processes (BP), cell component (CC), molecular function (MF), and categories of up or downregulated genes. **E)** GO most enrichment terms from the *dsFBXO32* and control comparison in the TNC. Signaling pathways are predominantly upregulated. **F)** GO most enrichment terms from the *dsFBXO32* and control comparison in the CNC. Signaling pathways are mostly downregulated

Figure 5. *in vitro* silencing of *dsFBXO32* yields melanocyte proliferation and migration.

A) Bilateral electroporation technique at the CNC level in E10 embryos. **B)** After CNC electroporation, the 3D skin explant is maintained for four days in *in vitro* condition. **C)** Melanogenesis takes place at the central longitudinal axis. **D)** Melanocytes are normally distributed at the skin epidermis. Melanocyte differentiation in **E-F)** control skin explants, **G-H)** *dsFBXO32* at the epidermis and dermis level. Notice the migration of melanocytes at the dermis. **I-J)** *FBXO32* overexpression in combination with human *FBXO32* WT. **K)** *FBXO32* overexpression in combination with human *FBXO32*^{G139S} showing **L)** melanocyte migration at the dermis. Scale bar: 500µm.

Figure 6. *FBXO32* induces melanocyte transformation and cytoskeleton remodeling.

A) Isolated cells from 3D skin explants previously electroporated were maintained *in vitro* for 4 days. Control cells exhibit bipolar morphology, whereas silencing of *FBXO32* results in multipolar morphology. **B)** Confocal images control, *dsFBXO32*, rescue *hFBXO32* WT, and rescue *hFBXO32*^{G139S} transfected cells to assess the expression of antibody against MelCAM to detect adhesion molecule (second row), Paxillin to detect focal adhesion plaque (third row). Magnification of each series shows the misregulation of paxillin at the filopodia and the increase in lamellipodia in *dsFBXO32* and mutant cells. Arrowhead showed blebbing, leading to invasive capacity in mutant cells. **C)** Scatter dot plot of filopodia length quantifications in melanocyte cells (median with interquartile range). ANOVA test was performed to compare conditions. **D)** Distribution of phalloidin accumulation in control, *dsFBXO32*, rescue *hFBXO32* WT and rescue *hFBXO32*^{G139S} to detect actin filaments (second row). Actin filaments were analyzed with Fiji Binary plugging (fourth row), illustrating phalloidin intensity, and skeletonized plugging (fifth row), showing actin filament branching. **E)** Bar chart showing relative expression of phalloidin in

different conditions, seen as intensity. n=number of filopodia analyzed from three independent experiments (**** P<0.0001). Error bars: SD. Scale bar in A: 50μm, scale bar in B and D: 25μm

Figure S1

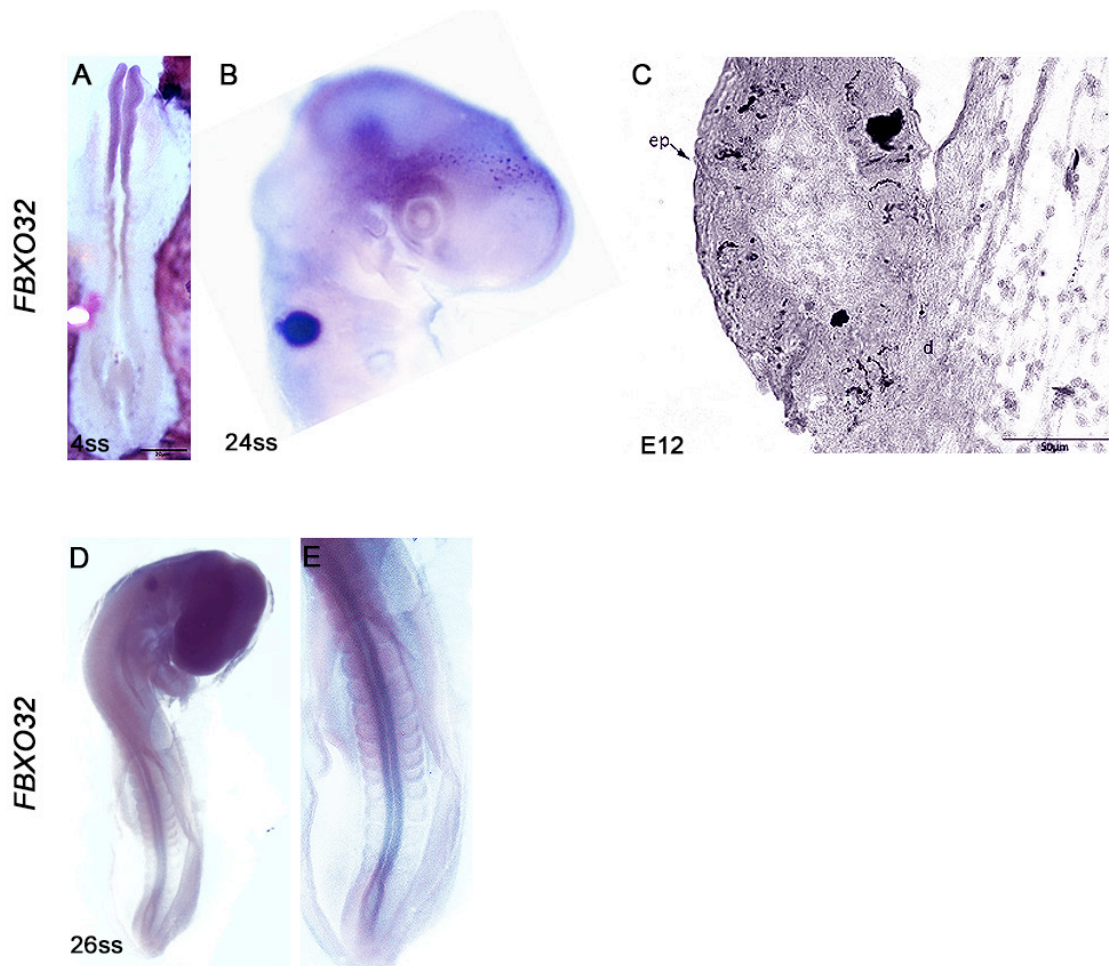


Figure S2

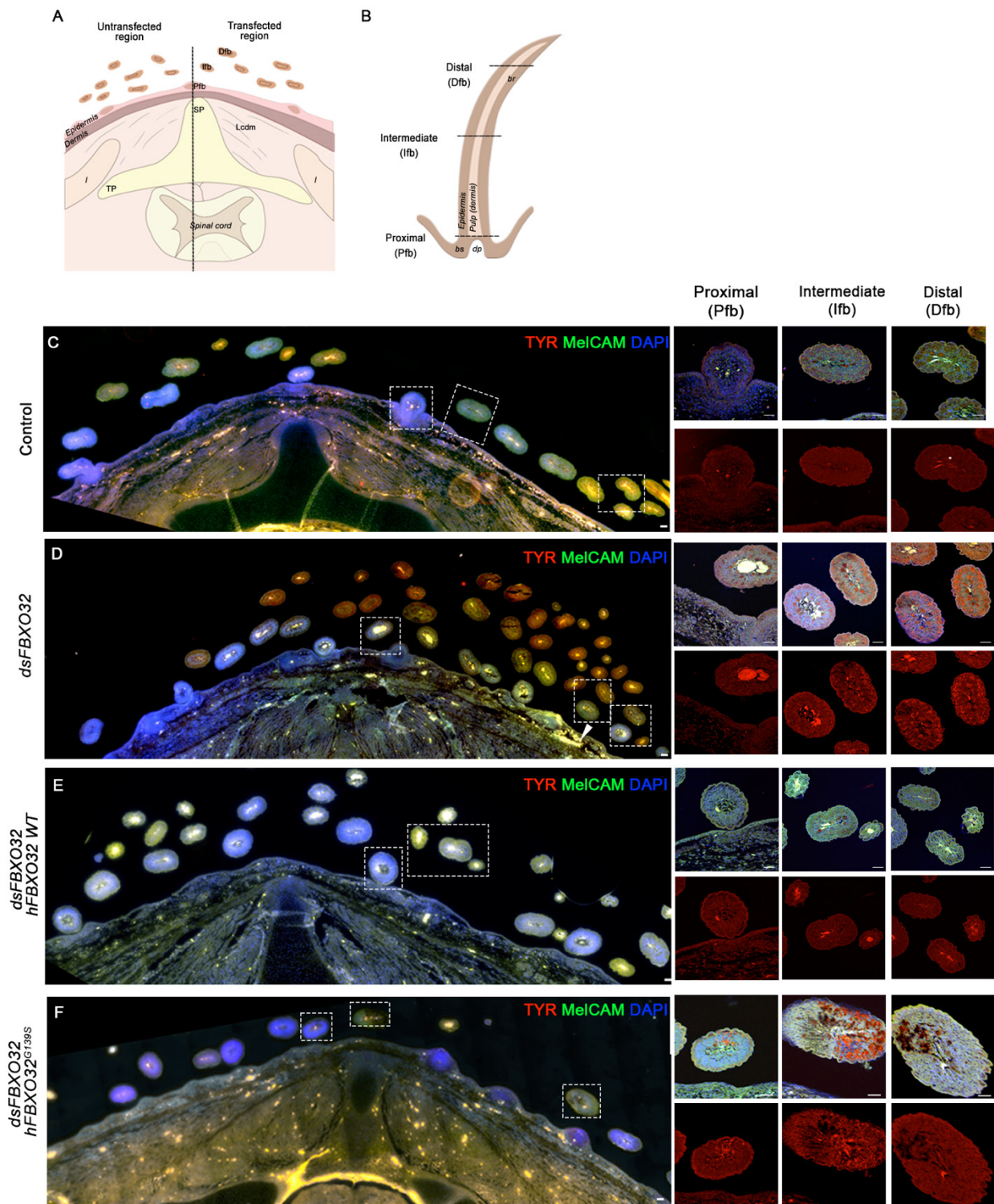


Figure S3

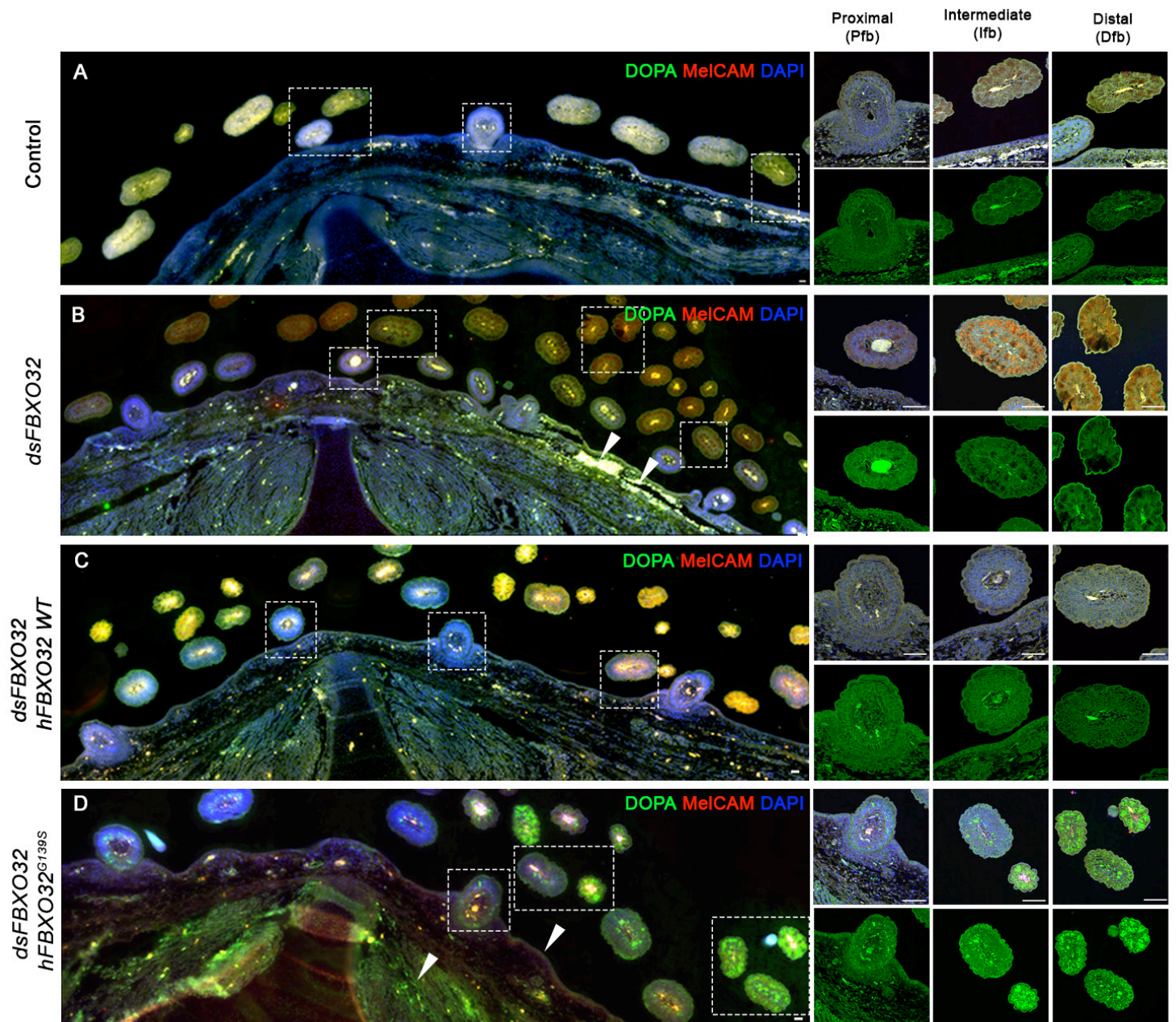


Figure S4

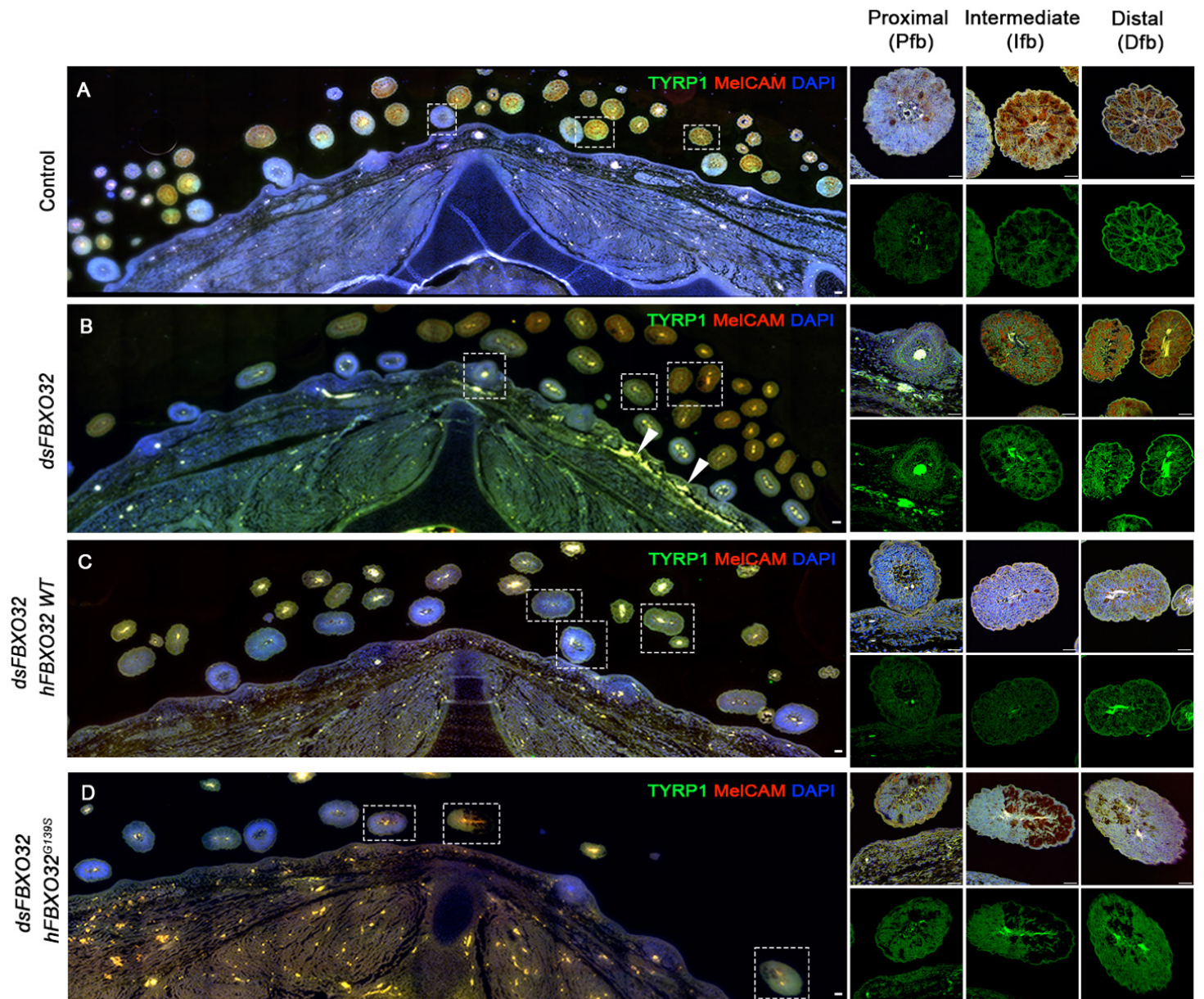


Figure S5

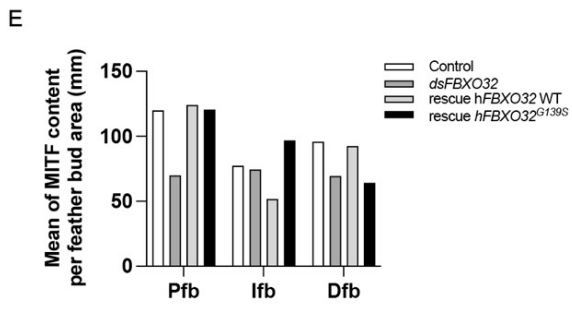
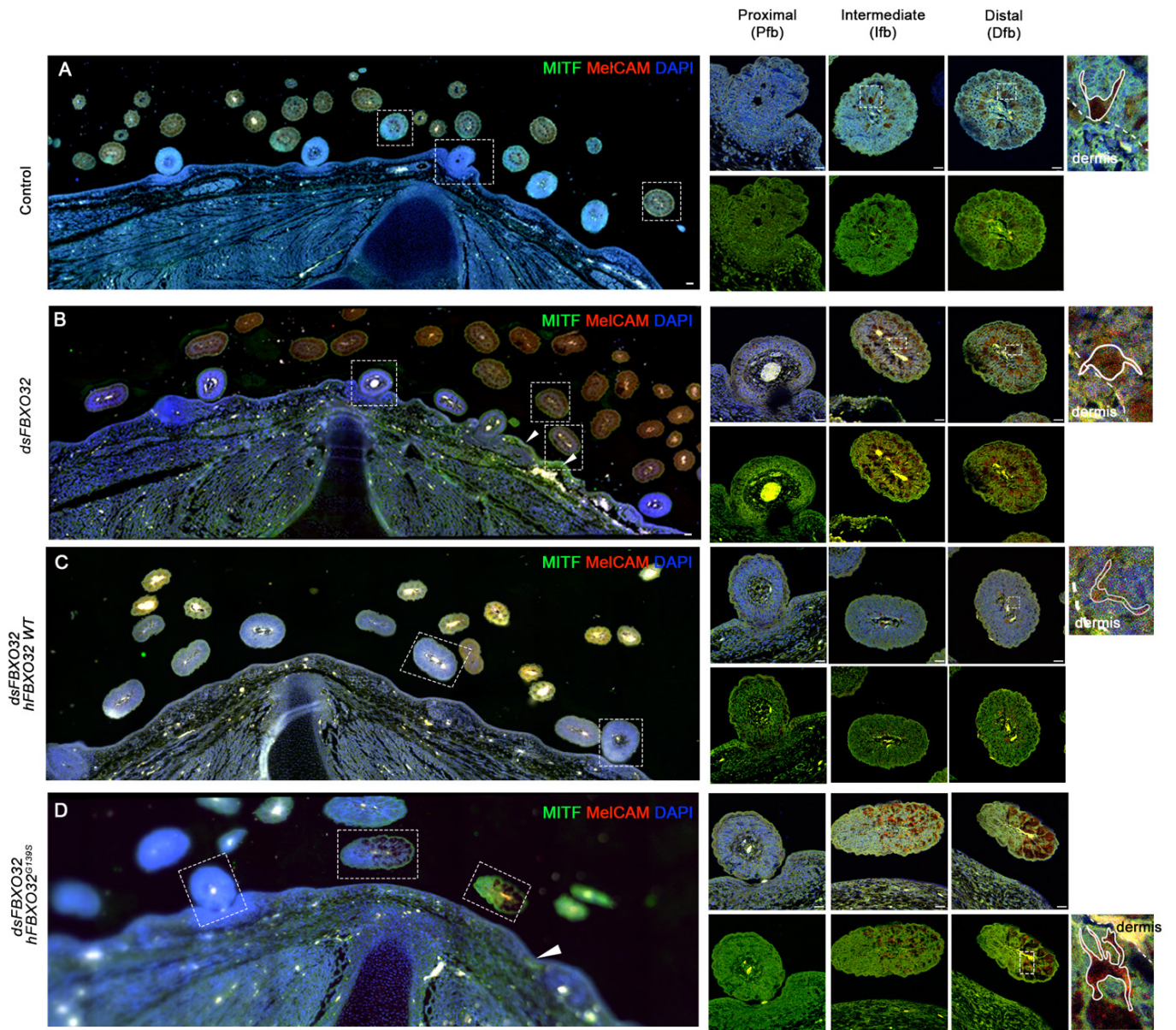
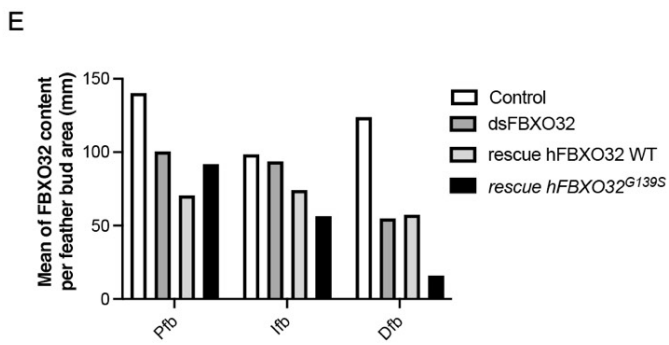
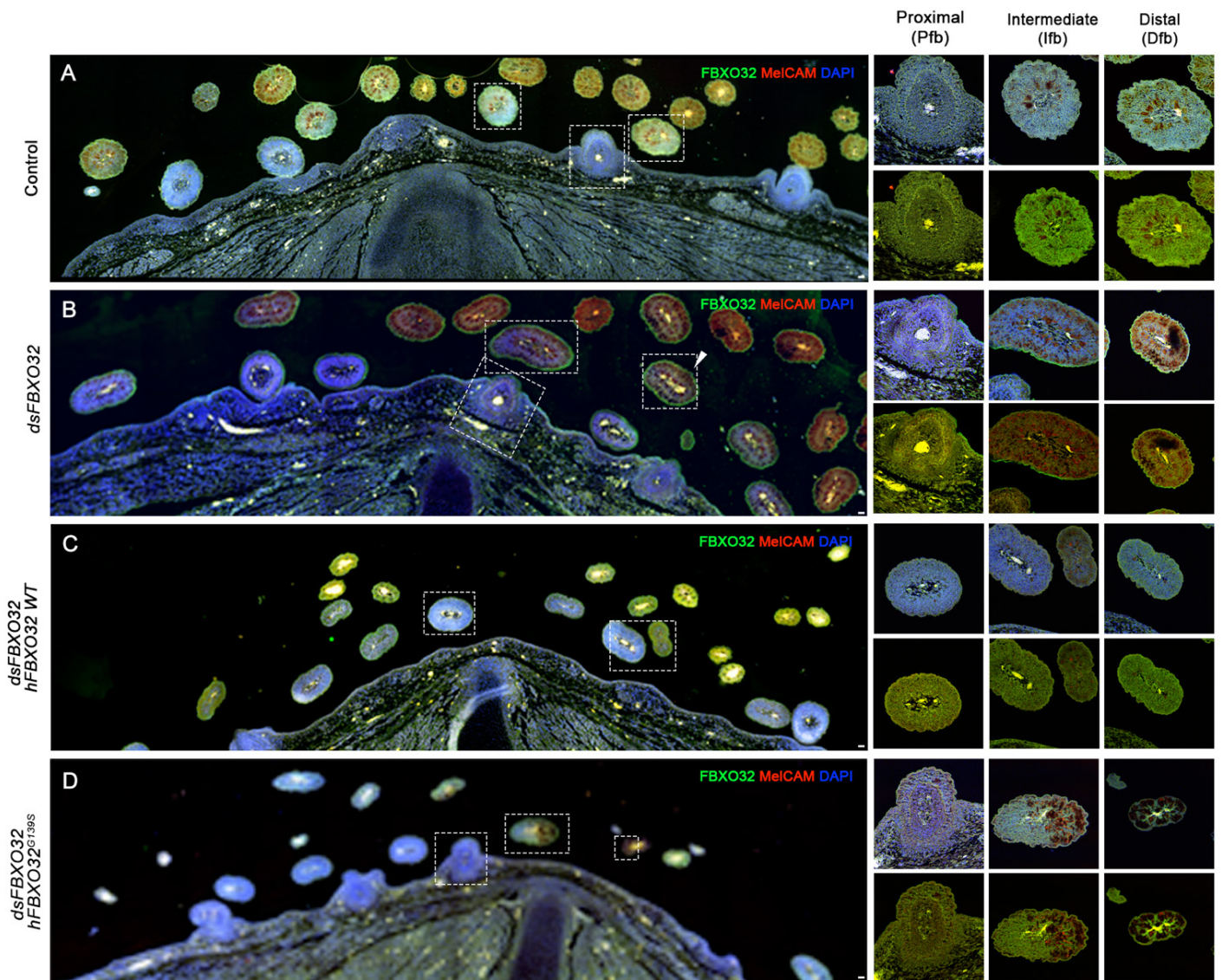


Figure S6



Supplemental figures

Figure S1. *FBXO32* transcripts are expressed in the CNC and TNC at different developmental stages.

A) transcripts are expressed in migratory FNC at 4ss embryos. **B)** Lateral view of hybridization for *FBXO32* transcripts at 24-26ss embryos. Transcripts are accumulated in migrating NCC at nasofrontal, retro-ocular, olfactory placode, and branchial-arches regions. **C)** Feather bud transversal sections of control embryos showing transcripts accumulation of *FBXO32* at the melanoblast-melanocyte lineage. **D-E)** Hybridisation for *FBXO32* in the neural tube at 26-24ssss.

Figure S2. inhibition of *FBXO32* at the trunk level exhibits a high accumulation of TH at the level of eumelanin pigmentation, potentially disturbing the onset of melanin synthesis.

A) Diagram of a trunk transversal section through the limbs. The dotted line indicated the untransfected and transfected region after unilateral electroporation. **B)** Diagram of the feather bud structure. Trunk section immunostaining against TYR and MelCAM in **C)** controls, **D)** *dsFBXO32*, **E)** *dsFBXO32* + h*FBXO32* WT and **F)** *dsFBXO32* + h*FBXO32* MUT. Arrowheads indicate double staining of TH and MelCAM at the dermis layer in D. Confocal images of proximal, intermediate, and distal feather buds show a merge of TYR, MelCAM, DAPI, and TH alone. SP: spinous process of the vertebra, TP: the transversal process of the vertebra, Lcdm: longus colli dorsalis muscle, I: ilium, Br: barb ridge, Bs: basal layer, Dp: dermal papilla, Ifb: intermediate feather bud, Dfb: distal feather bud, Pfb: proximal feather bud. Scale bar in mosaics trunk section and feather bud: 25µm.

Figure S3. *FBXO32* affects DOPA accumulation at melanocyte lineage

A-D) Immunohistochemistry in trunk section against DOPA and MelCAM in **A)** controls, **B)** *dsFBXO32*, **C)** co-electroporated with *dsFBXO32* + h*FBXO32* WT and **D)** co-electroporated with *dsFBXO32* + h*FBXO32* MUT. Confocal images of proximal, intermediate, and distal feather bud showing higher DOPA accumulation

in B and D. Arrowheads indicate DOPA localization at the level of the epidermis, dermis in C, and epidermis dorso-lateral muscle (longus colli dorsalis muscle) in D after *FBXO32* transfection. Scale bar in mosaics trunk section and feather bud magnification: 25µm.

Figure S4. *FBXO32* silencing alters TYRP1 accumulation at the trunk level.

A-D) Immunohistochemistry in trunk section against TYRP1 and MelCAM in **A)** controls, **B)** *dsFBXO32*, **C)** co-electroporated with *dsFBXO32* + h*FBXO32* WT and **D)** co-electroporated with *dsFBXO32* + h*FBXO32* MUT. Confocal images of proximal, intermediate, and distal feather buds show a merge of TYRP1, MelCAM, DAPI, and TYRP1 alone. Arrowheads indicate the colocalization of TYRP1 and MelCAM at the dermis layer. Scale bar in mosaics trunk section and feather bud magnification: 25µm.

Figure S5. Epistatic relation between *FBXO32* and MITF

A-D) Trunk section immunostaining against MITF and MelCAM in **A)** controls, **B)** *dsFBXO32*, **C)** co-electroporation with *dsFBXO32* + h*FBXO32* WT and **D)** co-electroporation with *dsFBXO32* + h*FBXO32* MUT. Arrowheads indicate the colocalization of MITF, MelCAM at the dermis layer in B. Confocal images of proximal, intermediate, and distal feather buds show a merge of MITF, MelCAM, DAPI, and MITF alone. Magnification of a unique melanocyte showing filopodia polarization towards the epidermis in A and C and to the dermis in B and D. **E)** Quantification of MITF content per feather bud are in all conditions. Pfb: proximal feather bud, lfb: intermediate feather bud, Dfb: distal feather bud. Scale bar in mosaics trunk section and feather bud magnification: 25µm.

Figure S6. Partial-efficient silencing of *FBXO32* at TNC.

A-D) Trunk section immunostaining against *FBXO32* and MelCAM in **A)** controls, **B)** *dsFBXO32*, **C)** co-electroporation with *dsFBXO32* + h*FBXO32* WT and **D)** co-electroporation with *dsFBXO32* + h*FBXO32* MUT. Arrowheads indicate the colocalization of *FBXO32* and MelCAM at the stratum corneum in B. Confocal images of proximal, intermediate, and distal feather buds show a merge of *FBXO32*, MelCAM, DAPI, and *FBXO32* alone. **E)** Quantification of *FBXO32* content per feather bud. *FBXO32* was partially inhibited in *dsFBXO32* embryos at the TNC. Pfb: proximal feather bud,

Ifb: intermediate feather bud, Dfb: distal feather bud. Scale bar in mosaics trunk section and feather bud magnification: 25 μ m.

9 Discussion

9.1 Main findings and significance

Melanoma arises due to a malignant transformation of melanocytes, the pigment cells that are embryonically derived from the NC (Strouse et al., 2005). When compared to adult melanoma, melanoma in children is a rare entity. Genetics variants detected in children or adolescents are not of the exact nature as those found in adults and, therefore, cannot be understood, investigated, and treated the same way. Considering the previous identification of *de novo* candidates' variants in childhood melanoma, my Ph.D. project presented here explores the biological significance of the new genetic variants in melanocyte differentiation. At the beginning of this project, four variants: *FBXO32*, *SOX10*, *DSCAM*, and *ALDH1L1*, were selected to analyze their biological significance during NC development. Then, an in-depth analysis was conducted on the gene *FBXO32* to determine whether the variant p.G139S could potentially impair melanocyte development. The results obtained during my Ph.D. evidence the role of all four candidate variants in normal melanocyte development and the deeper analysis and understanding of *FBXO32* implication in melanocyte transformation (**Table 7**).

- 1) I have demonstrated that all four variants are expressed in the NCCs and derivatives at three developmental stages: the onset of NCCs migration, during NCCs migration, and melanocyte differentiation. The detection of the transcript gives the proof concept of these genes' involvement in NC development to perform functional analysis.
- 2) The *FBXO32*, *SOX10*, *DSCAM*, and *ALDH1L1* gene inactivation at the CNC yields abnormal feather morphology, polarity, and vascularization. The *FBXO32* gene silencing results in eumelanin synthesis: contrary, *SOX10*, *DSCAM*, and *ALDH1L1* silencing results in melanin inhibition.
- 3) I have demonstrated that the variant, p.G139S, triggers melanocyte transformation in melanocyte polarity and enhances dermal vascularisation and eumelanin synthesis in TNC and CNC, and the abnormal phenotypes are alleviated and restored by the human *FBXO32* WT which can bypassed the detrimental effect of *FBXO32* loss-of-function.
- 4) The innovative *ex vivo* skin explant assay that I set up during this PhD demonstrated that *FBXO32* induces melanocyte migration toward the dermis.
- 5) At the cellular level, I demonstrated that *FBXO32*^{G139S} impairs filopodia length, lamellipodia, and promotes blebs protrusion formation, and provokes cell-cell

aggregates. These defects coincide with cytoskeleton and focal adhesion disassembly results in *FBXO32*^{G139S} and could be potentially involved in defective cell movement, cell misorientation in the epidermis, and aberrant back migration and dissemination toward dermal tissues

- 6) Two distinct differential gene enrichments were detected in the TNC and CNC at the transcriptomic level. Even though both TNC and CNC equally form melanocytes, when exposed to the detrimental effect of the same mutation, *FBXO32*^{G139S}, they exhibit similar phenotypical changes, but radically different gene enrichment profiling.
- 7) I established by RNAseq that two potential transcriptional networks of *FBXO32* are *ASIP* and *BAP1*. *FBXO32*^{G139S} results in downregulation of both genes suggesting that *FBXO32* might at least counteract melanogenesis by negatively downregulating *ASIP* to stimulate eumelanin synthesis

Table 7 *FBXO32* induces morphogenesis disruption in melanocyte differentiation

	TNC and CNC			
	Control	<i>dsFBXO32</i>	<i>dsFBXO32</i> + <i>hFBXO32</i> WT	<i>dsFBXO32</i> + <i>hFBXO32</i> ^{G139S}
Melanogenesis	Pheomelanin	Eumelanin	Pheomelanin	Eumelanin
Hypoplastic feather		YES		
Hyperplastic feather			YES	YES
Feather polarity	Normal	Disrupted	Normal	Disrupted

9.2 Silencing of *FBXO32*, *SOX10*, *DSCAM*, and *ALDH1L1* impairs melanocyte differentiation at the CNC

Initially, I investigated the biological role in melanocyte development of four candidate genes, *FBXO32*, *SOX10*, *DSCAM*, and *ALDH1L1*. Through *in situ* hybridization experiments, I proved that these four genes were expressed in neural crest cells at different stages of development in the chicken embryo. Then, I performed gene inactivation by RNAi electroporation at the CNC. I have demonstrated that the loss of expression of these genes led to phenotypes with abnormalities in melanocyte development, visible at both the cellular and anatomical levels. The gene *FBXO32* promotes melanocyte transformation by impairing polarity, increasing dermal vascularisation, and eumelanin synthesis. For this reason, my research project focused on the gene *FBXO32*, which gene silencing resulted in the most striking phenotypes. Our research project strategy was to assess rescue experiments in *FBXO32* using the human form of the gene carrying the *de novo* germline variant p.G139S detected in the children. To further understand if the genes *SOX10*, *DSCAM*, and *ALDH1L1* are involved in melanocyte transformation, we could follow our strategy by performing rescue experiments either with the human WT for the gene or the variant detected in the children. The variants corresponds to *SOX10*, p.R433Q, *DSCAM* both somatic p.E1825Q and p.G1460R identified in two different trios and *ALDH1L1*, p.R60H. Their effects will be studied in the melanoblast/melanocytic lineage at the anatomical, molecular, and cellular levels.

My results indicate the ongoing angiogenesis process by the increased vascularisation observed at the dermis level, supporting the idea that *FBXO32* can be involved in angiogenesis, which has a critical role in melanoma. Vascularization observed in both TNC and CNC could be studied by analyzing angiogenic growth factors such as Vascular Endothelial Cell Growth Factor (VEGF) and Basic Fibroblast Growth Factor (FGF). At the cephalic level, where CNC cells are capable of forming both melanocyte and perivascular cells, the coincident development of the vasculature in subectodermal tissues, is associated with a specific tropism of the *FBXO32*^{G139S} transfected CNC-derived melanocytes towards the vascular wall. Our observation suggests that such an angiotropism known as 'Pericyte mimicry" (Lugassy et al., 2020), could strengthen the noxious impact of *FBXO32*^{G139S} in CNC cells by favoring the systemic dissemination of transformed melanocytes.

9.3 *FBXO32* induces melanocyte transformation

Our longitudinal analysis in *FBXO32* from the onset of NC migration to melanoblast/melanocyte lineage shows reciprocates phenotypic. Aberration in melanocyte differentiation in TNC and CNC

compartments at different developmental stages. I investigated the MelCAM marker by immunolabelling, related to cell migration and melanoma progression and metastasis (Reid et al., 2013). Even if MelCAM is expected to not be detected in normal melanocytes, I observed its expression in control TNC tissue but increased accumulation in silencing and overexpression with *FBXO32*^{G139S}. This differential accumulation of MelCAM demonstrated by the *in vivo* experiments demonstrated the onset of melanocyte transformation. Moreover, we show that a differential percentage of MelCAM-positive cells correlates with the involvement of the *FBXO32* in melanocyte transformation.

9.4 *FBXO32* triggers eumelanin synthesis

Melanogenesis is an enzymatic chain reaction occurring in the melanosomes. Increased eumelanin synthesis occurs when *FBXO32* is silenced or upregulated by *in vivo* and *in vitro* assays. To understand if this effect is direct with gene enrichment, we bias our RNAseq data analysis at the two biological networks, in the melanosome where the melanin is synthesized and the MC1R signaling pathways. In the melanosome, genes related to eumelanogenesis included *TYR*, *DOPA*, and *TYRP1*. *TYR* and *TYRP1* are critical regulators in melanin synthesis and can indirectly reflect the melanin production content (Potrony et al., 2015). We first observed accumulation of *TYR* and *DOPA* evidenced in *hFBXO32*^{G139S} mature feather buds. The *FBXO32* silencing results in *TYRP1* accumulation in melanocytes at the dermis by immunolabelling. To analyze the biological transcription process behind, our RNAseq reveals that *DOPA* is upregulated in the overexpression of *hFBXO32* WT. When overexpressed with p.G139S, *FBXO32* results in *TYR* upregulation, whereas in control and overexpression with wild human type, *FBXO32* results in *TYR* downregulated. We observed in the transcriptional analysis an upregulation of *TYRP1* in controls in both TNC and CNC. These results are consistent with the potential of *FBXO32* in the first steps of the enzymatic reaction in melanin synthesis at the melanosome.

The principal receptor that regulates human pigmentation is *MC1R* via induction of the cAMP/protein kinase and the melanocortin's α -MSH and ASIP (Herraiz et al., 2021). *MC1R*, when stimulated by α -MSH, is a driver of eumelanogenesis. The binding of ASIP to *MC1R* prevents the stimulation of eumelanin synthesis, indirectly competing for the receptor binding α -MSH and blocking cAMP synthesis. Moreover, ASIP also modulates the expression of many genes involved in cell adhesion and other cellular processes other than pigmentation (Le Pape et al., 2008). My results demonstrated that overexpression of *hFBXO32* WT results in upregulation of *MC1R* in TNC and CNC controls.

Furthermore, *FBXO32* gene enrichment in α -MSH. The fact that we recurrently observe eumelanin synthesis related to *FBXO32* downregulation indicates its role in melanogenesis by direct regulation of genes involved in the process and indirectly activating the expression of the signaling process involved. Specifically, we observed the silencing of *FBXO32* and co-expression of *FBXO32*^{G139S} downregulation of *ASIP*. My results suggest that at least *FBXO32* acts by downregulation of *ASIP* to allow the binding of *MC1R* to α -MSH, thereby reducing cAMP production to trigger the eumelanin synthesis pathway (**Figure 9.1**). The mechanism for the *MC1R* to increase the risk of developing melanoma is not yet known. In our context, we can assume that *FBXO32*^{G139S} led to eumelanin stimulation production in melanocytes primarily by expected *TH*, *DOPA*, and *TYRP1* upregulation and *ASIP* downregulation activity. The results show a novel scenario of *FBXO32*^{G139S} involves in the melanogenesis program.

9.5 *FBXO32*'s effect on melanocyte cell extension formation

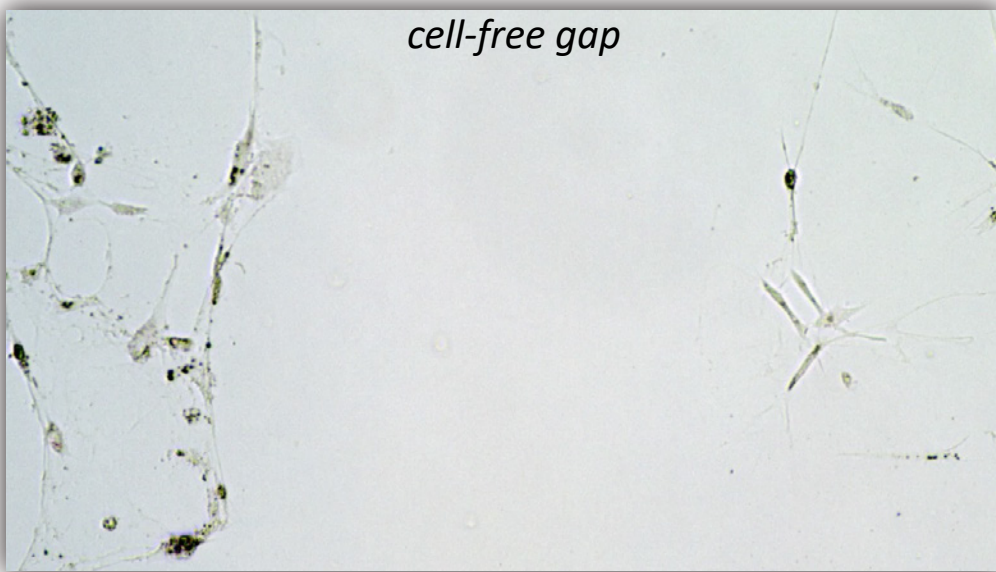
We have demonstrated the potential of *FBXO32*^{G139S} to induce cell migration towards the dermis. Considering this observation, we decided to investigate the melanocytic transformation capacities at the cellular level. My results show that *FBXO32* triggers filopodia length reduction, lamellipodia, and blebs formation, and the cells form aggregates. Lamellipodia have a significant role in driving cell migration by attaching to the substrate and generating forces to pull the cell forward (Yamaguchi & Condeelis, 2007), suggesting, that transfected melanocytes form tight lamellipodia protrusions to move collectively. During the radial growth phase, melanocytes exhibit abnormal proliferation, which limits and reduces their capacities to interact with keratinocytes. Then, transformed cells migrated a vertical growth phase from the epidermis to the dermis. The back migration towards the dermis, which occurs in the opposite direction to regular melanoblast migration during embryonic development, would be an essential step in the invasion (Bonaventure et al., 2013). In our experiments, we observed melanocyte migration to the dermis exclusively in *FBXO32*^{G139S} transfected cells; this observation indicates that this gene might impair cell migration, promotes cell dissemination, and pave the way for a possible invasion. To determine if *FBXO32*^{G139S} induces melanocyte invasion, we started a wound-healing assay using an insert culture (cell-free gap). Indeed, culture inserts, when compared with wound healing assays, yield more accurate and reliable results in terms of reproducibility between replicates (Pijuan et al., 2019). Even if I failed to create a confluent cell monolayer (90-95% confluence -due to the lockdown during the COVID-19 pandemic-), a critical assay to ensure cell migration, I evidenced the cell dynamics in normal melanocytes (Movie 1), and by using the Manual Tracking plugin of FIJI, I tracked cell trajectory tracks

Preliminary results show that *FBXO32*^{G139S} induces plasma membrane blebbing. Blebs are short spherical extensions of the plasma membrane devoid of actomyosin cortex contraction (Bonaventure et al., 2013). Blebs, lamellipodia, and filopodia can coexist at the leading edge of cells migration. Melanoma cells *in vitro* can adopt a range of morphologies during movement, ranging from elongated and mesenchymal to rounded and bleb-based (Ang Li et al., 2010). However, when cells are transfected with *FBXO32*^{G139S}, we observed lamellipodia and blebs formation, we can assume that the defective migration observed in the skin explants is a consequence of cell transformation triggered by the *FBXO32*^{G139S} variant.

In addition to filopodia, lamellipodia, and blebs, another type of membrane protrusion, invadopodia initiated melanoma metastasis by invading through the extracellular matrix (ECM) (Mousson et al., 2021). To degrade the ECM, cells secrete metalloproteases via actin-based invadopodia membrane protrusion (Hoshino et al., 2013; Leong et al., 2014; Hezhe Lu et al., 2016). We wondered if *FBXO32*^{G139S} would be sufficient to cause invasion in melanocyte transformation. To test if *FBXO32* can promote melanoma invasion, we could study 1) if *FBXO32* can trigger invadopodia structure formation by co-staining the cells for Paxillin, F-actin cortactin and membrane type-1 matrix metalloproteinase (MT1-MMP) markers, 2) to test whether inhibition of *FBXO32* or co-transfection with *hFBXO32*^{G139S} increase the ability to degrade extracellular matrix by gelatin degradation assay. I expected to observed to observe Paxillin and Cortactin colocalization in invadopodia formation. These tests can be paralleled with ongoing cell insert to demonstrate how *FBXO32*^{G139S} potentially led to melanocyte invasion.

Amongst the evidence in cell transformation in response to *FBXO32*^{G139S}, we observed an increased number of melanocytes in both *in vivo* and *in vitro* assays. I started to analyze cell density at differential time points, but again, due to the lockdown during the COVID-19 pandemic, my experiments were stopped dramatically without the possibility of conducting these critical experiments. It would be essential to assessed the ability of *FBXO32*^{G139S} to stimulate cell proliferation to understand the obtained results fully. I propose to assess a cell proliferation assay using Ki67 expressed through the activate cell cycle (G1, G2, S, and M phases) or Phosphohistone-H3 specific mitosis marker to measure proliferation in control and experimental conditions. I expect to observe accumulation of Ki67 or Phosphohistone-H3 markers in both *dsFBXO32* and *hFBXO32*^{G139S} and normal accumulation in control with recovery in *hFBXO32* WT cells.

Movie 1. Cell dynamics from during 24h isolated from control skin explant



9.6 *FBXO32* induces cytoskeleton remodeling

Cell migration is a complex process involving cell adhesion, protrusion, and contractility. It requires cell polarization and extension of protrusions and adhesion at the leading edge, coordinated with the disassembly of adhesion at the rear end of the cell (López-Colomé et al., 2017). Focal adhesion is robust and requires stable ECM contacts with cytoskeletal contractile stress fibers. Paxillin is a main component of focal adhesion, which functions primarily as a scaffolding protein for the assembly of the multi-protein complex to facilitate intracellular signaling (Brown & Turner, 2004; Deakin & Turner, 2014). Paxillin contributes to cell migration by maintaining the coordination of cell assembly and disassembly and the front and at the rear, respectively, by regulating focal adhesion dynamics (Webb et al., 2004). Data present herein reveal additional roles of *FBXO32* in focal adhesion disassembly in protrusive regions of the cells, significantly impaired in *FBXO32* transfected cells. Our results highlight the role of *FBXO32* as a mediator of focal adhesion formation. However, how the increased phospho-paxillin localization in the leading edges of *FBXO32*^{G139S} contributes to the cell migrations as aggregates is unclear. One way to explain an increase in the formation of focal adhesion is that paxillin is essential for the activation of focal adhesion pathways. To test this idea, we could study focal adhesion assembly, important in cell migration, by characterizing the FAK-Scr complex in the adhesion turnover by cell culture immunolabeling.

Moreover, we analyzed the topography of actin filaments by using a Phalloidin labeling, at the cellular level. My results indicate disruption of cytoskeleton organization in the overexpressed *FBXO32*^{G139S} cells leading to actin remodeling from stress fiber to edge ruffling. Actin filaments drive the extension of lamellipodia flat protrusions and filopodia to push the membrane (Ciobanasu et al., 2012). We assume that the filopodia shortening happened because *FBXO32*^{G139S} induces actin dynamics disassembly and the focal adhesion turnover (initiated by the study of paxillin). These defects could account for the back migration of the melanocytes observed in the dermis of the skin explant system.

9.7 *FBXO32*^{G139S} unfolds novel targets in melanocyte transformation

Few melanoma genes associated with childhood melanoma (first identified in adults) are implicated in the signaling pathways that control proliferation genes (*BRAF*, *NRAS*) (Charbel et al., 2014; Kinsler et al., 2013), growth and metabolism (*PTEN*) (Lu et al., 2015), cell cycle (*CDKN2A*) (Berg et al., 2004; Goldstein et al., 2018; Lu et al., 2015; Markovic et al., 1997), telomere maintenance (*TERT*) (Lu et al., 2015), and DNA repair (*BAP1*) (De La Fouchardière, 2017; de la Fouchardière et al., 2015). To investigate whether *FBXO32*^{G139S} could regulate common childhood

melanoma genes, we performed a gene-level exploratory analysis of gene enrichment profile from our RNAseq data in both TNC and CNC experimental series. Our research in *CDKN2A* demonstrated, as expected, no gene alterations due to *FBXO32* silencing or overexpression. Indeed, in cases of childhood melanoma, *CDKN2A* mutations have been reported to be rare, and no *CDK4* mutations have been reported (Berg et al., 2004; Rabbie et al., 2017). Unexpectedly, we detected downregulation of *CDK6* in *hFBXO32^{G139S}*. Genomic signatures of *CDK6* in childhood melanoma have never been described. In addition, overexpression experiments with *FBXO32* WT and *hFBXO32^{G139S}* showed downregulation of the cell cycles genes *BRAF* and the tumor suppressor *PTEN* involved in early-onset melanoma. How does *FBXO32^{G139S}* regulate its level of transcription? To answer this question, we could further validate our results obtained by other transcriptomic analyses such as RT-qPCR.

It is possible that other significant melanoma predisposing genes may influence the risk of disease in children-adolescent. The germline mutations of *BAP1* predisposition occur mainly in adults. Despite this, carriers frequently develop benign *BAP1* inactivation melanocytic nevi during childhood (de la Fouchardière et al., 2021). In the analysis of gene-gene interaction, our results demonstrated that *FBXO32^{G139S}* is implicated in the differential enrichment of *BAP1*. Specifically, *FBXO32^{G139S}* downregulated *BAP1* in both TNC and CNC. The *BAP1* gene encodes a nuclear deubiquitinate enzyme that acts as a tumor suppressor gene by the allelic "double hit" model of A. Knudson (Berger et al., 2011; de la Fouchardière, 2017; Goldstein, 2011). We can assume the synergistic post-transcriptional competition of *FBXO32* and *BAP1* in the ubiquitination system. While ubiquitination has long been associated with the degradation of membrane proteins by internalization and redirection to the proteasome, it is now known that the ubiquitination/deubiquitination switch is involved in many areas of cell regulation ranging from DNA repair or genome transcription to cell cycle progression, as well as other functions (stress response, apoptosis, differentiation, intercellular communication). In conclusion, we identified novel transcripts of *FBXO32: ASIP* and *BAP1* to be involved in melanogenesis and post-transcriptional regulation (**Figure 9.1**). Demonstrating a synergic relation between *FBXO32* and *BAP1* is a very promising line of research that deserves to be further pursued and analyzed, both in our functional models, and on tumor-derived tissues.

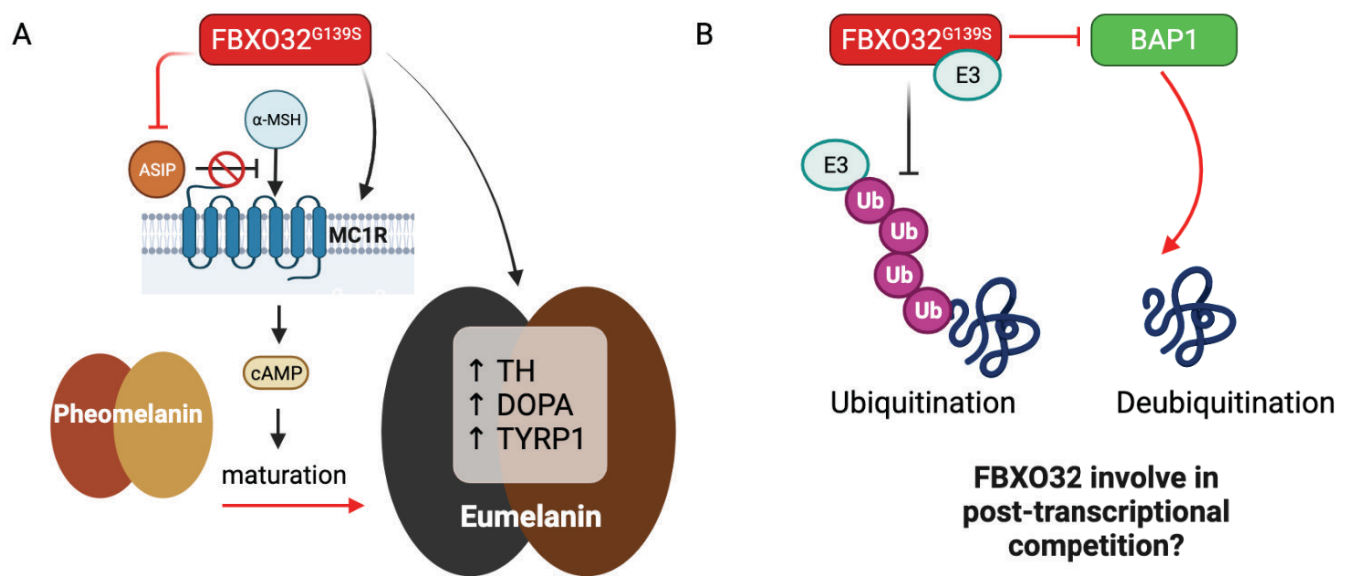


Figure 9.1 Schematic view of *FBXO32* network proposal in melanocyte transformation

A) Engage in eumelanogenesis and **B)** possible competition between *FBXO32* and *BAP1* post-transcriptional regulation .

9.8 Is *FBXO32* a TSG in childhood melanoma?

De novo mutations are a significant cause of severe early-onset genetic disorders (Acuna-Hidalgo et al., 2016). Our initial observation was that childhood melanoma does not have a familial predisposition to melanoma. This idea hints at analyzing carriers by WES in non-inherited childhood melanoma to identify *de novo* mutations. My research project precisely studies the role of the gene *FBXO32* during embryonic melanocyte development. My results bring *FBXO32* as a new candidate gene into the spotlight genomic landscape on this rare disease. We present a novel mechanism in which the inhibition of *FBXO32* modulates melanocyte transformation. Now, we wondered if *FBXO32* could act as a TSG in childhood melanoma. The reasoning behind this notion is that we observed phenotypic and transcriptional changes when the expression level of *FBXO32* is downregulated and overexpressed with the specific variant, p.G193S. Our *in vivo* at TNC and CNC and the *in vitro* skin explant and cell culture analysis showed that when *FBXO32* is downregulated, occurs a detrimental effect on the melanocyte lineage. To prove the concept of *FBXO32* as a tumor suppressor gene, we need to analyze the haploinsufficiency by monoallelic deletion (e.g., methylation) for inactivation of both alleles, according to Kudson's two-hit model hypothesis.

As described, *FBXO32* can act as both oncogene and TSG, depending on the cell lineage: as TSG in ovarian (Chou et al., 2010; Mei et al., 2015), colorectal carcinoma (Yuan et al., 2018), breast cancer (Zhou et al., 2017) an oncogene in breast cancer (Sahu et al., 2017). Significantly, enhanced degradation of TSG due to dysfunction of the ubiquitin proteasomal pathway or aberrant expression of E3 ligases may be associated with tumorigenesis (Singh Tekcham et al., 2020). In this project, we propose *FBXO32* as a TSG in the onset of melanoma during the malignant transformation of melanocytes (e.g., cell malignancy proliferation, possible invasion).

This dissertation contributes to shed a light on a novel interplay between upstream regulation of *de novo* candidate gene *FBXO32* in *ASIP* and *BAP1*. It combines *in vivo* and *in vitro* developmental analysis to understand the role of this variant in melanoblast/melanocyte lineage originating from the NC. Based on the evidence in which accumulation of eumelanin results in inhibition of *FBXO32*, we investigated the possible mechanism involved, which resulted in the downregulation of *ASIP*. Furthermore, we found the post-transcriptional gene *BAP1* downregulation by *FBXO32* inhibition.

My research contributes to the knowledge of *FBXO32* in the childhood melanoma field. To this end, the detection of the variant, p.G139S established a genetic diagnosis that can provide a future

prognosis based on data from other patients with similar mutations and, in the future, develop and apply the treatment.

10 Conclusion

During this PhD research project, we have contributed to understanding the biological role of the *de novo* candidate genes in childhood melanoma. The research project present here uses the chick embryo as an animal model pertinent for studying genes inactivation or overexpression during NCCs development; we also set up original *ex vivo* models which are relevant to the developmental context of childhood tumorigenicity. Since childhood melanoma lesions often appear at the extremities, we took advantage of the neural crest differential capacities at both CNC and TNC levels to test the biological effect of *FBXO32*. We have recapitulated gene silencing of *de novo* variants at different development stages, and I have demonstrated that at least *FBXO32*^{G139S} has a potential role in triggering melanocyte transformation, as I showed not only by *in vivo* and *in vitro* analysis at two developmental stages but also cellular level through *in vitro* cell analysis. I have demonstrated that *FBXO32*^{G139S} is involved in cytoskeleton remodeling at protrusion formation and focal adhesion disassembly, potentially inducing melanocyte invasion. Finally, I propose a new network between *FBXO32* - *ASIP* in eumelanogenesis and *FBXO32* - *BAP1* in the post-transcriptional ubiquitination proteasome system.

Childhood melanoma is a rare disease, and the current knowledge is based on the adults' genetics. The treatment of children and young adults does not rely on specific guidelines generally, young patients follow the same principles as adults (Ferrari et al., 2021), but the issue concerns the limited access to clinical trials and new drugs, which have been shown to alter the natural history of advanced melanomas dramatically. In the melanoma field, my research project is the first functional analysis to date to understand the mechanisms underlying melanocytic oncogenesis in children by functional analysis. We demonstrate the potential role of *FBXO32* to triggers melanocyte development. These results will be essential for identifying new biomarkers and could help in designing innovative therapeutic pipelines for pediatric melanoma.

11 Supplementary information

We further analyzed gene enrichment between the silencing of *FBXO32* versus controls and the correlation between the rescue with the *hFBXO32*^{G139S} versus *hFBXO32* WT in our RNA-seq data mining. We have done an exhaustive gene analysis screening from all gene in which we selected in total 1757 out of 19505 genes based on gene enrichment regarding proliferation and cell cycle (**Figure S11.1**), extracellular matrix (**Figure S11.2**), angiogenesis (**Figure S11.3**), apoptosis (**Figure S11.4**), EMT (**Figure S11.5**), ADAMs genes (**Figure S11.6**), and metalloproteinases (**Figure S11.7**), and gene involve in signaling pathways during development (**Figure S11.8**), Moreover, we detected unexpected targets as keratins (**Figure S11.9-10**) and realising hormones, surprisingly involve in melanoma (**Figure S11.11**).

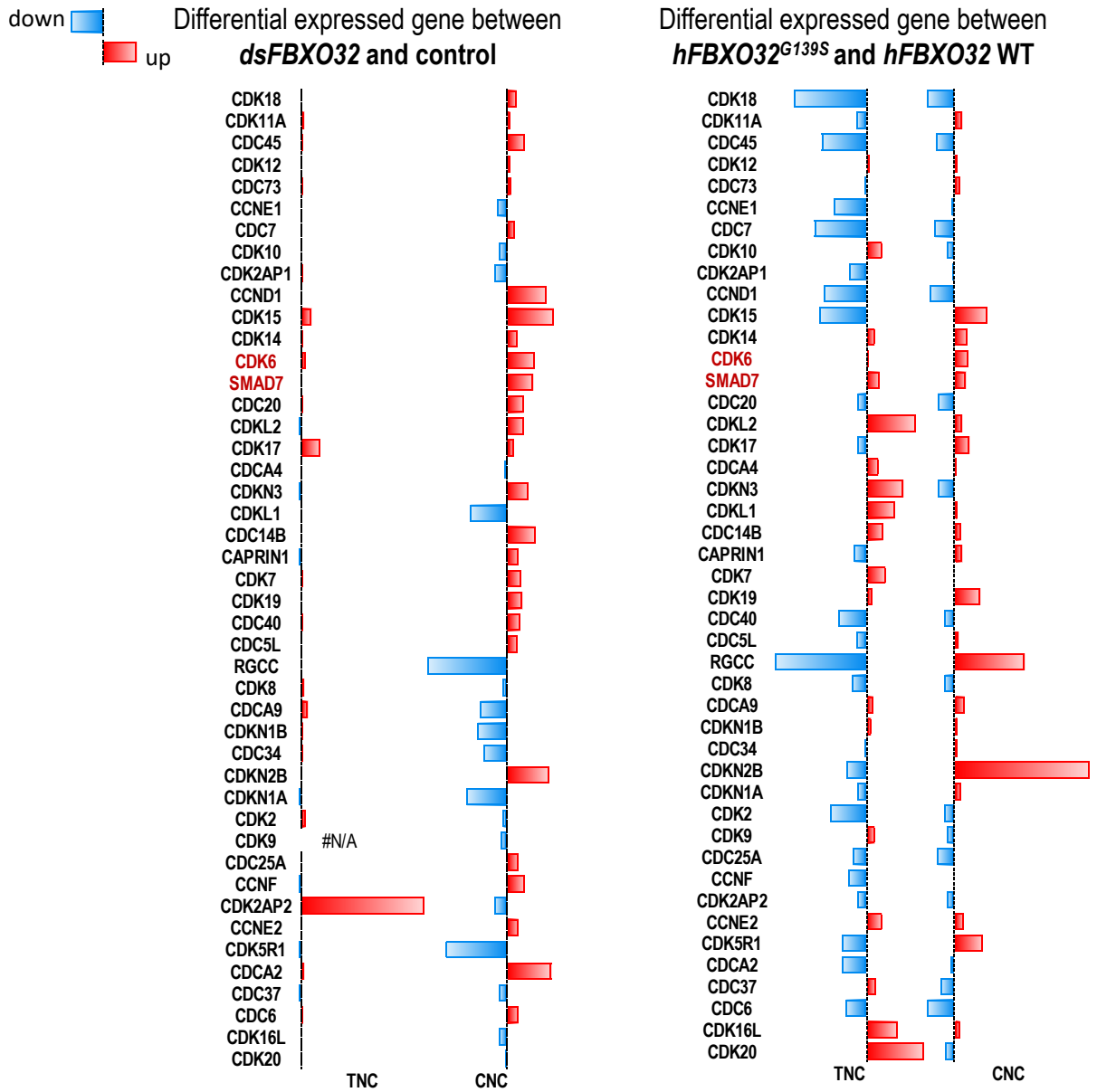


Figure S11. 1 Differential gene enrichment in proliferation and cell cycle genes

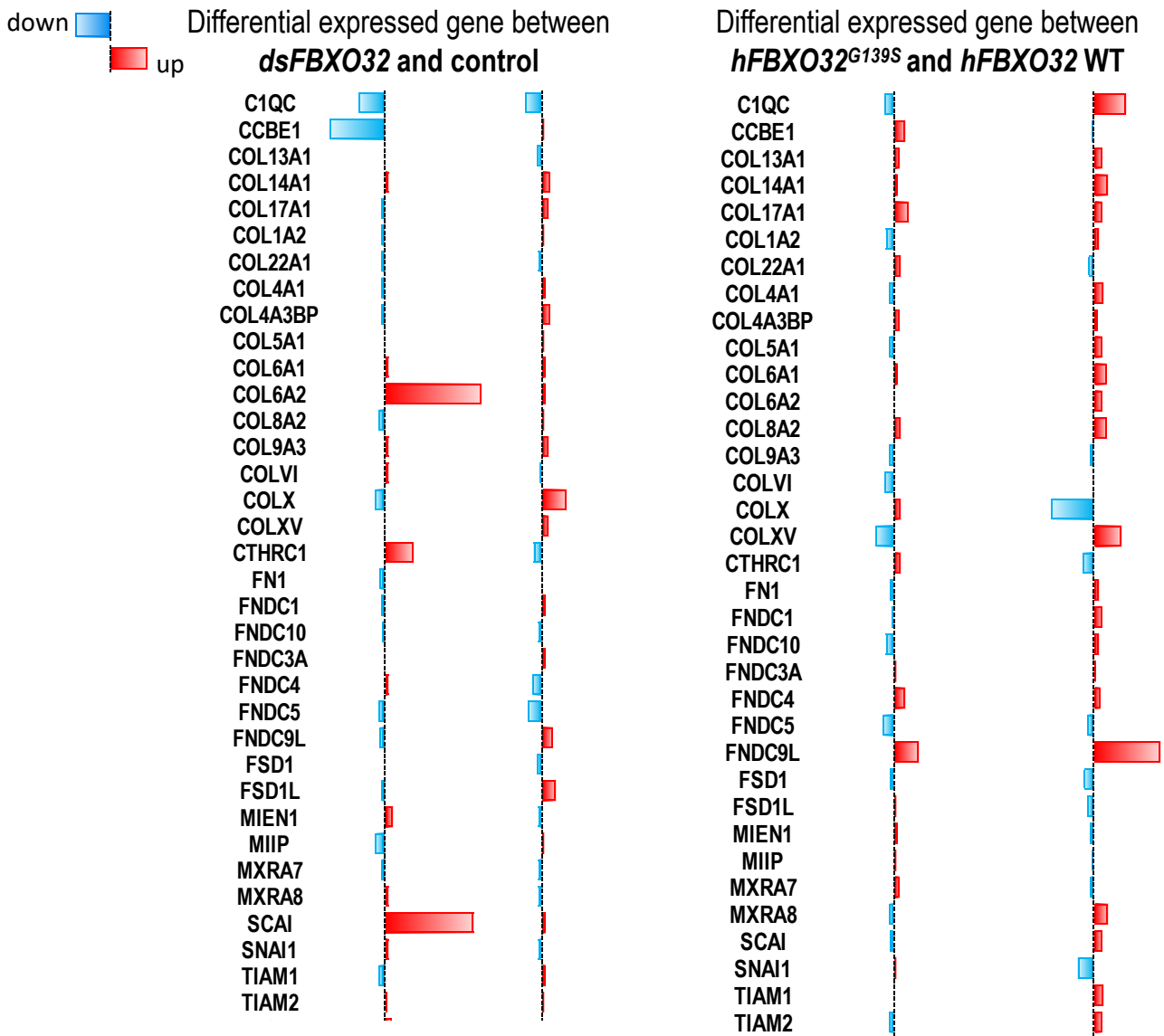




Figure S11. 2 Differential gene enrichment in extracellular matrix genes

down 
up 

Differential expressed gene between
dsFBXO32 and control

Differential expressed gene between
hFBXO32^{G139S} and *hFBXO32* WT

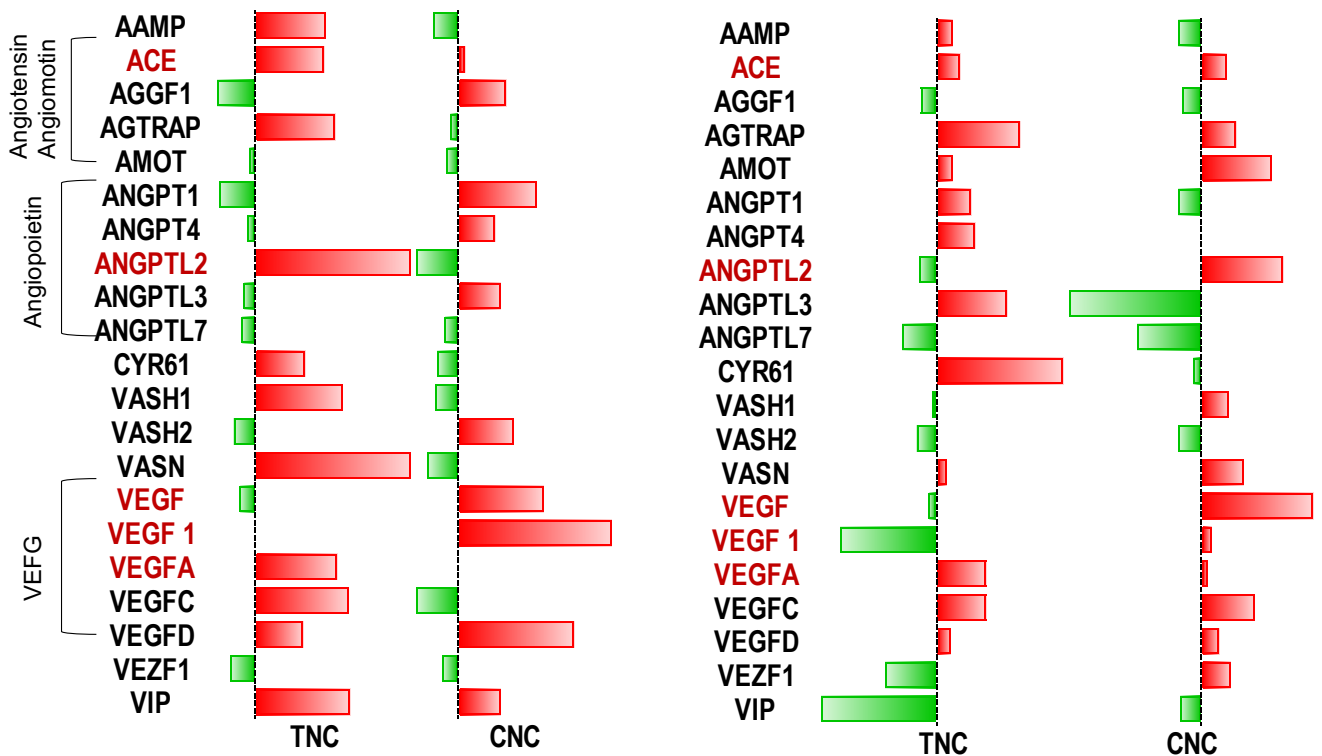


Figure S11. 3 Differential expressed genes involved in angiogenesis

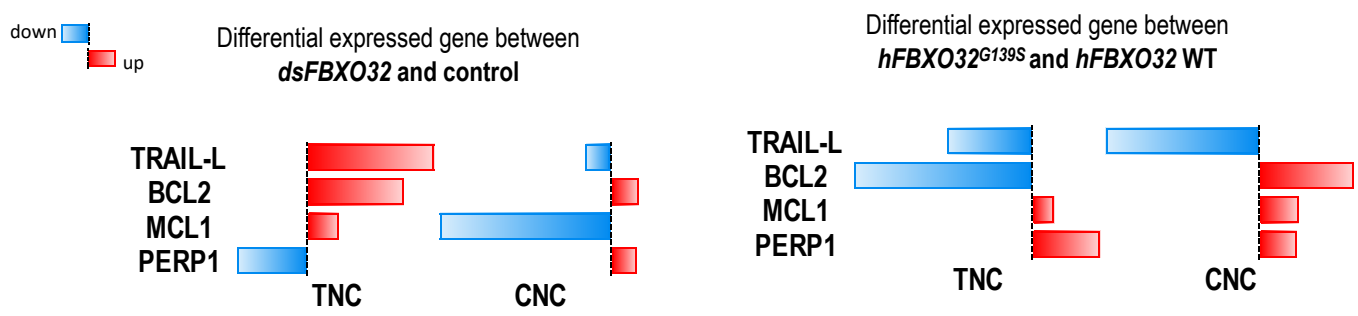
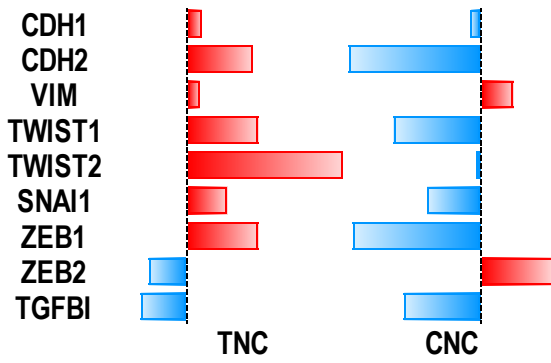


Figure S11. 4 Differential gene enrichment involved in apoptosis

down  up 

Differential expressed gene between
dsFBXO32 and control



Differential expressed gene between
hFBXO32^{G139S} and *hFBXO32* WT

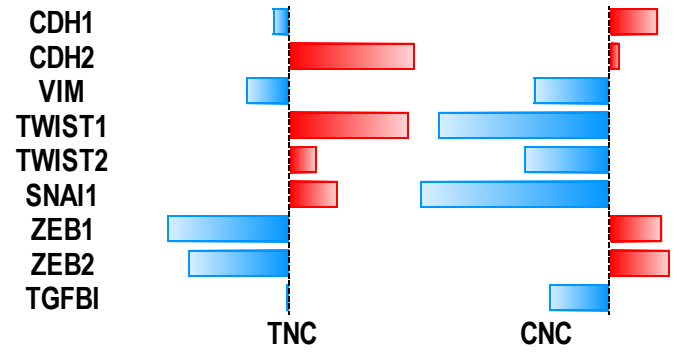
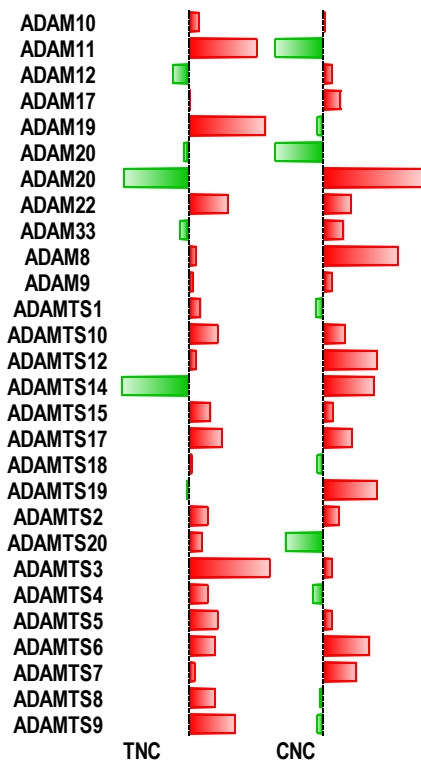


Figure S11. 5 Differential gene enrichment involved in EMT genes

down  up 

Differential expressed gene between
dsFBXO32 and control



Differential expressed gene between
hFBXO32^{G139S} and *hFBXO32* WT

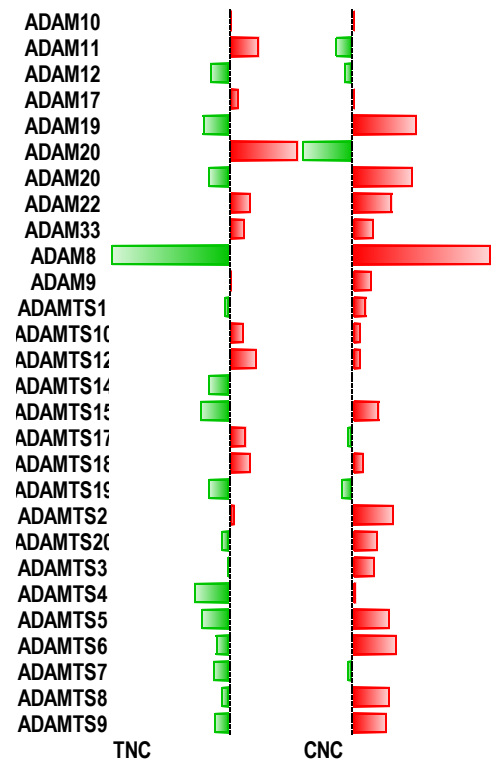


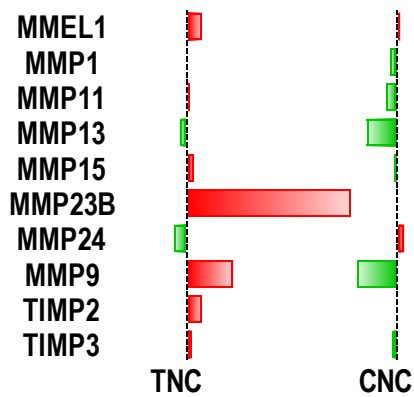


Figure S11. 6 Differential genes enrichment involved in disintegrant and metalloproteinase (ADAM)

down   up

Differential expressed gene between
dsFBXO32 and control



Differential expressed gene between
hFBXO32^{G139S} and *hFBXO32 WT*

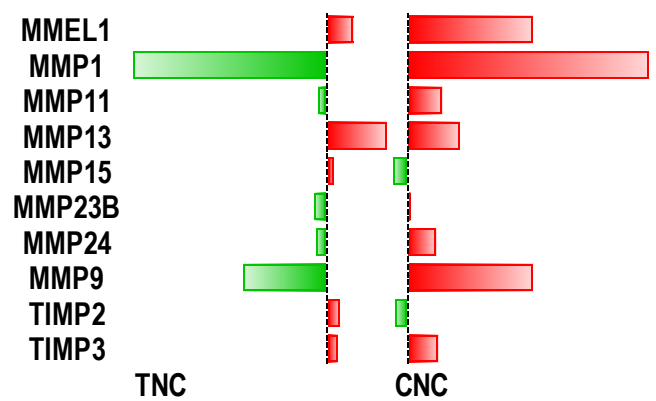




Figure S11. 7 Differential genes enrichment in metalloproteases, cell matrix degradation

down  up 

Differential expressed gene between *dsFBXO32* and control

Differential expressed gene between *hFBXO32^{G139S}* and *hFBXO32* WT

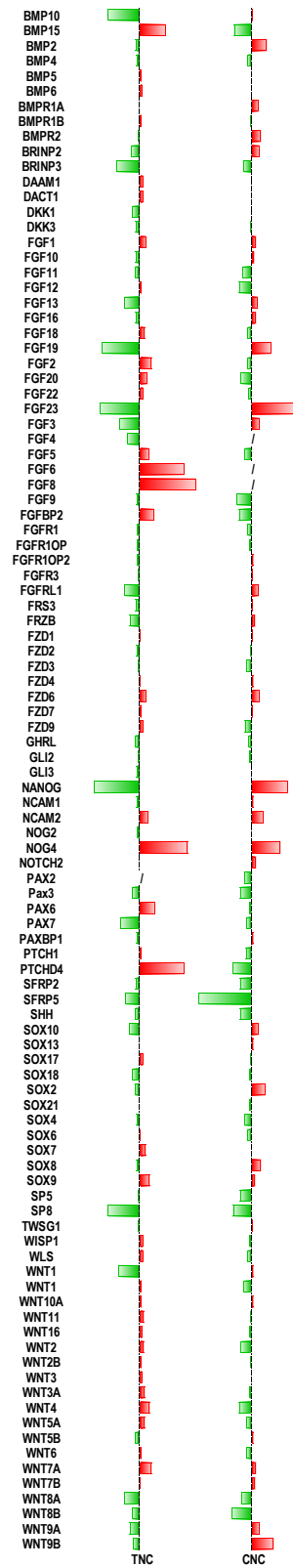
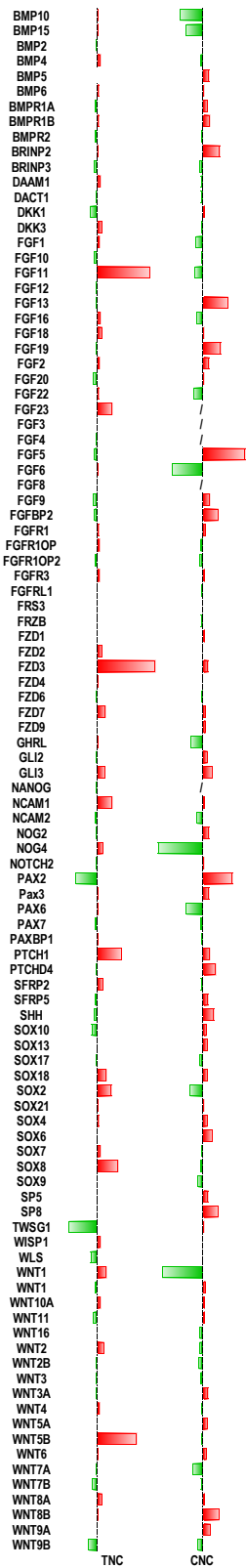


Figure S11. 8 Differential genes enrichment involved in developmental signaling pathways

Unexpected targets

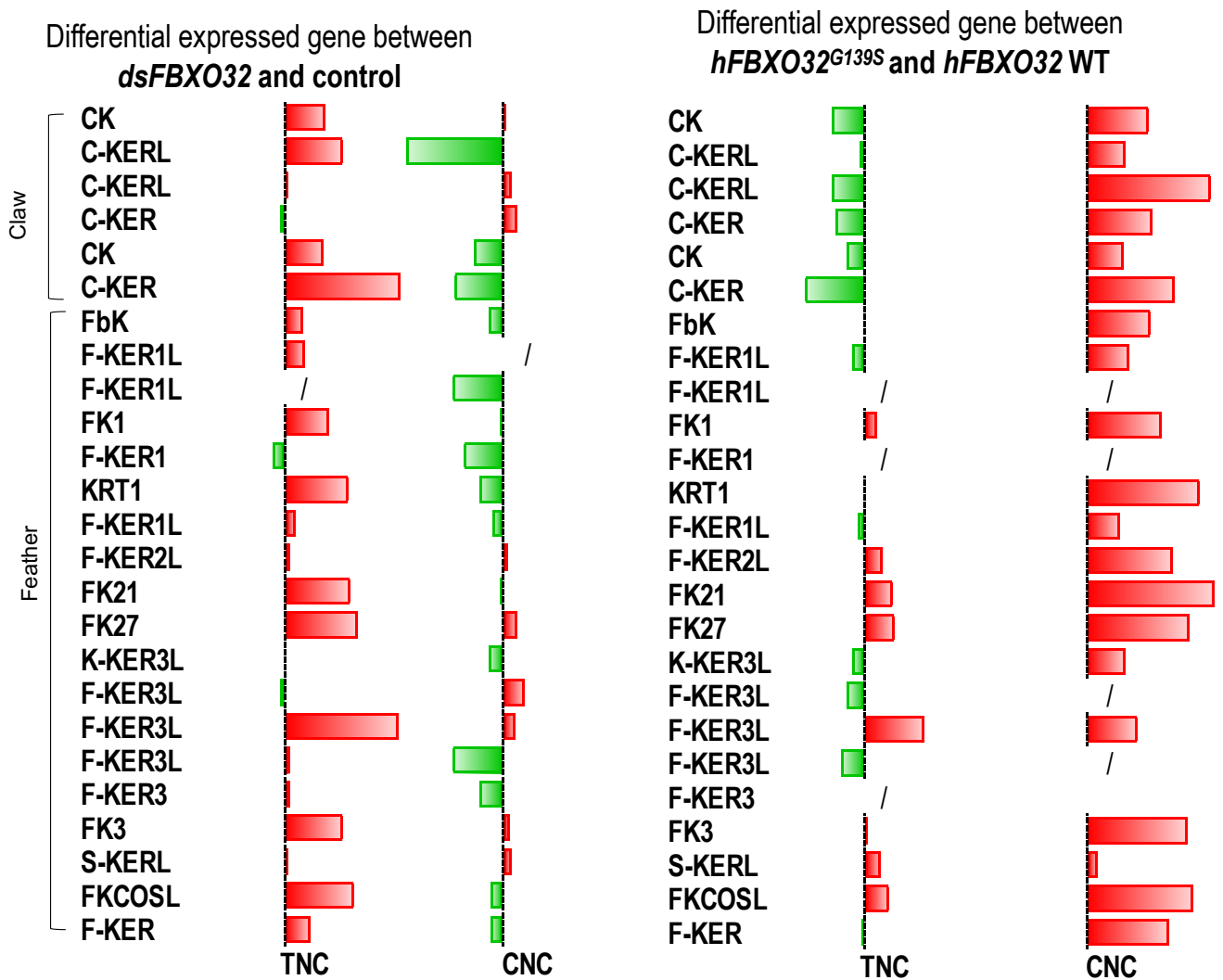


Figure S11. 9 Unexpected differentially expressed keratins genes

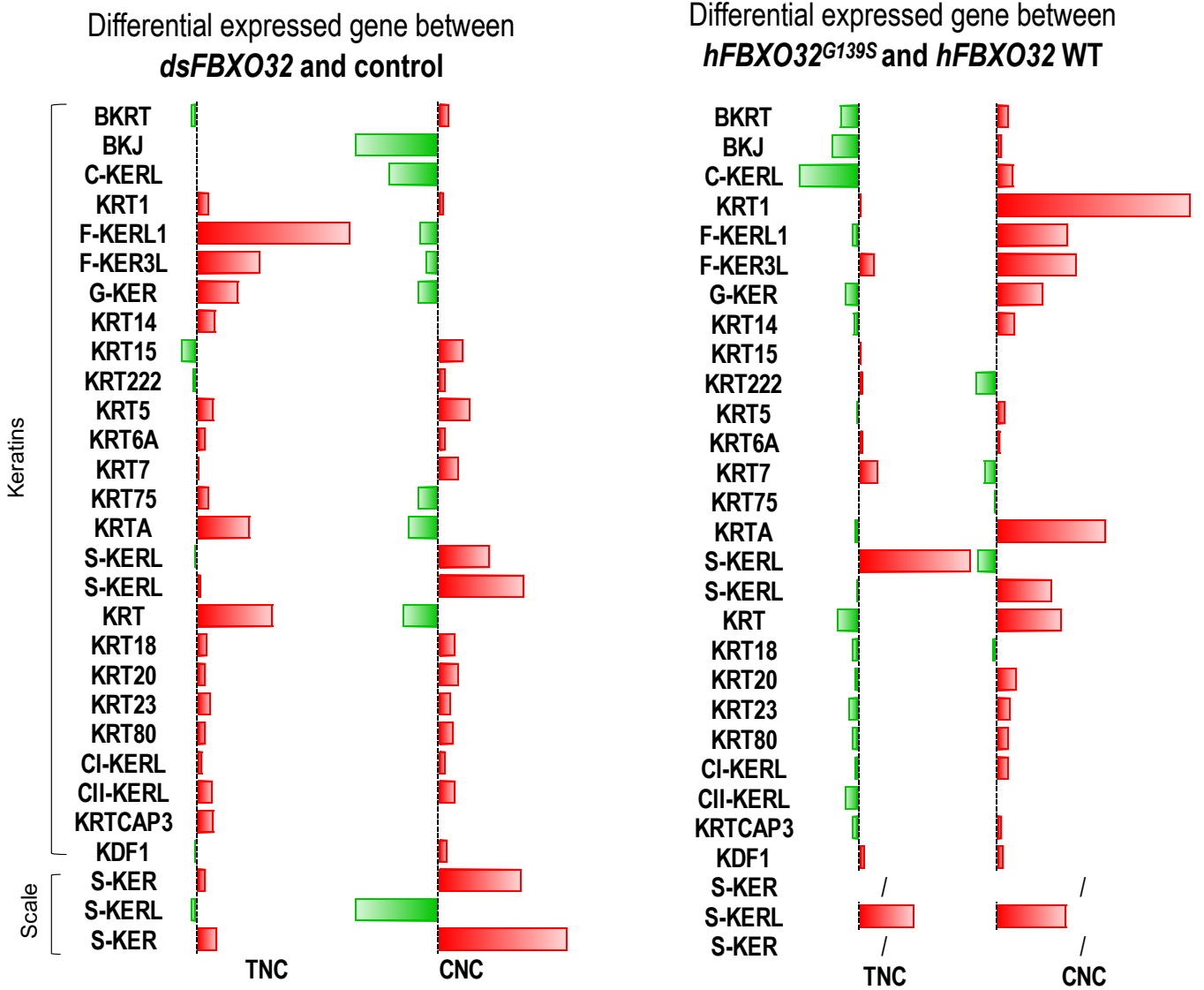


Figure S11. 10 Unexpected differentially expressed keratins genes

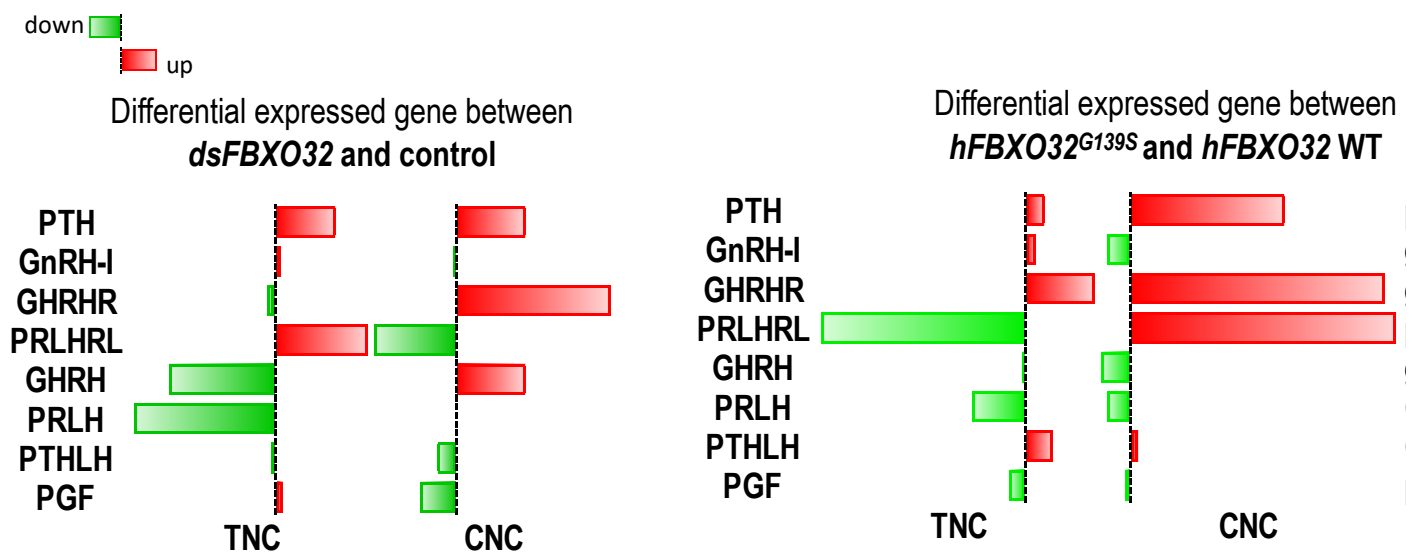


Figure S11. 11 Differentially expressed gene involved in releasing hormones

12 Bibliography

- Acuna-Hidalgo, R., Bo, T., Kwint, M. P., Van De Vorst, M., Pinelli, M., Veltman, J. A., Hoischen, A., Vissers, L. E. L. M., & Gilissen, C. (2015). Post-zygotic Point Mutations Are an Underrecognized Source of de Novo Genomic Variation. *American Journal of Human Genetics*, *97*(1), 67–74.
- Acuna-Hidalgo, R., Veltman, J. A., & Hoischen, A. (2016). New insights into the generation and role of de novo mutations in health and disease. *Genome Biology*, *17*(1), 1–19.
- Aguiar, D. P., Sghari, S., & Creuzet, S. (2014). The facial neural crest controls fore- and midbrain patterning by regulating Foxg1 expression through Smad1 activity. *Development (Cambridge, England)*, *141*(12), 2494–2505.
- Andermatt, I., Wilson, N., & Stoeckli, E. T. (2014). In ovo electroporation of miRNA-based-plasmids to investigate gene function in the developing neural tube. *Methods in Molecular Biology*, *1101*, 353–368.
- Baek, Y. S., Seo, J. Y., Song, J. Y., Lee, S. Y., Kim, A., & Jeon, J. (2019). Li-Fraumeni syndrome presenting as cutaneous melanoma in a child: case report and review of literature. *Journal of the European Academy of Dermatology and Venereology*, *33*(4), e174–e175.
- Baggiolini, A., Varum, S., Furrer, R., Correspondence, L. S., Mateos, J. M., Bettosini, D., John, N., Bonalli, M., Ziegler, U., Dimou, L., Clevers, H., & Sommer, L. (2015). Premigratory and Migratory Neural Crest Cells Are Multipotent In Vivo. *Cell Stem Cell*, *16*, 314–322.
- Bahrami, A., & Barnhill, R. L. (2018). Pathology and genomics of pediatric melanoma: A critical reexamination and new insights. *Pediatric Blood & Cancer*, *65*(2), e26792.
- Ballotti, R., & Bertolotto, C. (2017). Deregulated MITF sumoylation: A route to melanoma. *Molecular and Cellular Oncology*, *4*(4), 1–2.
- Barnhill, R. L., Flotte, T. J., Fleischli, M., & Perez-Atayde, A. (1995). Cutaneous melanoma and atypical spitz tumors in childhood. *Cancer*, *76*(10), 1833–1845.
- Bateman, C. M., Alpar, D., Ford, A. M., Colman, S. M., Wren, D., Morgan, M., Kearney, L., & Greaves, M. (2015). Evolutionary trajectories of hyperdiploid ALL in monozygotic twins. *Leukemia*, *29*(1), 58–65.
- Bauer, J., Curtin, J. A., Pinkel, D., & Bastian, B. C. (2007). Congenital melanocytic nevi frequently harbor NRAS mutations but no BRAF mutations. *Journal of Investigative Dermatology*, *127*(1), 179–182.
- Behjati, S., Maschietto, M., Williams, R. D., Side, L., Hubank, M., West, R., Pearson, K., Sebire, N.,

- Tarpey, P., Futreal, A., Brooks, T., Stratton, M. R., & Anderson, J. (2014). A Pathogenic Mosaic TP53 Mutation in Two Germ Layers Detected by Next Generation Sequencing. *PLoS Biology*, 9(5).
- Bell, R. E., & Levy, C. (2011). The three M's: Melanoma, microphthalmia-associated transcription factor and microRNA. *Pigment Cell and Melanoma Research*, 24(6), 1088–1106.
- Berg, P., Wennberg, A. M., Tuominen, R., Sander, B., Rozell, B. L., Platz, A., & Hansson, J. (2004). Germline CDKN2A mutations are rare in child and adolescent cutaneous melanoma. *Melanoma Research*, 14(4), 251–255.
- Berger, A. H., Knudson, A. G., & Pandolfi, P. P. (2011). A continuum model for tumour suppression. *Nature*, 476(7359), 163–169.
- Bertolotto, C. (2013). Melanoma: From Melanocyte to Genetic Alterations and Clinical Options. *Scientifica*, 2013, 1–22.
- Bertrand, J., Steingrimsson, E., Jouenne, F., Paillerets, B., & Larue, L. (2020). Melanoma Risk and Melanocyte Biology. *Acta Dermato Venereologica*, 100(11), adv00139.
- Biesecker, L. G., & Spinner, N. B. (2013). A genomic view of mosaicism and human disease. *Nature Reviews Genetics*, 14(5), 307–320.
- Bodine, S. C., Latres, E., Baumhueter, S., Lai, V. K. M., Nunez, L., Clarke, B. A., Poueymirou, W. T., Panaro, F. J., Erqian Na, Dharmarajan, K., Pan, Z. Q., Valenzuela, D. M., Dechiara, T. M., Stitt, T. N., Yancopoulos, G. D., & Glass, D. J. (2001). Identification of ubiquitin ligases required for skeletal muscle atrophy. *Science*, 294(5547), 1704–1708.
- Bonaventure, J., Domingues, M. J., & Larue, L. (2013). Cellular and molecular mechanisms controlling the migration of melanocytes and melanoma cells. *Pigment Cell & Melanoma Research*, 26(3), 316–325.
- Bressac-de Paillerets, B. (2020). Congenital naevus and melanoma in children: The contribution of genetics. *Annales de Dermatologie et de Venereologie*, 147(11), 703–705.
- Bronner-Fraser, M. (1986). Analysis of the Early Stages of Trunk Neural Crest Migration in Avian Embryos Using Monoclonal Antibody HNK-1. *Developmental Biology*, 55, 44–55.
- Bronner, M. E. (2012). Formation and migration of neural crest cells in the vertebrate embryo. *Histochemistry and Cell Biology*, 138(2), 179–186.
- Brown, M. C., & Turner, C. E. (2004). *Paxillin: Adapting to Change*.
- Busch, C., Krochmann, J., & Drews, U. (2013). The Chick Embryo as an Experimental System for Melanoma Cell Invasion. *PLoS ONE*, 8(1), 1–9.
- Campbell, L. B., Kreicher, K. L., Gittleman, H. R., Strodbeck, K., Barnholtz-Sloan, J., & Bordeaux, J. S. (2015). Melanoma incidence in children and adolescents: Decreasing trends in the United States. *Journal of Pediatrics*, 166(6), 1505–1513.
- Carreira, S., Goodall, J., Aksan, I., La Rocca, S. A., Galibert, M. D., Denat, L., Larue, L., & Goding, C.

- R. (2005). Mitf cooperates with Rb1 and activates p21Cip1 expression to regulate cell cycle progression. *Nature*, *433*(7027), 764–769.
- Carreira, S., Goodall, J., Denat, L., Rodriguez, M., Nuciforo, P., Hoek, K. S., Testori, A., Larue, L., & Goding, C. R. (2006). Mitf regulation of Dia1 controls melanoma proliferation and invasiveness. *Genes and Development*, *20*(24), 3426–3439.
- Ceballos, P., Ruiz -Maldonado, R., & Martin C., M. (1995). *CURRENT CONCEPTS MELANOMA IN CHILDREN*.
- Chang, W., Brohl, A. S., Patidar, R., Sindiri, S., Shern, J. F., Wei, J. S., Song, Y. K., Yohe, M. E., Gryder, B., Zhang, S., Calzone, K. A., Shivaprasad, N., Wen, X., Badgett, T. C., Miettinen, M., Hartman, K. R., League-Pascual, J. C., Trahair, T. N., Widemann, B. C., ... Khan, J. (2016). Multidimensional clinomics for precision therapy of children and adolescent young adults with relapsed and refractory cancer: A report from the center for cancer research. *Clinical Cancer Research*, *22*(15), 3810–3820.
- Charbel, C., Fontaine, R. H., Malouf, G. G., Picard, A., Kadlub, N., El-Murr, N., How-Kit, A., Su, X., Coulomb-L'Hermine, A., Tost, J., Mourah, S., Aractingi, S., & Guégan, S. (2014). NRAS mutation is the sole recurrent somatic mutation in large congenital melanocytic nevi. *Journal of Investigative Dermatology*, *134*(4), 1067–1074.
- Cheli, Y., Ohanna, M., Ballotti, R., & Bertolotto, C. (2010). Fifteen-year quest for microphthalmia-associated transcription factor target genes. *Pigment Cell and Melanoma Research*, *23*(1), 27–40.
- Chou, J. L., Su, H. Y., Chen, L. Y., Liao, Y. P., Hartman-Frey, C., Lai, Y. H., Yang, H. W., Deatherage, D. E., Kuo, C. T., Huang, Y. W., Yan, P. S., Hsiao, S. H., Tai, C. K., Lin, H. J. L., Davuluri, R. V., Chao, T. K., Nephew, K. P., Huang, T. H. M., Lai, H. C., & Chan, M. W. Y. (2010). Promoter hypermethylation of FBXO32, a novel TGF-B/SMAD4 target gene and tumor suppressor, is associated with poor prognosis in human ovarian cancer. *Laboratory Investigation*, *90*(3), 414–425.
- Ciobanasi, C., Faivre, B., & Le Clainche, C. (2012). Actin Dynamics Associated with Focal Adhesions. *International Journal of Cell Biology*, *2012*, 1–9.
- Clark, W. H., From, L., Bernardino, E. A., & Mihm, M. C. (1969). The Histogenesis and Biologic Behavior of Primary Human Malignant Melanomas of the Skin. *Cancer Research*, *29*(3), 705–727.
- Conway, E., Rossi, F., Fernandez-Perez, D., Ponzio, E., Ferrari, K. J., Zanotti, M., Manganaro, D., Rodighiero, S., Tamburri, S., & Pasini, D. (2021). BAP1 enhances Polycomb repression by counteracting widespread H2AK119ub1 deposition and chromatin condensation. *Molecular Cell*, *81*(17), 3526.
- Cordoro, K. M., Gupta, D., Frieden, I. J., McCalmont, T., & Kashani-Sabet, M. (2013). Pediatric

- melanoma: Results of a large cohort study and proposal for modified ABCD detection criteria for children. *Journal of the American Academy of Dermatology*, 68(6), 913–925.
- Costin, G.-E., & Hearing, V. J. (2007). Human skin pigmentation: melanocytes modulate skin color in response to stress. *The FASEB Journal*, 21(4), 976–994.
- Creuzet, S., Couly, G., & Le Douarin, N. M. (2005). Patterning the neural crest derivatives during development of the vertebrate head: insights from avian studies. *J. Anat*, 207, 447–459.
- Creuzet, S., Couly, G., Vincent, C., & Douarin, N. M. Le. (2002). *Negative effect of Hox gene expression on the development of the neural crest-derived facial skeleton*. 4313, 4301–4313.
- Creuzet, S. E. (2009). Neural crest contribution to forebrain development. *Seminars in Cell and Developmental Biology*, 20(6), 751–759.
- Creuzet, S. E. (2009). Regulation of pre-otic brain development by the cephalic neural crest. *Proceedings of the National Academy of Sciences of the United States of America*, 106(37), 15774–15779.
- Creuzet, S. E., Martinez, S., & Le Douarin, N. M. (2006). The cephalic neural crest exerts a critical effect on forebrain and midbrain development. *Proceedings of the National Academy of Sciences*, 103(38), 14033–14038.
- Creuzet, S., Schuler, B., & Le Douarin, N. (2004). Reciprocal relationships between Fgf8 and neural crest cells in facial and forebrain development. *Proceedings of the National Academy of Sciences*, 101(14), 4843–4847.
- D'Mello, S. A. N., Finlay, G. J., Baguley, B. C., & Askarian-Amiri, M. E. (2016). Signaling pathways in melanogenesis. *International Journal of Molecular Sciences*, 17(7), 1–18.
- Dal, G. M., Ergüner, B., Sađirođlu, M. S., Yüksel, B., Onat, O. E., Alkan, C., & Özçelik, T. (2014). Early postzygotic mutations contribute to de novo variation in a healthy monozygotic twin pair. *Journal of Medical Genetics*, 51(7), 455–459.
- de Andrade, K. C., Khincha MBBS, P. P., Hatton MS, J. N., Frone MS, M. N., Wegman-Ostrosky, T., Mai, P. L., Savage, S. A., Khincha, P. P., & César de Andrade, K. (2021). *Cancer incidence, patterns, and genotype-phenotype associations in individuals with pathogenic or likely pathogenic germline TP53 variants: an observational cohort study*.
- de la Fouchardière, A. (2017). BAP1 : un gène aux multiples fonctions impliqué dans de nombreux processus tumoraux. *Onco-Théragnostique*, VI(3), 11–16.
- De La Fouchardière, A. (2017). Mélanomes de l'enfant. *Tumeurs Pédiatriques*, VI(1), 62–67.
- de la Fouchardière, A., Boivin, F., Etchevers, H. C., & Macagno, N. (2021). Cutaneous Melanomas Arising during Childhood: An Overview of the Main Entities. *Dermatopathology*, 8(3), 301–314.
- de la Fouchardière, A., Cabaret, O., Savin, L., Combemale, P., Schwartz, H., Penet, C., Bonadona, V., Soufir, N., & Bressac-de Paillerets, B. (2015). Germline BAP1 mutations predispose also to

- multiple basal cell carcinomas. *Clinical Genetics*, 88(3), 273–277.
- De Souza, L. M., Robertson, B. M., & Robertson, G. P. (2017). Future of circulating tumor cells in the melanoma clinical and research laboratory settings. *Cancer Letters*, 392, 60–70.
- Deakin, N., & Turner, C. E. (2014). Paxillin inhibits HDAC6 to regulate microtubule acetylation, Golgi structure, and polarized migration. *Journal of Cell Biology*, 206, 395–413.
- Delloye-Bourgeois, C., & Castellani, V. (2019). Hijacking of Embryonic Programs by Neural Crest-Derived Neuroblastoma: From Physiological Migration to Metastatic Dissemination. *Frontiers in Molecular Neuroscience*, 12.
- Dessars, B., De Raeve, L. E., Housni, H. El, Debouck, C. J., Sidon, P. J., Morandini, R., Roseeuw, D., Ghanem, G. E., Vassart, G., & Heimann, P. (2007). Chromosomal translocations as a mechanism of BRAF activation in two cases of large congenital melanocytic nevi. *Journal of Investigative Dermatology*, 127(6), 1468–1470.
- Domingues, L., Hurbain, I., Gilles-Marsens, F., Sirés-Campos, J., André, N., Dewulf, M., Romao, M., Viaris de Lesegno, C., Macé, A.-S., Blouin, C., Guéré, C., Vié, K., Raposo, G., Lamaze, C., & Delevoeye, C. (2020). Coupling of melanocyte signaling and mechanics by caveolae is required for human skin pigmentation. *Nature Communications*, 11(1), 2988.
- Dong, J. M., Lau, L. S., Ng, Y. W., Lim, L., & Manser, E. (2009). Paxillin nuclear-cytoplasmic localization is regulated by phosphorylation of the LD4 motif: Evidence that nuclear paxillin promotes cell proliferation. *Biochemical Journal*, 418(1), 173–184.
- Du, J., Widlund, H. R., Horstmann, M. A., Ramaswamy, S., Ross, K., Huber, W. E., Nishimura, E. K., Golub, T. R., & Fisher, D. E. (2004). *Critical role of CDK2 for melanoma growth linked to its melanocyte-specific transcriptional regulation by MITF*.
- Dupin, E., Creuzet, S., & Le Douarin, N. M. (2006). The contribution of the neural crest to the vertebrate body. *Advances in Experimental Medicine and Biology*, 589, 96–119.
- Dupin, E., & Le Douarin, N. M. (2003a). Development of melanocyte precursors from the vertebrate neural crest. *Oncogene*, 22, 3016–3023.
- Dupin, E., & Le Douarin, N. M. (2003b). Development of melanocyte precursors from the vertebrate neural crest. *Oncogene*, 22, 3016–3023.
- Eggen, C. A. M., Durgaram, V. V. L., van Doorn, R., Mooi, W. J., Pardo, L. M., Pasmans, S. G. M. A., & Hollestein, L. M. (2017). Incidence and relative survival of melanoma in children and adolescents in the Netherlands, 1989–2013. *Journal of the European Academy of Dermatology and Venereology*, 32(6), 956–961.
- Elder, D. E., Bastian, B. C., Cree, I. A., Massi, D., & Scolyer, R. A. (2020). The 2018 World Health Organization classification of cutaneous, mucosal, and uveal melanoma detailed analysis of 9 distinct subtypes defined by their evolutionary pathway. *Archives of Pathology and Laboratory Medicine*, 144(4), 500–522.

- Erickson, C. A., & Goins, T. L. (1995). Avian neural crest cells can migrate in the dorsolateral path only if they are specified as melanocytes. *Development*, *121*(3), 915–924.
- Ernfors, P. (2010). Cellular origin and developmental mechanisms during the formation of skin melanocytes. *Experimental Cell Research*, *316*, 1397–1407.
- Etchevers, H. C., Vincent, C., Le Douarin, N. M., & Couly, G. F. (2001). The cephalic neural crest provides pericytes and smooth muscle cells to all blood vessels of the face and forebrain. *Development*, *128*(7), 1059–1068.
- Fang, D. (2002). Selective down-regulation of tyrosinase family gene TYRP1 by inhibition of the activity of melanocyte transcription factor, MITF. *Nucleic Acids Research*, *30*(14), 3096–3106.
- Ferrari, A., Lopez Almaraz, R., Reguerre, Y., Cesen, M., Bergamaschi, L., Indini, A., Schneider, D. T., Godzinski, J., Bien, E., Stachowicz-Stencel, T., Eigentler, T. K., Chiaravalli, S., Krawczyk, M. A., Pappo, A., Orbach, D., Bisogno, G., & Brecht, I. B. (2021). Cutaneous melanoma in children and adolescents: The EXPeRT/PARTNER diagnostic and therapeutic recommendations. *Pediatric Blood and Cancer*, *68*(S4), 1–11.
- Garcez, R. C., Le Douarin, N. M., & Creuzet, S. E. (2014). Combinatorial activity of Six1-2-4 genes in cephalic neural crest cells controls craniofacial and brain development. *Cellular and Molecular Life Sciences*, *71*, 2149–2164.
- Ghanem, G., & Fabrice, J. (2011). Tyrosinase related protein 1 (TYRP1/gp75) in human cutaneous melanoma. *Molecular Oncology*, *5*(2), 150–155.
- Gilissen, C., Hehir-Kwa, J. Y., Thung, D. T., Van De Vorst, M., Van Bon, B. W. M., Willemsen, M. H., Kwint, M., Janssen, I. M., Hoischen, A., Schenck, A., Leach, R., Klein, R., Tearle, R., Bo, T., Pfundt, R., Yntema, H. G., De Vries, B. B. A., Kleefstra, T., Brunner, H. G., ... Veltman, J. A. (2014). Genome sequencing identifies major causes of severe intellectual disability. *Nature*, *511*(7509), 344–347.
- Gilissen, C., Hehir-Kwa, J. Y., Tjwan Thung, D., van de Vorst, M., M van Bon, B. W., Willemsen, M. H., Kwint, M., Janssen, I. M., Hoischen, A., Schenck, A., Leach, R., Klein, R., Tearle, R., Bo, T., Pfundt, R., Yntema, H. G., A de Vries, B. B., Kleefstra, T., Brunner, H. G., ... Veltman, J. A. (2014). *Genome sequencing identifies major causes of severe intellectual disability*.
- Giovannone, D., Ortega, B., Reyes, M., El-Ghali, N., Rabadí, M., Sao, S., & de Bellard, M. E. (2015). Chicken trunk neural crest migration visualized with HNK1. *Acta Histochemica*, *117*(3), 255–266.
- Giuliano, S., Cheli, Y., Ohanna, M., Bonet, C., Beuret, L., Bille, K., Loubat, A., Hofman, V., Hofman, P., Ponzio, G., Bahadoran, P., Ballotti, R., & Bertolotto, C. (2010). Microphthalmia-associated transcription factor controls the DNA damage response and a lineage-specific senescence program in melanomas. *Cancer Research*, *70*(9), 3813–3822.
- Goding, C. R. (2011). A picture of Mitf in melanoma immortality. *Oncogene*, *30*, 2304–2306.

- Goldstein, A. M. (2011). Germline BAP1 mutations and tumor susceptibility. *Nature Genetics*, 43(10), 925–926.
- Goldstein, A. M., Chan, M., Harland, M., Hayward, N. K., Demenais, F., Bishop, T., Azizi, E., Bergman, W., Bianchi-Scarra, G., Bruno, W., Calista, D., Albright, L. A. C., Chaudru, V., Chompret, A., Cuellar, F., Elder, D. E., Ghiorzo, P., Gillanders, E. M., Gruis, N. A., ... Yakobson, E. (2007). Features associated with germline CDKN2A mutations: a GenoMEL study of melanoma-prone families from three continents. *J Med Genet*, 44, 99–106.
- Goldstein, A. M., Stidd, K. C., Yang, X. R., Fraser, M. C., & Tucker, M. A. (2018). Pediatric melanoma in melanoma-prone families. *Cancer*, 124(18), 3715–3723.
- Gomes, M. D., Lecker, S. H., Jagoe, R. T., Navon, A., & Goldberg, A. L. (2001). Atrogin-1, a muscle-specific F-box protein highly expressed during muscle atrophy. *Proceedings of the National Academy of Sciences of the United States of America*, 98(25), 14440–14445.
- Gröbner, S. N., Worst, B. C., Weischenfeldt, J., Buchhalter, I., Kleinheinz, K., Rudneva, V. A., Johann, P. D., Balasubramanian, G. P., Segura-Wang, M., Brabetz, S., Bender, S., Hutter, B., Sturm, D., Pfaff, E., Hübschmann, D., Zipprich, G., Heinold, M., Eils, J., Lawerenz, C., ... Pfister, S. M. (2018). The landscape of genomic alterations across childhood cancers. *Nature*, 555(7696), 321–327.
- Gruis, N. A., van der Velden, P., Sandkuijl, L., Prins, D., Weaver-Feldhaus, J., Kamb, A., Bergman, W., & Frants, R. (1995). Homozygotes for CDKN2 (p16) germline mutation in Dutch familial melanoma kindreds. *Nature Genetics*, 10(3), 351–353.
- Gudbjartsson, D. F., Sulem, P., Stacey, S. N., Goldstein, A. M., Rafnar, T., Sigurgeirsson, B., Benediktsdottir, K. R., Thorisdottir, K., Ragnarsson, R., Sveinsdottir, S. G., Magnusson, V., Lindblom, A., Kostulas, K., Botella-Estrada, R., Soriano, V., Juberías, P., Grasa, M., Saez, B., Andres, R., ... Stefansson, K. (2008). ASIP and TYR pigmentation variants associate with cutaneous melanoma and basal cell carcinoma. *Nature Genetics*, 40(7), 886–891.
- Habel, N., El-Hachem, N., Soysouvanh, F., Hadhiri-Bziouche, H., Giuliano, S., Nguyen, S., Horák, P., Gay, A.-S., Debayle, D., Nottet, N., Béranger, G., Paillerets, B. B., Bertolotto, C., & Ballotti, R. (2020). FBXO32 links ubiquitination to epigenetic reprogramming of melanoma cells. *Cell Death & Differentiation*.
- Haber, D. A., & Velculescu, V. E. (2014). Blood-based analyses of cancer: Circulating tumor cells and circulating tumor DNA. *Cancer Discovery*, 4(6), 650–661.
- Hamburger, V., & Hamilton, H. L. (1951). A series of normal stages in the development of the chick embryo. *Journal of Morphology*, 88(1), 49–92.
- Hamre, M. R., Chuba, P., Bakhshi, S., Thomas, R., & Severson, R. K. (2002). Cutaneous melanoma in childhood and adolescence. *Pediatric Hematology and Oncology*, 19(5), 309–317.
- Herraiz, C., Martínez-Vicente, I., & Maresca, V. (2021). The α -melanocyte-stimulating

- hormone/melanocortin-1 receptor interaction: A driver of pleiotropic effects beyond pigmentation. *Pigment Cell and Melanoma Research*, 34(4), 748–761.
- His, W., & His, W. (1868). *Untersuchungen über die erste Anlage des Wirbelthierleibes: die erste Entwicklung des Hühnchens im Ei*. F.C.W. Vogel,.
- Hodis, E., Watson, I. R., Kryukov, G. V., Arold, S. T., Imielinski, M., Theurillat, J. P., Nickerson, E., Auclair, D., Li, L., Place, C., Dicara, D., Ramos, A. H., Lawrence, M. S., Cibulskis, K., Sivachenko, A., Voet, D., Saksena, G., Stransky, N., Onofrio, R. C., ... Chin, L. (2012). A landscape of driver mutations in melanoma. *Cell*, 150(2), 251–263.
- Horn, S., Figl, A., Rachakonda, P. S., Fischer, C., Sucker, A., Gast, A., Kadel, S., Moll, I., Nagore, E., Hemminki, K., Schadendorf, D., & Kumar, R. (2013). TERT Promoter Mutations in Familial and Sporadic Melanoma. *Science*, 339(6122), 959–961.
- Hoshino, D., Kirkbride, K. C., Costello, K., Clark, E. S., Sinha, S., Grega-Larson, N., Tyska, M. J., & Weaver, A. M. (2013). Exosome secretion is enhanced by invadopodia and drives invasive behavior. *Cell Reports*, 5(5), 1159–1168.
- Huang, F. W., Hodis, E., Jue Xu, M., Kryukov, G. V., Chin, L., & Garraway, L. A. (2013). Highly recurrent TERT promoter mutations in human melanoma. *Scienceexpress*.
- Hudson, L. D. (2001). MELANOMA 2001. *Southern Medical Journal*, 94(9), 851–852.
- Jen, M., Murphy, M., & Grant-Kels, J. M. (2009). Childhood melanoma. *Clinics in Dermatology*, 27(6), 529–536.
- Ji, Z., Mohammed, H., Webber, A., Ridsdale, J., Han, N., Carroll, J. S., & Sharrocks, A. D. (2014). The forkhead transcription factor FOXK2 acts as a chromatin targeting factor for the BAP1-containing histone deubiquitinase complex. *Nucleic Acids Research*, 42(10), 6232–6242.
- Jin, Z. B., Li, Z., Liu, Z., Jiang, Y., Cai, X. B., & Wu, J. (2018). Identification of de novo germline mutations and causal genes for sporadic diseases using trio-based whole-exome/genome sequencing. *Biological Reviews*, 93(2), 1014–1031.
- Jonsson, H., Magnusdottir, E., Eggertsson, H. P., Stefansson, O. A., Arnadottir, G. A., Eiriksson, O., Zink, F., Helgason, E. A., Jonsdottir, I., Gylfason, A., Jonasdottir, A., Jonasdottir, A., Beyter, D., Steingrimsdottir, T., Norddahl, G. L., Magnusson, O. T., Masson, G., Halldorsson, B. V., Thorsteinsdottir, U., ... Stefansson, K. (2021). Differences between germline genomes of monozygotic twins. *Nature Genetics*, 53(1), 27–34.
- Kain, K. H., Miller, J. W. I., Jones-Paris, C. R., Thomason, R. T., Lewis, J. D., Bader, D. M., Barnett, J. V., & Zijlstra, A. (2014). The chick embryo as an expanding experimental model for cancer and cardiovascular research. *Dev Dyn*, 243(2), 216–228.
- Kalirai, H., Shahidipour, H., Coupland, S. E., & Luyten, G. (2015). Use of the Chick Embryo Model in Uveal Melanoma. *Ocular Oncology and Pathology*, 1(3), 133–140.
- Kamb, A., Shattuck-Eidens, D., Liu, Q., Gruis, N. A., Ding, W., Hussey, C., Tran, T., Miki, Y., Weaver-

- Feldhaus, J., McClure, M., Aitken, J. F., Anderson, D. E., Bergman, W., Frants, R., Goldgar, D. E., Green, A., MacLennan, R., Martin, N. G., Meyer, L. J., ... Cannin-Albright, L. A. (1994). Analysis of the p16 gene (CDKN2) as a candidate for the chromosome 9p melanoma susceptibility locus. *Nature*, *8*.
- Kanitakis, J. (2002). Anatomy, histology and immunohistochemistry of normal human skin. *European Journal of Dermatology: EJD*, *12*(4), 390–391.
- Karaman, S., & Detmar, M. (2014). Mechanisms of lymphatic metastasis. *The Journal of Clinical Investigation*, *124*(3), 922.
- Katahira, T., & Nakamura, H. (2003). Gene silencing in chick embryos with a vector-based small interfering RNA system. *Development Growth and Differentiation*, *45*(4), 361–367.
- Khaled, M., Levy, C., & Fisher, D. E. (2010). Control of melanocyte differentiation by a MITF-PDE4D3 homeostatic circuit. *Genes and Development*, *24*(20), 2276–2281.
- Kimura, J., Katahira, T., Araki, I., & Nakamura, H. (2004). Possible role of Hes5 for the rostrocaudal polarity formation of the tectum. *Development Growth and Differentiation*, *46*(3), 219–227.
- Kinsler, V. A., O'Hare, P., Bulstrode, N., Calonje, J. E., Chong, W. K., Hargrave, D., Jacques, T., Lomas, D., Sebire, N. J., & Slater, O. (2017). Melanoma in congenital melanocytic naevi. *British Journal of Dermatology*, *176*(5), 1131–1143.
- Kinsler, Veronica A., Abu-Amero, S., Budd, P., Jackson, I. J., Ring, S. M., Northstone, K., Atherton, D. J., Bulstrode, N. W., Stanier, P., Hennekam, R. C., Sebire, N. J., Moore, G. E., & Healy, E. (2012). Germline melanocortin-1-receptor genotype is associated with severity of cutaneous phenotype in congenital melanocytic nevi: A role for MC1R in human fetal development. *Journal of Investigative Dermatology*, *132*(8), 2026–2032.
- Kinsler, Veronica A, Thomas, A. C., Ishida, M., Bulstrode, N. W., Loughlin, S., Hing, S., Chalker, J., Mckenzie, K., Abu-amero, S., Slater, O., Chanudet, E., Palmer, R., Morrogh, D., Stanier, P., Healy, E., Sebire, N. J., & Moore, G. E. (2013). Multiple Congenital Melanocytic Nevi and Neurocutaneous Melanosis Are Caused by Postzygotic Mutations in Codon 61 of NRAS. *Journal of Investigative Dermatology*, *133*(9), 2229–2236.
- Kipreos, E. T., & Pagano, M. (2000). The F-box protein family. *Genome Biology*, *1*(5), XIX–XX.
- Kollipara, R., Cooley, L. D., Horii, K. A., Hetherington, M. L., Leboit, P. E., Singh, V., & Zwick, D. L. (2014). Spitzoid melanoma in a child with Li-Fraumeni syndrome. *Pediatric and Developmental Pathology*, *17*(1), 64–69.
- Kos, R., Tucker, R. P., Hall, R., Duong, T. D., & Erickson, C. A. (2003). Methods for Introducing Morpholinos into the Chicken Embryo. *Developmental Dynamics*, *226*, 470–477.
- Kraemer, K. H., Lee, M., Andrews, A. D., & Lambert, W. C. (1994). *The role of Sunlight and DNA Repair in of Melanoma and Nonmelanoma Skin Cancer*.
- Ku, C. S., Tan, E. K., & Cooper, D. N. (2013). From the periphery to centre stage: De novo single

- nucleotide variants play a key role in human genetic disease. *Journal of Medical Genetics*, 50(4), 203–211.
- Kulesa, P. M., Bailey, C. M., Kasemeier-Kulesa, J. C., & McLennan, R. (2010). Cranial neural crest migration: New rules for an old road. In *Developmental Biology* (Vol. 344, Issue 2, pp. 543–554). Academic Press Inc.
- Kunimoto, R., Jimbow, K., Tanimura, A., Sato, M., Horimoto, K., Hayashi, T., Hisahara, S., Sugino, T., Hirobe, T., Yamashita, T., & Horio, Y. (2014). SIRT1 regulates lamellipodium extension and migration of melanoma cells. *Journal of Investigative Dermatology*, 134(6), 1693–1700.
- Kuo, B. R., & Erickson, C. A. (2010). *Cell Adhesion & Migration Regional differences in neural crest morphogenesis*.
- Le Douarin, N., Creuzet, S., Couly, G., & Dupin, E. (2004). Neural crest cell plasticity and its limits. *Development*, 24, 4637–4650.
- Le Douarin, N., & Kalcheim, C. (1999). The Neural Crest: Source of the Pigment Cells. In *The Neural Crest*.
- Le Douarin, N. M. (2004). The avian embryo as a model to study the development of the neural crest: a long and still ongoing story. *Mechanisms of Development*, 121, 1089–1102.
- Le Douarin, N. M., Brito, J. M., & Creuzet, S. (2007). Role of the neural crest in face and brain development. *Brain Research Reviews*, 55(2), 237–247.
- Le Douarin, N. M., Couly, G., & Creuzet, S. E. (2012). The neural crest is a powerful regulator of pre-otic brain development. *Developmental Biology*, 366(1), 74–82.
- Le Douarin, N. M., Creuzet, S., Couly, G., & Dupin, E. (2004). Neural crest cell plasticity and its limits. *Development*, 131(19), 4637–4650.
- Le Douarin, N. M., & Teillet, M. A. M. (1974). Experimental analysis of the migration and differentiation of neuroblasts of the autonomic nervous system and of neurectodermal mesenchymal derivatives, using a biological cell marking technique. *Developmental Biology*, 41(1), 162–184.
- Le Lievre, C. S., & Le Douarin, N. M. (1975). Mesenchymal derivatives of the neural crest: analysis of chimaeric quail and chick embryos. In *Embryol. exp. Morph* (Vol. 34).
- Le Lièvre, C. S., & Le Douarin, N. M. (1975). Mesenchymal derivatives of the neural crest: analysis of chimaeric quail and chick embryos. *Journal of Embryology and Experimental Morphology*, 34(1), 125–154.
- Le Pape, E., Wakamatsu, K., Ito, S., Wolber, R., & Hearing, V. J. (2008). Regulation of eumelanin / pheomelanin synthesis and visible pigmentation in melanocytes by ligands of the melanocortin 1 receptor. *Pigment Cell & Melanoma Research*, 21(4), 477.
- Lee, S., Barnhill, R. L., Dummer, R., Dalton, J., Wu, J., Pappo, A., & Bahrami, A. (2015). TERT Promoter Mutations Are Predictive of Aggressive Clinical Behavior in Patients with Spitzoid

- Melanocytic Neoplasms OPEN. *Scientific Reports* |, 5, 11200.
- Leong, H. S., Robertson, A. E., Stoletov, K., Leith, S. J., Chin, C. A., Chien, A. E., Hague, M. N., Ablack, A., Carmine-Simmen, K., McPherson, V. A., Postenka, C. O., Turley, E. A., Courtneidge, S. A., Chambers, A. F., & Lewis, J. D. (2014). Invadopodia Are Required for Cancer Cell Extravasation and Are a Therapeutic Target for Metastasis. *Cell Reports*, 8(5), 1558–1570.
- Li, A., Dawson, J. C., Forero-Vargas, M., Spence, H. J., Yu, X., König, I., Anderson, K., & Machesky, L. M. (2010). The Actin-Bundling Protein Fascin Stabilizes Actin in Invadopodia and Potentiates Protrusive Invasion. *Current Biology*, 20(4), 339–345.
- Li, F. P., & Fraumeni, J. F. (1969). Soft-tissue sarcomas, breast cancer, and other neoplasms. A familial syndrome? *Annals of Internal Medicine*, 71(4), 747–752.
- Lin, J. Y., & Fisher, D. E. (2007). Melanocyte biology and skin pigmentation. *Nature*, 445(7130), 843–850.
- Loercher, A. E., Tank, E. M. H., Delston, R. B., & Harbour, J. W. (2005). MITF links differentiation with cell cycle arrest in melanocytes by transcriptional activation of INK4A. *Journal of Cell Biology*, 168(1), 35–40.
- López-Colomé, A. M., Lee-Rivera, I., Benavides-Hidalgo, R., & López, E. (2017). Paxillin: A crossroad in pathological cell migration. *Journal of Hematology and Oncology*, 10(1), 1–15.
- Lu, C., Zhang, J., Nagahawatte, P., Easton, J., Lee, S., Liu, Z., Ding, L., Wyczalkowski, M. A., Valentine, M., Navid, F., Mulder, H., Tatevossian, R. G., Dalton, J., Davenport, J., Yin, Z., Edmonson, M., Rusch, M., Wu, G., Li, Y., ... Bahrami, A. (2015). The genomic landscape of childhood and adolescent melanoma. *Journal of Investigative Dermatology*, 135(3), 816–823.
- Lu, H., Liu, S., Zhang, G., Kwong, L. N., Zhu, Y., Miller, J. P., Hu, Y., Zhong, W., Zeng, J., Wu, L., Krepler, C., Sproesser, K., Xiao, M., Xu, W., Karakousis, G. C., Schuchter, L. M., Field, J., Zhang, P. J., Herlyn, M., ... Guo, W. (2016). Oncogenic BRAF-Mediated Melanoma Cell Invasion. *Cell Reports*, 15(9), 2012–2024.
- Lugassy, C., Kleinman, H. K., Vermeulen, P. B., & Barnhill, R. L. (2020). Angiotropism, pericytic mimicry and extravascular migratory metastasis: an embryogenesis-derived program of tumor spread. *Angiogenesis*, 23(1), 27–41.
- Markovic, O., Markovic, N., Whiteman, D. C., Milligan, A., Welch, J., Green, A. C., & Hayward, N. K. (1997). *Germline CDKN2A Mutations in Childhood Melanoma*.
- Matichard, E., Verpillat, P., Meziani, R., Gérard, B., Descamps, V., Legroux, E., Burnouf, M., Bertrand, G., Bouscarat, F., Archimbaud, A., Picard, C., Ollivaud, L., Basset-Seguin, N., Kerob, D., Lanternier, G., & Lebbe, C. (2004). Melanocortin 1 receptor (MC1R) gene variants may increase the risk of melanoma in France independently of clinical risk factors and UV exposure. *J Med Genet*, 41, 13.
- McGill, G. G., Horstmann, M., Widlund, H. R., Du, J., Motyckova, G., Nishimura, E. K., Lin, Y.,

- Ramaswamy, S., Avery, W., Ding, H., Jordan, S. A., Jackson, I. J., Korsmeyer, S. J., Golub, T. R., & Fisher, D. E. (2002). Bcl2 Regulation by the Melanocyte Master Regulator Mitf Modulates Lineage Survival and Melanoma Cell Viability. *Cell*, *109*(6), 707–718.
- McRae, J., Clayton, S., Fitzgerald, TW, & Authors), (299 more. (2017). *Prevalence and architecture of de novo mutations in developmental disorders*.
- Mei, Z., Zhang, D., Hu, B., Wang, J., Shen, X., & Xiao, W. (2015). FBXO32 targets c-Myc for proteasomal degradation and inhibits c-Myc activity. *Journal of Biological Chemistry*, *290*(26), 16202–16214.
- Mort, R. L., Jackson, I. J., & Elizabeth Patton, E. (2015). The melanocyte lineage in development and disease. *Development (Cambridge)*, *142*(4), 620–632.
- Mousson, A., Legrand, M., Steffan, T., Vauchelles, R., Carl, P., Gies, J.-P., Lehmann, M., Zuber, G., De Mey, J., Dujardin, D., Sick, E., & Rondé, P. (2021). Inhibiting FAK–Paxillin Interaction Reduces Migration and Invadopodia-Mediated Matrix Degradation in Metastatic Melanoma Cells. *Cancers*, *13*(8), 1871.
- Muramatsu, T., Mizutani, Y., Ohmori, Y., & Okumura, J. I. (1997). Comparison of three nonviral transfection methods for foreign gene expression in early chicken embryos in ovo. *Biochemical and Biophysical Research Communications*, *230*(2), 376–380.
- Nakamaura, H., Katahira, T., Sato, T., Watanabe, Y., & Funahashi, J. I. (2004). Gain- and loss-of-function in chick embryos by electroporation. *Mechanisms of Development*, *121*(9), 1137–1143.
- Nasti, T. H., & Timares, L. (2015). MC1R, eumelanin and pheomelanin: Their role in determining the susceptibility to skin cancer. *Photochemistry and Photobiology*, *91*(1), 188–200.
- National Cancer Institute. (2018). *SEER cancer Stat Facts: Melanoma of the Skin*. SEER Stat Fact Sheets: Melanoma of the Skin.
- Niwa, T., Mochii, M., Nakamura, A., & Shiojiri, N. (2002). Plumage pigmentation and expression of its regulatory genes during quail development – histochemical analysis using Bh (black at hatch) mutants. *Mechanisms of Development*, *118*(1–2), 139–146.
- O’roak, B. J., Vives, L., Girirajan, S., Karakoc, E., Krumm, N., Coe, B. P., Levy, R., Ko, A., Lee, C., Smith, J. D., Turner, E. H., Stanaway, I. B., Vernet, B., Malig, M., Baker, C., Reilly, B., Akey, J. M., Borenstein, E., Rieder, M. J., ... Eichler, E. E. (2012). Sporadic autism exomes reveal a highly interconnected protein network of de novo mutations HHS Public Access. *Nature*, *485*(7397), 246–250.
- Olmeda, D., Cerezo-Wallis, D., Riveiro-Falkenbach, E., Pennacchi, P. C., Contreras-Alcalde, M., Ibarz, N., Cifdaloz, M., Catena, X., Calvo, T. G., Cañón, E., Alonso, D., Suarez, J., Osterloh, L., Graña, O., Mulero, F., Megías, D., Cañamero, M., Martínez-Torrecedrada, J., Mondal, C., ... Soengas, M. S. (2017). Whole body imaging of lymphovascular niches identifies

- premetastatic roles of MIDKINE. *Nature*, 546(7660), 676.
- Pappo, A. S. (2003). Melanoma in children and adolescents. *European Journal of Cancer*, 39(18), 2651–2661.
- Paterson, E. K., Fielder, T. J., Macgregor, G. R., Ito, S., Wakamatsu, K., Gillen, D. L., Eby, V., Boissy, R. E., & Ganesan, A. K. (2015). *Tyrosinase Depletion Prevents the Maturation of Melanosomes in the Mouse Hair Follicle*.
- Pawlikowska, P., Tayoun, T., Oulhen, M., Faugoux, V., Rouffiac, V., & Aberlenc, A. (2020). Exploitation of the chick embryo chorioallantoic membrane (CAM) as a platform for anti-metastatic drug testing. *Scientific Reports*.
- Pekarik, V., Bourikas, D., Miglino, N., Joset, P., Preiswerk, S., & Stoeckli, E. T. (2003). Screening for gene function in chicken embryo using RNAi and electroporation. *Nature Biotechnology*, 21(1), 93–96.
- Pellegrini, C., Botta, F., Massi, D., Martorelli, C., Facchetti, F., Gandini, S., Maisonneuve, P., Avril, M.-F., Demenais, F., Bressac-de Paillerets, B., Hoiom, V., Cust, A. E., Anton-Culver, H., Gruber, S. B., Gallagher, R. P., Marrett, L., Zanetti, R., Dwyer, T., Thomas, N. E., ... Wong, T. H. (2019). MC1R variants in childhood and adolescent melanoma: a retrospective pooled analysis of a multicentre cohort. *The Lancet Child & Adolescent Health*, 3(5), 332–342.
- Pellegrini, C., Fagnoli, M. C., Suppa, M., & Peris, K. (2012). MC1R variants predisposing to concomitant primary cutaneous melanoma in a monozygotic twin pair. *BMC Medical Genetics*, 13(1), 1.
- Pijuan, J., Barceló, C., Moreno, D. F., Maiques, O., Sisó, P., Marti, R. M., Macià, A., & Panosa, A. (2019). In vitro Cell Migration, Invasion, and Adhesion Assays: From Cell Imaging to Data Analysis. *Frontiers in Cell and Developmental Biology*, 7, 107.
- Poduri, A., Evrony, G., Cai, X., & Walsh, C. (2013). Somatic Mutation, Genomic Variation, and Neurological Disease. *Science*, 341, 934–940.
- Potrony, M., Badenas, C., Aguilera, P., Puig-Butille, J. A., Carrera, C., Malveyh, J., & Puig, S. (2015). Update in genetic susceptibility in melanoma. *Annals of Translational Medicine*, 3(15), 210.
- Potterf, S. B., Mollaaghbabab, R., Hou, L., Southard-Smith, E. M., Hornyak, T. J., Arnheiter, H., & Pavan, W. J. (2001). Analysis of SOX10 function in neural crest-derived melanocyte development: SOX10-dependent transcriptional control of dopachrome tautomerase. *Developmental Biology*, 237(2), 245–257.
- Rabbie, R., Rashid, M., Arance, A. M., Sánchez, M., Tell-Marti, G., Potrony, M., Conill, C., van Doorn, R., Dentro, S., Gruis, N. A., Corrie, P., Iyer, V., Robles-Espinoza, C. D., Puig-Butille, J. A., Puig, S., & Adams, D. J. (2017). Genomic analysis and clinical management of adolescent cutaneous melanoma. *Pigment Cell and Melanoma Research*, 30(3), 307–316.
- Randle, S. J., & Laman, H. (2016). F-box protein interactions with the hallmark pathways in

- cancer. In *Seminars in Cancer Biology* (Vol. 36, pp. 3–17). Academic Press.
- Reedy, M. V., Faraco, C. D., & Erickson, C. A. (1998). The delayed entry of thoracic neural crest cells into the dorsolateral path is a consequence of the late emigration of melanogenic neural crest cells from the neural tube. *Developmental Biology*, *200*(2), 234–246.
- Reid, A. L., Millward, M., Pearce, R., Lee, M., Frank, M. H., Ireland, A., Monshizadeh, L., Rai, T., Heenan, P., Medic, S., Kumarasinghe, P., & Ziman, M. (2013). Markers of circulating tumour cells in the peripheral blood of patients with melanoma correlate with disease recurrence and progression. *British Journal of Dermatology*, *168*(1), 85–92.
- Renaux-Petel, M., Charbonnier, F., Théry, J. C., Fermey, P., Lienard, G., Bou, J., Coutant, S., Vezain, M., Kasper, E., Fourneaux, S., Manase, S., Blanluet, M., Leheup, B., Mansuy, L., Champigneulle, J., Chappé, C., Longy, M., Sévenet, N., Paillerets, B. B. De, ... Bougeard, G. (2018). Contribution of de novo and mosaic TP53 mutations to Li-Fraumeni syndrome. *Journal of Medical Genetics*, *55*(3), 173–180.
- Rentzsch, P., Witten, D., Cooper, G. M., Shendure, J., & Kircher, M. (2019). CADD: Predicting the deleteriousness of variants throughout the human genome. *Nucleic Acids Research*, *47*(D1), D886–D894.
- Ribatti, D., & Tamma, R. (2019). The chick embryo chorioallantoic membrane as an in vivo experimental model to study multiple myeloma. In *Enzymes* (1st ed., Vol. 46). Elsevier Inc.
- Rodriguez, M. S., Dargemont, C., & Hay, R. T. (2000). *SUMO-1 Conjugation in Vivo Requires Both a Consensus Modification Motif and Nuclear Targeting**.
- Sahu, S. K., Tiwari, N., Pataskar, A., Zhuang, Y., Borisova, M., Diken, M., Strand, S., Beli, P., & Tiwari, V. K. (2017). FBXO32 promotes microenvironment underlying epithelial-mesenchymal transition via CtBP1 during tumour metastasis and brain development. *Nature Communications*, *8*(1), 1–18.
- Sanders, S. J., Murtha, M. T., Gupta, A. R., Murdoch, J. D., Raubeson, M. J., Willsey, A. J., Ercan-Sencicek, A. G., Di Lullo, N. M., Parikshak, N. N., Stein, J. L., Walker, M. F., Ober, G. T., Teran, N. A., Song, Y., El-Fishawy, P., Murtha, R. C., Choi, M., Overton, J. D., Bjornson, R. D., ... State, M. W. (2012). De novo mutations revealed by whole exome sequencing are strongly associated with autism. *Nature*, *485*(7397), 237.
- Sanders, S. J., Murtha, M. T., Gupta, A. R., Murdoch, J. D., Raubeson, M. J., Willsey, A. J., Ercan-Sencicek, A. G., M., D. N., Parikshak, N. N., Stein, J. L., Walker, M. F., Ober, G. T., Teran, N. A., Song, Y., El-Fishawy, P., Murtha, R. C., Choi, M., Overton, J. D., Bjornson, R. D., ... State, M. W. (2013). De novo mutations revealed by whole exome sequencing are strongly associated with autism. *Nature*.
- Sanger, F., Nicklen, S., & Coulson, R. (1977). DNA sequencing with chain-terminating inhibitors. *Proc Natl Acad Sci*, *74*(12), 5463–5467.

- Satyamoorthy, K., Muyrers, J., Meier, F., Patel, D., & Herlyn, M. (2001). Mel-CAM-specific genetic suppressor elements inhibit melanoma growth and invasion through loss of gap junctional communication. *Oncogene*, *20*(34), 4676–4684.
- Schaefer, K. S., Doughman, Y. Q., Fisher, S. A., & Watanabe, M. (2004). Dynamic Patterns of Apoptosis in the Developing Chicken Heart. *Developmental Dynamics*, *229*(3), 489–499.
- Ségurel, L., Wyman, M. J., & Przeworski, M. (2014). Determinants of Mutation Rate Variation in the Human Germline. *Annual Review of Genomics and Human Genetics*, *15*(1), 47–70.
- Serbedzija, G. N., Bronner-Fraser, M., & Fraser, S. E. (1994). Developmental potential of trunk neural crest cells in the mouse. *Development*, *120*(7), 1709–1718.
- Serrano, M., Lee, H.-W., & Chin, L. (1996). Role of the INK4a Locus in Tumor Suppression and Cell Mortality. In *Cell* (Vol. 85).
- Seynaeve, B., Lee, S., Borah, S., Park, Y., Pappo, A., Kirkwood, J. M., & Bahrami, A. (2017). Genetic and Epigenetic Alterations of TERT Are Associated with Inferior Outcome in Adolescent and Young Adult Patients with Melanoma. *Scientific Reports*, *7*(1), 45704.
- Shain, A. H., & Bastian, B. C. (2016). From melanocytes to melanomas. *Nature Reviews Cancer*, *16*(6), 345–358.
- Shain, A. H., Yeh, I., Kovalyshyn, I., Sriharan, A., Talevich, E., Gagnon, A., Dummer, R., North, J., Pincus, L., Ruben, B., Rickaby, W., D'Arrigo, C., Robson, A., & Bastian, B. C. (2015). The Genetic Evolution of Melanoma from Precursor Lesions. *New England Journal of Medicine*, *373*(20), 1926–1936.
- Singh Tekcham, D., Chen, D., Liu, Y., Ling, T., Zhang, Y., Chen, H., Wang, W., Otkur, W., Qi, H., Xia, T., Liu, X., Piao, H., & Liu, H. (2020). *F-box proteins and cancer: an update from functional and regulatory mechanism to therapeutic clinical prospects*. *10*(9), 4150–4167.
- Slominski, R. M., Zmijewski, M. A., & Slominski, A. T. (2015). The role of melanin pigment in melanoma. *Experimental Dermatology*, *24*(4), 258–259.
- Song, Y., Lin, M., Liu, Y., Wang, Z. W., & Zhu, X. (2019). Emerging role of F-box proteins in the regulation of epithelial-mesenchymal transition and stem cells in human cancers. *Stem Cell Research and Therapy*, *10*(1), 1–11.
- Southard-smith, E. M., Kos, L., & Pavan, W. J. (1998). Mutation Disrupts Neural Crest Development in. *Nature Genetics*, *18*(january), 60–64.
- Spitz, S. (1948). *MELANOMAS OF CHILDHOOD*.
- Stefanaki, C., Chardalias, L., Soura, E., Katsarou, A., & Stratigos, A. (2017). Paediatric melanoma. *Journal of the European Academy of Dermatology and Venereology*, *31*(10), 1604–1615.
- Strouse, J. J., Fears, T. R., Tucker, M. A., & Wayne, A. S. (2005). Pediatric melanoma: Risk factor and survival analysis of the Surveillance, Epidemiology and End Results database. *Journal of Clinical Oncology*, *23*(21), 4735–4741.

- Sturm, R. A., Duffy, D. L., Box, N. F., Chen, W., Smit, D. J., Brown, D. L., Stow, J. L., Leonard, J. H., & Martin, N. G. (2003). The role of melanocortin-1 receptor polymorphism in skin cancer risk phenotypes. *Pigment Cell Research*, *16*(3), 266–272.
- Tan, J., Yang, X., Zhuang, L., Jiang, X., Chen, W., Puay, L. L., Karuturi, R. K. M., Tan, P. B. O., Liu, E. T., & Yu, Q. (2007). Pharmacologic disruption of polycomb-repressive complex 2-mediated gene repression selectively induces apoptosis in cancer cells. *Genes and Development*, *21*(9), 1050–1063.
- Tanaka, N., Kosaka, T., Miyazaki, Y., Mikami, S., Niwa, N., Otsuka, Y., Minamishima, Y. A., Mizuno, R., Kikuchi, E., Miyajima, A., Sabe, H., Okada, Y., Uhlén, P., Suematsu, M., & Oya, M. (2016). Acquired platinum resistance involves epithelial to mesenchymal transition through ubiquitin ligase FBXO32 dysregulation. *JCI Insight*, *1*(18).
- Tassabehji, M., Newton, V. E., & Read, A. P. (1994). Waardenburg syndrome type 2 caused by mutations in the human microphthalmia (MITF) gene. *Nature Genetics*, *8*(3), 251–255.
- Thomas, A. J., & Erickson, C. A. (2008). The making of a melanocyte: the specification of melanoblasts from the neural crest. *Pigment Cell & Melanoma Research*, *21*(6), 598–610.
- Thomas, A. J., & Erickson, C. A. (2009). FOXD3 regulates the lineage switch between neural crest-derived glial cells and pigment cells by repressing MITF through a non-canonical mechanism. *Development (Cambridge, England)*, *136*, 1849–1858.
- Vallarelli, A. F., Rachakonda, P. S., André, J., Heidenreich, B., Riffaud, L., Bensussan, A., Kumar, R., & Dumaz, N. (2016). TERT promoter mutations in melanoma render TERT expression dependent on MAPK pathway activation. *Oncotarget*, *7*(33), 53127.
- Valverde, P., Healy, E., Sikkink, S., Haldane, F., Thody, A. J., Carothers, A., Jackson, I. J., & Rees, J. L. (1996). *The Asp84Glu variant of the melanocortin 1 receptor (MC1R) is associated with melanoma*. *5*(10).
- Velasco-Velázquez, M. A., Salinas-Jazmín, N., Mendoza-Patiño, N., & Mandoki, J. J. (2008). *Reduced paxillin expression contributes to the antimetastatic effect of 4-hydroxycoumarin on B16-F10 melanoma cells*.
- Veltman, J. A., & Brunner, H. G. (2012). De novo mutations in human genetic disease. *Nature Reviews Genetics*, *13*(8), 565–575.
- Vissers, L. E. L. M., De Ligt, J., Gilissen, C., Janssen, I., Steehouwer, M., De Vries, P., Van Lier, B., Arts, P., Wieskamp, N., Del Rosario, M., Van Bon, B. W. M., Hoischen, A., De Vries, B. B. A., Brunner, H. G., & Veltman, J. A. (2010). A de novo paradigm for mental retardation. *Nature Genetics*, *42*(12), 1109–1112.
- Wang, Z., Liu, P., Inuzuka, H., & Wei, W. (2014). Roles of F-box proteins in cancer. *Nature Reviews Cancer*, *14*(4), 233–247.
- Webb, D. J., Donais, K., Whitmore, L. A., Thomas, S. M., Turner, C. E., Parsons, J. T., & Horwitz, A. F.

- (2004). FAK-Src signalling through paxillin, ERK and MLCK regulates adhesion disassembly. *Nature Cell Biology*, 6(2), 154–161.
- Wiesner, T., Murali, R., Fried, I., Cerroni, L., Busam, K., Kutzner, H., & Bastian, B. C. (2012). A Distinct Subset of Atypical Spitz Tumors is Characterized by BRAF Mutation and Loss of BAP1 Expression. *American Journal of Surgical Pathology*, 36(6), 818–830.
- Wiesner, T., Obenauf, A. C., Murali, R., Fried, I., Griewank, K. G., Ulz, P., Windpassinger, C., Wackernagel, W., Loy, S., Wolf, I., Viale, A., Lash, A. E., Pirun, M., Socci, N. D., Rütten, A., Palmedo, G., Abramson, D., Offit, K., Ott, A., ... Speicher, M. R. (2011). Germline mutations in BAP1 predispose to melanocytic tumors. *Nature Genetics*, 43(10), 1018–1021.
- Wilson, N. H., & Stoeckli, E. T. (2011). Cell type specific, traceable gene silencing for functional gene analysis during vertebrate neural development. *Nucleic Acids Research*, 39(20).
- Wong, J. R., Harris, J. K., Rodriguez-Galindo, C., & Johnson, K. J. (2013). Incidence of Childhood and Adolescent Melanoma in the United States: 1973–2009. *Pediatrics*, 131(5), 846–854.
- Yamagata, M., & Sanes, J. R. (2008). Dscam and Sidekick proteins direct lamina-specific synaptic connections in vertebrate retina. *Nature*, 451(7177), 465–469.
- Yamaguchi, H., & Condeelis, J. (2007). Regulation of the actin cytoskeleton in cancer cell migration and invasion. *Biochimica et Biophysica Acta*, 1773(5), 642.
- Yang, C., Li, X., Li, Q., Fu, S., Li, H., Guo, Z., Lin, J., & Zhao, S. (2014). Evaluation of three different promoters driving gene expression in developing chicken embryo by using in vivo electroporation Evaluation of three different promoters in vivo. *Genetics and Molecular Research*, 13(1), 1270–1277.
- Yokoyama, S., Woods, S. L., Boyle, G. M., Aoude, L. G., Macgregor, S., Zismann, V., Gartside, M., Cust, A. E., Haq, R., Harland, M., Taylor, J. C., Duffy, D. L., Holohan, K., Dutton-Regester, K., Palmer, J. M., Bonazzi, V., Stark, M. S., Symmons, J., Law, M. H., ... Brown, K. M. (2011). A novel recurrent mutation in MITF predisposes to familial and sporadic melanoma. *Nature*, 480.
- Yu, H., Pak, H., Hammond-Martel, I., Ghram, M., Rodrigue, A., Daou, S., Barbour, H., Corbeil, L., Hébert, J., Drobetsky, E., Masson, J. Y., Di Noia, J. M., & Affar, E. B. (n.d.). *Tumor suppressor and deubiquitinase BAP1 promotes DNA double-strand break repair*.
- Yuan, X., Zhang, Z., Jiang, K., Wang, X., & Li, Y. (2018). Preliminary study of the role F-box protein 32 (FBXO32) in colorectal neoplasms through the transforming growth factor beta (TGF- β)/Smad4 signalling pathway. *Medical Science Monitor*, 24, 1080–1088.
- Zarrizi, R., Menard, J. A., Belting, M., & Massoumi, R. (2014). Deubiquitination of γ -tubulin by BAP1 prevents chromosome instability in breast cancer cells. *Cancer Research*, 74(22), 6499–6508.
- Zhou, H., Liu, Y., Zhu, R., Ding, F., Wan, Y., Li, Y., & Liu, Z. (2017). FBXO32 suppresses breast

cancer tumorigenesis through targeting KLF4 to proteasomal degradation. *Nature Publishing Group*, 36, 3312–3321.